Cauchy-Characteristic Matching In General Relativity

by

B. Szilágyi

M.S., University of Timişoara, Romania, 1994

Submitted to the Graduate Faculty

of Arts and Sciences in partial fulfillment

of the requirements for the degree of

Doctor of Philosophy

University of Pittsburgh

2000

Cauchy-Characteristic Matching In General Relativity

B. Szilágyi, Ph.D.
University of Pittsburgh, 2000

The problem of self-gravitating, isolated systems is undoubtedly an important and intriguing area of research in General Relativity. However, due to the involved nature of Einstein's equations physicists found themselves unable to fully explore such systems.

From Einstein's theory we know that besides the electromagnetic spectrum, objects like quasars, active galactic nuclei, pulsars and black holes also generate a physical signal of purely gravitational nature. Now scientists involved in the Laser Interferometic Gravitational Observatory (LIGO) project are feverishly trying to build an instrument that will detect it.

While the theory of gravitational radiation has been developed using sophisticated mathematical techniques, the actual form of the signal from a given source is impossible to determine analytically. The need to investigate this and related problems has led to the creation of the field of numerical relativity.

Immediately two major approaches emerged. The first one formulates the gravitational radiation problem as a standard Cauchy initial value problem. The advantage of this approach is that it is able to handle regions of space-time where strong fields are present and caustics in the wavefronts are likely to form. But it suffers from some inherent disadvantages when it comes to the prediction of gravitational radiation waveforms.

Another approach is the Characteristic Initial value problem. This method is unable to treat regions of space-time where caustics form but it is uniquely suited to study radiation problems because it describes space-time in terms of radiation wavefronts.

The fact that the advantages and disadvantages of these two systems are complementary suggests that one may want to use the two of them together. In a full nonlinear problem it would be advantageous to evolve the inner (strong field) region using Cauchy evolution and the outer (radiation) region with the Characteristic approach. Cauchy Characteristic Matching enables one to evolve the whole space-time matching the boundaries of Cauchy and Characteristic evolution. The methodology of Cauchy Characteristic Matching has been successful in numerical evolution of the spherically symmetric Klein-Gordon-Einstein field equations as well as for 3-D non-linear wave equations. In this thesis the same methodology is studied in the context of the Einstein equations.

ACKNOWLEDGMENTS

First of all, I want to thank my advisor, Jeffrey Winicour. His wisdom and patience made this work possible. Without his continuous input I would not have been able to accomplish the work being done the last four years. In him I found not only an immense source of knowledge but also a source of guidance and encouragement so crucial in scientific research.

I would also like to thank Roberto Gómez for the many things I have learned from him in physics, computers, and many other things while working together.

During these years the Relativity Group of the University of Pittsburgh made the Department of Physics a warm environment of work.

I would like to thank Sascha Husa for important discussions on a variety of subjects. Also, I would like to thank Yosef Zlochower for his suggestions to improve the manuscript.

Finally, I want to express how much the unconditional support of my wife, Anita, meant to me during these years. She and our children, Ábrahám and Abigél, are a refreshing environment. My parents, Imre and Márta, have always thought of me with warm hearts, waiting for the return of their son who wandered to such a remote school. Without the input of these people I would have been a very depressed and ineffective person.

To Anita, Ábrahám and Abigél

CONTENTS

LIST OF FIGURES

1. INTRODUCTION

1.1 The investigation of general relativistic astrophysical systems

Self gravitating isolated systems represent an interesting and challenging area of physics. The Einstein equations describe how the presence of massive compact objects like quasars or black-holes change the geometry of space-time. On the other hand, the exterior of these objects is free of matter and is affected to a much lesser extent by the interior dynamics of these systems.

These objects are too remote to allow for direct observation of their structure. Instead, physicists and astronomers can build various antennae designed to detect the electromagnetic and the gravitational signals emitted by these isolated systems. One of these antennae is LIGO, the Laser Interferometer Gravitational-Wave Observatory, built by scientists at Caltech and MIT, with funding from the National Science Foundation. LIGO consists of a pair of high-precision laser interferometers. The laser beams are contained in an L-shaped vacuum installation, with 4 km long arms. Each arm contains mirrors that cause the laser beam to bounce back and forth between them hundreds of times before it interferes with the beam from the other arm. As gravitational radiation passes, the structure of space-time between the mirrors changes. This change amounts to a change in the distance between the mirrors. Thus the propagation of the laser-beam between these mirrors is perturbed, causing a change in the interference pattern. The change in distance between these mirrors, however, could be as little as one part in 1000 of the size of a proton. This illustrates the difficulty physicists face when trying to detect gravitational radiation by direct methods.

The existence of gravity-waves was hypothetical until J. H. Taylor and R. A. Hulse detected them indirectly in 1974. Using the radio telescope at Arecibo, Puerto Rico, they made a series of precise measurements of radio pulses emitted by two neutron stars orbiting around one another. They found that the orbital of spin these objects was increasing. They also showed that the rate of this speed-up confirmed the predictions of general

relativity for massive stars shedding orbital energy in the form of gravity waves. For their discovery, the two scientists were awarded the 1993 Nobel Prize in physics.

A correct interpretation of the gravitational signals requires understanding how they propagate and interact with the antenna. One also needs to know how these signals are generated. The strongly nonlinear character of the Einstein equations prohibits us from solving them analytically except in the weak field limit and for some highly symmetrical configurations. Thus approximation techniques are used.

One of the most promising ways to tackle the field equations of General Relativity is the simulation of curved space-time via a finite-difference approximation. This proceeds as follows:

- Choose a coordinate system suitable to describe the physical system.

- Define an initial surface with respect to the coordinate-choice. The initial surface represents a 3-dimensional subset of the 4-dimensional space-time to be simulated. The fourth dimension defines the direction in which the numerical simulation proceeds to evolve space-time.

- Represent the three-dimensional initial surface by a discrete grid-structure. Evolution in the direction of the fourth coordinate is done via small, discrete "time-steps".

- Represent the field equations by a finite-difference evolution algorithm. When doing so, the partial differential operator ∂ is approximated by finite a difference operator D_Δ. The finite difference approximation is consistent if $\lim_{\Delta \to 0} D_\Delta f = \partial f$.

Although the methodology might sound straight-forward, the real life situation is much more involved. In general relativity there are no preferred coordinate systems. The coordinates must be adapted to the system. In the case of the propagation of gravitational radiation a natural coordinate system is defined by the characteristics of space-time – the curves along which disturbances propagate. The characteristic approach has been successful in numerical simulations of highly dynamical space-times. Furthermore, with use of radial compactification techniques, the evolved space-time region can be extended to infinity where the antennae are effectively located. However, Einstein's equations imply that in certain circumstances the light rays (characteristics) refocus. Thus a coordinate system that is based on characteristics may become singular.

Another approach is based upon the Cauchy problem for general relativity. It provides initial data on an arbitrary space-like surface and then

evolves space-time as a function of an arbitrarily defined time-coordinate. The Cauchy approach avoids the focusing problem but it has its own drawbacks. One is the choice of the right coordinates, where "right" means "one that works," i.e. does not encounter singularities. Another is that the Cauchy problem suffers from structural disadvantages when evolving gravitational radiation. Since the observer is practically at infinity with respect to the gravitational source, the Cauchy grid must be extended to infinity as well. This is not possible in any finite computational tool, because compactification cannot resolve the waveform of the radiation. Since radiation propagates along light-like characteristics, grid-points distributed in a spatial direction are not efficient.

Another major problem in numerical relativity is the choice of evolution equations. The Einstein system, although written in a beautifully compact form, cannot be used in their original form for numerical simulation. Instead, one has to use combinations of various components of the Einstein tensor as numerical evolution equations. Ideally one wants to recast the original Einstein system in a first-order symmetric-hyperbolic form since those systems have well understood mathematical properties which can be well-handled in a numerical context. However these first order forms become quite complicated, with a large number of auxiliary variables and equations. Even today's supercomputers are slow when simulating space-time via those systems. Thus it is preferable to trade a first-order symmetric-hyperbolic system for one with less variables, but with mathematical properties which are harder to understand. The evolution equations for the characteristic initial value problem, as first provided by Bondi [1], form a set of equations well suited for numerical simulation. From the many available Cauchy systems we have adopted the Arnowitt-Deser-Misner (ADM) system [2, 3] which is based upon the Hamiltonian formulation of general relativity.

1.2 Cauchy-characteristic matching in general relativity

Given the complementary strengths and weaknesses of the characteristic and Cauchy formulations, the strategy we pursue in this thesis is that of Cauchy-Characteristic Matching, where the strong-field region is described by Cauchy evolution, the weak-field region is described by Characteristic evolution and the interface between the two domains is handled by Cauchy-Characteristic Matching (CCM).

CCM has been successfully applied to the problem of nonlinear scalar waves propagating in a 3-D Euclidean space [4], CCM has been used to evolve the spherical collapse of a self-gravitating scalar field onto a black

hole [5].

In order to be able to build a routine that interfaces the boundary of two evolution systems, one needs to make sure that the the finite-difference representation of the field-equations is numerically stable in both domains. Furthermore, one needs to assure that these numeric field-equations are able to handle the matching boundary conditions properly. These conditions are not satisfied if physically spurious exponential modes are generated. The characteristic code is a robustly stable evolution algorithm, which is able to handle boundaries. However, the ADM system needs an appropriate treatment of the boundary in order to avoid spurious exponentially growing modes. At the boundary one must prescribe the radiation degrees of freedom and then use an appropriate set of boundary equations that determine the remaining components of the metric tensor.

Furthermore, since the coordinates of the Cauchy system are arbitrary while the coordinates of the characteristic system are based on the light-cone structure of space-time, one needs to perform a non-trivial coordinate transformation when matching the characteristic and Cauchy evolution equations.

At the end of this thesis we lay out a problem for future research. Specifically, although we have identified a stable way of applying boundary conditions with the linearized ADM equations in Cartesian coordinates for the case of a boundary aligned to the spatial grid-structure, application of a spherical boundary (a prerequisite of the CCM) for a Cartesian ADM code is non-trivial.

1.3 Preview

The contents of this thesis is outlined as follows:

Chapter 2 gives a brief description of the Cauchy and Characteristic formulations of the equations of General Relativity. At the end of the chapter the concept of Cauchy Characteristic Matching (CCM) is briefly presented. Next, in Chapter 3, the Pitt Null Code is described. First the underlying physics is presented, i.e. the characteristic slicing, the spin-weighted metric functions and the equations describing the evolution of space-time. The end of the chapter shows how one can use characteristic evolution to numerically evolve black-hole space-times.

Chapter 4 defines the concept of Cauchy Characteristic Matching first for a spherically symmetric scalar wave, next for a 3-D scalar field. Then the same concept is outlined for the case of general relativity. To make the understanding of the details easier, first a geometrical description is given. Chapters 5 and 6 describe the two modules of CCM (extraction and

injection) in detail. Along with the presentation of the matching modules, calibration tests are provided to show proper second-order accuracy for a number of test-beds.

Next, in Chapter 7, we study the stability properties of CCM. As it is shown, the numerical noise of the individual modules do not excite any short-time instabilities. However, in order to analyze the long-term stability properties of matching, one needs to assure that both the Cauchy and the characteristic evolution codes are able to deal with the discretization error that is inherent to numerical boundary algorithms. This issue is addressed in Chapter 8. As it is shown, the characteristic code is able to deal with constraint violating boundary modes of high frequency without signs of numerical instabilities. However, as shown in the same chapter, the Cauchy code using the ADM equations is numerically unstable unless the boundary conditions are treated properly. A major contribution of this thesis is that, in the context of linearized gravitational theory, Cartesian coordinates, we have elucidated the appropriate boundary conditions on the faces of a cube for the coupled set of partial-differential equations that form the principal part of the ADM equations. In particular, one should not specify boundary values for six metric components but provide boundary data for the two radiation degrees of freedom and use a set of boundary constraints to determine the remaining four components of the spatial metric tensor.

The stability of the injection module requires a spherical boundary condition for the Cartesian Cauchy code. As discussed in Chapter 9, for the ADM system this implies use of boundary constraints in spherical coordinates. The question of spherical boundary constraints applied to a Cartesian grid is a complicated problem.

1.4   New developments in this thesis

The work presented in this thesis is the result of the work of a number of people. It is not easy to separate the individual contributions. Jeffrey Winicour had a most significant role in this work. Besides him Joe Welling, Roberto Gómez, Philip Papadopoulos, Luis Lehner, and Nigel Bishop had important contributions as well. The formalism and the code used in Cauchy-Characteristic Matching (CCM) is based on the work of these people.

The years that I was present in the Pittsburgh numerical relativity group were marked by a close collaboration with Roberto Gómez. During our collaboration, Roberto has taught me much about the physical background of our work, scientific programming as well as code-optimizing on various supercomputer platforms.

When I started to work in the group most of the code developing of the extraction module was already done. My contribution to the extraction was the calibration of the module. This work included the development of Maple algebra scripts that provided the analytic results needed for convergence tests.

The injection module in its current form was was developed by Roberto and myself. To assure the proper convergence rate for the various interpolation routines involved as well as for the whole module, I used a number of test-beds.

The stability runs of CCM had been the subject of our work for years. Although Roberto had a significant input to the question of stability of CCM, the experiments described in Chapter 7 were designed and performed by myself.

Another area of collaboration was the numerical study described in Chapter 8. Here Roberto's part was the development of the linearized Cauchy evolution codes for the various evolution algorithms. My part was the analysis, design and implementation of the boundary routines as well as the test-runs that concluded in a stable boundary-algorithm for the linearized ADM system. These are the first robustly stable Cauchy evolutions of a bounded gravitational system. This is my major contribution to the work described in this thesis.

I also made some contributions to the development of the formalism used in the study of axisymmetric event horizons and of the characteristic code itself.

2. AN OVERVIEW OF NUMERICAL RELATIVITY

2.1 Introduction

Since Einstein first wrote down the equations of general relativity (GR) in 1916, only a limited class of analytical solutions have been found. The first solution, the space-time metric of a "point charge" was written down not by Einstein but by Schwarzschild about one year after the field equations were defined.

As always, when exact analytic approaches become too cumbersome, approximations are used to further investigate the space of solutions. Approximations on an analytic level give perturbative solutions around known exact solutions. On the numeric level one can approximate the space-time continuum by a discrete set of points, write down the field equations as a set of finite-difference equations and use computer power to evolve regions of space-time.

Perhaps the first crisp definition of numerical relativity was given by Charles Misner in 1957 [6]:

> First we assume that have a computing machine better than anything we have now, and many programmers and a lot of money, and you want to look at a nice pretty solution of the Einstein equations. The computer wants to know from you what are the values of $g_{\mu\nu}$ and $\partial_t g_{\mu\nu}$ at some initial surface. Mme. Foures [Y. Choquet-Bruhat] has told us that to get these initial condition you must specify something else and hand over that problem, the problem of the initial values, to a smaller computer first, before you start on what Lichnerowicz called the evolutionary problem. The small computer would prepare the initial conditions for the big one. Then the theory, while not guaranteeing solutions for the whole future, says that it will be some finite time before anything blows up.

Still, more than forty years after this statement, when one wants to build a general relativistic code, several problems arise:

- First of all one has to determine whether the field equations are well posed or not, i.e. Does it make sense to treat the system as a set of coupled evolution equations with some suitable initial data, with boundary-values to be provided at the edge of the evolution zone? Or does the system have attributes similar to an elliptic equation where "evolution" as a function of "time" makes no mathematical sense?

- Next one has to rewrite the original field equations in a form that is suitable for numerical evolution. This question is related to the previous one in the sense that if one recasts the equations as a first-order symmetric-hyperbolic system of equations, then the numerical implementation becomes a lengthy but straightforward problem.

- Another related problem is that, despite their exponential growth, computer resources are still a limiting factor and so one might want to trade a system with a large number of variables and clear mathematical properties to one with six or maybe twelve variables, but with mathematical properties yet to be understood.

- A fourth issue that appears when doing finite-differencing is the question of numerical instabilities. This problem, if not studied carefully for the adopted discretization scheme, might give rise to non-physical exponential modes which eventually make the physical content of the numerical simulation worthless. As it will be seen, the stability properties of a code depend not only on the evolution scheme being used but also on the treatment of the boundary.

Despite the difficulties that arise there have been great successes attached to the domain of numerical relativity which motivate further search for development. One discovery, which had not been anticipated purely by analytic approaches, is the critical phenomena found when simulating spherically symmetric gravitational collapse. On the analytic side, Christodoulou made a penetrating study of the existence and uniqueness of solutions to the characteristic initial value problem [7, 8, 9, 10]. He showed that weak initial data evolve to Minkowski space asymptotically in time, but that sufficiently strong data form a horizon.[1] In the latter case, he showed that the geometry is asymptotically Schwarzschild in the approach to $\mathcal{I}^+$ (future time infinity) from outside the horizon. What this analytic tour-de-force did not reveal was the remarkable critical behavior in the transition between these two regimes, which was discovered by Choptuik [11, 12] using computational simulation.

---

[1] For a definition of the "horizon" of a black hole see Section 3.4.

Another major result of numerical relativity was the numerical simulations of axisymmetric space-times that enabled evolution of dynamical black holes [13, 14, 15, 16, 17, 18]. Grid-sucking (gridpoints falling into black holes), the importance of the right choice of time slicing, numerical instabilities, and the question of boundaries are just some of the issues that demanded attention.

Besides these (and many other) numeric results of mainly theoretic significance there is another reason why numerical relativity can have a significant role in our understanding of the fundamental laws of our universe. There is a good hope that through the building and use of laser interferometers (LIGO, VIRGO, etc.) gravitational radiation will be detected. This data needs to be confirmed and interpreted, at least in part, by numerical simulations. The events most likely to be detected are rotating black holes inspiraling into each other – a problem that requires full 3-dimensional treatment. There are post-Newtonian approaches [19, 20] on the analytic side that provide approximate information for some phases of the inspiral, but the full picture is unlikely to be completed without the use of accurate 3-D numerical simulation.

The question of evolution equations also demands attention. If one counts the number of equations or field components, at first sight it seems that there are ten components of the symmetric, 4×4 Einstein tensor to be solved, a number that fits perfectly the ten "independent" components of the metric tensor. The obvious solution, then, would be that one should do numerical simulations solving for all components of the Einstein equations. This approach, however, does not take into account the different quantities involved in the Einstein system. As it will be seen in subsequent sections, certain degrees of freedom in the space-time metric correspond to gauge choices (choice of coordinates) which have neither physical meaning nor associated evolution equations. The equations governing these gauge degrees of freedom are constraints, which if satisfied in some 3-D subspace of the space-time manifold, will be satisfied throughout the whole space-time, provided the rest of the Einstein equations are satisfied.

Thus the issue of coordinates and the related question of separating the Einstein equations into evolution equations and constraints are the first questions that will be addressed in the following sections.

2.2 Coordinates

In general relativity the arc-length between two points in space-time can be computed using the 4-metric. In the case of two infinitesimally close points

A and B the four-distance ds^2 can be computed using

$$ds^2 = g_{\mu\nu}dx^\mu dx^\nu \tag{2.1}$$

where $g_{\mu\nu}$ is the 4×4 symmetric metric tensor and $dx^\mu = x^\mu(A) - x^\mu(B)$. (Here and throughout this thesis Greek indices run from 0 to 3, while lowercase Latin indices correspond to spatial dimensions and they run from 1 to 3.) The distance between these two points is called *spacelike, null,* or *timelike* if ds^2 is positive, zero, or negative. This definition can be extended to coordinates as well: keeping three of the four coordinates fixed and varying one leads to a positive, zero or negative value of ds^2, defining spacelike, null, and timelike coordinates. Vectors fall in similar categories with respect to the sign of their length-square

$$v^\nu v_\nu = g_{\mu\nu}v^\nu v^\mu. \tag{2.2}$$

The lack of physical meaning associated to the coordinates implies that there are no restrictions in their choice – a freedom that can be helpful or, at times, confusing. The simplest form of the metric tensor $g_{\mu\nu}$ at a given point corresponds to a coordinate system where $g_{\mu\nu}$ is diagonal, but this cannot, in general, be done locally in the neighborhood of a point. In other words, at each point in space-time there is a Minkowski frame (in which space-time is described by the Minkowski metric) but, except for the trivial cases, there is no analogue of inertial coordinates in the neighborhood of the point. However, the number of positive and negative elements of the diagonalized metric is an invariant global property of the space-time manifold. This defines the *signature* of the metric which in our convention is $[-, +, +, +]$.

2.3 The Cauchy formulation

2.3.1 The "3+1" slicing of space-time

In the numerical simulation of a time-dependent system, one evolves some set of physical quantities as a function of time, i.e.

- provide some initial (Cauchy) data at $t = 0$

- use the evolution equations to determine the fields at any point of the evolution domain at a later time t.

One of the problems of setting up the equivalent problem for the Einstein equations is that the notion of *time* is coordinate-dependent and has no unique physical meaning. One chooses it in some suitable manner and then sets up the Cauchy problem. For this reason we do the following [21]:
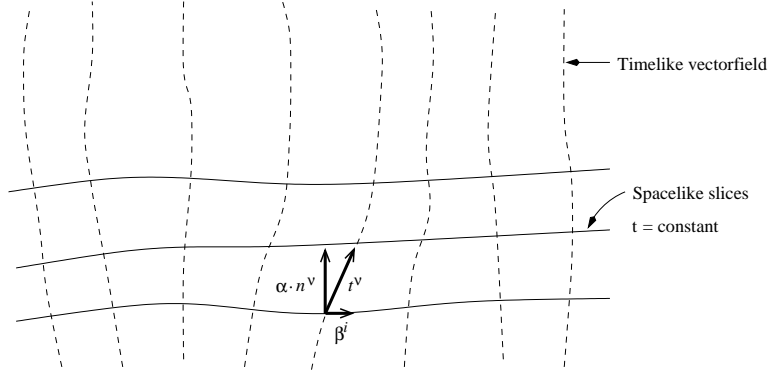
Fig. 2.1: Illustration of the "3+1" slicing.

- pick a function t and a vector field t^μ such that the surfaces, Σ_t, of constant t are spacelike Cauchy surfaces satisfying $t^\mu \nabla_\mu t = 1$;

- choose evolution equations based upon the choice of (t, Σ_t);

- provide initial data on Σ_0;

- compute the metric fields at later times $t > 0$ via the evolution equations.

Figure 2.1 illustrates the resulting "3+1" slicing approach.

In the coordinate system $\{x^\mu\}$, with $x^0 = t$, the Einstein and Ricci tensors $G_{\mu\nu}$ and $R_{\mu\nu}$ are given by

$$G_{\mu\nu} = R_{\mu\nu} - \frac{1}{2}g_{\mu\nu}R \tag{2.3}$$

$$R_{\mu\nu} = -\frac{1}{2}g^{\alpha\beta}\left\{-2\partial_\beta\partial_{(\nu}g_{\mu)\alpha} + \partial_\alpha\partial_\beta g_{\mu\nu} + \partial_\mu\partial_\nu g_{\alpha\beta}\right\}$$
$$+F_{\mu\nu}(g, \partial g), \tag{2.4}$$

where $F_{\mu\nu}(g, \partial g)$ is a non-linear term in the metric and its first derivatives. As it can be seen from Eqs. (2.3) - (2.4), the field equations involve up to second time derivatives of the metric. For this reason initial data consists of specifying the metric $g_{\mu\nu}$ and its time-derivative $\partial_t g_{\mu\nu}$ on Σ_0.

Let n^ν be the unit normal to the Σ_t surfaces. The equations

$$G_{\mu\nu}n^\nu = 0 \tag{2.5}$$

contain no second time derivatives of any of the metric components, i.e. they are fully specified by the initial data. These four equations (or any

combination of them) can be viewed as initial value constraints. As a consequence of the Bianchi identity

$$\nabla^\mu G_{\mu\nu} = 0, \tag{2.6}$$

if the constraints are initially satisfied and the spatial components of the Einstein tensor vanish everywhere, then the constraints are also globally satisfied.

Since four of the ten components of the metric tensor can be fixed by the choice of gauge, it is a perfect match that the six remaining components can be evolved by requiring that the six spatial components of the Einstein tensor (or some combination of those with the constraints) be satisfied.

As already stated on page 8, when trying to "evolve" a system of equations one might face problems of well-posedness. It is a classic result of Choquet-Bruhat [22] that the "3+1" splitting described above gives rise to a well-posed initial value problem in harmonic coordinates (i.e. in coordinates x^μ that satisfy the wave equation $\nabla_\nu \nabla^\nu x^\mu = 0$).

Given a $t = $ constant surface Σ_t, its normal vector n^a, and the 4-metric $g_{\mu\nu}$, the 3-metric $^{(3)}g_{\mu\nu}$ of the surface Σ_t is given by

$$^{(3)}g_{\mu\nu} = g_{\mu\nu} + n_\mu n_\nu. \tag{2.7}$$

The evolution proceeds in the t-direction, tangent to the "evolution" vector t^α satisfying $t^\alpha \partial_\alpha = \partial_t$.

The lapse α and the shift vector β^μ are defined by

$$t^\mu = \alpha\, n^\mu + \beta^\mu, \tag{2.8}$$

i.e. the lapse is equal to the projection of t^μ onto the unit normal n^μ to Σ_t, while the shift is the projection of t^μ onto the Cauchy surface Σ_t.

Next we must choose the evolution equations. Given the "3+1" slicing, one natural choice would be the spatial components of the Einstein tensor. However, as seen from numerical experiments presented in Chapter 8, these Einstein tensor components do not provide a set of evolution equations suitable for numerical evolution. A more suitable choice, referred to as "Standard ADM" system, comes from a Hamiltonian formulation of the theory [2].

2.3.2 The "Standard ADM" system

The ADM evolution equations are a first-order in time, second-order in space system, defined by

$$\partial_t\, ^{(3)}g_{ij} \quad - \quad \mathcal{L}_\beta\, ^{(3)}g_{ij} = -2\alpha\, ^{(3)}K_{ij}, \tag{2.9}$$

$$\partial_t \,^{(3)}K_{ij} \quad - \quad \mathcal{L}_\beta \,^{(3)}K_{ij} = -D_i D_j \alpha$$
$$+ \quad \alpha \left(\,^{(3)}R_{ij} + \,^{(3)}K \,^{(3)}K_{ij} - 2 \,^{(3)}K_i^l \,^{(3)}K_{lj} \right). \quad (2.10)$$

The symbol $\mathcal{L}_v$ stands for Lie-derivative along a vector field v^ρ. For a tensor field $T_{\mu\nu}$ it can be computed using

$$\mathcal{L}_v T_{\mu\nu} = v^\rho \partial_\rho T_{\mu\nu} + T_{\rho\nu} \partial_\mu v^\rho + T_{\mu\rho} \partial_\nu v^\rho. \quad (2.11)$$

The covariant derivative D is defined as the three-dimensional derivative operator with respect to $^{(3)}g_{ij}$.

Equation (2.9) defines the extrinsic curvature of the Cauchy slice Σ_t according to

$$^{(3)}K_{ij} = \frac{1}{2}\mathcal{L}_n \,^{(3)}g_{ij}. \quad (2.12)$$

The Hamiltonian and the momentum constraints are defined by

$$\mathcal{C} \quad = \quad ^{(3)}R - \,^{(3)}K_{ij} \,^{(3)}K^{ij} + \,^{(3)}K^2, \quad (2.13)$$
$$\mathcal{C}^i \quad = \quad D_j \left(\,^{(3)}K^{ij} - \,^{(3)}g^{ij} \,^{(3)}K \right). \quad (2.14)$$

Although the evolution equations (2.9) - (2.10) appear to be compact, their explicit forms are lengthy expressions. The number of variables (six metric components $^{(3)}g_{ij}$ and six extrinsic curvature components $^{(3)}K_{ij}$) is appealing for numerical simulations but the system cannot be put into a first-order symmetric-hyperbolic form. Thus its mathematical properties are difficult to understand. Chapter 8 contains a study of the linearized ADM system from a numerical point of view.

2.4 The characteristic formulation

The gauge freedom inherent in the "3+1" formalism can be extremely useful or, in some cases, confusing. The spacelike surfaces can be chosen to facilitate the description of general relativistic objects such as black holes, etc.

As an alternative, the *Characteristic Formulation* uses a foliation of space-time by null hypersurfaces which facilitates the description of waves. This section gives a brief description of the choice of the coordinates and the form of the metric. More detailed discussion can be found in [1, 23, 24] as well as in Chapter 3.

2.4.1   The null foliation of space-time

The construction proceeds as follows:

- Choose a spacelike, closed, convex 2-surface.

- Choose some angular coordinates, say (θ, ϕ), that uniquely describe the points of the 2-surface.

- Transport the 2-surface along a timelike vector field to obtain a 3-surface referred to as the *timelike world-tube* Γ.

- A "2+1" slicing of the world-tube (similar to the "3+1" method) provides a time-coordinate u on Γ.

  So far the parameters (u, θ, ϕ) describing the 3-surface Γ have been established.

- Unless caustics or other topological "defects" are present, the out-going null-rays emanating from the world-tube associates a unique point to any space-time point in the exterior. This provides a natural extension of the coordinates (u, θ, ϕ) to the exterior space-time.

- Finally, choose a radial coordinate by requiring that the metric of surfaces $u = $ constant, $r = $ constant have form $r^2 h_{AB} dx^A dx^B$, with $\det(h_{AB}) = \det(q_{AB})$ where q_{AB} is the unit-sphere metric.[2] The coordinate r is sometimes referred to as the surface-area coordinate.

Much of the gauge freedom of general relativity is fixed in the characteristic formulation by geometric choices. In fact the only gauge freedom present in this formulation is the choice and parameterization of the world-tube, i.e. the coordinates (u, θ, ϕ). The only drawback of the characteristic approach is that the formalism is difficult to adapt to the description of space-time regions with caustics.

Figure 2.2 illustrates the null foliation of space-time.

2.4.2   The metric and its interpretation

With coordinates described in Section 2.4.1 the space-time metric takes the Bondi-Sachs form [1, 23, 24]

---

[2] Here and in subsequent expressions of this work capital Latin letters $A, B, C, \ldots$ are used to indicate angular coordinates.

Timelike
worldtube

Null
hypersurface

r

r

r

r

(θ,ϕ)

$u = $ constant

(θ,ϕ)
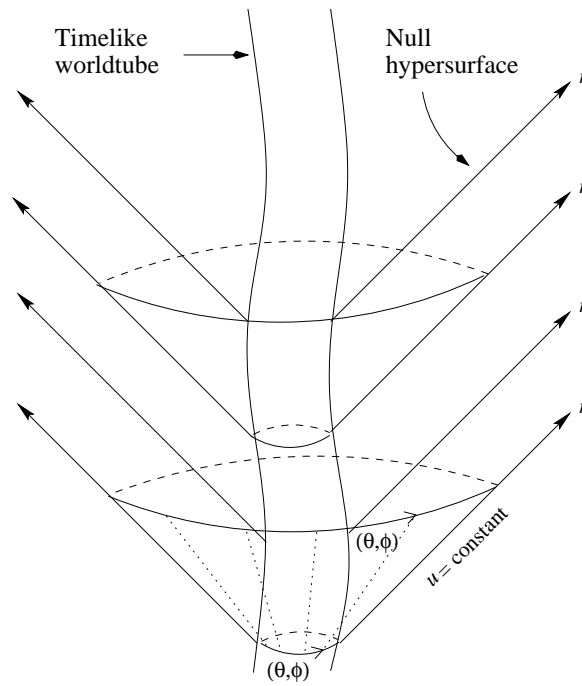
Fig. 2.2: Null Foliation of space-time.

$$ds^2 = -\left(e^{2\beta}V/r - r^2 h_{AB}U^A U^B\right)du^2 - 2e^{2\beta}du\,dr$$
$$-2r^2 h_{AB}U^B du dx^A + r^2 h_{AB}dx^A dx^B. \qquad (2.15)$$

Because the construction of the coordinates is based upon the lightcone structure of space-time, quantities built out of the metric components have geometrical meaning. Six real field variables appear in the metric: V, β, U^A and h_{AB}. The symmetric 2-tensor h_{AB} represents the conformal geometry of the surfaces defined by $dr = du = 0$. The requirement $\det(h_{AB}) = \det(q_{AB})$ reduces h_{AB} to the two radiative degrees of freedom. The scalar field β measures the *expansion* of the light rays as they propagate outward. The function V is the analog of the Newtonian potential, and its asymptotic expansion contains the mass aspect of the system.

Further understanding of the metric components (including the gauge functions U^A) stems from the intrinsic metric of the $r = $ constant surfaces,

$$\gamma_{ij}dx^i dx^j = -e^{2\beta}\frac{V}{r}du^2 + r^2 h_{AB}\left(dx^A - U^A du\right)\left(dx^B - U^B du\right). \quad (2.16)$$

The "2+1" decomposition of the world-tube is used to define the coordinates (u, θ, ϕ) and identifies $g_{AB} = r^2 h_{AB}$ as the metric of the 2-surfaces of constant u which foliate it. The square of the lapse is $e^{2\beta}V/r$ while the 2-dimensional shift vector on the world-tube is given by $(-U^A)$.

2.4.3   *Field equations*

The vacuum Einstein equations $G_{\mu\nu} = 0$ divide into three categories, as pointed out by Bondi [1]. The equations corresponding to the Ricci tensor components R_{rr}, R_{rA} and $h^{AB}R_{AB}$ contain no derivatives with respect to u. These equations involve the metric only within $u = $ constant hypersurfaces, which motivates calling them *hypersurface equations*. The equations $R_{AB} - h_{AB}h^{CD}R_{CD}/2$ contain first derivatives with respect to u as well as second radial and angular derivatives. Their solution at a space-time point involves use of the metric components in a 4-dimensional neighborhood of that point. They are called *evolution equations* and describe the propagation of gravitational radiation. They correspond to the general-relativistic version of the scalar wave equation in retarded spherical coordinates (u, r, θ, ϕ). The third category consists of *conservation equations* which contain no second radial-derivatives. These are the analogues, with respect to an r-foliation, of the traditional constraints in a Cauchy formalism (see page 12). Bondi used the Bianchi identities to show that one of them, the conservation condition $R_r^r = 0$ is automatically fulfilled by virtue of the other equations. He further showed that the remaining conservation

equations

$$R^r_u = 0, \quad R^r_A = 0 \tag{2.17}$$

are satisfied on a complete outgoing null cone if they hold on a single spherical cross-section. Explicit expressions for the hypersurface equations the evolution equation and the conservation laws can be found in [25].

Chapter 3 is dedicated to the description and applications of the Pitt Null Code, a numerical implementation of the characteristic formalism.

2.5   Alternative formulations

In recent years various systems of hyperbolic equations deduced form Einstein's equations have been proposed by Abrahams, Anderson, Choquet-Bruhat and York [26, 27], Bona and Masso [28], Choquet-Bruhat and Ruggeri [29], Friedrich [30], Frittelli and Reula [31], Iriondo, Lequizamon and Reula [32]. Mixed elliptic and hyperbolic systems have also been formulated by Christodoulou and Klainerman [33], Rendall [34], Choquet-Bruhat [35], Shibata and Nakamura [36]. For the Baumgarte-Shapiro system (derived from the ADM equations) see [37]. Other hyperbolic systems related to [37] have been discussed by Alcubierre, Brügmann, Miller and Suen [38], Frittelli and Reula [39], and Friedrich and Rendall [40]. Hübner has implemented numerical evolution based upon a hyperbolic formalism for global Cauchy evolution of compactified space-time [41, 42, 43, 44]. (Please note that the list is intended to be informative rather than exhaustive.)

While on a mathematical level the properties of first-order hyperbolic systems are much better understood than those of higher-order non-hyperbolic ones, there are considerably more variables and equations to be evolved. This issue might eventually be solved as available computational resources increase.

2.6   Cauchy-Characteristic Matching (CCM)

As portrayed in the previous sections, the Cauchy and the characteristic approaches have complementary strengths and weaknesses. Cauchy evolution has promising ability to evolve strong field regions of space-time but it is limited to a finite spatial region, which introduces an artificial outer boundary. Characteristic evolution, if used with a compactified radial coordinate, allows the incorporation of future null infinity within a finite computational grid. However, in turn, it suffers from complications due to gravitational fields causing focusing of the light rays. Unification of both methods seems to be a promising way of taking advantage of each formalisms' strengths. The methodology called Cauchy-Characteristic Matching (CCM) utilizes

Cauchy evolution within some prescribed timelike world-tube, but replaces the need for an outer boundary condition by matching to a characteristic evolution in the exterior of this world-tube. This provides a global solution and allows calculation of the gravitational wave-form reaching future null infinity [24, 45, 46, 47].

The methodology of CCM has been successful in numerical evolution of the spherically symmetric Klein-Gordon-Einstein field equations as well as for 3-D non-linear wave equations [48, 4].

A detailed description of the full 3-D CCM for the case of Einstein equations will be provided in chapters 4-7.

3. THE CHARACTERISTIC CODE

This chapter provides a description of a 3-D characteristic code known as the Pitt Null Code. The code was developed over a period of fifteen years by the Pitt numerical relativity group. The final version was completed by Luis Lehner, whose thesis [25] is used as primary reference throughout most of this chapter.

3.1 The physical algorithm

3.1.1 Coordinates

The choice of coordinates is based on the characteristic foliation of space-time as described in Section 2.4.1. Although some of the coordinate freedom is fixed by geometric considerations, the choice of the angular coordinates on the world-tube is arbitrary. Furthermore, radial compactification is employed to describe space-time out to future null infinity.

Angular coordinates

Since both the topology of the world-tube Γ and the topology of future null infinity $\mathcal{I}^+$ are S^2, it is natural to adopt a spherical coordinate system (θ, ϕ). However, this does not provide a smooth covering of the S^2. Our solution is to use two stereographic coordinate patches to cover the sphere, an approach that has been successful in several applications [4, 49]. This removes the singularity at the poles but, since the two patches overlap, there is a problem of consistency between the two patches.

Let θ and ϕ label the points on the sphere in the usual way. The two angular degrees of freedom are combined into a single complex stereographic coordinate $\zeta = q + Ip$, defined on the north patch by

$$\zeta_N = \tan\left(\frac{\theta}{2}\right) e^{I\phi}, \tag{3.1}$$

with $I = \sqrt{-1}$. The coordinate ζ_N provides a smooth description of the sphere everywhere except at the point $\theta = \pi$. Analogously $\zeta_S = 1/\zeta_N$

provides a smooth coordinatization except for the north pole. The patches described by ζ_N, ζ_S are sufficient to cover the sphere, with some overlap region.

Now let Ψ be a smooth scalar field on the sphere. The consistency condition that $\Psi(\zeta, \bar{\zeta})$ (and its derivatives) be equal on the two patches is

$$\Psi_N \left[\zeta_N, \bar{\zeta}_N \right] = \Psi_S \left[\zeta_S(\zeta_N, \bar{\zeta}_N), \bar{\zeta}_S(\zeta_N, \bar{\zeta}_N) \right], \tag{3.2}$$

in the overlap region.

Radial compactification

Asymptotically flat space-times can be given rigorous interpretation in the limit $r \to \infty$ along a null hypersurface (holding u constant) with the use of compactification techniques [50]. The surface area coordinate r is mapped into a finite range by the transformation [51]

$$x := \frac{r}{r+1}. \tag{3.3}$$

Space-time fields are globally defined in the interval $x_1 \leq x \leq 1$, where x_1 denotes the location of the inner radial grid-boundary. Future null infinity ($\mathcal{I}^+$) is described by $x = 1$.

3.1.2 Equations

The eth formalism

Spin-weighted fields

With the coordinates defined as described in Section 3.1.1, one could write out the Einstein equations in terms of partial derivatives of the metric functions. However, the equations can be written more conveniently using the (*eth*) $\eth$-formalism [52, 53, 54, 49].

In this formalism tensor fields on the sphere are replaced by spin-weighted fields. The result is a compact and efficient manner of treating tensors on a sphere as well as their derivatives.

The distance squared between two infinitesimally close points on a unit sphere can be written as

$$ds^2 = q_{AB} dx^A dx^B, \tag{3.4}$$

where the 2-metric q_{AB} is defined by the choice of angular coordinates:

$$q_{AB} = \mathrm{diag}\left(4/(1 + \zeta\bar{\zeta})^2, 4/(1 + \zeta\bar{\zeta})^2 \right). \tag{3.5}$$

One can rewrite q_{AB} in terms of a complex basis vector q_A (dyad) as

$$q_{AB} = (q_A\bar{q}_B + \bar{q}_A q_B)/2, \qquad (3.6)$$

where q^A satisfied $q^A q_A = 0$ and $q^A \bar{q}_A = 2$.[1] A possible choice of q^A (on the two patches) is given by

$$q_S^A = (1 + \zeta_S\bar{\zeta}_S) \cdot (\delta_2^A + I\delta_3^A), \qquad (3.7)$$
$$q_N^A = (1 + \zeta_N\bar{\zeta}_N) \cdot (\delta_2^A + I\delta_3^A). \qquad (3.8)$$

In the overlap between the patches the two dyads q_N^A and q_S^A are related by $q_N^A = e^{I\alpha}q_S^A$, where $e^{I\alpha} = -\bar{\zeta}_S/\zeta_S$.

Having introduced a complex basis one can represent any vector field on the sphere in the form $v = q^A v_A$. In the overlap region the vector transformation law between the two basis q_S^A and q_N^A translates into $v_N = e^{I\alpha}v_S$. Furthermore, any tensor field $v_{A_1...A_n}$ can be represented by 2^{n-1} different complex scalar fields of the form

$$v = t^{A_1}\ldots t^{A_n}\, v_{A_1}\ldots v_{A_n}, \qquad (3.9)$$

where t^A stands either for q^A or $\bar{q}^A$. Assuming that in Eq. (3.9) the dyad q^A occurs p times (and its complex conjugate, $\bar{q}^A$ occurs $n - p$ times), the transformation law of the complex scalar v between the two patches is given by $v_N = e^{Is\alpha}v_S$, where $s = 2p - n$. The spin-weight of the field v is given by the integer s.

Spin-weighted derivatives

The technique used to express tensor fields in terms of spin-weighted fields extends to covariant derivatives, since a covariant derivative of a tensor is another tensor. Given a spin s quantity F the *eth* operators $\eth$ and $\bar{\eth}$ are defined by [55]:

$$\eth F = q^A D_A F = q^A \partial_A F + \zeta\, s\, F, \qquad (3.10)$$
$$\bar{\eth} F = \bar{q}^A D_A F = \bar{q}^A \partial_A F - \bar{\zeta}\, s\, F. \qquad (3.11)$$

The spin of $\eth F$ is $s + 1$ while $\bar{\eth} F$ has spin $s - 1$.

Spin-weighted equations

In order to use the formalism described in the previous section we introduce the complex spin-weighted quantities $J = h_{AB}q^A q^B/2$, $K = h_{AB}q^A\bar{q}^B/2$

---

[1] Here we depart from other conventions [53] to avoid factors of $\sqrt{2}$.

and $U = U^A q_A$. In addition, we exchange the real variable V with the function $W = (V - r)/r^2$. The determinant condition $\det(h_{AB}) = \det(q_{AB})$ translates into $1 = K^2 - J\bar{J}$, which determines K in terms of J. The spin-weight of J is 2, and the function U has spin-weight 1, while K, W, and β have zero spin-weight. Complex conjugation of a spin-weighted quantity gives a spin-weight of equal magnitude and opposite sign. Thus, for example, the spin-weight of $\bar{U}$ is -1.

The vacuum Einstein equations $G_{\mu\nu} = 0$ can be decomposed into spin-weighted terms as well [56, 57, 55]. As described in Section 2.4.3, these divide into hypersurface equations, evolution equations and conservation equations.

Hypersurface equations

The Ricci tensor component $R_{rr} = 0$ implies

$$\beta_{,r} = N_\beta, \tag{3.12}$$

where N_β contains quadratically aspherical terms, i.e. terms that are quadratic in the deviation from spherical symmetry [46]. For reference we give the full non-linear hypersurface equation for β (see [55], Eq. (A1)):

$$\beta_{,r} = \frac{r}{8}\left(J_{,r}\bar{J}_{,r} - (K_{,r})^2 \right). \tag{3.13}$$

The equations $R_{rA} = 0$ imply

$$U_{,r} = r^{-2}e^{2\beta}Q + N_U, \tag{3.14}$$
$$(r^2 Q)_{,r} = -r^2(\bar{\eth}J + \eth K)_{,r} + 2r^4\eth(r^{-2}\beta)_{,r} + N_Q, \tag{3.15}$$

where Q is used as an intermediate variable to eliminate second radial derivatives of U and the quadratically aspherical terms are included in N_U and N_Q.

The equation for W is given by $R_{AB}h^{AB} = 0$, i.e.

$$W_{,r} = \frac{1}{2}e^{2\beta}\mathcal{R} - 1 - e^\beta\eth\bar{\eth}e^\beta + \frac{1}{4}r^{-2}(r^4(\eth\bar{U} + \bar{\eth}U))_{,r} + N_W, \tag{3.16}$$

where the quadratically aspherical terms are included in N_W. The quantity $\mathcal{R}$ is the curvature scalar of $u = \text{constant } r = \text{constant}$ surfaces and it is computed using

$$\mathcal{R} = 2K - \eth\bar{\eth}K + \frac{1}{2}(\bar{\eth}^2 J + \eth^2\bar{J}) + \frac{1}{4K}(\bar{\eth}\bar{J}\eth J - \bar{\eth}J\eth\bar{J}). \tag{3.17}$$

The hypersurface equations (3.12) - (3.16) contain angular and radial derivatives but no time derivatives of the metric functions. Given J on

a $u =$ constant hypersurface, these equations propagate β, U, Q and W along the radial direction, in terms of integration constants on an inner world-tube.

Evolution equations

The evolution equations $R_{AB} - h_{AB}h^{CD}R_{CD}/2$ together with the determinant condition $\det(h_{AB}) = \det(q_{AB})$ result in the equation for J

$$
\begin{aligned}
2(rJ)_{,ur} - \left(r^{-1}V(rJ)_{,r}\right)_{,r} &= -r^{-1}(r^2\eth U)_{,r} + 2r^{-1}e^\beta\eth^2 e^\beta \\
&\quad -(r^{-1}W)_{,r}J + N_J,
\end{aligned} \tag{3.18}
$$

where the quadratically aspherical terms are included in N_J.

Conservation equations

For a world-tube given by $r =$ constant the conservation equations take the form [55]

$$
\begin{aligned}
\beta_{,u} &= \mathcal{K}_\beta, & (3.19) \\
Q_{,u} &= -2\eth\beta_{,u} - q^A\mathcal{K}_A, & (3.20)
\end{aligned}
$$

where $\mathcal{K}_\beta, \mathcal{K}_A$ are purely null-hypersurface terms (composed out of β, U^A, V and h_{AB} and their r and x^A derivatives). They determine the evolution of the integration constants on the inner world-tube.

3.2 The construction of the code

The Pitt Null Code is a general relativistic code solving a discretized version of the Einstein equations in the context of a null foliation of space-time, as described in Section 2.4.1. In this section we outline the finite-difference implementation of the Pitt Null Code. For further details see [58, 25].

3.2.1 The structure of the numerical grid

The compactified radial coordinate x is discretized as $x_i = x_1 + (i-1)\Delta x$ where $i = 1\ldots N_x$ and $\Delta x = (1 - x_1)/(N_x - 1)$. The point $x_{N_x} = 1$ lies at null infinity. The point x_1 has to lie on or inside the world-tube,[2]

---

[2] Most of the time, when running the characteristic code by itself, the innermost radial gridpoint will lay on the world-tube. However, as it will be seen in Chapter 4, in the framework of Cauchy-Characteristic Matching, the world-tube may have a location that changes with respect to the characteristic grid structure during the code evolution, but it is always outside the innermost radial gridpoint. In this chapter we make the assumption that the innermost radial gridpoint is on the world-tube Γ, i.e. $x_1 = x_{|\Gamma}$.

i.e. $x_1 \leq x_{|\Gamma}$. The stereographic coordinate $\zeta = q + Ip$ is discretized by $q_j = -1 + (j - 3)\Delta$ and $p_k = -1 + (k - 3)\Delta$, where $j, k = 1 \ldots N_\zeta$ and $\Delta = 2/(N_\zeta - 5)$. The evolution proceeds with time-step Δu subject to the Courant-Friedrichs-Levy (CFL) condition which states that the numerical domain of dependence of the finite difference equations must contain the analytic domain of dependence of the original equations.

The fields J, β, Q, and W are represented by their values on this rectangular grid, e.g. $J^n_{ijk} = J(u_n, x_i, q_j, p_k)$. As first shown in [51], stability requirements suggest that the field U is represented by values at the midpoints $x_{i+\frac{1}{2}} = x_i + \Delta x/2$ on a radially staggered grid (so that $U^n_{ijk} = U(u_n, x_{i+\frac{1}{2}}, q_j, p_k)$). In addition the variables must be chosen such that they are regular functions of x throughout the whole numerical grid, including the outermost gridpoint. This requires [59] that $W(x)$ be replaced by $\tilde{W}(x) = r^{-2}W(x)$ in the numerical scheme.

3.2.2   Boundary values

The boundary data to be supplied on the timelike world-tube are the metric functions J, β, U, W. Furthermore, one needs to supply J on the first null hypersurface (initial data), which can be provided free of constraints in the null–timelike boundary problem. The world-tube data must satisfy conservation laws. Numerically one can either provide constrained boundary data or, to test the robustness of the numerical algorithm, one can put any data onto the world-tube and see whether the code handles the constraint-violating modes.

3.2.3   The eth module

Computing the action of $\eth$ and $\bar{\eth}$ on various fields involves angular derivatives. For the sake of clarity we illustrate how the module works for the case of computing $\eth U$, with U given on all angular gridpoints on both patches. First one computes the necessary partial derivatives using second-order centered finite difference expressions, e.g. $U_{,q} = \frac{U_{j+1} - U_{j-1}}{2\Delta} + O(\Delta^2)$. These are computed everywhere except at the edges of the angular grid. Then one constructs the quantity $\eth U$ up to $O(\Delta^2)$ accuracy throughout the angular grid except for the edges. The missing values at the grid boundaries are obtained from the values computed on the other patch, using the appropriate spin-weighted transformation rule combined with a 2-D quadratic polynomial interpolator. The width of the overlap region between the two angular grid patches is designed specifically so that this interpolation can be done properly.

3.2.4 Hypersurface equations

Having eliminated second radial derivatives with the use of the intermediate variable Q, the radial discretization of the hypersurface equations becomes straightforward. In the following we shall give explicit finite-difference expressions for the radial algorithm of the hypersurface equations in the quasispherical approximation [55, 25]. The additional terms that enter when solving for the full 3-D problem do not introduce any qualitatively new terms.

1. *Equation for β:* In the quasispherical approximation β remains independent of r. Thus, its value is completely defined by its boundary value:

$$\beta_i = \beta_{|\Gamma}. \tag{3.21}$$

2. *Equation for Q:* Re-expressing radial derivatives in terms of derivatives with respect to x, one obtains the rule for propagating Q

$$2Q + x(1-x)Q_{,x} = -x(1-x)(\bar{\eth}J + \eth K)_{,x} - 4\eth\beta, \tag{3.22}$$

where the quadratically aspherical terms are omitted. Replacing x-derivatives with their second-order finite-difference approximation and the value $Q_{i-1/2}$ by the average $(Q_i + Q_{i-1})/2$, one obtains an expression that involves values of Q, J, K and β at the points x_i and x_{i-1}:

$$
\begin{aligned}
Q_i \quad + \quad & Q_{i-1} + x_{i-\frac{1}{2}}\left(1 - x_{i-\frac{1}{2}}\right)\frac{Q_i - Q_{i-1}}{2\Delta x} = \\
& -x_{i-\frac{1}{2}}\left(1 - x_{i-\frac{1}{2}}\right)\left(\bar{\eth}\frac{J_i - J_{i-1}}{2\Delta x} + \eth\frac{K_i - K_{i-1}}{2\Delta x}\right) \\
& -2\eth\left(\beta_i + \beta_{i-1}\right) + O(\Delta^3),
\end{aligned}
\tag{3.23}
$$

which can easily be solved for Q_i. After a radial march that proceeds from Γ to $\mathcal{I}^+$, the global truncation error in Q is $O(\Delta^2)$.

3. *Equation for U:* In the quasispherical approximation, in terms of the variable x, the hypersurface equation for U is

$$U_{,x} = \frac{e^{2\beta}Q}{r_1 x^2}, \tag{3.24}$$

where r_1 is the location of the innermost radial gridpoint in terms of the coordinate r. The discretized rule for updating U is

$$U_i = U_{i-1} + \frac{e^{2\beta_i}Q_i}{r_1 x_i^2}\Delta x + O(\Delta^3) \tag{3.25}$$

for all points except the point $x_{\frac{3}{2}}$, lying just outside Γ. At that point U, is written as a Taylor expansion around the world-tube:

$$U_1 = U_{|\Gamma} + U_{,x|\Gamma}\left(x_{1+\frac{1}{2}} - x_{|\Gamma}\right) + O(\Delta^2). \qquad (3.26)$$

The algorithm provides values of U with $O(\Delta^2)$ global error.

4. *Equation for W:* In terms of $\tilde{W} = W/r^2$ and its x-derivatives, the equation for W within the quasispherical approximation reduces to

$$
\begin{aligned}
x^2\tilde{W}_{,x} + 2\frac{x}{1-x}\tilde{W} \;=\; & \frac{1}{2}e^{2\beta}\mathcal{R} - 1 - e^{\beta}\eth\bar{\eth}e^{\beta} \\
& + \frac{1}{4}x^2\left(\eth\bar{U} + \bar{\eth}U\right)_{,x} \\
& + \frac{x}{1-x}\left(\eth\bar{U} + \bar{\eth}U\right). \qquad (3.27)
\end{aligned}
$$

The corresponding finite-difference rule for propagating $\tilde{W}$ is

$$
\begin{aligned}
x_{i-\frac{1}{2}}^2\left(1 - x_{i-\frac{1}{2}}\right)\frac{\tilde{W}_i - \tilde{W}_{i-1}}{\Delta x} + x_{i-\frac{1}{2}}\left(\tilde{W}_i + \tilde{W}_{i-1}\right) = & \\
\frac{1}{2}\left(1 - x_{i-\frac{1}{2}}\right)\Big(\frac{1}{2}e^{2\beta_i}\mathcal{R}_i + \frac{1}{2}e^{2\beta_{i-1}}\mathcal{R}_{i-1} & \\
-2 - e^{\beta_i}\eth\bar{\eth}e^{\beta_i} - e^{\beta_{i-1}}\eth\bar{\eth}e^{\beta_{i-1}}\Big) & \\
+\frac{1}{4}x_{i-\frac{1}{2}}^2\left(1 - x_{i-\frac{1}{2}}\right)\left(\eth\frac{\bar{U}_i - \bar{U}_{i-2}}{2\Delta x} + \bar{\eth}\frac{U_i - U_{i-2}}{2\Delta x}\right) & \\
+x_{i-\frac{1}{2}}\left(\eth\bar{U}_{i-1} + \bar{\eth}U_{i-1}\right) + O(\Delta^3). & \qquad (3.28)
\end{aligned}
$$

In carrying out the radial march the error in $\tilde{W}$ is $O(\Delta^2)$ except for the outermost radial gridpoint where a numerical analysis implies that the error is $O(\Delta^2 \log \Delta)$.

3.2.5 Evolution equation

The numeric implementation of the evolution equation for J is based on an algorithm that has proved successful in the axisymmetric case [51, 60].

Let Ψ be a scalar field with a source on a flat background. In spherical, retarded-time coordinates, the scalar wave equation $\square\Psi = S$ can be written as

$$\square^{(2)}\psi = -\frac{L^2\psi}{r^2} + rS, \qquad (3.29)$$
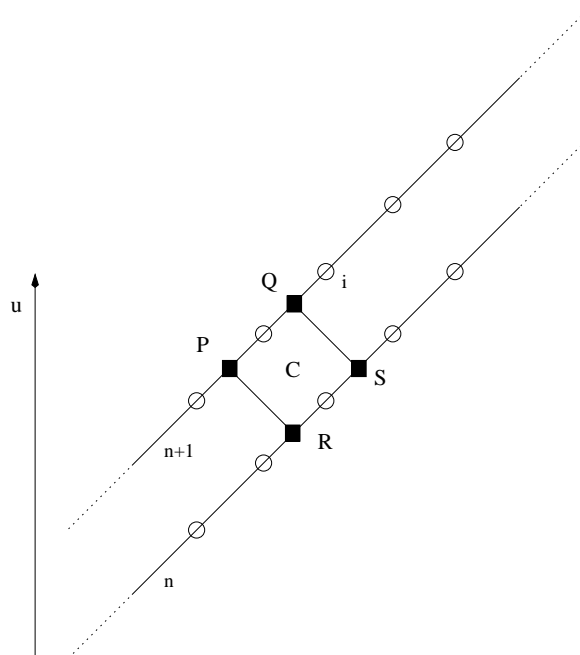
Fig. 3.1: The null parallelogram.

where $\psi = r\Psi$, L is the angular momentum operator and $\square^{(2)}$ is the (flat) 2-dimensional wave operator intrinsic to the (u, r) plane. The operator $\square^{(2)}$ can be written as

$$\square^{(2)}\psi = 2\psi_{,ur} - \psi_{,rr} = \psi_{,uv}, \tag{3.30}$$

where $v = u + 2r$.

Next a null parallelogram $\mathcal{A}$ is built out of a set of two outgoing null geodesic segments (PQ, RS), lying on two null cones that are Δu apart, and two incoming null geodesic segments (RP, SQ) that are Δr apart. Integration of Eq. (3.29) over $\mathcal{A}$ gives

$$\psi_Q = \psi_P + \psi_S - \psi_R + \frac{1}{2}\int_{\mathcal{A}} du\, dr \left[-\frac{L^2\psi}{r^2} + rS \right]. \tag{3.31}$$

To extend the null-parallelogram algorithm to the case of the gravitational evolution equation [58, 25] we first rewrite Eq. (3.18) in the form

$$e^{2\beta}\square^{(2)}(rJ) = \mathcal{H}, \tag{3.32}$$

where $\square^{(2)}$ is now the 2-D wave operator in the curved space-time

$$\square^{(2)}\psi = e^{-2\beta}\left[2\psi_{,ru} - \left(\frac{V}{r}\psi_{,r} \right)_{,r} \right], \tag{3.33}$$

and

$$\mathcal{H} = -r^{-1}\left(r^2\eth U \right)_{,r} + 2r^{-1}e^{\beta}\eth^2 e^{\beta} - \left(r^{-1}W \right)_{,r}J + N_J. \tag{3.34}$$

Integrating Eq. (3.32) over the null parallelogram $\mathcal{A}$ one obtains

$$(rJ)_Q = (rJ)_P + (rJ)_S - (rJ)_R + \frac{1}{2}\int_{\mathcal{A}} du\, dr\, \mathcal{H}. \tag{3.35}$$

Since the segments (RP, SQ) are ingoing null geodesics, their orientation with respect to the fixed numerical grid vary as the background metric changes. This means that one cannot construct the parallelogram $\mathcal{A}$ with corners lying on numerical gridpoints. Numerical analysis and experimentation show [61] that a stable algorithm results by placing this parallelogram so that the sides formed by the incoming rays intersect adjacent u-hypersurfaces at equal but opposite x-displacement from the neighboring gridpoints. The values of rJ at the vertices of the parallelogram are approximated to second-order accuracy by linear interpolation between nearest neighbor gridpoints on the same outgoing characteristic. The integrand

is approximated by its value at the center C of the parallelogram. The resulting equation is

$$(rJ)_Q = (rJ)_P + (rJ)_S - (rJ)_R + \frac{1}{2}\Delta u\,(r_Q - r_P + r_S - r_R)\,\mathcal{H}_C. \quad (3.36)$$

After the appropriate interpolations, the value of rJ at the i-th gridpoint is updated according to the finite-difference expression [25]

$$
\begin{aligned}
(rJ)_i^{n+1} &= \mathcal{F}\left[(rJ)_{i-1}^{n+1}, (rJ)_{i-2}^{n+1}, (rJ)_{i+1}^n, (rJ)_i^n, (rJ)_{i-1}^n\right] \\
&+ \frac{1}{2}\Delta u\,(r_Q - r_P + r_S - r_R)\,\mathcal{H}_C,
\end{aligned}
\quad (3.37)
$$

where the symbol $\mathcal{F}$ is a linear function in the (rJ)'s and J is given at all gridpoints at level u_n and at gridpoints $x_1 \ldots x_{i-1}$ at level u_{n+1}. In the quasispherical approximation the expression Eq. (3.37) provides an explicit algorithm for updating (rJ) via an outgoing radial march. However, with the quadratically aspherical terms included, the right-hand-side of Eq. (3.37) contains $J_{,u}$ which requires the unknown value J_i^{n+1} when computing $\mathcal{F}$ in the center of the computational cell. Thus an iterative approach is used [58]:

1. First the value J_i^n is copied into J_i^{n+1}. This provides an initial guess value in the point $(n+1, i)$ with an error of $O(\Delta)$.

2. Next the function $\mathcal{F}$ is computed at the center of the computational cell. As already stated, this requires use of J_i^{n+1}.

3. Using Eq. (3.37) a corrected value for J_i^{n+1} is computed.

4. Points (2) and (3) are repeated a sufficient number of times to ensure convergence.

On level u_n the finite-difference stencil contains the four points $x_{i-2} \ldots x_{i+1}$; on level u_{n+1}, the three points $x_{i-2} \ldots x_i$. The use of four points at level u_n introduces dissipation which cures non-linear instabilities that otherwise would occur. In order to obtain an accurate global discretization at infinity, the evolution variable $\Phi = xJ$ is used. For further details please refer to [58, 25].

3.2.6 Stability and accuracy tests

The code was tested for stability and accuracy. A harsh stability test was performed by providing random initial and boundary data of $O(\Delta^2 \cdot 10^{-6})$ and running it for 2000 "crossing times," where one crossing time is the

time it takes light to go across the world-tube in a flat background. The code showed no signs of instability [62].

To check the accuracy of the code runs were performed with larger and larger grid-sizes, using the same physical parameters. The numeric results were compared to the analytic solution. The following test-beds were used to check convergence:

- Quasispherical waves. A linearized solution of the quasispherical equations (involving a spherical harmonic with angular momentum $\ell = 6$) was run with a very small amplitude ($|J| = 10^{-9}$). The inner boundary was set to $r_1 = 1$ and the wave was evolved numerically between $u_i = 0$ and $u_f = 0.5$.

- Boost and rotation symmetric solutions. A family of non-linear solutions called SIMPLE, with exact boost and rotation symmetry [51] was also used. The field variables are

$$J = \frac{(1+\Sigma)^4 - 16}{8(1+\Sigma)^2}, \tag{3.38}$$

$$\beta = \log\frac{(1+\Sigma)}{2\sqrt{\Sigma}}, \tag{3.39}$$

$$U = -\frac{a^2\, r\, \Lambda}{\Sigma}, \tag{3.40}$$

$$\tilde{W} = \frac{1}{r}\left(-1 + \frac{1}{\Sigma}\right) + a\, r^2\, \frac{(2\, \Xi - 1)}{\Sigma}, \tag{3.41}$$

where

$$\Sigma = \sqrt{1 + a^2\, r^2\, \Xi}, \quad \Lambda = \frac{2\,\zeta\,(1 - \zeta\bar{\zeta})}{\left(1 + \zeta\bar{\zeta}\right)^2} \quad \text{and} \quad \Xi = \frac{4\zeta\bar{\zeta}}{\left(1 + \zeta\bar{\zeta}\right)^2}. \tag{3.42}$$

Because of its cylindrical symmetry this solution is not asymptotically flat, but it is used to construct an asymptotically flat solution by smoothly pasting it to asymptotically flat null data outside some radius R_0. The resulting solution provides a non-linear test inside the domain of dependence of the analytic (unmixed) solution.

- Schwarzschild in rotating coordinates. In a null frame that rotates with angular velocity ω according to $\phi \to \tilde{\phi} + \omega u$, the Schwarzschild metric can be written as

$$\begin{aligned}
ds^2 &= -\left(1 - \frac{2m}{r} - \omega^2 r^2 \sin^2\theta\right) du^2 - 2\, du\, dr \\
&\quad + 2\,\omega\, r^2 \sin^2\theta\, du\, d\phi + r^2 q_{AB}\, dx^A\, dx^B.
\end{aligned} \tag{3.43}$$

The test was performed with the choices $r_1 = 3m$, $\omega = 0.5$, $m = 1$. The metric fields were evolved numerically between $u_i = 0$ and $u_f = 0.5$.

These tests show that the code is second-order accurate. See [25] for details.

3.3 The news

As mentioned in Section 2.1, a prime motivation for numerical relativity is the prediction/interpretation of waveforms for laser interferometer detectors of gravitational radiation such as LIGO, VIRGO, etc. So far we have discussed the construction of a code that evolves the gravitational radiation to future null infinity $\mathcal{I}^+$ if appropriate boundary data is given on an inner timelike boundary Γ. One needs to connect quantities evolved by this code to data that the detectors will actually measure. In short, the effects of gravitational radiation on experimental apparatus can be understood as follows:

Consider linearized gravitational waves propagating through a flat, empty region of space-time. Let (t, x, y, z) be Cartesian coordinates, with metric $g_{\mu\nu} = \eta_{\mu\nu} + \varepsilon h_{\mu\nu}$. As a further restriction, require that $h_{\mu\nu}$ satisfy the "TT" (tracefree-transverse) gauge constraints, $h_{0\mu}^{TT} = 0$, $\delta^{jk}h_{ij,k}^{TT} = 0$, and $\delta^{ij}h_{ij}^{TT} = 0$. A gravitational plane-wave propagating in the z-direction is defined by the functions [63]

$$h_{xx}^{TT} - h_{yy}^{TT} = \Re\left(A_+ e^{-I\omega(t-z)}\right), \tag{3.44}$$

$$h_{xy}^{TT} = h_{yx}^{TT} = \Re\left(A_\times e^{-I\omega(t-z)}\right). \tag{3.45}$$

Consider a ring that, in absence of gravitational fields, is a perfect circle. Both polarization modes transform the ring into ellipses. The length of the axes of the ellipse oscillate according to the oscillating metric components (3.44), (3.45). The main axes will be along the Cartesian x- and y-directions for the "+" mode and at an angle of $\pi/4$ from the x- and y-axis for the "$\times$" mode. Figure 3.2 illustrates the effects of the two polarization modes.

Even though in a flat background gravitational radiation can be described analytically, one faces difficulties in a general relativistic context. In classical mechanics energy is defined as the quantity whose conservation is related to the homogeneity of time [64]. In electromagnetism, radiation is defined as a phenomena that carries energy-momentum. Since *time* in general relativity has no unique physical meaning, one faces difficulties when defining energy. The problem was solved by the definition of asymptotically flat space-times [50]. Space-times are referred to as asymptotically flat if an

The "+" polarization mode   The "x" polarization mode
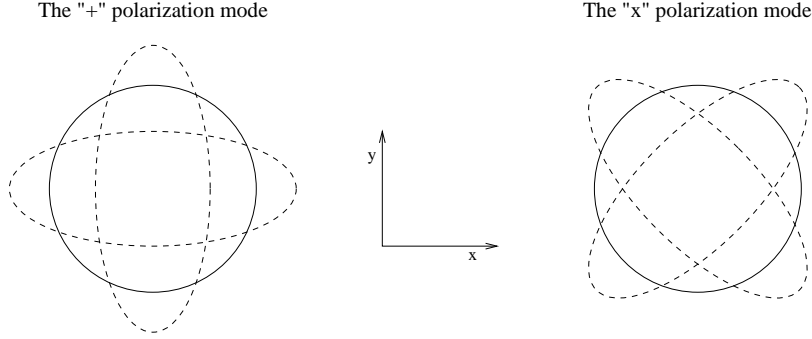
Fig. 3.2: The "+" and the "×" polarization modes of a gravitational plane-wave propagating in a flat background along the z axis.

appropriate boundary representing the "points at infinity" can be "added" to the space-time in a suitable way. At these "points" the induced metric is in fact flat and quantities like the energy carried away by gravitational radiation, and the notion of total energy, can be defined unambiguously.

The formalism of calculating the gravitational radiation and a description of the numerical module that does this is described in [65, 59, 66, 49, 55, 25]. An important module of the Pitt Null Code provides the waveforms detected by a gravitational radiation antenna.

In the case of gravitational radiation antenna such as LIGO or VIRGO the test object used to measure the effects of gravitational radiation is not a sphere but a set of mirrors and laser beams. Specifically, in the LIGO detectors, one uses a pair of 4 km long laser-beams that are at right angle. These beams define the x and y axes of the reference frame. Thus if a "+" mode is present, it causes a change in the relative lengths of the arms of the detector. Although this change is typically orders of magnitude below the size of the proton, a precise interferometer might be able to detect the effects of the radiation. Furthermore, using data from the two LIGO sites and from the other similar detectors from Europe, Japan and Australia, the background noise can be filtered out in a very effective way. Comparing the time-delay between the signals as detected at the various sites, one can also determine the position of the source of the gravitational radiation.

3.3.1   Sources of gravitational radiation

Although the universe contains a countless number of sources of gravitational radiation, most of them cannot be detected because of the weakness of the gravitational signal that reaches the Earth. However, dynamic astro-

physical systems such as coalescing compact binaries are good candidates for emitting gravitational waves which can be detected by an observer on earth. These systems consist of either two neutron stars, two black holes or one of each. Due to their small size (~ 20 km in case of a neutron star), they can orbit each other at close range and a high orbital frequency (up to ~ 500 Hz). In these coalescing binaries gravitational waves are emitted with a high efficiency. Thus, for instance, a double neutron star system which is 500 km apart radiates away most of its potential energy within minutes. The rate at which gravitational radiation is emitted increases as the co-orbiting objects approach each other. The typical waveform produced during this accelerated inspiral is a chirp signal [67] (see Figure 3.3). To first order the chirp signal can be described by the change of its frequency over time $\dot{f}$ and by its amplitude A:

$$\dot{f} \quad \propto \quad M_c^{5/3} f^{11/3} + \begin{pmatrix} \text{relativistic corrections} \\ M_1, M_2, S_1, S_2 \end{pmatrix} \tag{3.46}$$

$$A \quad \propto \quad k_{\text{orbit}} M_c^{5/3} \frac{f^{2/3}}{r} \tag{3.47}$$

with M_c the chirp mass

$$M_c = \frac{(M_1 \, M_2)^{3/5}}{(M_1 + M_2)^{1/5}}, \tag{3.48}$$

f the orbital frequency, M_1, M_2, S_1 and S_2 the mass and spin of the two compact objects, respectively, k_{orbit} a constant accounting for the inclination of the source orbital plane and r the distance of the detector to the source. The details of the exact waveform of the inspiral event provide further information about the system itself such as the eccentricity of the orbit, the spin and the mass of the objects (see, for example, [69]).

While the coalescence of two neutron stars can be described by analytic approximations, the case of two black holes poses a much more complex problem. The coalescence of the binary black-hole system is roughly divided into three phases [70]:

- During the first phase, the *inspiral*, the two black holes are well separated and the waveform of the emitted gravitational waveform can be determined via post-Newtonian approaches (see, e.g. [71, 72, 73, 74]). During this phase the gravitational radiation reaction time-scale is much longer than the orbital period. The inspiral ends when the binary orbit becomes relativistically dynamically unstable at an orbital separation of $r \sim 6M$, where M is the total mass of the binary. [75, 76]. The gravitational waves from the inspiral carry encoded
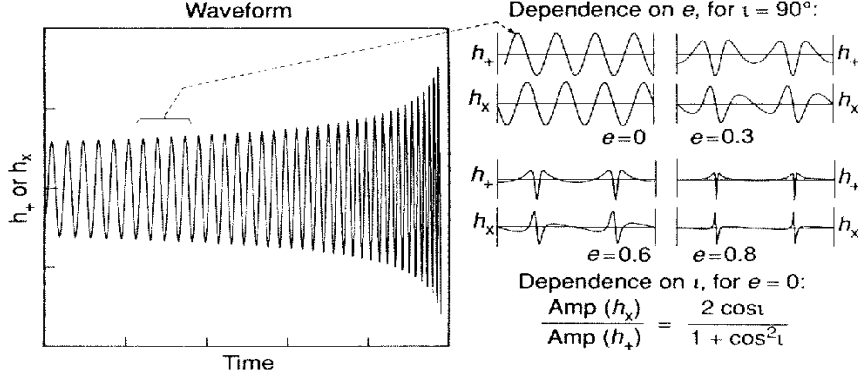
Fig. 3.3: Chirp waveform from an inspiral event of a compact binary system [68]. On the right the dependency of the waveform of the orbital eccentricity e and the orbital inclination ι is shown.

within them the masses and spins of the two black holes, some of the orbital elements of the binary, and the distance to the binary [77, 78].

- Towards the end of the inspiral, the black holes make a gradual transition from a radiation-reaction driven inspiral to a freely-falling plunge [75, 79, 80]. This phase is referred to as the *merger*. Gravitational waves emitted during this process are expected to be rich in information about the dynamics of relativistic gravity in a highly nonlinear, highly dynamic regime. This is the phase in which numerical relativity has an important role, since the highly non-linear character of the merger prohibits use of perturbative approaches.

- In the final state the system settles down to a stationary Kerr state. Thus the nonlinear dynamics of the merger gradually become more and more describable as oscillations of this final black hole's quasi-normal modes [81, 82]. The corresponding emitted gravitational waves consist of a superposition of exponentially damped sinusoids. This phase is often referred to as the *ring-down* phase. The waves from the ring-down carry information about the mass and spin of the final black hole [83, 84].

In order to obtain a rough estimate of the amplitude of the observed strain (relative length-change) $h = \Delta L/L$ caused by a gravitational wave from a typical astrophysical source one can use a dimensional argument

together with the approximation that gravitational radiation couples to the quadrupole moment only. Denoting the quadrupole of the mass distribution of a source by Q, we write [85]:

$$h \sim \frac{G\ddot{Q}}{c^4 r} \sim \frac{G(E_{\text{kin}}^{\text{non-symm.}}/c^2)}{c^2 r} \tag{3.49}$$

with G the gravitational constant and $E_{\text{kin}}^{\text{non-symm.}}$ the non symmetric part of the kinetic energy. Setting the non-symmetric energy equal to one solar mass

$$E_{\text{kin}}^{\text{non-symm.}}/c^2 \sim M_\odot,$$

and assuming that the source is located at inter-galactic or cosmological distances, one obtains a strain estimate of order

$$h \quad \lesssim \quad 10^{-21} \qquad \text{Virgo cluster,} \tag{3.50}$$
$$h \quad \lesssim \quad 10^{-23} \qquad \text{Hubble distance.} \tag{3.51}$$

For a detector with a baseline of 10^4 m the relativistic length changes become of order

$$\Delta L = hL \lesssim 10^{-19}\,\text{m} \quad \text{to} \quad 10^{-17}\,\text{m}. \tag{3.52}$$

This is a rather optimistic estimate. Most sources will radiate significantly less energy in gravitational waves.

Similarly, one can estimate the upper bound for the frequencies of gravitational waves [85]. A gravitational wave source cannot be much smaller than its Schwarzschild radius $2GM/c^2$, and cannot emit strongly at periods shorter than the light travel time $4\pi GM/c^3$ around its circumference. This yields a maximum frequency of

$$f \lesssim \frac{c^3}{4\pi GM} \simeq 10^4\,\text{Hz}\,\frac{M_\odot}{M}. \tag{3.53}$$

The rate at which black-hole coalescences occur is discussed, for instance, in [70]. For *solar mass* binaries with total masses in the range $10M_\odot \lesssim M \lesssim 50M_\odot$ the rate of coalescence in the Universe is expected to be about $1/100,000$ years in our Galaxy, or several per year within a distance of 200Mpc [86, 87, 88, 89, 90]. For *intermediate mass* black hole binaries, with total masses in the range $50M_\odot \lesssim M \lesssim$ (a few) $\times 10^3 M_\odot$, there is little observational evidence. Still, even if the coalescence rate of intermediate mass black-hole binaries is $\sim 10^{-4}$ that of neutron-star binaries (which is thought to be $\sim 10^{-5}\text{yr}^{-1}$ in our Galaxy), the black-hole sources would still be seen more often by LIGO than the neutron-star sources, and thus could be the first detected type of source. As regard as *supermassive*

black hole binaries, there is a variety of strong circumstantial evidence that supermassive black holes, in the mass range $10^6 - 10^9 M_\odot$ exist in quasars and active galactic nuclei. Also, $\sim 25\% - 50\%$ of nearby massive spiral and elliptical galaxies are expected to harbor quiescent supermassive black holes. A main scientific goal of space-based gravity wave detectors, such as LISA, is to detect various phenomena related to such black holes. These include capture of compact stars [91, 92, 78, 93, 94], the formation of super-massive black holes [91, 92], as well as the collision of these in the context of Galaxy mergers [95, 77, 91, 92, 78, 96, 97]. Such events would be detectable throughout the observable universe with large signal to noise ratios [92, 78]. The overall event rate for these phenomena is uncertain, but could be one or more events per year.

3.4 Black hole evolution

Consider a space-time containing a singularity. According to the cosmic censorship principle the singularity is hidden by an event horizon that causally disconnects the singularity from future null infinity $\mathcal{I}^+$. The region delimited by the event horizon is called a black hole. Inside the black-hole horizon the lightcones are tilted inwards so that no light ray can escape.

The issue of black hole evolution is one of the most demanding problems in numerical relativity. As it was first suggested in [98], in order to avoid the singularity, one can excise its neighborhood. Recently [5, 99] it was shown that the black-hole region can be evolved by a characteristic evolution based upon ingoing null cones. These null cones are truncated at an inner boundary (see Figure 3.4).

The construction of the ingoing null coordinate system is the analog of the outgoing case (see Section 2.4.1) except that after the construction and coordinatization of the timelike world-tube one uses ingoing null rays (instead of outgoing ones) to coordinatize the space-time region inside Γ. The space-time metric takes the ingoing Bondi-Sachs form

$$
\begin{aligned}
ds^2 &= \left(e^{2\beta}\frac{V}{r} + r^2 h_{AB} U^A U^B \right) dv^2 + 2e^{2\beta} dv\, dr \\
&\quad -2r^2 h_{AB} U^B dv\, dx^A + r^2 h_{AB} dx^A\, dx^B.
\end{aligned} \tag{3.54}
$$

The analytical and numerical toolkit used for the outgoing formulation can be refurbished for the incoming case via the substitution [5]

$$
\beta \to \beta + I\pi/2. \tag{3.55}
$$

The black hole is contained inside the timelike world-tube Γ. In order to perform black-hole simulations, in addition to initial and boundary data
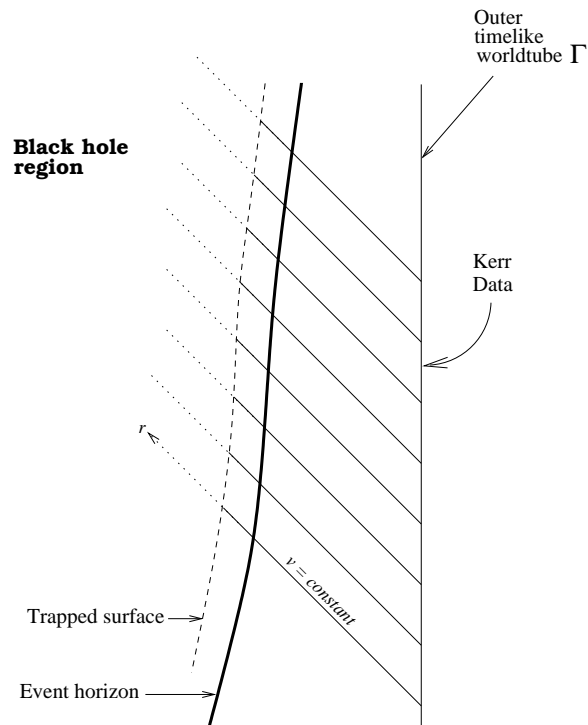
Fig. 3.4: The space-time region surrounding the black hole as described by an ingoing null foliation. The region close to the singularity is excised from the computational domain by means of locating a trapped surface, as described in Section 3.4.3.

one needs an excision algorithm that locates an inner boundary such that the code avoids the singularity.

3.4.1 Outer boundary data

As stated in Section 3.2.2, the characteristic code needs the values J, β, U, W (as well as $U_{,r}$) at the outer boundary Γ. In a number of cases the space-time metric is known in Cartesian coordinates but not in Bondi coordinates. A global coordinate transformation from Cartesian to Bondi coordinates requires knowledge of the light-cones emanating from Γ, for the given space-time. In most cases this is complicated. Here we use an alternative approach. With the Cartesian metric provided around the world-tube Γ, a numeric module – the extraction module (see Chapter 5, also [46, 47]) – is used to perform the coordinate transformation locally, computing the characteristic boundary quantities J, β, U and W around Γ.

The space-time metric of the Kerr (spinning) black hole in Cartesian Kerr Schild coordinates takes the form [100]

$$ds^2 = -dt^2 + dx^2 + dy^2 + dz^2 + 2Hk_\mu k_\nu dx^\mu dx^\nu, \qquad (3.56)$$

where k_μ is tangent to an ingoing congruence of twisting light rays and H is a potential given by

$$H = \frac{M_k r_k^3}{r_k^4 + a^2 z^2}, \qquad (3.57)$$

with

$$\frac{x^2 + y^2}{r_k^2 + a^2} + \frac{z^2}{r_k^2} = 1. \qquad (3.58)$$

The parameter a defines the angular momentum of the spinning black hole. The Schwarzschild metric can be obtained by setting $a = 0$.

Boundary data for a Kerr black-hole simulation is constructed by using the metric (3.56) as input for the extraction module and using the output as boundary data for the characteristic code.

Alternatively, for the case of the Schwarzschild metric, a gauge transformation $(t, x, y, z) \rightarrow (t', x', y', z')$ is first performed where the primed frame (t', x', y', z') wobbles, rotates, or is boosted with respect to the unprimed frame (t, x, y, z). Then the extraction module computes the coordinate transformation locally (around Γ) from the primed Cartesian coordinates to Bondi coordinates. It should be noted that the physics described by the primed Cartesian frame is the same as for the unprimed Cartesian frame. The gauge transformation amounts to making the world-tube wobble, rotate, or boost with respect to the singularity.

For the wobbling case the coordinates x'^{α} are defined by

$$t' = t, \ z' = z, \tag{3.59}$$
$$x' = (x+b)\cos\omega t - y\sin\omega t, \tag{3.60}$$
$$y' = (x+b)\sin\omega t + y\cos\omega t. \tag{3.61}$$

A very similar coordinate transformation gives the space-time metric of a black hole in rotating coordinates:

$$t' = t, \ z' = z, \tag{3.62}$$
$$x' = x\cos\omega(t+r_c) - y\sin\omega(t+r_c), \tag{3.63}$$
$$y' = x\sin\omega(t+r_c) + y\cos\omega(t+r_c), \tag{3.64}$$

with $r_c^2 = x^2 + y^2 + z^2$. In this case the null metric quantities are known analytically:

$$J = 0, \ \ \beta = 0, \tag{3.65}$$
$$U = I\omega\sin\theta\, e^{I\phi}, \tag{3.66}$$
$$V = -r + 2M_s. \tag{3.67}$$

The boosted frame is defined by

$$x' = x, \ y' = y, \tag{3.68}$$
$$z' = z\cosh\alpha - t\sinh\alpha, \tag{3.69}$$
$$t' = t\cosh\alpha - z\sinh\alpha. \tag{3.70}$$

When using the gauge conditions (3.68) - (3.70), the world-tube Γ is boosted with respect to the singularity. Thus one must stop the characteristic evolution before Γ reaches the horizon of the black-hole.

3.4.2   Initial data

In addition to boundary data on Γ, the characteristic evolution needs initial data, i.e. the constraint-free function J on the initial null-hypersurface.

Since the black hole is either rotating or moving with respect to Γ the initial null-hypersurface is not necessarily spherically symmetric and initial data cannot be given analytically. Let the incoming null vector n^a and the complex spacelike vector m^a span the tangent space to the null hypersurface (see Figure 3.5).

In constructing the initial data for a moving black-hole we require that the Weyl tensor component $C_{abcd}\, n^a n^c m^b m^d$ (corresponding to Ψ_4 in
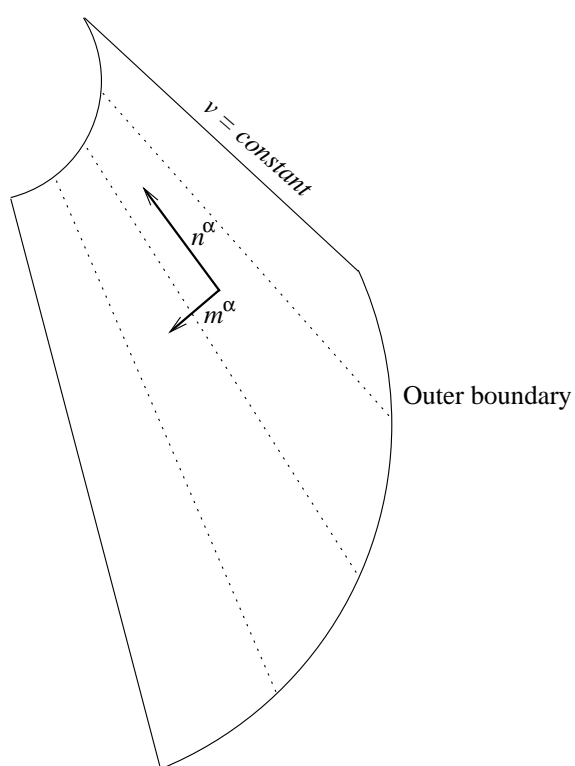
Fig. 3.5: Section of an ingoing null hypersurface.

Newman-Penrose terminology [101]) vanish on the initial (non-symmetric) null hypersurface [99]:

$$\left(r^2 J_{,r}\right)_{,r} - 2\beta_{,r}\left(r^2 J\right)_{,r} - \frac{r^2}{2}J\left(J_{,r}\bar{J}_{,r} - K_{,r}^2\right) = 0. \qquad (3.71)$$

In the linearized regime this corresponds to the condition that the outgoing radiation is set to zero. Combining this condition with the hypersurface equation (3.13) for β one obtains

$$r^2\left(r^2 J_{,r}\right)_{,r} - 2\beta_{,r}\left(r^4 J\right)_{,r} = 0, \qquad (3.72)$$

an equation that can be solved numerically in terms of boundary values for J and $J_{,r}$ on the world-tube.

We set $J = 0$ to prescribe initial data for a rotating black-hole space-time (see Eq. (3.62) - (3.64)) in which no gravitational radiation is present.

In the case of a Kerr (spinning) black hole, construction of characteristic data on the initial null-hypersurface is more complicated. One approach is to give Kerr boundary data on Γ and let the initial null hypersurface describe a space-time region containing a distorted Kerr black-hole with some radiation. The characteristic evolution causes some of this radiation to fall into the black hole and some to propagate outward. The radiation that hits Γ is reflected since the world-tube corresponds to a stationary Kerr space-time. Eventually all (initial) radiation falls into the black hole.

3.4.3 Singularity excision

Given the boundary data and initial data, the ingoing characteristic code still needs an inner boundary algorithm, when evolving black-hole space-times. This algorithm is necessary so that the evolution code does not reach the singularity.

Since singularities are causally disconnected from $\mathcal{I}^+$, one can cut out a space-time region inside the black-hole horizon without introducing unphysical effects on the phenomena outside the horizon. This is called singularity excision [98] – a technique that has become standard in black-hole simulations.

Normally for a convex, topologically S^2 surface the light rays emitted in the outward normal direction form a divergent beam. However gravitational lensing can refocus light rays so that in special circumstances (such as the neighborhood of singularities) the outgoing light cones from the surface converge. Such a surface is called trapped. In the limit in which the outgoing light cone neither expands nor converges we obtain a marginally trapped

surface (MTS). Under reasonable physical circumstances these trapped surfaces always lie inside black-hole event horizons. Thus (marginally) trapped surfaces are a guide for determining the region of space-time to be excised.

For a given slice $\mathcal{S}$ of an ingoing null hypersurface $\mathcal{N}_v$, defined by $r = R(v, x^A)$, the divergence Θ_l of the outgoing null normals is given by [5]

$$
\begin{aligned}
\frac{r^2 e^{2\beta}}{2}\Theta_l \;=\; & -V - \frac{1}{\sqrt{q}} \left[\sqrt{q} \left(e^{2\beta} h^{AB} R_{,B} - r^2 U^A \right) \right]_{,A} \\
& -r \left(r^{-1} e^{2\beta} h^{AB} \right)_{,r} R_{,A} R_{,B} + r^2 U^A_{,r} R_{,A}.
\end{aligned}
\tag{3.73}
$$

The slice is marginally trapped if $\Theta_l = 0$.

Solving for Eq. (3.73) is numerically difficult. Alternatively [25] one can identify the largest $r = $ constant slice of $\mathcal{N}_v$ that satisfies the algebraic inequality $Q \leq 0$ where

$$
Q = -V + \frac{r^2}{\sqrt{q}} \left(\sqrt{q} U^A \right)_{,A}.
\tag{3.74}
$$

This surface is either trapped or marginally trapped, and is called the Q-boundary. Solving Eq. (3.74) is computationally more efficient but the Q-boundary makes less efficient use of gridpoints then a MTS. Both approaches were implemented for the characteristic code. For details see [25].

3.4.4   Results

In all the above test cases the characteristic code proved able to stably and accurately evolve dynamic space-time regions containing a single black hole. The tests show not only that the evolution code can handle highly non-linear space-time dynamics, but they also indicate that the extraction module is able to provide the necessary boundary data in a time-dependent, non-linear regime. For further details see [102, 99].

3.5   The binary problem

Section 3.4 discusses simulation of single-black-hole space-times via characteristic evolution. However, the binary problem is still unsolved. The light-cone structure of the space-time region between two spinning, co-orbiting black holes is far from trivial. It is not possible to adapt the characteristic code to handle the caustics and crossovers that are formed during the coalescence. Still, one could use characteristic evolution matched to a Cauchy evolution such that the Cauchy code does not have to deal with excision. (See Figure 3.6.) The characteristic code can solve both the outer and the
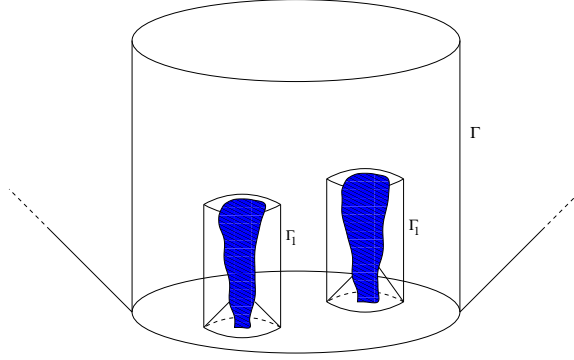
Fig. 3.6: A possible scenario for early stage binary evolution.

inner boundary problems. The missing element is a matching algorithm between the Cauchy and characteristic codes, as described in chapters 4-7.

There is another scenario in which characteristic evolution can be used. As first demonstrated for the axisymmetric case [103] and then for more generic cases [104], horizon structures for black-hole merger can be constructed as stand-alone items with almost no assumption about the surrounding space-time. The time-reversed picture gives a white-hole horizon that in the remote past is asymptotically in equilibrium as a Kerr white hole. An initial perturbation of the white-hole is amplified and causes a fission of the horizon, the time-reversed scenario of a black-hole collision. The binary horizon structure obtained by these analytic means is consistent with the numerical results in [13, 14, 15, 16, 17, 18, 105, 106]. The construction of such event horizons is outlined in the following section.

3.5.1 Construction and structure of binary event horizons

A black hole event horizon is a special null hypersurface with light rays emerging from an initial caustic-crossover region, where the horizon forms, and then expanding asymptotically to a constant surface area. The caustics that play a role in generic horizon formation correspond to elementary caustics studied in catastrophe optics. Caustics are 2-dimensional surfaces where focusing of light rays results in infinite intensity. In the case of event horizons the intensity is finite on the crossover set, where distinct light rays traced back on the horizon collide. Please refer to Figure 3.7 (left) for an illustration of a black hole event horizon.

In the case of an axisymmetric head-on collision of two black holes (see Figure 3.7, right), the event horizon has the shape of a trouser where
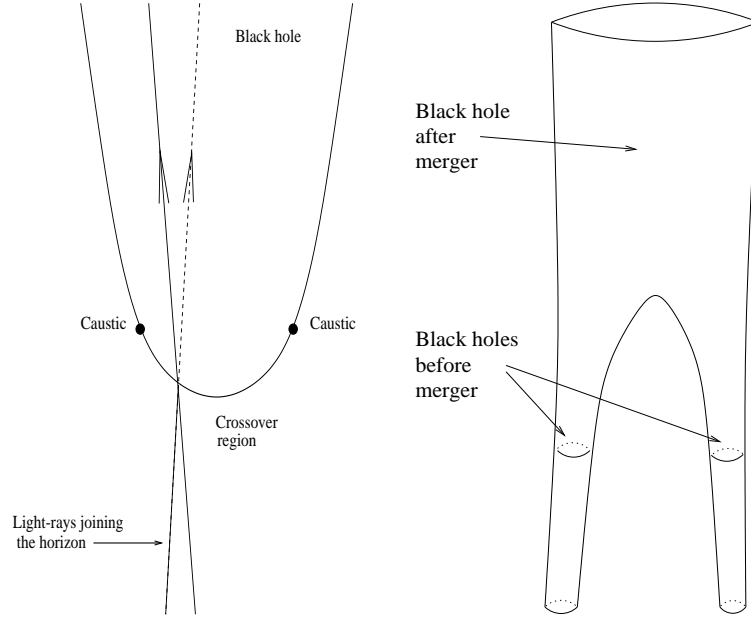
Fig. 3.7: On the left: a single black-hole event horizon. On the right: head-on collision of black holes.

the legs represent the holes before collision. In the vacuum case these extend forever into the past, although their cross-sectional area becomes vanishingly small [103, 107]. In a different scenario, gravitational collapse of a rotating cluster leads to formation of a torus-shaped horizon which eventually closes up forming an asymptotically spherical black-hole. The toroidal phase is also present in generic black hole mergers. A sequence of 3-D slices of a generic merger horizon can be seen on Figure 3.8.

In [103] such axisymmetric horizons are constructed as stand-alone objects, without prescribing the properties of the surrounding space-time. In a following paper [104] the methodology is extended to the case of more generic event horizons. In these papers the direction of time is reversed, thus providing geometries of white-hole horizons. As stand-alone objects, white-hole horizons correspond to black-hole horizons, the difference being the orientation of the time-coordinate axis. Black hole horizons have an ever increasing area while the surface area of white-hole horizons is continuously decreasing. The geometric optics construction outlined below is based on the caustics and the crossover sets that determine the formation of event horizons.
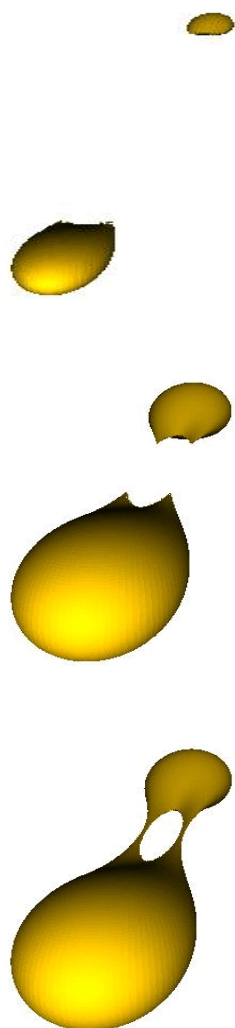
Fig. 3.8: Space-like, 2-D slices of a generic merger event horizon. The slice on the bottom shows a late, toroidal phase.
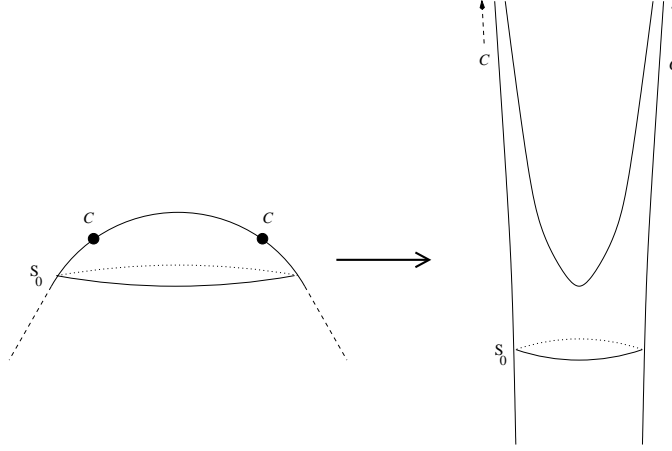
Fig. 3.9: The effect of re-mapping $u = u(\hat{u})$.

Let $\mathcal{S}_0$ be a smooth convex surface embedded in Minkowski space at constant time $\hat{t} = 0$. Let $\hat{\mathcal{H}}^-$ be the null surface described by a light beam that comes from past null infinity, crosses $\mathcal{S}_0$ perpendicularly, and pinches off to the future of $\mathcal{S}_0$. By convention $\hat{\mathcal{H}}^-$ ends at points where two light-rays cross each other. These endpoints consist of a set of caustic points $\mathcal{C}$, where neighboring rays focus, and a set of non-focal crossover points $\mathcal{X}$, where distinct null rays meet.

Let $\hat{\gamma}_{ab}$ be the degenerate metric of the 3-dimensional null surface $\hat{\mathcal{H}}^-$ coordinatized by $(\hat{u}, \theta, \phi)$. A conformal metric $\gamma_{ab} = \Omega^2 \hat{\gamma}_{ab}$ is constructed which describes the intrinsic geometry of a null hypersurface $\mathcal{H}^-$ with an affine parameter u along its null rays. The dependence $u = u(\hat{u})$ is defined by the requirement that the projection of the Einstein tensor onto $\mathcal{H}^-$ vanishes. (Here the projected Einstein tensor is computed viewing γ_{ab} as the metric of $\mathcal{H}^-$ in the frame (u, θ, ϕ). In addition the conformal factor Ω^2 is chosen such that the resulting conformal null hypersurface $\mathcal{H}^-$ is smooth and its radius R has a finite limit R_∞ as $u \to -\infty$. Once Ω is chosen the remaining gauge freedom in u can be fixed by setting $u = \hat{u} = u_0$ on $\mathcal{S}_0$. The interesting feature of this mechanism is that in this new parametrization of $\mathcal{H}$ the caustic points $\mathcal{C}$ will not be reached by any null rays before $u \to \infty$ while crossover points belonging to $\mathcal{X}$ at any finite distance from the caustic points will be reached by null rays at a finite u. As it can be seen on Figure 3.9, a trouser-shaped null hypersurface is generated that represents the event-horizon of a fissioning white hole. In the reversed time-direction, it is a horizon of two merging black holes.

3.5.2   Evolution of exterior geometry

A prime application of the conformal horizon model is the calculation of the radiation emitted by colliding black holes [107].

The time-reversal of the bifurcating white-hole horizon $\mathcal{H}^-$ is a horizon of colliding black holes, $\mathcal{H}$. This 3-dimensional null hypersurface serves as inner boundary for a characteristic evolution. The evolution is carried out along a family of ingoing null hypersurfaces J_v which intersect the horizon in topological spheres. The evolution is restricted to the period from merger to ring-down, or else the inner boundary would be intersected by ingoing null hypersurfaces in disjoint pieces. The evolution proceeds backward. The first ingoing null hypersurface J^+ intersects $\mathcal{H}^+$ in $\mathcal{S}_0$, as illustrated in Figure 3.10. Locating $\mathcal{S}_0$ at a late quasi-stationary time implies that the ingoing null hypersurface J^+ approximates $\mathcal{I}^+$. Thus the conformal model of the horizon of a black hole collision can be used as characteristic initial data to construct a vacuum space-time covering a very interesting nonlinear domain from merger to ring-down.
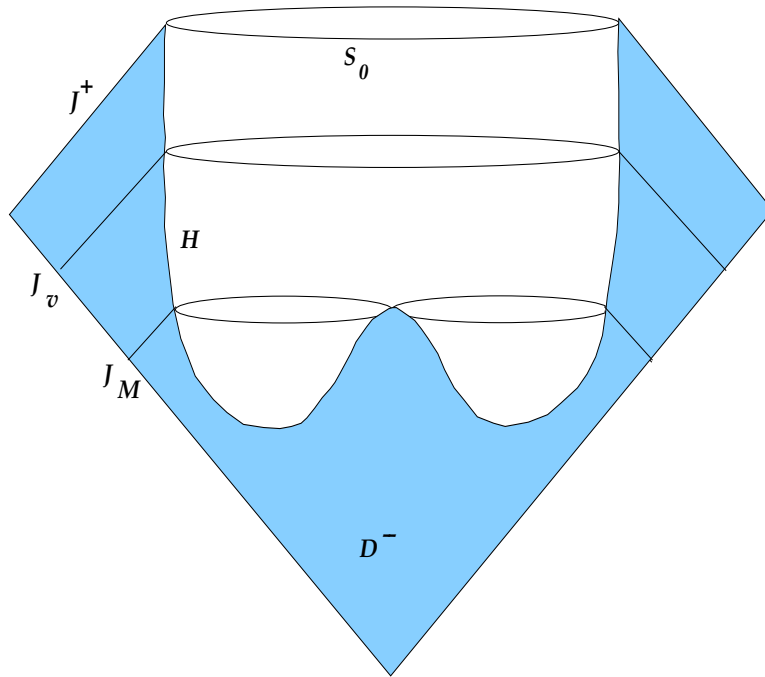
Fig. 3.10: Space-time evolution from merger to ring-down via a time-reversed characteristic evolution.

4. CAUCHY-CHARACTERISTIC MATCHING

The characteristic description of space-time has proven to be a very appropriate framework for evolving gravitational radiation from some timelike world-tube Γ to future null infinity $\mathcal{I}^+$. The drawback of the approach is in its inability to treat space-time regions where refocusing occurs for the null geodesics that define its coordinate system. By implication, the problem of two coalescing black holes will not be solved by solely characteristic evolution. In a Cauchy algorithm, coordinates are chosen arbitrarily so that caustics do not necessarily present a coordinate problem. However, a Cauchy algorithm based upon a spacelike foliation cannot be defined globally and requires an outer boundary where an artificial boundary condition can introduce spurious back radiation that contaminates the evolution.

The methodology of Cauchy-Characteristic Matching (CCM) adopted here is one that is very much proper to general relativity: that of describing space-time with multiple coordinate patches. CCM is designed to handle the interface between a Cauchy and a characteristic patch [108, 45] in a scenario where the black-hole dynamics is described in the interior of a timelike world-tube Γ by a Cauchy code while the radiation is carried from the world-tube Γ to future null infinity $\mathcal{I}^+$ by a characteristic code.

CCM has been successfully applied in a number of instances. The first of these was the problem of non-linear scalar waves propagating in a 3-D Euclidean space [4]. Performance for the matching algorithm was compared with local and nonlocal radiation boundary conditions proposed in the computational physics literature. For linear problems CCM outperformed all local boundary conditions and was about as accurate (for similar grid resolution) as the best nonlocal conditions. In terms of computational expense CCM has far outperformed the nonlocal approaches. The same holds true with regard to accuracy in the non-linear regime, where CCM turned out to be significantly more accurate than all other methods tested.

In another instance, a two-fold version of CCM has been used to evolve globally the spherical collapse of a self-gravitating scalar field onto a black hole [5]. The black hole (with excised singularity) and its surrounding region were described by an ingoing null foliation. This patch was matched to a Cauchy region, which in turn was matched to an exterior, outgoing

characteristic code carrying out the radiation to $\mathcal{I}^+$. Although it has spherical symmetry, the model has shown the fitness of the multi-patch approach (including CCM) to deal with singular space-times.

The Southampton group has worked out the formalism of CCM for the case of Einstein equations with axial symmetry [109, 110, 111, 112, 113]. However, a numerically stable implementation of the axisymmetric general relativistic CCM is yet to be borne out.

In the following sections the principles of CCM are described – first for a scalar field [4], then for the case of general relativity [47]. The two modules of the general relativistic CCM – extraction and injection – are described in further detail in the following chapters.

4.1   Cauchy-characteristic evolution in a flat background

Let Ψ be a smooth solution of the scalar wave equation. In Cartesian coordinates (t, x, y, z) it satisfies

$$\partial_{tt}\Psi = (\partial_{xx} + \partial_{yy} + \partial_{zz})\,\Psi. \tag{4.1}$$

In stereographic spherical coordinates (r, q, p) (see page 19) and a retarded time coordinate $u = t - r$ the field equation (4.1) takes the form

$$2\partial_{ur}\psi = \partial_{rr}\psi + \frac{P^2}{4r^2}\,(\partial_{qq} + \partial_{pp})\,\psi, \tag{4.2}$$

where $\psi = r\Psi$ and $P = 1 + q^2 + p^2$. In CCM, Eq. (4.1) is evolved up to some radius R_m using a Cauchy algorithm, while a characteristic algorithm integrates Eq. (4.2) for $r \geq R_m$. The matching procedures ensure that, in the continuum limit, Ψ and its derivatives are continuous across the spherical boundary $r = R_m$ so that spurious back reflection does not occur.

4.1.1   The spherically symmetric case

Analytic discussion

For the simple case of spherical symmetry the Cauchy version of the wave equation (4.1) reduces to

$$\partial_{tt}\psi = \partial_{rr}\psi, \tag{4.3}$$

while the characteristic version (4.2) becomes

$$2\partial_{ur}\psi = \partial_{rr}\psi. \tag{4.4}$$

The evolution algorithm proceeds schematically as follows (see Figure 4.1):
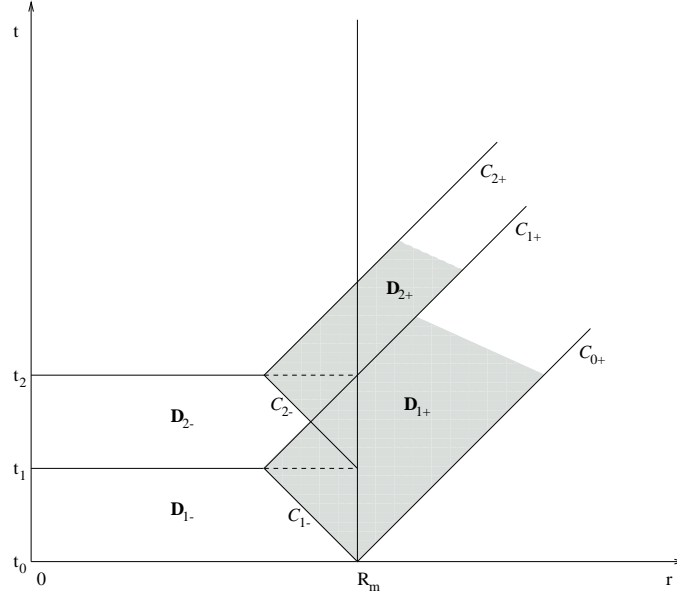
Fig. 4.1: The matching scheme for the spherically symmetric case. The symbols $\mathbf{D}_{1\pm}, \mathbf{D}_{2\pm}$ stand for domains of dependence while $C_{0+}, C_{1\pm}, C_{2\pm}$ stand for outgoing (ingoing) characteristics.

- At the setup of the evolution one needs to provide initial data in the domain $t = t_0, r \leq R_m$ and on the outgoing characteristic C_{0+}.

- Using the Cauchy initial data the evolution proceeds throughout the domain of dependence $\mathbf{D}_{1-}$, determining the data on the ingoing characteristic C_{1-}.

- Using the initial data C_{0+} and the boundary data C_{1-} the characteristic evolution determines data in the domain $\mathbf{D}_{1+}$. This allows completion of the Cauchy data at $t = t_1$ all the way out to $r = R_m$.

- These steps can now be iterated: Cauchy data is now available to evolve throughout the domain $\mathbf{D}_{2-}$ including C_{2-}, which determines the characteristic data to evolve through $\mathbf{D}_{2+}$, etc.

Finite differencing

In the discretized version of Cauchy-characteristic evolution the crisscross pattern of characteristics inside the radius R_m is at the scale of grid spacing.

The matching algorithm in this case is a cross-grid interpolation scheme which in the continuum limit makes the sphere R_m transparent to the wave propagation.

The Cauchy equation (4.3) is discretized using a standard second-order finite-difference scheme:

$$\frac{\psi_i^{n+1} - 2\psi_i^n + \psi_i^{n-1}}{(\Delta t)^2} = \frac{\psi_{i+1}^n - 2\psi_i^n + \psi_{i-1}^n}{(\Delta r)^2} + O(\Delta^2). \qquad (4.5)$$

The characteristic evolution uses the null parallelogram algorithm (see Section 3.2.5).

Figure 4.2 is a diagram illustrating the interpolation scheme. The radius R_m is defined by $R_m - R_B = \kappa \Delta r$, where κ is an arbitrary parameter. Although in the spherically symmetric case the introduction of κ is not crucial, it becomes important in higher dimensions. In 3-D the Cauchy domain is represented by a Cartesian grid and the characteristic domain is described by a spherical grid-structure. By implication the boundary gridpoints of the two evolution domains do not coincide. Thus it is important that the 1-D matching algorithm works for a range of κ that leaves room for applying a generalization of the same algorithm for 3-D non-aligned grid-boundaries. Given Ψ at all Cauchy points on level t_n except for the boundary point D and at all characteristic gridpoints up to level u_{n-1}, the field values Ψ_E and Ψ_F are obtained by radial interpolation along the null characteristics u_{n-1} and u_{n-2}. Next the characteristic and Cauchy boundary values Ψ_C and Ψ_D are computed by interpolation along the Cauchy surface t_n. With new boundary values provided, the evolution schemes can proceed to update points at the next levels t_{n+1} and u_n. Interpolators are quadratic such that the resulting error is $O(\Delta^4)$. This will assure second-order accuracy for the overall evolution scheme. The algorithm is numerically stable for a wide range of gap sizes $0 \leq \kappa \leq 2$.

4.1.2 The 3-D case

In a 3-dimensional application, the Cauchy field is represented on a Cartesian grid that consists of points equally spaced in all directions:

$$x_i = -a + (i-1)h, \;\; y_j = -a + (j-1)h, \;\; z_k = -a + (k-1)h, \qquad (4.6)$$

$(1 \leq i,j,k \leq 2M)$ where $h = 2a/(2M-1)$. The angular and radial dimensions in the characteristic grid are discretized in the same fashion as for the GR characteristic code (see Section 3.1.1). The inner boundary of the characteristic grid is a spherical shell of radius $R_m = a - h/2$, centered at the origin of Cartesian coordinates. Cartesian gridpoints are classified
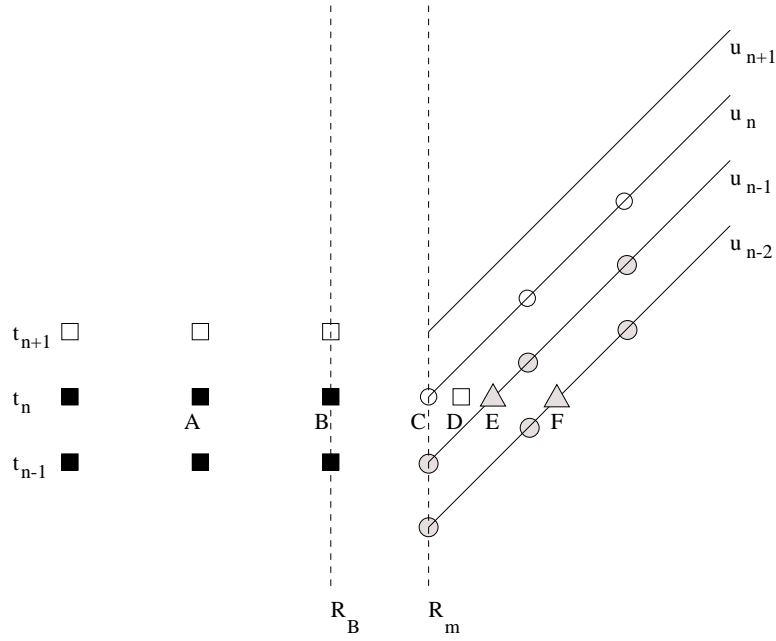
Fig. 4.2: The matching interpolation scheme for the spherically symmetric case. The points A, B, D are Cauchy gridpoints with D at the boundary. The point C is the boundary gridpoint of the outgoing characteristic u_n. Points E and F are at the intersection of the Cauchy time level t_n and the outgoing characteristics u_{n-1}, u_{n-2}.

according to their position with respect to the boundary sphere of radius R_m. Points inside the sphere are called *interior* or *evolution points*; nearest neighbors of evolution points which are on or outside the sphere R_m are called *boundary points*. The remaining gridpoints are not used.

The Cauchy evolution algorithm is the 3-D extension of Eq. (4.5). The characteristic algorithm is a 3-D null parallelogram algorithm.

As in the spherically symmetric case, the 3-D matching algorithm reduces to a cross-grid interpolation scheme. Generalizing Figure 4.2 into three dimensions, the points C, E, and F are spheres at level t_n, with radii $R_C = R_m, \quad R_E = R_m + K\Delta t, \quad R_F = R_m + 2K\Delta t$, while A, B and D stand for Cartesian grid-points. Field values on the outer two spheres E and F are obtained from interpolation along characteristic hypersurfaces. Next follows a 3-D routine that updates the Cartesian boundary points E and the sphere C using a quadratic interpolation scheme between the outer spheres E, F and the Cartesian points A, B. (This 3-D interpolation scheme is described in detail in Section 9.1.)

The parameter K must be chosen to assure that the field values at point D are provided by interpolation instead of extrapolation. In [4] the choice

$$K = [h/2\Delta t] + 1 \tag{4.7}$$

is used, where the brackets denote the integer part.

It should be noted that in [4] an external source-term and a non-linear self-coupling term was added to the right-hand-side of the scalar wave equation (4.1) and (4.2) without degrading the performance of CCM.

4.2   Cauchy-characteristic evolution in general relativity

Having described the architecture of CCM for the case of a scalar wave in a flat background, the following section examines the application to general relativity. The algebraic details of CCM are discussed in Chapters 5 and 6. Here it is presented from a more geometric point of view. Once CCM is understood on this geometric level, the details become more transparent.

The main concept of CCM for general relativity is the same as for other field equations: a timelike world-tube is used to match between a Cauchy and a characteristic region. The two evolution codes provide boundary data for each other, similar to the flat-background scalar wave case.

There are two major new features that appear only when evolving the Einstein equations (as opposed to evolving some scalar field). One is a non-trivial, dynamic coordinate transformation that has to be done numerically time-step after time-step. The other is the consistency between boundary
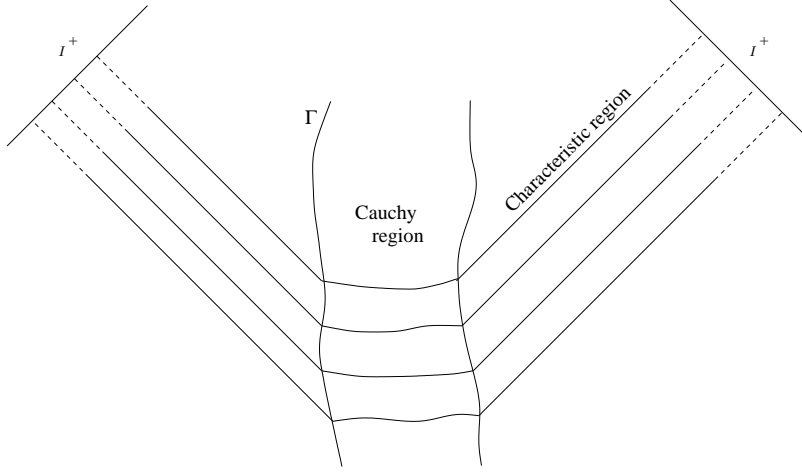
Fig. 4.3: A sketch of the matching scheme for the case of general relativity. The inside of the timelike world-tube Γ is evolved by a Cauchy code while its exterior is evolved by a characteristic code.

conditions and the coupled tensorial field equations. The first issue is discussed in the remainder of this chapter with further details in Chapters 5 and 6, while the second issue is addressed in Chapters 8 and 9.

CCM proceeds as follows: Let t^α be a timelike vector field. Using "3+1" slicing one can define the Cartesian coordinates (t, x, y, z) in a region of the space-time. Let Γ be a timelike world-tube defined by $(x^2+y^2+z^2)_{|\Gamma} = R_\Gamma^2$, with R_Γ^2 constant. The coordinates (x, y, z) induce a natural stereographic coordinate system (q, p) on Γ by the transformation

$$q(x^i) = \frac{x}{R_\Gamma \pm z}, \quad p(x^i) = \pm\frac{y}{R_\Gamma \pm z} \tag{4.8}$$

on the north $(+)$ and south $(-)$ patches. These coordinates are related to the complex stereographic coordinate ζ used in the characteristic code (see Chapter 3) by $\zeta = q + I \cdot p$. This completes the "2+1" description of the timelike world-tube Γ and the necessary ingredients to construct an outgoing characteristic coordinate system $y^\beta = (u, r, y^A)$.[1] The retarded time-coordinate u is fixed by $u_{|\Gamma} = t_{|\Gamma}$, while r stands for the Bondi surface-area coordinate (see Section 3.1.1). The coordinates y^β provide a description of the exterior of Γ, provided light rays leaving Γ in the outgoing normal direction do not refocus.

---

[1] Here and in further instances the notation y^A denotes angular coordinates: $y^2 = q, y^3 = p$.

The coordinatization of the Cauchy region inside Γ is largely arbitrary while the description of the outside characteristic region is uniquely determined by the choice of lapse and shift in the parametrization of Γ. This fundamental difference between the two coordinate systems explains why the issue of coordinate transformation at Γ is a nontrivial problem. If one recalls that the characteristic coordinates are radially aligned to null-geodesics and that the light-ray paths are defined by the (dynamic) space-time metric, one can easily see that the Jacobian determining the coordinate transformation involved in CCM is dynamic as well.

The CCM algorithm for general relativity consists of the following two parts:

- *Extraction.* Cauchy data is passed onto the characteristic evolution. This involves a coordinate transformation from Cartesian to Bondi coordinates.

- *Injection.* Characteristic data is passed onto the Cauchy evolution. This involves a coordinate transformation from Bondi to Cartesian coordinates.

4.2.1 Extraction

In extraction, the coordinate transformation must be carried out in a neighborhood of the world-tube, not just on it. This is because the surfaces Γ_t do not, in general, correspond to surfaces of constant Bondi r. Thus Γ typically intersects characteristic radial gridlines between gridpoints. Since the overall desired computational accuracy is $O(\Delta^2)$ and since the distance between Γ_t and nearest radial gridpoints is $O(\Delta)$, one needs to compute not only the null metric on Γ but its radial derivatives as well. The transformation between Cartesian and Bondi coordinates is done first by transforming from Cartesian to affine null coordinates, then from affine null to Bondi coordinates.

Among the building elements of the Jacobian between the Cauchy and affine null coordinates are the generators ℓ^α of the outgoing null geodesics that are normal to Γ_t. The vector ℓ^α can easily be computed at the world-tube using the Cartesian metric, lapse, and shift:

$$\ell^\alpha_{|\Gamma} = \left(\frac{n^\alpha + s^\alpha}{\alpha - {}^{(3)}g_{ij}\beta^i s^j} \right)_{|\Gamma}, \tag{4.9}$$

where s^α is a spatial unit vector that is normal to Γ_t in the outward direction, while n^α is a timelike vector field normal to the $t =$ constant Cauchy slice Σ_t. The denominator in Eq. (4.9) is determined by the normalization

condition $\ell^\alpha t_\alpha = -1$. In the flat space-time case, using Minkowski coordinates, the components of the null vector at the world-tube are $\ell^\alpha_{|\Gamma} = (1, \frac{x^i}{R_\Gamma})$.

The null geodesics leaving the world-tube along ℓ^α are described in the neighborhood of Γ, in Cartesian coordinates, by

$$x^\alpha = x^{(0)\alpha} + \ell^{(0)\alpha}\lambda + \ell^{(0)\alpha}_{,\lambda}\lambda^2 + O(\lambda^3), \tag{4.10}$$

where the notation $x^{(0)\alpha} \equiv x^\alpha_{|\Gamma}$, etc. is employed. The λ-derivative of the null vector ℓ^α is computed using the geodesic equation

$$\ell^\alpha_{,\lambda} + \Gamma^\alpha_{\mu\nu}\ell^\mu\ell^\nu = 0, \tag{4.11}$$

where

$$\Gamma^\alpha_{\mu\nu} = \frac{1}{2}\, g^{\alpha\beta}\left[\, g_{\mu\beta,\nu} +\, g_{\nu\beta,\mu} -\, g_{\nu\mu,\beta}\,\right]. \tag{4.12}$$

The metric in affine null coordinates $\tilde{y}^{\tilde{\alpha}} = (u, \lambda, y^A)$ is computed using

$$\tilde{\eta}_{\tilde{\alpha}\tilde{\beta}} = \frac{\partial x^\mu}{\partial \tilde{y}^{\tilde{\alpha}}}\frac{\partial x^\nu}{\partial \tilde{y}^{\tilde{\beta}}}\, g_{\mu\nu}. \tag{4.13}$$

Given the coordinate transformation $x^\mu = x^\mu(\tilde{y}^{\tilde{\alpha}})$ up to $O(\lambda^3)$, the Jacobian (which includes λ-derivatives of x^α) is known around the world-tube up to $O(\lambda^2)$.

The second transformation from affine coordinates (u, λ, q, p) to Bondi coordinates $y^\alpha = (u, r, q, p)$ can be understood as follows:

The area dA of a 2-D surface-element $dq \cdot dp$ is determined by the the square root of the determinant of the angular metric $\tilde{\eta}_{\tilde{A}\tilde{B}}$. This quantity clearly depends on the radial coordinate. (E.g. in the case of flat space-time and the usual (r, θ, ϕ) coordinates the angular metric is diag($r^2, r^2 \sin^2 \theta$)). Let dA_1 stand for the area $dq \cdot dp$ on the unit sphere. The Bondi surface area coordinate r is defined as the square root of the ratio dA/dA_1, i.e.:

$$r = \left(\frac{\det(\tilde{\eta}_{\tilde{A}\tilde{B}})}{\det(q_{AB})}\right)^{\frac{1}{4}} = \frac{P}{2}\left(\det(\tilde{\eta}_{\tilde{A}\tilde{B}})\right)^{\frac{1}{4}}. \tag{4.14}$$

where we have used Eq. (3.5). The derivative of the surface-area coordinate with respect to the affine parameter along a null geodesic labeled by some (q, p) is related to the expansion of the light-rays, i.e.

$$r_{,\lambda} = e^{-2\beta}. \tag{4.15}$$

Equation (4.14) provides r around the world-tube up to $O(\lambda^2)$ – the same order to which the metric elements $\tilde{\eta}_{\tilde{\alpha}\tilde{\beta}}$ are computed. Computing

the Bondi metric $\eta_{\alpha\beta}$ involves terms with $r_{,\lambda}$. For this reason, without additional information, the radial derivative of the Bondi metric cannot be computed on Γ. The missing information $r_{,\lambda\lambda}$ is obtained using the β-hypersurface equation (3.13) and the relation

$$\beta_{,\lambda} = -\frac{\eta_{,\lambda}^{ru}}{2\eta^{ru}} = -\frac{r_{,\lambda\lambda}}{2r_{,\lambda}}. \qquad (4.16)$$

For further details see Chapter 5.

As a last step, given the Bondi metric $\eta_{\alpha\beta}$ in the neighborhood of Γ up to $O(\lambda^2)$ one needs to read off the Bondi functions J, β, U, W at the world-tube, along with their radial derivatives. This can be done immediately given the definition of these functions ($U \equiv q_A U^A, J \equiv q^A q^B h_{AB}, W \equiv (V - r)/r^2$), and the form of the contravariant Bondi metric:

$$\eta^{\alpha\beta} = \begin{bmatrix} 0 & -e^{-2\beta} & 0 & 0 \\ -e^{-2\beta} & e^{-2\beta}\dfrac{V}{r} & -e^{-2\beta}U^2 & -e^{-2\beta}U^3 \\ 0 & -e^{-2\beta}U^2 & r^{-2}h^{22} & r^{-2}h^{23} \\ 0 & -e^{-2\beta}U^3 & r^{-2}h^{32} & r^{-2}h^{33} \end{bmatrix}. \qquad (4.17)$$

4.2.2 Injection

With extraction providing the coordinate transformation in a neighborhood of Γ, injection does not involve much additional algebra. When reversing the coordinate transformation (i.e. from Bondi coordinates $y^\beta = (u, r, q, p)$ to Cartesian coordinates $x^\alpha = (t, x, y, z)$) one can invert the Jacobian and obtain the necessary information. An even simpler approach is to compute the contravariant Cartesian metric g^{ij}, which involves the same Jacobian matrix as needed for computing the covariant Bondi metric (see [21]). The reverse coordinate transformation is performed on a set $\mathcal{S}_{Null}$ of null grid-points in the neighborhood of the world-tube Γ. The position of these points is fixed in Bondi coordinates. However, due to the dynamic nature of the coordinate transformation, the same set of points has a time-dependent location in the Cartesian frame. Thus, in addition to computing the Cartesian metric components on $\mathcal{S}_{Null}$, these gridpoints are labeled by values $x^\alpha = f(y^\beta)$ computed as a Taylor expansion around Γ.

The next problem is purely numeric: we need to transfer data from $\mathcal{S}_{Null}$ to the set of boundary points of the Cartesian grid, $\mathcal{S}_{Cauchy}$. Similar to the case of scalar matching, this is done in two steps: first interpolate metric information onto a spherical grid contained in Σ_t that surrounds the

set of Cartesian points $\mathcal{S}_{Cauchy}$, then use a 3-D interpolation algorithm to transfer the boundary information from this spherical grid onto the Cartesian boundary points.

Let Λ be a Cartesian spherical world-tube with (constant) radius $R_\Lambda = R_\Gamma + O(\Delta x)$, concentric with Γ. Let Λ_t be the intersection of Λ with the Cauchy slice Σ_t. The injection world-tube Λ must be chosen such that the sphere Λ_t surrounds $\mathcal{S}_{Cauchy}$ at all t.

Information needs to be transferred from $\mathcal{S}_{null}$ to Λ_t, then from Λ_t to $\mathcal{S}_{Cauchy}$. The elements of $\mathcal{S}_{null}$ are labeled by their Bondi (u, r, y^A) and Cartesian (t, x, y, z) coordinates. They form a subset of a regular Bondi grid. In terms of their Cartesian coordinates, however, they form an irregular 4-D grid which changes from time-step to time-step.

In order to get data onto the sphere Λ_t, first data is interpolated onto the world-tube Λ from neighboring null gridpoints. Then a time-interpolation is performed to determine Cauchy boundary data on Λ_t. Finally, a 3-D interpolation is performed within the Cauchy slice Σ_t in order to obtain the Cauchy metric at the boundary-points $\mathcal{S}_{Cauchy}$ of the Cartesian grid. The interpolation algorithm and the algebra employed in the injection are described in detail in Chapter 6. An illustration of the interpolation schemes involved in the injection can be seen in Figure 4.4.
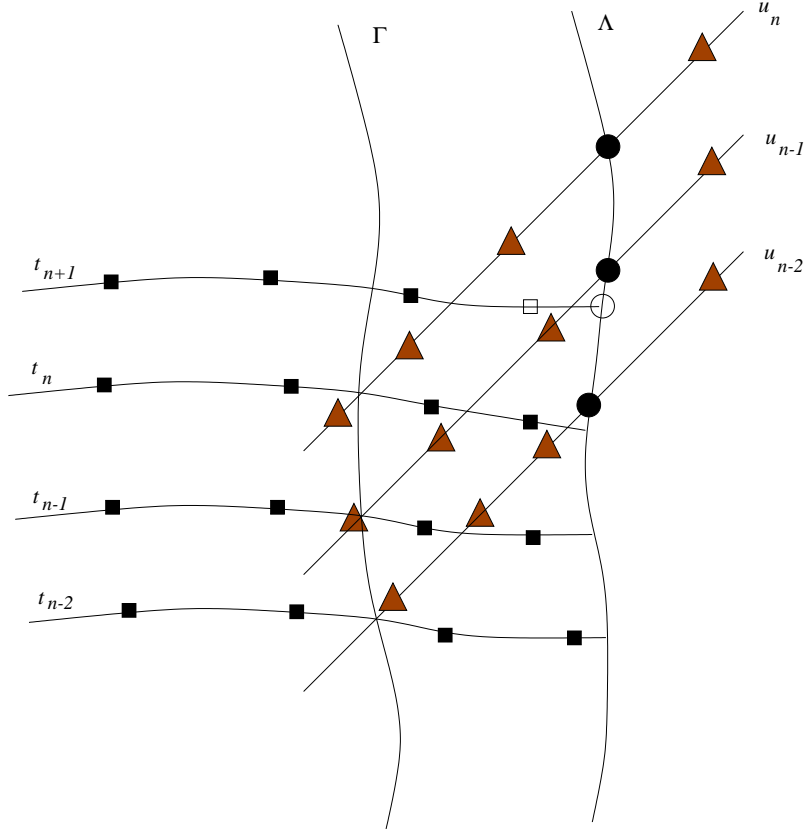
Fig. 4.4: A sketch of the interpolation scheme for the the injection. Cauchy evolution and boundary points are represented by filled and empty squares. Null gridpoints are represented by triangles. The filled circles stand for points on Λ where the Cartesian metric has been computed from null data at neighboring gridpoints. The empty circle indicates the sphere Λ_t where one needs to obtain Cauchy boundary data by time interpolation.

5. THE EXTRACTION MODULE

This chapter describes the extraction module, a numerical algorithm designed to extract characteristic boundary data from a Cauchy evolution domain.

The first step in the extraction module is getting data from the Cauchy grid onto the world-tube Γ by means of an interpolation algorithm. Then a lengthy algebraic calculation is performed to determine the Bondi variables J, β, U, W and their radial derivatives on Γ. During extraction, the world-tube Γ is located in Bondi coordinates and then the set of characteristic boundary gridpoints is defined. Finally, the functions J, β, U and W are placed onto these boundary points. (The characteristic evolution proceeds from these points to future null infinity $\mathcal{I}^+$.) A detailed description of these steps is given in the following sections. The latter part of the chapter is devoted to calibration tests and their results.

5.1 Interpolation schemes

There are several ways to transfer data from a Cartesian grid to a spherical grid. Issues that need to be considered include desired accuracy, numerical stability and computational efficiency. In addition, filtering techniques might be useful for producing smooth output.

5.1.1 Cubic, 3-D interpolator

A straightforward approach to the problem is a 3-D cubic interpolator. Given a smooth function $F(x, y, z)$ that is known on a 3-D grid $F_{[I,J,K]} = F(x_{[I]}, y_{[J]}, z_{[K]})$, the algorithm for computing F and its Cartesian derivatives $\partial F/\partial x^i$ on a stereographic gridpoint $M(q, p)$ is the following:

- First locate the Cartesian cell containing M, i.e. find (I_0, J_0, K_0) such that

$$x_{[I_0]} \leq x_M < x_{[I_0+1]}, \quad y_{[J_0]} \leq y_M < y_{[J_0+1]}, \quad z_{[K_0]} \leq z_M < z_{[K_0+1]}. \tag{5.1}$$

The numerical stencil used for the interpolation is a set of 64 Cartesian gridpoints $(x^i)_{[I,J,K]}$, $I_0 - 1 \leq I \leq I_0 + 2$, $\quad J_0 - 1 \leq J \leq J_0 + 2$, $K_0 - 1 \leq K \leq K_0 + 2$, that form the cell (I_0, J_0, K_0) and its 26 neighboring cells.

- Next, using the grid values $F_{[I,J,K]}$ at the gridpoints of the interpolation stencil, construct a polynomial

$$\mathcal{P}_F(x, y, z) = \sum_{i,j,k=0}^{3} c_{i,j,k}(x - x_{[I_0]})^i (y - y_{[J_0]})^j (z - z_{[K_0]})^k \quad (5.2)$$

with the coefficients $c_{i,j,k}$ determined by $\mathcal{P}_F(x_{[I]}, y_{[J]}, z_{[K]}) = F_{[I,J,K]}$ at the 64 gridpoints.

- Last, the function F and its derivatives are constructed at the stereographic gridpoint M from the interpolation polynomial according to

$$F(x_M, y_M, z_M) = \mathcal{P}_F(x_M, y_M, z_M) + O(\Delta^4), \quad (5.3)$$

$$\frac{\partial}{\partial x^i} F(x_M, y_M, z_M) = \frac{\partial}{\partial x^i} \mathcal{P}_F(x_M, y_M, z_M) + O(\Delta^3). \quad (5.4)$$

A 2-D version of the cubic interpolation scheme can be seen in Figure 5.1.

The approach is straightforward to implement, easy to test, and has a well defined accuracy. However, its extended interpolation stencil could potentially lead to instability of the matching algorithm. The interpolation stencil gridpoints must be inside the injection world-tube Λ. These gridpoints are at most $2\sqrt{3}\Delta x$ away from Γ. Thus, in order to be able to use the cubic polynomial interpolator described above, the injection world-tube must have a radius $R_\Lambda \approx R_\Gamma + 2\sqrt{3}\Delta x$ or larger. Since the injection strategy is based on a Taylor expansion around the extraction world-tube Γ, this can effect the accuracy of matching.

5.1.2 Best fit algorithm

As an alternative to polynomial interpolation another algorithm was tested to transfer data between the Cartesian and spherical grid-structure. This algorithm is based on least-square fit.

General linear least-squares

Let φ be a function known at a discrete set of points $(x_l, y_l, z_l)_{l=1...N_p}$, and let $\{F_a(x, y, z)\}_{a=1..M_f}$ be a set of M_f linearly independent functions. The
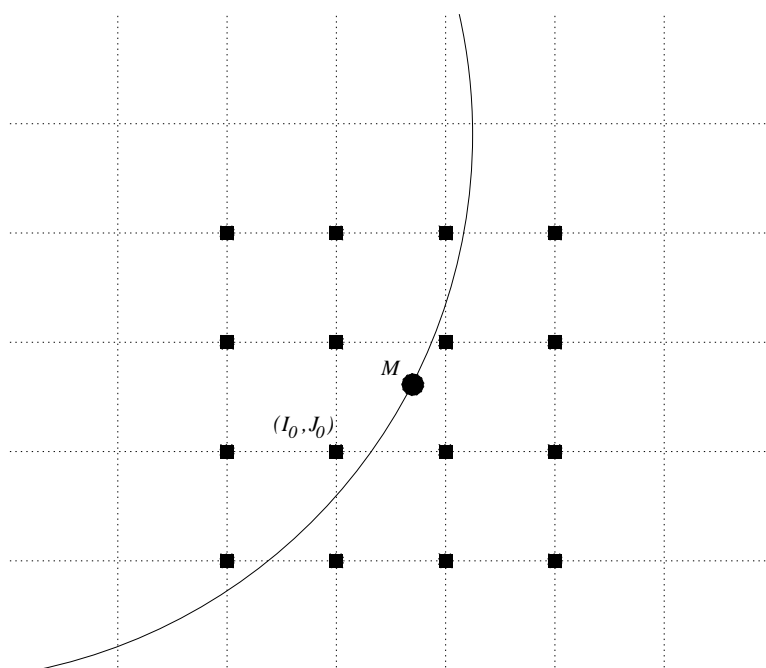
Fig. 5.1: A 2-D version of the cubic interpolation scheme. Data from the Carte-
sian gridpoints marked with filled squares is used to obtain interpolated
data at a point M on the sphere.

set of coefficients $\{C_a\}_{a=1..M_f}$ that minimize the merit function

$$\chi^2 = \sum_{l=1}^{N_p} \left[\varphi(x_l, y_l, z_l) - \sum_{a=1}^{M_f} C_a F_a(x_l, y_l, z_l) \right]^2 \qquad (5.5)$$

can be computed solving a linear algebraic equation [114]:

$$\sum_{a=1}^{M_f} \alpha_{ab} C_b = \beta_b, \qquad b = 1 \ldots M_f, \qquad (5.6)$$

where

$$\alpha_{ab} = \sum_{l=1}^{N_p} F_a(x_l, y_l, z_l) \cdot F_b(x_l, y_l, z_l), \qquad (5.7)$$

$$\beta_a = \sum_{l=1}^{N_p} F_a(x_l, y_l, z_l) \cdot \varphi(x_l, y_l, z_l). \qquad (5.8)$$

Note that the matrix α_{ab} does not depend on the actual data $\varphi(x_l, y_l, z_l)$, it depends only on the coordinates of the data-points $(x_l, y_l, z_l)_{l=1\ldots N_p}$. The matrix equation (5.6) is solved using LU decomposition.[1]

Basis-functions

The set of basis-functions is chosen to be:

$$F_{iklp}(r_0; x, y, z) = \left(\frac{x}{r}\right)^i \left(\frac{y}{r}\right)^{(l-i-k)} \left(\frac{z}{r}\right)^k \left(\frac{r_0}{r} - 1\right)^p, \qquad (5.9)$$

where

$$k = 0 \ldots 1, \qquad (5.10)$$
$$i = 0 \ldots l - k, \qquad (5.11)$$
$$l = 0 \ldots l_{max}, \qquad (5.12)$$
$$p = 0 \ldots p_{max}, \qquad (5.13)$$
$$r = \sqrt{x^2 + y^2 + z^2}. \qquad (5.14)$$

For any given r_0, the set of basis-functions are determined by the set of three parameters: $(l_{max}, p_{min}, p_{max})$.

---

[1] The term LU decomposition stands for an algorithm in which one decomposes a matrix into a lower triangular and an upper triangular matrix. (See [114], pp.31ff.)

The fitting zone is always a spherical shell of thickness of a few grid-zones. Defining r_0 as the average of the outer and inner radii of the fitting zone the renormalized radial coordinate $r_0/r - 1$ takes values around zero which is advantageous if we think of the radial fitting as a kind of expansion in series.

Making a least-square fit of the numerical data to a linear combination of this set of functions gives an analytic function that smoothly approximates our data.

Fitting in the extraction

In order to transfer data from the Cauchy grid to the world-tube the following needs to be done:

- choose a set of basis-functions (by specifying $(l_{max}, p_{min}, p_{max})$);

- define a fitting zone (a spherical shell surrounding the sphere Γ_t);

- use Cauchy data points within this shell to construct a smooth representation of the "3+1" data:

$$g_{ij} \quad \rightarrow \quad \sum_{a=1}^{M_f} C_a^{g_{ij}} F_a(x, y, z), \qquad (5.15)$$

$$\alpha \quad \rightarrow \quad \sum_{a=1}^{M_f} C_a^{\alpha} F_a(x, y, z), \qquad (5.16)$$

$$\beta^i \quad \rightarrow \quad \sum_{a=1}^{M_f} C_a^{\beta^i} F_a(x, y, z); \qquad (5.17)$$

- evaluate the above constructed smooth functions on the sphere Γ_t.

Since the location of Γ_t in coordinates (x, y, z) is independent of t, the set of points used in the extraction-fitting is the same. Thus the matrix α_{ab} given by Eq. (5.7) does not need to be computed at each iteration. This also means that the LU decomposition of α_{ab} needs to be done only once, at the first time-step.

The time derivative of the Cauchy data on the world-tube is smoothly represented by

$$\dot{g}_{ij} \quad \rightarrow \quad \sum_{a=1}^{M_f} \dot{C}_a^{g_{ij}} F_a(x, y, z), \qquad (5.18)$$

$$\dot{\alpha} \;\; \rightarrow \;\; \sum_{a=1}^{M_f} \dot{C}_a^{\alpha} F_a(x,y,z), \tag{5.19}$$

$$\dot{\beta}^i \;\; \rightarrow \;\; \sum_{a=1}^{M_f} \dot{C}_a^{\beta^i} F_a(x,y,z), \tag{5.20}$$

where $\dot{C}_a^{g_{ij}}, \dot{C}_a^{\alpha}, \dot{C}_a^{\beta^i}$ are obtained by finite differencing in time.

Space-derivatives are computed either by first computing the space-derivatives of the Cauchy functions α, β^i, g_{ij} at the Cartesian gridpoints and then fitting them onto Γ_t, or by computing the quantities

$$g_{ij,k} \;\; \rightarrow \;\; \sum_{a=1}^{M_f} C_a^{g_{ij}} \frac{\partial F_a}{\partial x^k}, \tag{5.21}$$

$$\alpha_{,k} \;\; \rightarrow \;\; \sum_{a=1}^{M_f} C_a^{\alpha} \frac{\partial F_a}{\partial x^k}, \tag{5.22}$$

$$\beta^i_{,k} \;\; \rightarrow \;\; \sum_{a=1}^{M_f} C_a^{\beta^i} \frac{\partial F_a}{\partial x^k}. \tag{5.23}$$

A weakness is that the algorithm does not have a well defined accuracy. An argument for using it is that it can work with a Cartesian "stencil" much more compact than the 3-D cubic polynomial interpolator.

A similar algorithm was adopted to replace some of the polynomial interpolation from the injection routine. However, at least for the chosen settings, this fitting technique induced short-time instabilities in the injection module. This led to abandoning the use of fitting.

5.2 Algebra

Next we describe in detail the algebraic calculations performed in the extraction module. The presentation is based on [47].

5.2.1 Parameterization of the world-tube

The $t = $ constant surfaces of the world-tube Γ are topologically spherical, and they can be parametrized by labels $\tilde{y}^{\tilde{A}}, \tilde{A} = [2,3]$. Future oriented null rays are parametrized by their labels $\tilde{y}^{\tilde{A}}$ on Γ_t and an affine parameter λ along the radial direction, with $\lambda = 0$ on the world-tube. The angular coordinates are $\tilde{y}^2 = q = \Re(\zeta)$ and $\tilde{y}^3 = p = \Im(\zeta)$ with ζ being the complex stereographic coordinate as described in Section 3.1.1. The two-surface Σ_t

is represented by a discrete numeric grid-structure identical to the angular grid-structure of the characteristic code (see Section 3.2.1).

The Cartesian coordinates (x, y, z) of a particular point on Γ_t can be written as functions of the angular coordinates $\zeta = q + Ip$ and the radius R_Γ of the extraction world-tube using

$$x(\tilde{y}^A) \;=\; 2R_\Gamma \cdot \left(\frac{\Re(\zeta)}{1 + \zeta\bar{\zeta}} \right), \tag{5.24}$$

$$y(\tilde{y}^A) \;=\; \pm 2R_\Gamma \cdot \left(\frac{\Im(\zeta)}{1 + \zeta\bar{\zeta}} \right), \tag{5.25}$$

$$z(\tilde{y}^A) \;=\; \pm R_\Gamma \cdot \left(\frac{1 - \zeta\bar{\zeta}}{1 + \zeta\bar{\zeta}} \right). \tag{5.26}$$

The reverse expressions $\tilde{y}^{\tilde{A}} = f(x^i)$ are given by Eq. (4.8).

5.2.2   4-D geometry around the world-tube

The geometry around the world-tube is fully specified by the 4-D metric. These determine the unit normal n^α to the Cauchy slices Σ_t as well as the outward pointing normal s^α to the world-tube Γ. The vectors n^α and s^α are used to determine the directions of the outgoing null radial geodesics – an element necessary to compute the coordinate transformation between the Cartesian and the (affine) null coordinates.

From a numerical point of view the first step is getting the Cauchy metric information onto Γ_t by means of interpolation, fitting, etc. as described in the previous section. The ADM code operates with the the 3-D metric $^{(3)}g_{ij}$, lapse function α, and the shift vector β^i. In order to reconstruct the full 4-D metric $g_{\mu\nu}$ and its derivatives $g_{\mu\nu,\rho}$ we use

$$g_{ij} \;=\; {}^{(3)}g_{ij}, \tag{5.27}$$

$$g_{it} \;=\; {}^{(3)}g_{ij}\beta^j, \tag{5.28}$$

$$g_{tt} \;=\; -\alpha^2 + g_{it}\beta^i, \tag{5.29}$$

$$g_{it,\rho} \;=\; {}^{(3)}g_{ij,\rho}\beta^j + {}^{(3)}g_{ij}\beta^j_{,\rho}, \tag{5.30}$$

$$g_{tt,\rho} \;=\; -2\alpha\alpha_{,\rho} + {}^{(3)}g_{ij,\rho}\beta^i\beta^j + 2\,{}^{(3)}g_{ij}\beta^i\beta^j_{,\rho}. \tag{5.31}$$

It follows from the definition of lapse and shift (see Section 2.3.1) that the unit normal n^μ to the $t = $ constant hypersurfaces can be written as

$$n^\mu = \frac{1}{\alpha}\left(1, -\beta^i\right). \tag{5.32}$$

Let $s^\alpha = (0, s^i)$ be the outward pointing unit normal to the sphere Γ_t. By construction s^i lies in Σ_t, and it can be expressed in terms of

$$q^i = \frac{\partial x^i}{\partial \tilde{y}^2}, \quad p^i = \frac{\partial x^i}{\partial \tilde{y}^3}, \tag{5.33}$$

which can be computed analytically from Eqs. (5.24) - (5.26). Using the unit antisymmetries ϵ_{ijk}, we obtain the spatial components of the normal 1-form σ_i

$$\sigma_i = \epsilon_{ijk} q^j p^k, \tag{5.34}$$

with norm $\sigma = \sqrt{\sigma_i \sigma_j {}^{(3)} g^{ij}}$. Then the vector s^i is equal to the contravariant, renormalized vector σ^i:

$$s^i = {}^{(3)} g^{ij} \frac{\sigma_j}{\sigma}. \tag{5.35}$$

The generators ℓ^μ of the outgoing null cone through Γ_t are given on the world-tube by the vectors n^μ and s^μ, normalized such that $\ell^\mu t_\mu = -1$, that is,

$$\ell^\mu = \frac{n^\mu + s^\mu}{\alpha - {}^{(3)} g_{ij} \beta^i s^j}. \tag{5.36}$$

This supplies all the necessary elements on the world-tube Γ_t to perform the first coordinate transformation from Cartesian coordinates $x^\mu = (t, x, y, z)$ into affine null coordinates $\tilde{y}^{\tilde{\nu}} = (u, \lambda, q, p)$. Once we have the metric in affine null coordinates it takes only a few more algebraic steps to obtain the Bondi metric, from which we can extract the Bondi metric variables J, β, U and W in terms of a Taylor expansion around the world-tube Γ.

5.2.3 Coordinate transformation

The coordinate transformation $x^\alpha \to \tilde{y}^{\tilde{\beta}}$ needs to be performed in a neighborhood of the world-tube Γ.

The standard approach in carrying through coordinate transformations is to compute the Jacobian $\partial x^\mu / \partial \tilde{y}^{\tilde{\alpha}}$, then use the tensorial transformation rule

$$\tilde{\eta}_{\tilde{\alpha}\tilde{\beta}} = \frac{\partial x^\mu}{\partial \tilde{y}^{\tilde{\alpha}}} \frac{\partial x^\nu}{\partial \tilde{y}^{\tilde{\beta}}} {}^{(4)} g_{\mu\nu}. \tag{5.37}$$

However, the geometric properties of the affine null coordinate system make this task easier because four out of the ten components of the 4×4 symmetric tensor are given by

$$\tilde{\eta}_{\lambda\lambda} = 0, \quad \tilde{\eta}_{\lambda\tilde{A}} = 0, \quad \tilde{\eta}_{\lambda u} = -1. \tag{5.38}$$

The first of these conditions indicates that the radial coordinate λ is null, the second one is implied by the fact that the null vector ℓ^μ is normal to Γ, while the last condition is a consequence of λ being an affine parameter. The additional degree of freedom in the choice of λ is eliminated by

$$\lambda_{|\Gamma} = 0. \tag{5.39}$$

At this point six independent metric functions remain. The part of the coordinate transformation that is still missing is

$$J^\mu_{\tilde\alpha} \equiv \frac{\partial x^\mu}{\partial \tilde y^{\tilde\alpha}} = x^{(0)\mu}_{,\tilde\alpha} + x^{(1)\mu}_{,\tilde\alpha}\lambda + O(\lambda^2), \text{ for } \tilde y^{\tilde\alpha} = (u,q,p). \tag{5.40}$$

By construction the coordinates t and u are related by $u_{|\Gamma} = t_{|\Gamma}$ and $(\partial t/\partial u)_{|\Gamma} = 1$. Furthermore, since the location of Γ_t in Cartesian coordinates is time-independent, only the angular derivatives of $x^{(0)}(\equiv x_{|\Gamma})$ survive in Eq. (5.40). These can easily be computed using Eqs. (5.24) - (5.26).

The harder task in the coordinate transformation is the evaluation of the $O(\lambda)$ part. This can be done starting from

$$x^\mu_{,\lambda\tilde A} = \ell^\mu_{,\tilde A}, \quad x^\mu_{,\lambda u} = \ell^\mu_{,u}. \tag{5.41}$$

Since the null vector ℓ^μ depends on the Cauchy metric components, the terms listed in Eq. (5.41) involve derivatives of the Cauchy metric as well as zeroth order Jacobian terms. In order to compute the derivatives of ℓ^μ first derivatives of n^μ are computed. Then derivatives of the spacelike vector s^i follow.

Since the vector n^μ is the unit normal to the Cauchy surfaces Σ_t, it is entirely determined by the choice of lapse and shift. The Cartesian derivatives

$$n^i_{,\nu} = \frac{1}{\alpha^2}\left(\alpha_{,\nu}\beta^i - \alpha\beta^i_{,\nu}\right), \quad n^t_{,\nu} = -\frac{1}{\alpha^2}\alpha_{,\nu} \tag{5.42}$$

can be used to compute derivatives with respect to (u,q,p) via

$$n^\mu_{,\tilde A} = n^\mu_{,j}x^j_{,\tilde A}, \tag{5.43}$$

$$n^\mu_{,u|\Gamma} = n^\mu_{,t|\Gamma}. \tag{5.44}$$

The vector s^i is constructed from the time-independent vector σ^i and the metric tensor components. Its time derivatives are

$$\begin{aligned}
s^i_{,t} &= g^{ik}_{,t}\frac{\sigma_k}{\sigma} - g^{ik}\frac{\sigma_k\sigma_{,t}}{\sigma^2} = -g^{im}g^{kn}g_{mn,t}\frac{\sigma_k}{\sigma} - s^i\frac{\sigma_{,t}}{\sigma} \\
&= -g^{im}g_{mn,t}s^n - s^i\frac{\sigma_{,t}}{\sigma}. \tag{5.45}
\end{aligned}$$

Here the quantity σ (the norm of σ^i) is time-dependent because the metric tensor used to build the norm of a vector varies with time. Thus

$$2\sigma\sigma_{,t} = \left(\sigma^2\right)_{,t} = g^{kl}_{,t}\sigma_k\sigma_l = -g^{km}g^{ln}g_{mn,t}\sigma_k\sigma_l = -s^m s^n g_{mn,t}\sigma^2. \quad (5.46)$$

Substituting Eq. (5.46) into Eq. (5.45) one obtains

$$s^i_{,t} = \left(-g^{im} + s^i\frac{1}{2}s^m\right)g_{mn,t}s^n. \quad (5.47)$$

Similarly, it follows from Eq. (5.35) that

$$\begin{aligned}
s^i_{,\tilde{A}} &= g^{ik}_{,j}x^j_{,\tilde{A}}\frac{\sigma_k}{\sigma} + g^{ik}\frac{\sigma_{k,\tilde{A}}}{\sigma} - g^{ik}\frac{\sigma_k\sigma_{,\tilde{A}}}{\sigma^2} \\
&= -g^{in}g^{km}g_{mn,j}\,x^j_{,\tilde{A}}\frac{\sigma_k}{\sigma} + g^{ik}\frac{\sigma_{k,\tilde{A}}}{\sigma} - s^i\frac{\sigma_{,\tilde{A}}}{\sigma}, \quad (5.48)
\end{aligned}$$

where the $\sigma_{k,\tilde{A}}$ are obtained from the analytic expressions (5.33), and $\sigma_{,\tilde{A}}$ from

$$\begin{aligned}
2\sigma\sigma_{,\tilde{A}} &= \left(\sigma^2\right)_{,\tilde{A}} = \left(g^{kl}\sigma_k\sigma_l\right)_{,\tilde{A}} = g^{kl}_{,j}x^j_{,\tilde{A}}\sigma_k\sigma_l + 2\,g^{kl}\sigma_l\sigma_{k,\tilde{A}} \\
&= -g^{km}g^{ln}g_{mn,j}x^j_{,\tilde{A}}\sigma_k\sigma_l + 2\,g^{kl}\sigma_l\sigma_{k,\tilde{A}} \\
&= -s^m s^n g_{mn,j}x^j_{,\tilde{A}}\sigma^2 + 2s^k\sigma\sigma_{k,\tilde{A}}. \quad (5.49)
\end{aligned}$$

Collecting Eqs. (5.48) and (5.49), the angular derivatives of s^i are:

$$\begin{aligned}
s^i_{,\tilde{A}} &= -g^{in}s^m g_{mn,j}\,x^j_{,\tilde{A}} + g^{ik}\frac{\sigma_{k,\tilde{A}}}{\sigma} + s^i\left(\frac{1}{2}s^m s^n g_{mn,j}x^j_{,\tilde{A}} - s^k\frac{\sigma_{k,\tilde{A}}}{\sigma}\right) \\
&= \left(g^{in} - s^i s^n\right)\frac{\sigma_{n,\tilde{A}}}{\sigma} + \left(-g^{in} + \frac{1}{2}s^i s^n\right)s^m g_{mn,j}x^j \quad (5.50)
\end{aligned}$$

5.2.4   The affine null metric

One of the useful quantities in computing the null metric $\tilde{\eta}_{\tilde{\alpha}\tilde{\beta}}$ is the λ-derivative of the Cartesian tensor $g_{\alpha\beta}$:

$$g_{\alpha\beta,\lambda|\Gamma} = \left(\frac{\partial g_{\alpha\beta}}{\partial x^\mu}\right)_{|\Gamma}\left(\frac{\partial x^\mu}{\partial\lambda}\right)_{|\Gamma} = g^{(0)}_{\alpha\beta,\mu}\ell^{(0)\mu}. \quad (5.51)$$

The null metric can be expanded around Γ as follows

$$\tilde{\eta}_{\tilde{\alpha}\tilde{\beta}} = \tilde{\eta}^{(0)}_{\tilde{\alpha}\tilde{\beta}} + \tilde{\eta}^{(0)}_{\tilde{\alpha}\tilde{\beta},\lambda}\lambda + O(\lambda^2), \quad (5.52)$$

where the zeroth order coefficients are given by

$$
\begin{aligned}
\tilde{\eta}_{u\tilde{u}}^{(0)} &= g_{tt|\Gamma}, \\
\tilde{\eta}_{u\tilde{A}}^{(0)} &= x^i_{,\tilde{A}} g_{it|\Gamma}, \\
\tilde{\eta}_{\tilde{A}\tilde{B}}^{(0)} &= x^i_{,\tilde{A}} x^j_{,\tilde{B}} g_{ij|\Gamma},
\end{aligned}
\tag{5.53}
$$

and the first-order terms are

$$
\begin{aligned}
\tilde{\eta}_{uu,\lambda}^{(0)} &= \left[g_{tt,\lambda} + 2\,\ell^\mu_{,u} g_{\mu t} \right]_{|\Gamma} + O(\lambda), \\
\tilde{\eta}_{u\tilde{A},\lambda}^{(0)} &= \left[x^k_{,\tilde{A}} \left(\ell^\mu_{,u} g_{k\mu} + g_{kt,\lambda} \right) + \ell^k_{,\tilde{A}} g_{kt} + \ell^t_{,\tilde{A}} g_{tt} \right]_{|\Gamma} + O(\lambda), \\
\tilde{\eta}_{\tilde{A}\tilde{B},\lambda}^{(0)} &= \left[x^k_{,\tilde{A}} x^l_{,\tilde{B}} g_{kl,\lambda} + \left(\ell^\mu_{,\tilde{A}} x^l_{,\tilde{B}} + \ell^\mu_{,\tilde{B}} x^l_{,\tilde{A}} \right) g_{\mu l} \right]_{|\Gamma} + O(\lambda).
\end{aligned}
\tag{5.54}
$$

Recall that the components $\tilde{\eta}_{\lambda\tilde{\beta}}$ are given by Eq. (5.38).

Given the covariant null metric $\tilde{\eta}_{\tilde{\alpha}\tilde{\beta}}$ as an expansion up to $O(\lambda^2)$, its contravariant form $\tilde{\eta}^{\tilde{\alpha}\tilde{\beta}}$ is known to the same order

$$
\tilde{\eta}^{\tilde{\mu}\tilde{\nu}} = \tilde{\eta}^{(0)\,\tilde{\mu}\tilde{\nu}} + \tilde{\eta}^{(0)\tilde{\mu}\tilde{\nu}}_{,\lambda} \lambda + O(\lambda^2),
\tag{5.55}
$$

using

$$
\tilde{\eta}^{\tilde{\mu}\tilde{\alpha}} \tilde{\eta}_{\tilde{\alpha}\tilde{\nu}} = \delta^{\tilde{\mu}}_{\tilde{\nu}}, \quad \tilde{\eta}^{\tilde{\mu}\tilde{\nu}}_{,\lambda} = -\tilde{\eta}^{\tilde{\mu}\tilde{\alpha}} \tilde{\eta}^{\tilde{\beta}\tilde{\nu}} \tilde{\eta}_{\tilde{\alpha}\tilde{\beta},\lambda}.
\tag{5.56}
$$

Similar to the case of the covariant metric, the components $\tilde{\eta}^{\lambda\tilde{\alpha}}$ are determined by the null coordinate conditions

$$
\tilde{\eta}^{\lambda u} = -1, \quad \tilde{\eta}^{u\tilde{A}} = \tilde{\eta}^{uu} = 0,
\tag{5.57}
$$

a consequence of Eq. (5.38). As a result, the contravariant null metric can be computed by

$$
\begin{aligned}
\tilde{\eta}^{\tilde{A}\tilde{B}} \tilde{\eta}_{\tilde{B}\tilde{C}} &= \delta^{\tilde{A}}_{\tilde{C}}, \\
\tilde{\eta}^{\lambda\tilde{A}} &= \tilde{\eta}^{\tilde{A}\tilde{B}} \tilde{\eta}_{\tilde{B}u}, \\
\tilde{\eta}^{\lambda\lambda} &= -\tilde{\eta}_{uu} + \tilde{\eta}^{\lambda\tilde{A}} \tilde{\eta}_{\tilde{A}u},
\end{aligned}
\tag{5.58}
$$

with the first-order terms given by

$$
\begin{aligned}
\tilde{\eta}^{\tilde{A}\tilde{B}}_{,\lambda} &= -\tilde{\eta}^{\tilde{A}\tilde{C}} \tilde{\eta}^{\tilde{B}\tilde{D}} \tilde{\eta}_{\tilde{C}\tilde{D},\lambda}, \\
\tilde{\eta}^{\lambda\tilde{A}}_{,\lambda} &= \tilde{\eta}^{\tilde{A}\tilde{B}} \left(\tilde{\eta}_{u\tilde{B},\lambda} - \tilde{\eta}^{\lambda\tilde{C}} \tilde{\eta}_{\tilde{C}\tilde{B},\lambda} \right), \\
\tilde{\eta}^{\lambda\lambda}_{,\lambda} &= -\tilde{\eta}_{uu,\lambda} + 2\,\tilde{\eta}^{\lambda\tilde{A}} \tilde{\eta}_{u\tilde{A},\lambda} - \tilde{\eta}^{\lambda\tilde{A}} \tilde{\eta}^{\lambda\tilde{B}} \tilde{\eta}_{\tilde{A}\tilde{B},\lambda}.
\end{aligned}
\tag{5.59}
$$

5.2.5 Metric in Bondi coordinates

By convention the angular coordinates used in the Bondi frame are defined to be the same as the angular coordinates used in the affine null frame, i.e. $y^A \equiv \tilde{y}^{\tilde{A}} = (q, p)$. As a consequence, switching from affine null coordinates $\tilde{y}^{\tilde{\mu}} = (u, \lambda, \tilde{y}^{\tilde{A}})$ to Bondi coordinates $y^\mu = (u, r, y^A)$ amounts to trading the affine parameter λ for the surface area coordinate $r = r(u, \lambda, y^A)$ defined by

$$r = \left(\frac{\det(\tilde{\eta}_{\tilde{A}\tilde{B}})}{\det(q_{AB})} \right)^{\frac{1}{4}} = \frac{2}{P} \det(\tilde{\eta}_{\tilde{A}\tilde{B}})^{\frac{1}{4}}, \tag{5.60}$$

where we have used $\det(q_{AB}) = 16/(1 + q^2 + p^2)^4 = 16/P^4$.

The only nontrivial elements of the Jacobian $\partial y^\alpha/\partial \tilde{y}^{\tilde{\beta}}$ are $r_{,\lambda}$, $r_{,\tilde{A}}$ and $r_{,u}$, which can be computed using

$$r_{,\lambda} = \frac{r}{4} \tilde{\eta}^{\tilde{A}\tilde{B}} \tilde{\eta}_{\tilde{A}\tilde{B},\lambda}, \tag{5.61}$$

$$r_{,\tilde{C}} = \frac{r}{4} \left(\tilde{\eta}^{\tilde{A}\tilde{B}} \tilde{\eta}_{\tilde{A}\tilde{B},\tilde{C}} - \frac{\det(q_{\tilde{A}\tilde{B}})_{,\tilde{C}}}{\det(q_{\tilde{A}\tilde{B}})} \right), \tag{5.62}$$

$$r_{,u} = \frac{r}{4} \tilde{\eta}^{\tilde{A}\tilde{B}} \tilde{\eta}_{\tilde{A}\tilde{B},u}. \tag{5.63}$$

The terms involved in computing $r_{,\tilde{C}}$ can be obtained via

$$\frac{\det(q_{\tilde{A}\tilde{B}})_{,\tilde{C}}}{\det(q_{\tilde{A}\tilde{B}})} = -\frac{8\,\tilde{y}^{\tilde{C}}}{P},$$

$$\tilde{\eta}_{\tilde{A}\tilde{B},\tilde{C}} = \left(x^i_{,\tilde{A}\tilde{C}} x^j_{,\tilde{B}} + x^i_{,\tilde{A}} x^j_{,\tilde{B}\tilde{C}} \right) g_{ij}$$
$$+ x^i_{,\tilde{A}} x^j_{,\tilde{B}} x^k_{,\tilde{C}} g_{ij,k} \tag{5.64}$$

where the $x^i_{,\tilde{A}\tilde{C}}$ are given functions of (q, p). Furthermore, when computing $r_{,u}$, we need the u-derivative of the affine null metric, which, according to Eq. (5.53), is given by

$$\tilde{\eta}_{\tilde{A}\tilde{B},u} = \left[x^i_{,\tilde{A}} x^j_{,\tilde{B}} g_{ij,t} \right]_{|\Gamma} + O(\lambda). \tag{5.65}$$

The Bondi metric $\eta^{\alpha\beta}$ is then obtained from

$$\eta^{\alpha\beta} = \frac{\partial y^\alpha}{\partial \tilde{y}^\mu} \frac{\partial y^\beta}{\partial \tilde{y}^\nu} \tilde{\eta}^{\tilde{\mu}\tilde{\nu}}. \tag{5.66}$$

Since the only difference between the affine and the Bondi null frames is the radial coordinate, we only need to compute the metric elements η^{rr},

η^{rA} and η^{ru}, the rest of the tensor $\eta^{\alpha\beta}$ being identical with $\tilde{\eta}^{\tilde{\alpha}\tilde{\beta}}$. Using Eq. (5.57),

$$
\begin{aligned}
\eta^{rr} &= r_{,\tilde{\alpha}}\, r_{,\tilde{\beta}}\, \tilde{\eta}^{\tilde{\alpha}\tilde{\beta}} = (r_{,\lambda})^2\, \tilde{\eta}^{\lambda\lambda} + 2\, r_{,\lambda}\, \left(r_{,\tilde{A}}\, \tilde{\eta}^{\lambda\tilde{A}} - r_{,u} \right) + r_{,\tilde{A}}\, r_{,\tilde{B}}\, \tilde{\eta}^{\tilde{A}\tilde{B}} \\
\eta^{rA} &= r_{,\tilde{\alpha}}\, \tilde{\eta}^{\tilde{\alpha}\tilde{A}} = r_{,\lambda}\, \tilde{\eta}^{\lambda\tilde{A}} + r_{,\tilde{B}}\, \tilde{\eta}^{\tilde{A}\tilde{B}} \\
\eta^{ru} &= r_{,\tilde{\alpha}}\, \tilde{\eta}^{\tilde{\alpha}u} = -r_{,\lambda}
\end{aligned}
\tag{5.67}
$$

At this point we are one step away from obtaining the Bondi metric variables J, U, β, W and passing them to the characteristic code as boundary data.

5.2.6   Boundary data for the characteristic code

Recall from Section 4.2.1 that the null gridpoints do not necessarily lie *on* the world-tube Γ. Moreover, the position of individual null gridpoints with respect to Γ can differ from time-step to time-step. In particular, gridpoints that are just inside of Γ at $t = t_{[N]}$ could end up outside of it at $t = t_{[N+1]}$. Thus, in order to provide boundary data for the characteristic code, the following steps must be made:

- compute the Bondi metric variables around the world-tube up to $O(\lambda^2)$

- localize the world-tube-slice Γ_t in Bondi coordinates

- insert the Bondi functions onto the characteristic gridpoints neighboring Γ_t.

Then, the characteristic code has the necessary data to evolve the metric functions from the world-tube to the outer boundary.[2]

In order to compute the Bondi metric variables, the contravariant Bondi metric is written in the form given by Eq. (4.17). The functions $J, \beta, U,$ and W can now be expressed in terms of known quantities on the world-tube, as described in the next sections. Although these functions have already been defined in Chapter 3, their definition is repeated here for the ease of reading.

---

[2] In the case of an ingoing null simulation, the evolution proceeds from Γ to the inner (possibly excised) boundary. See Section 3.4 for an example.

The metric of the sphere J

Given r and $r_{,\lambda}$ and noting that

$$\eta_{AB} = \tilde{\eta}_{AB} \equiv r^2 h_{AB}, \tag{5.68}$$

h_{AB} and its derivative can be obtained from

$$
\begin{aligned}
h_{AB} &= \frac{1}{r^2}\eta_{AB}, \\
h_{AB,\lambda} &= \frac{1}{r^2}\left(\eta_{AB,\lambda} - \frac{2\,r_{,\lambda}}{r}\eta_{AB}\right).
\end{aligned}
\tag{5.69}
$$

In terms of q^A, $\bar{q}^A$, and h_{AB}, the metric functions J and K are then defined as follows:

$$J \equiv \frac{1}{2}q^A q^B h_{AB}, \quad K \equiv \frac{1}{2}q^A \bar{q}^B h_{AB}. \tag{5.70}$$

As stated in Section 3, the determinant condition $\det(h_{AB}) = \det(q_{AB})$ implies $1 = K^2 - J\bar{J}$. Thus, it suffices to evaluate J, which can be computed as an expansion around Γ

$$J(y^\alpha) = J^{(0)} + J^{(0)}_{,\lambda}\lambda + O(\lambda^2), \tag{5.71}$$

with $J^{(0)}$ and $J^{(0)}_{,\lambda}$ given by

$$
\begin{aligned}
J^{(0)} &= \left(\frac{1}{2\,r^2}q^A q^B \eta_{AB}\right)_{|\Gamma}, \\
J^{(0)}_{,\lambda} &= \left(\frac{1}{2\,r^2}q^A q^B \eta_{AB,\lambda} - 2\frac{r_{,\lambda}}{r}J\right)_{|\Gamma}.
\end{aligned}
\tag{5.72}
$$

The "expansion factor" β

From inspection of Eq. (4.17) one can see that

$$\eta^{ru} = -e^{-2\beta}. \tag{5.73}$$

Substituting the last of Eqs. (5.67) into Eq. (5.73), one obtains

$$\beta = -\frac{1}{2}\log(r_{,\lambda}). \tag{5.74}$$

The first-order derivative term $\beta^{(0)}_{,\lambda}$ involves $r^{(0)}_{,\lambda\lambda}$ which in turn involves second derivatives of the Cauchy metric (or curvature terms). In order to

avoid the associated algebraic (and numeric) complications, we use the first differential order characteristic equation (3.13).

At a constant angle (q, p) the relation $\partial_\lambda = r_{,\lambda}\partial_r$ holds. This allows an exchange of the r-derivatives in Eq. (3.13) with λ-derivatives:

$$\beta_{,\lambda} = \frac{r}{8\,r_{,\lambda}}\left(J_{,\lambda}\bar{J}_{,\lambda} - (K_{,\lambda})^2\right). \tag{5.75}$$

Equation (5.75), shows how the derivative with respect to the affine parameter of the expansion of light rays is a quadratic term, i.e. it vanishes in linearized theory.

Substituting Eq. (5.70) into Eq. (5.75), we obtain

$$\beta_{,\lambda} = \frac{r}{8\,r_{,\lambda}}\left(J_{,\lambda}\bar{J}_{,\lambda} - \frac{1}{1 + J\bar{J}}\left[\Re\left(\bar{J}J_{,\lambda}\right)\right]^2\right). \tag{5.76}$$

Equations (5.74) and (5.76) hold globally and thus provide a way to compute $\beta^{(0)} = \beta_{|\Gamma}$ and $\beta_{,\lambda}^{(0)} = \beta_{,\lambda|\Gamma}$ Then, the expansion for β around Γ can be written

$$\beta(y^\alpha) = \beta^{(0)} + \beta_{,\lambda}^{(0)}\lambda + O(\lambda^2). \tag{5.77}$$

In addition, using Eq. (5.74) $r_{,\lambda\lambda}$ can be computed in terms of the known quantities $\beta_{,\lambda}$ and $r_{,\lambda}$:

$$\beta_{,\lambda} = \partial_\lambda\left(-\frac{1}{2}\log\left(r_{,\lambda}\right)\right) = -\frac{r_{,\lambda\lambda}}{2r_{,\lambda}}. \tag{5.78}$$

The "shift" U

The metric function U is expressed, using Eq. (5.67), as

$$U \equiv U^A q_A = \frac{\eta^{rA}}{\eta^{ru}}q_A = -\left(\tilde{\eta}^{\lambda\tilde{A}} + \frac{r_{,\tilde{B}}}{r_{,\lambda}}\tilde{\eta}^{\tilde{A}\tilde{B}}\right)q_{\tilde{A}}, \tag{5.79}$$

The λ derivative of U will be given by

$$
\begin{aligned}
U_{,\lambda} &= -\left[\tilde{\eta}^{\lambda\tilde{A}}_{,\lambda} + \left(\frac{r_{,\lambda\tilde{B}}}{r_{,\lambda}} - \frac{r_{,\tilde{B}}\,r_{,\lambda\lambda}}{r^2_{,\lambda}}\right)\tilde{\eta}^{\tilde{A}\tilde{B}} + \frac{r_{,\tilde{B}}}{r_{,\lambda}}\tilde{\eta}^{\tilde{A}\tilde{B}}_{,\lambda}\right]q_{\tilde{A}}, \\
&= -\left(\tilde{\eta}^{\lambda\tilde{A}}_{,\lambda} + \frac{r_{,\lambda\tilde{B}}}{r_{,\lambda}}\tilde{\eta}^{\tilde{A}\tilde{B}} + \frac{r_{,\tilde{B}}}{r_{,\lambda}}\tilde{\eta}^{\tilde{A}\tilde{B}}_{,\lambda}\right)q_{\tilde{A}} \\
&\quad + 2\beta_{,\lambda}\left(U + \tilde{\eta}^{\lambda\tilde{A}}q_{\tilde{A}}\right), \tag{5.80}
\end{aligned}
$$

where Eq. (5.78) was used to eliminate $r_{,\lambda\lambda}$ in the last line.

Then applying Eqs. (5.79) - (5.80) around the world-tube, U is found to second-order accuracy by:

$$U(y^\alpha) = U^{(0)} + U^{(0)}_{,\lambda}\lambda + O(\lambda^2). \tag{5.81}$$

The "potential" W

Recall from Eq. (4.17) that

$$\eta^{rr} = e^{-2\beta}\frac{V}{r}, \quad \eta^{ur} = -e^{-2\beta}. \tag{5.82}$$

Thus the function V is given by

$$V \equiv -r\eta^{rr}/\eta^{ru}. \tag{5.83}$$

For Minkowski space, $\eta^{rr} = -\eta^{ru} = 1$ so that the asymptotic value of V is given by $V = r$. Thus, in the characteristic code, V is replaced with the function $W \equiv (V - r)/r^2$. In terms of the affine contravariant null metric $\tilde{\eta}^{\tilde{\alpha}\tilde{\beta}}$, W can be expressed as

$$W = \frac{1}{r}\left(\frac{\eta^{rr}}{r_{,\lambda}} - 1\right) = \frac{1}{r}\left(r_{,\lambda}\tilde{\eta}^{\lambda\lambda} + 2\left(r_{,\tilde{A}}\,\tilde{\eta}^{\lambda\tilde{A}} - r_{,u}\right) + \frac{r_{,\tilde{A}}\,r_{,\tilde{B}}}{r_{,\lambda}}\tilde{\eta}^{\tilde{A}\tilde{B}} - 1\right), \tag{5.84}$$

with the radial derivative term $W_{,\lambda}$ given by

$$
\begin{aligned}
W_{,\lambda} &= -\frac{r_{,\lambda}}{r}W + \frac{1}{r}\left(r_{,\lambda}\tilde{\eta}^{\lambda\lambda} + 2\left(r_{,\tilde{A}}\,\tilde{\eta}^{\lambda\tilde{A}} - r_{,u}\right) + \frac{r_{,\tilde{A}}\,r_{,\tilde{B}}}{r_{,\lambda}}\tilde{\eta}^{\tilde{A}\tilde{B}} - 1\right)_{,\lambda} \\
&= -\frac{r_{,\lambda}}{r}\left(\left(\frac{r_{,\lambda}}{r} + 2\,\beta_{,\lambda}\right)\tilde{\eta}^{\lambda\lambda} - \tilde{\eta}^{\lambda\lambda}_{,\lambda} - \frac{1}{r}\right) + \frac{2}{r}\left(\frac{r_{,\lambda}r_{,u}}{r} - r_{,\lambda u}\right) \\
&\quad + \frac{2}{r}\left(r_{,\lambda\tilde{A}} - \frac{r_{,\lambda}r_{,\tilde{A}}}{r}\right)\tilde{\eta}^{\lambda\tilde{A}} + 2\frac{r_{,\tilde{A}}}{r}\tilde{\eta}^{\lambda\tilde{A}}_{,\lambda} \\
&\quad + \frac{r_{,\tilde{B}}}{r\,r_{,\lambda}}\left(2\,r_{,\lambda\tilde{A}}\tilde{\eta}^{\tilde{A}\tilde{B}} + 2\,\beta_{,\lambda}r_{,\tilde{A}} + r_{,\tilde{A}}\tilde{\eta}^{\tilde{A}\tilde{B}}_{,\lambda}\right) - \frac{r_{,\tilde{A}}\,r_{,\tilde{B}}}{r^2}\tilde{\eta}^{\tilde{A}\tilde{B}}. \tag{5.85}
\end{aligned}
$$

With Eqs. (5.84) - (5.85) evaluated on the world-tube Γ, W is found to second-order accuracy by

$$W(y^\alpha) = W^{(0)} + W^{(0)}_{,\lambda}\lambda + O(\lambda^2). \tag{5.86}$$

At this point the four Bondi metric functions J, β, U, W have been obtained as Taylor-expansions around Γ, up to $O(\lambda^2)$. The location of the

world-tube Γ in the Bondi frame is now known, since at any point of Γ the four Bondi coordinate values (u, r, q, p) are known from the extraction. Let M be a gridpoint on Γ, labeled by the angular coordinates $(q_{[I]}, p_{[J]})$. For a given time-step $t_{[N]}$ let $r_{[K]}$ be the nearest neighbor of M in the radial direction. Then the extraction provides boundary data for the characteristic code by setting[3]

$$J_{[I,J,K]} \;\;=\;\; J_{[I,J]}^{(0)} + \frac{r_{[K]} - r_{[I,J]}^{(0)}}{r_{,\lambda[I,J]}^{(0)}} \cdot J_{,\lambda[I,J]}^{(0)} + O(\Delta^2), \qquad (5.87)$$

$$\beta_{[I,J,K]} \;\;=\;\; \beta_{[I,J]}^{(0)} + \frac{r_{[K]} - r_{[I,J]}^{(0)}}{r_{,\lambda[I,J]}^{(0)}} \cdot \beta_{,\lambda[I,J]}^{(0)} + O(\Delta^2), \qquad (5.88)$$

$$W_{[I,J,K]} \;\;=\;\; W_{[I,J]}^{(0)} + \frac{r_{[K]} - r_{[I,J]}^{(0)}}{r_{,\lambda[I,J]}^{(0)}} \cdot W_{,\lambda[I,J]}^{(0)} + O(\Delta^2), \qquad (5.89)$$

and

$$U_{[I,J,K]} \;\;=\;\; U_{[I,J]}^{(0)} + \frac{r_{[K+\frac{1}{2}]} - r_{[I,J]}^{(0)}}{r_{,\lambda[I,J]}^{(0)}} \cdot U_{,\lambda[I,J]}^{(0)} + O(\Delta^2), \qquad (5.90)$$

where we have taken in account the fact that the field U is represented on a radially staggered grid. Furthermore, since the characteristic equations involve second derivatives of U, its boundary data must be provided at an additional radial gridpoint neighboring the world-tube Γ.

5.3   Calibration of the extraction module

Given the amount of algebraic calculations involved in extraction, one needs a number of test-beds to assure that they are implemented correctly. Furthermore, finite differencing and interpolation involved in the module also needs to be checked for proper convergence.

In calibration we have first worked out analytically all quantities involved in the extraction. Then, to check proper second-order convergence of the extraction module, we have compared the numerical output of the module with the analytic functions for finer and finer resolution, keeping all physical parameters fixed.

---

[3] In fact, at this point the extraction module uses the compactified coordinate x (as defined in Eq. (3.3)) instead of the Bondi radial coordinate r, i.e. it first locates Γ in terms of the x-grid, then expands the world-tube values of J, β, U, W in terms of $(x - x^{(0)})$. However, the difference between the two approaches is $O(\Delta^2)$, which is insignificant.

It is worth noting that the Jacobian of the Cartesian-Bondi transformation is used not only in the extraction but also in the injection. Thus we have checked convergence not only for the numeric Bondi metric but also for the Cartesian-Bondi Jacobian as computed by the extraction module.

Two classes of analytic solutions were used. The first class consisted of solutions known in Cauchy coordinates. Given the Cauchy metric we used the algebraic steps prescribed in the extraction to obtain the Bondi-Cartesian coordinate transformation as well as the Bondi metric as an expansion around the world-tube Γ. The second class of analytic solutions was provided in Bondi coordinates. In this case the Cartesian coordinates were defined by hand, i.e. we defined the Cartesian frame by prescribing the functions $x^\alpha = f(y^\beta)$. The approach is straightforward and algorithmic for both classes, but the actual calculations are quite lengthy. Thus convergence tests not only validate the numerical implementation, but also provide a consistency check between the numeric and algebraic calculations.

5.3.1   Minkowski space

For the case of Minkowski space-time the lightcone structure is known analytically. Thus the coordinate transformation can be given globally (instead of as an expansion around Γ). The Cauchy metric in Cartesian coordinates (t, x, y, z) is

$$g_{\mu\nu} = \mathrm{diag}[-1, 1, 1, 1]. \tag{5.91}$$

The first coordinate transformation $(t, x, y, z) \rightarrow (u, \lambda, q, p)$ is defined by

$$t = u + \lambda, \tag{5.92}$$

$$x = 2(R_\Gamma + \lambda)\frac{q}{P}, \tag{5.93}$$

$$y = \pm 2(R_\Gamma + \lambda)\frac{p}{P}, \tag{5.94}$$

$$z = \pm(R_\Gamma + \lambda)\frac{2 - P}{P}, \tag{5.95}$$

where $P = 1 + q^2 + p^2$ and the $+(-)$ sign corresponds to the north (south) patch. The null vector in the two coordinate patches is given by

$$\ell^\mu = \left(1, \ \frac{2q}{P}, \ \pm\frac{2p}{P}, \ \pm\frac{2 - P}{P}\right). \tag{5.96}$$

The second coordinate transformation $(u, \lambda, q, p) \rightarrow (u, r, q, p)$ is defined by $r = R_\Gamma + \lambda$. The Bondi metric variables are known globally: $J = \beta = U = W = 0$. The analytic results were reproduced by the numerical calculations to machine precision.

5.3.2 *Teukolsky waves*

The Cauchy metric

Next results are presented for a linearized solution that describes propagation of a time-symmetric quadrupole wave (Teukolsky wave) for unit lapse, zero shift. The Cauchy 3-metric in coordinates (z, ρ, ϕ) is given by ([115], p. 282f):

$$g_{zz} = 1 + 3D\cos^4\theta + 6(B - C)\cos^3\theta + 3C - A, \qquad (5.97)$$

$$g_{\rho\rho} = 1 + 3D\sin^2\theta\cos^2\theta - A, \qquad (5.98)$$

$$g_{z\rho} = 3\sin\theta\cos\theta(D\cos^2\theta + B - C), \qquad (5.99)$$

$$g_{\phi\phi} = \rho^2(1 + 3(A - C)\sin^2\theta - A), \qquad (5.100)$$

where $\theta = \arccos(z/r)$. The functions A, B, C and D are given by

$$A = 3\left[\frac{F^{(2)}}{r^3} + \frac{3F^{(1)}}{r^4} + \frac{3F}{r^5}\right], \qquad (5.101)$$

$$B = -\left[\frac{F^{(3)}}{r^2} + \frac{3\,F^{(2)}}{r^3} + \frac{6\,F^{(1)}}{r^4} + \frac{6\,F}{r^5}\right], \qquad (5.102)$$

$$C = \frac{1}{4}\left[\frac{F^{(4)}}{r} + \frac{2\,F^{(3)}}{r^2} + \frac{9\,F^{(2)}}{r^3} + \frac{21\,F^{(1)}}{r^4} + \frac{21\,F}{r^5}\right], \qquad (5.103)$$

$$D = A + C - 2B, \qquad (5.104)$$

$$F = f(t + r) - f(t - r), \qquad (5.105)$$

$$F^{(n)} \equiv \left[\frac{d^n f(x)}{dx^n}\right]_{x=t+r} - \left[\frac{d^n f(x)}{dx^n}\right]_{x=t-r}, \qquad (5.106)$$

with $r = \sqrt{x^2 + y^2 + z^2}$ and

$$f(x) = \varepsilon x\, e^{-(x/\varpi)^2}, \qquad (5.107)$$

so that at $t = 0$ we obtain a Gaussian pulse of width ϖ around the origin of the coordinate system.

The coordinate transformation $(z, \rho, \phi) \to (x, y, z)$ is defined in the usual way $\rho^2 = x \cdot x + y \cdot y$, $\phi = \arctan(y/x)$, providing the 3-metric in Cartesian coordinates.

The extraction quantities

The algebraic expressions involved in extraction are worked out up to $O(\varepsilon^2)$.

For the quadrupole solution described above the null vector $\ell^{(0)\mu}$ has the form

$$\ell^{(0)t} = 1, \tag{5.108}$$

$$\ell^{(0)x} = 2\frac{q}{P} + \varepsilon\frac{q}{P}\left(\gamma_1 + \frac{\gamma_2}{P} - \frac{\gamma_2}{P^2}\right) + O(\varepsilon^2), \tag{5.109}$$

$$\ell^{(0)y} = \pm 2\frac{p}{P} \pm \varepsilon\frac{p}{P}\left(\gamma_1 + \frac{\gamma_2}{P} - \frac{\gamma_2}{P^2}\right) + O(\varepsilon^2), \tag{5.110}$$

$$\ell^{(0)z} = \pm\frac{2-P}{P} + \varepsilon\left(\gamma_3 + \frac{\gamma_4}{P} \pm \frac{3\gamma_2}{2P^2} \mp \frac{\gamma_2}{P^3}\right) + O(\varepsilon^2). \tag{5.111}$$

The λ-derivative of the null vector at the world-tube Γ is given by

$$\ell^{(0)t}_{,\lambda} = \varepsilon\frac{6-6P+P^2}{P^2}\gamma_9, \tag{5.112}$$

$$\ell^{(0)x}_{,\lambda} = \varepsilon\frac{q}{P}\left(\gamma_5 + \frac{\gamma_6}{P} - \frac{\gamma_6}{P^2}\right), \tag{5.113}$$

$$\ell^{(0)y}_{,\lambda} = \pm\varepsilon\frac{p}{P}\left(\gamma_5 + \frac{\gamma_6}{P} - \frac{\gamma_6}{P^2}\right), \tag{5.114}$$

$$\ell^{(0)z}_{,\lambda} = \varepsilon\left(\gamma_7 + \frac{\gamma_8}{P} \pm \frac{3\gamma_6}{2P^2} \mp \frac{\gamma_6}{P^3}\right). \tag{5.115}$$

Equations (5.108) - (5.111) and (5.112) - (5.115) give some of the components of the Jacobian $\partial x^\alpha/\partial\tilde{y}^{\tilde{\beta}}$. The ones that still need to be specified are angular and time derivatives of ℓ^μ and $\ell^\mu_{,\lambda}$.

The expansion of the Bondi coordinate $r(u,\lambda,q,p)$ around Γ is given by

$$\begin{aligned} r(u,q,p,\lambda) = R_\Gamma \quad &+ \quad \varepsilon\frac{6-6P+P^2}{P^2}\gamma_{10} \\ &+ \quad \left(1 - \varepsilon\frac{6-6P+P^2}{P^2}\gamma_{11}\right)\lambda \\ &+ \quad O(\varepsilon^2)\,O(\lambda^2). \end{aligned} \tag{5.116}$$

The characteristic functions J, U, W can be expanded around the world-tube as follows:

$$J = \varepsilon\frac{q^2 - p^2 + 2Iqp}{P^2}\left(\gamma_{12} + \lambda\gamma_{13} + O(\lambda^2)\right) + O(\varepsilon^2), \tag{5.117}$$

$$U = \varepsilon\frac{(P-2)(q+Ip)}{P^2}\left(\gamma_{14} + \lambda\gamma_{15} + O(\lambda^2)\right) + O(\varepsilon^2), \tag{5.118}$$

$$W = \varepsilon\frac{6-6P+P^2}{P^2}\left(\gamma_{16} + \lambda\gamma_{17} + O(\lambda^2)\right) + O(\varepsilon^2). \tag{5.119}$$

The function $\beta^{(0)}$ is known once $r_{,\lambda}$ is given (see Eq. (5.74)). In linearized theory, one can write $\beta = \beta^{(0)} + O(\varepsilon^2)$ since, as it can be seen in Eq. (5.75), the expression $\beta_{,\lambda}$ is fully non-linear.
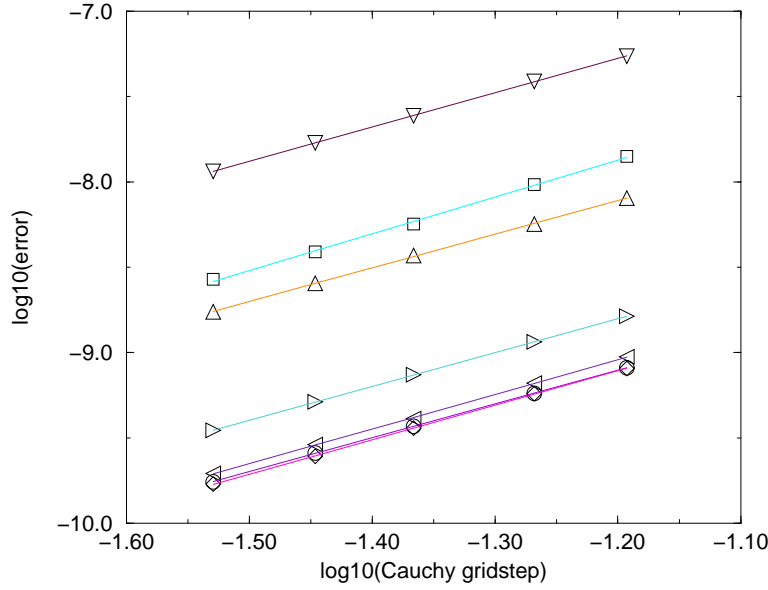
Fig. 5.2: Convergence test of the Bondi metric quantities J, $J_{,\lambda}$, β, U, $U_{,\lambda}$, W, $W_{,\lambda}$ for the quadrupole linear waves. The function $\beta_{,\lambda}$ has been omitted because it is $O(\varepsilon^2)$. The error is measured with the ℓ_∞ norm of the difference between numeric and analytic values, which was found to be $O(\Delta^{1.97})$. Parameters are $t = 2, R_\Gamma = 1, \varepsilon = 10^{-8}, \varpi = 0.5$.

The symbols $\gamma_{1\dots17}$ stand for functions defined on Γ that depend on the retarded-time coordinate u but not on the angular coordinates (q, p). Explicit expressions for $\gamma_{1\dots17}$ can be found in Appendix A.

Numeric results

The numeric extraction quantities were compared against the analytic results for grid sizes $32, 48, 64, 80$ and 96. All extraction quantities have been found to be second-order accurate, as seen from the slope of the convergence plot of the Bondi metric variables on the world-tube in Figure 5.2.

5.3.3   SIMPLE

Another test-bed was constructed starting from the non-linear, static, axisymmetric solution SIMPLE as described in [51]. The solution has already been mentioned on page 30 as a test-bed for the characteristic code. Here

we use it in a different gauge so that the axis of symmetry lies in the y-direction. This results in a more thorough test of the extraction algebra since the stereographic coordinate patches are symmetrized around the z-axis.

The space-time metric in Bondi null coordinates (u, r, θ, ϕ) takes the form

$$ds^2 \ ((\hat{V}/r)e^{2\hat{\beta}} - \hat{U}^2 r^2 e^{2\hat{\gamma}})du^2 + 2e^{2\hat{\beta}}du\,dr + 2\hat{U}r^2 e^{2\hat{\gamma}}du\,d\theta$$
$$-r^2(e^{2\hat{\gamma}}d\theta^2 + e^{-2\hat{\gamma}}sin^2\theta d\phi^2), \quad (5.120)$$

where

$$2e^{\hat{\gamma}} = 1 + \Sigma, \quad e^{2\hat{\beta}} = \frac{(1+\Sigma)^2}{4\Sigma}, \quad (5.121)$$

$$\hat{U} = -\frac{a^2\rho\sqrt{r^2 - \rho^2}}{r\Sigma}, \quad (5.122)$$

$$\hat{V} = \frac{r(2a^2\rho^2 - a^2r^2 + 1)}{\Sigma}, \quad (5.123)$$

$\rho = r\sin\theta, \Sigma = \sqrt{1 + a^2\rho^2}$, and a is a free scale parameter.

A coordinate transformation $(u, r, \theta, \phi) \rightarrow (u, \lambda, \theta, \phi)$ is first performed by solving the differential equation

$$d\lambda = e^{2\hat{\beta}}dr. \quad (5.124)$$

Even though $\hat{\beta}$ is known in terms of r, Eq. (5.124) cannot be integrated in closed form. Therefore $\hat{\beta}$ (and all subsequent expressions) are expanded in terms of a. Then, one obtains

$$\lambda + R_\Gamma = r + \frac{1}{80}r^5 sin(\theta)^4 a^4 + \cdots, \quad (5.125)$$

which determines r as a function of λ:

$$r = (\lambda + R_\Gamma) - \frac{1}{80}(\lambda + R_\Gamma)^5 sin(\theta)^4 a^4 + \cdots. \quad (5.126)$$

Here the integration constant of Eq. (5.124) has been fixed by the gauge condition

$$\lambda_{|a=0} = r - R_\Gamma. \quad (5.127)$$

This coordinate transformation provides an affine null metric. To change the axis of symmetry of the space-time first a Cartesian frame $(t, \hat{x}, \hat{y}, \hat{z})$ is defined by

$$u \ = \ t - \lambda, \quad (\lambda + R_\Gamma)^2 \ = \ \hat{x}^2 + \hat{y}^2 + \hat{z}^2,$$
$$\theta \ = \ \arccos\left(\frac{\hat{z}}{\lambda + R_\Gamma}\right), \quad \phi \ = \ \arccos\left(\frac{\hat{x}}{\sqrt{\hat{x}^2 + \hat{y}^2}}\right), \quad (5.128)$$

then the y and z axes are rotated by 90^0 according to

$$\hat{x} = x, \quad \hat{y} = z, \quad \hat{z} = -y. \tag{5.129}$$

Thus a Cartesian solution is constructed (in coordinates (t, x, y, z)), symmetric with respect to the y-axis. Using this Cauchy metric the algebraic steps prescribed by the extraction routine are followed to compute in the neighborhood of Γ the lightcone generators ℓ^α, the affine and the Bondi null metric, and the metric variables J, β, U, W.

In order to be able to give values for a that exploit the non-linear feature of the test-bed, we have worked out the expansion terms up to $O(a^{12})$. Expressions for r, J, β, U, W and their λ-derivatives can be found in Appendix B.

The extraction code showed proper, second order convergent behavior to the analytic results.

5.3.4 *Schwarzschild in differentially rotating null coordinates*

The Schwarzschild metric in outgoing Kerr-Schild coordinates $\hat{x}^\alpha$ is given by

$$ds^2 = -d\hat{t}^2 + d\hat{x}^2 + d\hat{y}^2 + d\hat{z}^2 + \frac{2m}{\hat{r}}(-d\hat{t} + \frac{\hat{x}d\hat{x} + \hat{y}d\hat{y} + \hat{z}d\hat{z}}{\hat{r}})^2, \tag{5.130}$$

where $\hat{r}^2 = \hat{x}^2 + \hat{y}^2 + \hat{z}^2$. (Equation (5.130) is obtained from the metric of a Kerr black hole Eq. (3.56), with angular momentum set to zero.) This metric and its derivatives on the world-tube $\hat{x}^2 + \hat{y}^2 + \hat{z}^2 = R_\Gamma^2$ can be used to provide the boundary values for a null coordinate system based upon the family of outgoing null cones emanating from the $\hat{t} = $ constant foliation. In a simple choice of null coordinates $\hat{y}^\alpha = (\hat{u}, \hat{r}, \hat{\theta}, \hat{\phi})$ associated with $\hat{x}^\alpha$ we have $\hat{u} = \hat{t} - \hat{r} + R_\Gamma$, $\hat{r} = \sqrt{\hat{x}^2 + \hat{y}^2 + \hat{z}^2}$, $\cos(\hat{\theta}) = \hat{z}/\sqrt{\hat{x}^2 + \hat{y}^2 + \hat{z}^2}$, $\tan(\hat{\phi}) = \hat{y}/\hat{x}$. This leads to the Eddington-Finkelstein version of the Schwarzschild metric,

$$ds^2 = -(1 - 2m/\hat{r})d\hat{u}^2 - 2d\hat{u}d\hat{r} - \hat{r}^2 q_{AB}d\hat{y}^A d\hat{y}^B. \tag{5.131}$$

The world-tube and the outgoing null cones have intrinsically spherically symmetric geometries. We obtain a non-spherically symmetric null metric, suitable for code testing, by introducing gauge freedom. We set $\hat{u} = u + \psi(u)$, $\hat{r} = r$, $\hat{\theta} = \theta$ and $\hat{\phi} = \phi + \xi(u, \theta)$, which leads to time-dependent β, J and U.

Unfortunately, no r-dependence in J can be introduced this way. The spherical symmetry of the null cone requires that its shear vanish, i.e. that $m^\alpha m^\beta k_{\alpha;\beta} = 0$, where k^α and the complex spacelike vector m^α span the

space tangent to the null hypersurface. In a null coordinate system (u, r, y^A) with angular metric h_{AB}, the shear free condition can be formulated as

$$q^A q^B (k_{A;B} - \frac{1}{2} h_{AB} h^{CD} k_{C;D}) = 0, \qquad (5.132)$$

which is equivalent to the requirement that $J_{,r} = 0$. So gauge transformations that preserve the world-tube and its foliation can introduce a non-vanishing J but $J_{,r}$ and consequently $\beta_{,r}$ vanish.

The Cartesian coordinates $\hat{x}^\alpha$ are also related to a differentially rotating Cartesian frame by x^α by $\hat{t} = t + \psi$, $\hat{x} = x \cos \xi - y \sin \xi$, $\hat{y} = x \sin \xi + y \cos \xi$ and $\hat{z} = z$. The x^α and y^α frames are related by the standard construction $u = t - r + R_\Gamma$, $r^2 = x^2 + y^2 + z^2$, $\theta(x, y, z) = \arccos(z/r)$, and $\phi = \text{arccot}(x/y)$.

The code tests are based upon extraction from the x^α frame to obtain the null metric in the y^α frame and on the reverse injection process. The explicit form of the Cartesian and null metrics are listed below.

Analytic results in Cartesian and Bondi coordinates

The Cartesian 3-metric, the lapse, and the shift are

$$g_{xx} = 1 \quad + \quad \frac{2 x^2 m}{r^3} - \frac{2 xyz \xi_\theta}{r^2 \rho} - \frac{2 x^2 z \rho \, \xi_\theta \, \xi_u}{r^3} + \frac{x^2 \rho^2 \xi_u{}^2}{r^2} + \frac{2 xy \xi_u}{r}$$

$$+ \quad \frac{x^2 z^2 \xi_\theta{}^2}{r^4} - \frac{x^2 (r - 2 m) \psi'(u)^2}{r^3} + \frac{4 x^2 m \psi'(u)}{r^3}, \qquad (5.133)$$

$$g_{yy} = 1 \quad + \quad \frac{2 y^2 m}{r^3} + \frac{2 xyz \xi_\theta}{r^2 \rho} - \frac{2 y^2 z \rho \xi_\theta \, \xi_u}{r^3} + \frac{y^2 \rho^2 \xi_u{}^2}{r^2} - \frac{2 xy \xi_u}{r}$$

$$+ \quad \frac{y^2 z^2 \xi_\theta{}^2}{r^4} - \frac{y^2 (r - 2 m) \psi'(u)^2}{r^3} + \frac{4 y^2 m \psi'(u)}{r^3}, \qquad (5.134)$$

$$g_{zz} = 1 \quad + \quad \frac{2 z^2 m}{r^3} + \frac{\rho^4 \xi_\theta{}^2}{r^4} + \frac{2 z \rho^3 \xi_\theta \xi_u}{r^3} + \frac{z^2 \rho^2 \xi_u{}^2}{r^2}$$

$$+ \quad \frac{z^2 (2 m - r) \psi'(u)^2}{r^3} + \frac{4 z^2 m \psi'(u)}{r^3}, \qquad (5.135)$$

$$g_{xy} = \quad \frac{2 xy m}{r^3} + \frac{xyz^2 \xi_\theta{}^2}{r^4} + \frac{(x^2 - y^2) \, z \, \xi_\theta}{r^2 \rho}$$

$$- \quad \frac{2 xyz \rho \xi_\theta \, \xi_u}{r^3} + \frac{xy \rho^2 \xi_u{}^2}{r^2} - \frac{(x^2 - y^2) \, \xi_u}{r}$$

$$- \quad \frac{xy (r - 2 m) \psi'(u)^2}{r^3} + \frac{4 xy m \psi'(u)}{r^3}, \qquad (5.136)$$

$$g_{xz} = \frac{2\,xzm}{r^3} - \frac{xz\rho^2\xi_\theta{}^2}{r^4} + \frac{y\rho\xi_\theta}{r^2}$$

$$+ \frac{x\rho\left(\rho^2 - z^2\right)\xi_\theta\,\xi_u}{r^3} + \frac{xz\rho^2\xi_u{}^2}{r^2}$$

$$+ \frac{xz\left(2\,m - r\right)\psi'(u)^2}{r^3} + \frac{4\,xzm\psi'(u)}{r^3} + \frac{yz\,\xi_u}{r}, \qquad (5.137)$$

$$g_{yz} = \frac{2\,yzm}{r^3} - \frac{yz\rho^2\xi_\theta{}^2}{r^4} - \frac{x\rho\xi_\theta}{r^2}$$

$$+ \frac{y\rho\left(\rho^2 - z^2\right)\xi_u\,\xi_\theta}{r^3} + \frac{yz\rho^2\xi_u{}^2}{r^2}$$

$$+ \frac{yz\left(2\,m - r\right)\psi'(u)^2}{r^3} + \frac{4\,yzm\psi'(u)}{r^3} - \frac{xz\xi_u}{r}, \qquad (5.138)$$

$$\alpha = \sqrt{\frac{1 + \psi'(u)}{1 + \frac{2m}{r} - \psi'(u)\left(1 - \frac{2m}{r}\right)}}, \qquad (5.139)$$

$$\beta^x = \frac{-2\,xm + x\left(r - 2\,m\right)\psi'(u) - yr^2\xi_u}{r\left[-\left(r - 2\,m\right)\psi'(u) + 2\,m + r\right]}, \qquad (5.140)$$

$$\beta^y = \frac{-2\,ym + y\left(r - 2\,m\right)\psi'(u) + xr^2\xi_u}{r\left[-\left(r - 2\,m\right)\psi'(u) + 2\,m + r\right]}, \qquad (5.141)$$

$$\beta^z = \frac{-2\,zm + z\left(r - 2\,m\right)\psi'(u)}{r\left[-\left(r - 2\,m\right)\psi'(u) + 2\,m + r\right]}, \qquad (5.142)$$

where

$$\rho = \sqrt{x^2 + y^2},$$
$$r = \sqrt{x^2 + y^2 + z^2},$$
$$\xi_\theta = \frac{\partial}{\partial\theta}\xi(u, \theta),$$
$$\xi_u = \frac{\partial}{\partial u}\xi(u, \theta),$$

with $\theta(x, y, z) = \arccos(z/r)$, and $u = t - r + R_\Gamma$.

Here $(u, r, \theta, \phi = \arccos(x/y))$ are the differentially rotating null coordinates y^α. The Bondi metric variables are

$$J = \frac{\left[2\left(q^2 - p^2\right) + 4iqp\right]}{P}\left[\frac{\xi_\theta^2}{P} + \frac{i\xi_\theta}{\sqrt{p^2 + q^2}}\right], \qquad (5.143)$$

$$J_{,\lambda} = 0, \qquad (5.144)$$

$$\beta = \frac{\ln(1 + \psi'(u))}{2}, \qquad (5.145)$$

$$\beta_{,\lambda} = 0, \tag{5.146}$$

$$U = \pm\frac{2\,\xi_u\,(p - Iq)}{P}, \tag{5.147}$$

$$U_{,\lambda} = 0, \tag{5.148}$$

$$W = \frac{(r - 2\,m)\,(1 + \psi'(u)) - r}{r^2}, \tag{5.149}$$

$$W_{,\lambda} = \frac{(-r + 4\,m)\,\psi'(u) + 4\,m}{r^3\,(1 + \psi'(u))}, \tag{5.150}$$

with $P = 1 + p^2 + q^2$, using the positive (negative) sign for the north (south) patch. Also it is known that

$$\begin{aligned}
\theta_N(q, p) &= 2\arctan(\sqrt{p^2 + q^2}), \\
\theta_S(q, p) &= 2\operatorname{arccot}(\sqrt{p^2 + q^2}).
\end{aligned}$$

The coordinate transformation $(u, \lambda, q, p) \to (t, x, y, z)$ is given by

$$x = 2\frac{\left(R_\Gamma + \frac{\lambda}{1 + \psi'(u)}\right) q}{1 + q^2 + p^2},$$

$$y = \pm 2\frac{\left(R_\Gamma + \frac{\lambda}{1 + \psi'(u)}\right) p}{1 + q^2 + p^2},$$

$$z = \pm\frac{\left(R_\Gamma + \frac{\lambda}{1 + \psi'(u)}\right) \cdot \left(1 - p^2 - q^2\right)}{1 + q^2 + p^2} \tag{5.151}$$

$$t = u + \frac{\lambda}{1 + \psi'(u)}. \tag{5.152}$$

All components of the null vector ℓ^α corresponding to this coordinate transformation are independent of λ:

$$\ell^\alpha_{,\lambda} = 0. \tag{5.153}$$

Test Results

With all extraction quantities worked out analytically, the solution provides a useful test-bed in calibrating the extraction module. Thus convergence rates were measured not only for the Bondi functions but also for the various terms involved in the coordinate transformations. The numeric results of the extraction module exhibited second order convergence to the analytic solution.

5.3.5 Dynamic black-hole space-times

In addition to the tests described in Sections 5.3.1 - 5.3.4, there are a number of test-beds used for calibrating the characteristic evolution whose boundary conditions were provided by the extraction module (see Section 3.4). The performance of those tests is not only a successful test of the characteristic code, but it also proves that the extraction module is able to provide boundary data for the characteristic code.

6. THE INJECTION MODULE

The injection module consists of a set of numerical routines that are designed to construct Cauchy boundary data. The module starts from the characteristic metric functions, performs the coordinate transformation

$$(u, r, q, p) \rightarrow (t, x, y, z),$$

and uses a number of interpolation routines to obtain the Cauchy metric at the Cartesian boundary gridpoints.

This chapter describes the injection module and its calibration in detail.

6.1 The physical algorithm

In injection, one first needs to define a 4-D region of space-time (with respect to the Bondi frame (y^β)) that surrounds the boundary of the Cauchy evolution domain. This is done using the location of the extraction worldtube Γ as computed in the extraction and the fact that injection will occur in an $O(\Delta)$ neighborhood of Γ.

In this region the Cartesian coordinates $x^\alpha = (t, x, y, z)$ need to be expressed as functions of the Bondi coordinates, i.e. we need the dependence $x^\alpha = f(y^\beta)$. We also need the Jacobian terms $\partial x^i / \partial y^\beta$. First the parameter λ is computed as an integral starting from $\Gamma_{u=t}$:

$$\lambda(y^\beta) = \int_{\Gamma_u}^r \frac{dr}{r_{,\lambda}} = \int_{\Gamma_u}^r e^{2\beta} dr \tag{6.1}$$

where β is known from the characteristic evolution. During the integration of Eq. (6.1) the coordinates (u, q, p) are held fixed.

Next the values (x^α) are evaluated as an expansion around Γ:

$$x^\alpha = x^{(0)\alpha} + \lambda \ell^{(0)\alpha} + O(\lambda^2). \tag{6.2}$$

The Jacobian terms $\partial x^i / \partial y^A$ and $\partial x^i / \partial u$ can be computed up to $O(\lambda^2)$, by taking angular and time derivatives of Eq. (6.2). The remaining Jacobian

terms $\partial x^i / \partial r$ are computed in the same manner as x^α, i.e. as an expansion around Γ:

$$x^i_{,r} = \frac{\partial x^i}{\partial \lambda} \frac{\partial \lambda}{\partial r} = e^{2\beta} \left(\ell^{(0)i} + \lambda \ell^{(0)i}_{,\lambda} + O(\lambda^2) \right). \tag{6.3}$$

In Eqs. (6.2) - (6.3) the quantities $x^{(0)\alpha}, \ell^{(0)\alpha}$ and $\ell^{(0)\alpha}_{,\lambda}$ are provided by the extraction module.

Next the Bondi metric tensor $\eta^{\alpha\beta}$ is constructed using the values J, β, U and W:

$$\eta^{rr} = e^{-2\beta} \left(r \cdot W + 1 \right), \tag{6.4}$$

$$\eta^{rq} = -\frac{P}{2} e^{-2\beta} \cdot \Re(U), \tag{6.5}$$

$$\eta^{rp} = -\frac{P}{2} e^{-2\beta} \cdot \Im(U), \tag{6.6}$$

$$\eta^{qq} = \left(\frac{P}{2r} \right)^2 \left(K - \Re(J) \right), \tag{6.7}$$

$$\eta^{qp} = \left(\frac{P}{2r} \right)^2 \left(-\Im(J) \right), \tag{6.8}$$

$$\eta^{pp} = \left(\frac{P}{2r} \right)^2 \left(K + \Re(J) \right), \tag{6.9}$$

$$\eta^{ru} = -e^{-2\beta}, \quad \eta^{qu} = \eta^{pu} = \eta^{uu} = 0. \tag{6.10}$$

The spatial components of the Cauchy metric are then given by

$$g^{ij} = \frac{\partial x^i}{\partial y^\alpha} \frac{\partial x^j}{\partial y^\beta} \eta^{\alpha\beta}. \tag{6.11}$$

Recall that Eqs. (6.1) - (6.11) are applied in an infinitesimal, 4-D neighborhood of the spacelike Cauchy boundary region. Thus the 4-metric components g^{ij} can be evaluated at the Cauchy injection time t_{inj}. Furthermore, at this time-level the gauge functions α, β^i (lapse and shift) are known. Also, recall from Section 2.3.1 that for a Cauchy slice $\Sigma_{t_{inj}}$ with time-like unit normal $n^\alpha = \left(\frac{1}{\alpha}, \frac{-\beta^i}{\alpha} \right)$ the space-time metric components g^{ij} and the intrinsic metric $^{(3)}g^{ij}$ of the 3-D Cauchy surface are related by

$$^{(3)}g^{ij}_{|t_{inj}} = g^{ij}_{|t_{inj}} + n^i n^j. \tag{6.12}$$

Thus, we have obtained the contravariant 3-metric $^{(3)}g^{ij}$ at the injection time t_{inj}. Given that $^{(3)}g^{ij}\, ^{(3)}g_{jk} = \delta^i_k$, the covariant 3-metric $^{(3)}g_{ij|t_{inj}}$ is obtained via an elementary matrix inversion.

6.2 Implementation

Let $\left\{\Lambda^{[I]}\right\}_{I=1\cdots M}$ be a set of spherical world-tubes concentric with Γ with radii $R^{[I]}$, defined by $\sqrt{x^2 + y^2 + z^2} = R^{[I]}$. Let $\Lambda_t^{[I]}$ denote the intersection of $\Lambda^{[I]}$ with the Cauchy slice Σ_t. Let the set of Cartesian radii $R^{[I]}$ be equally spaced, with $R^{[I+1]} - R^{[I]} = O(\Delta)$, such that all Cauchy boundary points are contained between the two spheres $\Lambda_t^{[1]}$ and $\Lambda_t^{[M]}$ for all t. Note that in previous chapters, for simplicity, a single injection world-tube Λ was introduced which in the current context is identified with $\Lambda^{[M]}$, i.e. $R_\Lambda \equiv R^{[M]}$.

Defining a 4-D space-time region that surrounds the Cauchy boundary region amounts to selecting a subset $\mathcal{S}_{Null}$ of the characteristic grid that surrounds the set of world-tubes $\left\{\Lambda^{[I]}\right\}_{I=1\cdots M}$ in a 4-D sense.

This subset $\mathcal{S}_{null}$ extends from the extraction world-tube Γ to a few grid-zones outside the injection world-tube $\Lambda^{[M]}$. Since the location of $\Lambda^{[M]}$ is defined with respect to Cartesian coordinates, in the Bondi frame it changes shape and location during the numerical evolution. Thus the choice of $\mathcal{S}_{null}$ can be done in two ways:

- Choose $\mathcal{S}_{null}$ once (at the first iteration) such that it surrounds not only $\Lambda^{[M]}$ but a sphere of a larger radius $(1 + f) \cdot R^{[M]}$ with $f > 0$ a safety factor. Then the correctness of the choice of f needs to be monitored time-step after time-step.

- Another alternative is to choose $\mathcal{S}_{null}$ dynamically, i.e. at each time-step localize $\Lambda_t^{[M]}$ in Bondi coordinates and use null gridpoints that adequately cover the Cauchy injection points.

The current implementation of the injection module uses the first way.

Let u_n label the last time level of the characteristic evolution. Then computation of the Cartesian coordinate values (x^α) and of the Jacobian terms $\partial x^i / \partial y^\beta$ is done at the retarded time $u_{n-1/2} \equiv u_n - \frac{1}{2}\Delta u$, where $\Delta u = \Delta t$. Furthermore, the $O(\lambda)$ terms of $\partial x^i / \partial y^A$ are computed via second-order finite-difference formulae for the angular derivatives, with the $O(1)$ terms known analytically. In a similar way, with a vanishing $O(1)$ term in $\partial x^i / \partial u$, the $O(\lambda)$ term is computed using

$$\left(\frac{\partial x^i}{\partial u}\right)_{|u_{n-1/2}} = \frac{x_{u_n}^i - x_{u_{n-1}}^i}{\Delta u} + O(\Delta^2). \tag{6.13}$$

The contravariant Bondi and Cauchy metric components are computed using Eqs. (6.4) - (6.10) and (6.11) applied at $u = u_{n-1/2}$.

At this point the Cauchy metric components g^{ij} are known on a set of gridpoints (r_k, q_i, p_j), at a number of retarded time levels $u_{n-1/2}, u_{n-3/2}$, etc. (Results from previous time-steps are assumed to be known.) Furthermore, all characteristic gridpoints are labeled not only by their Bondi coordinates (u, r, q, p), but also by their Cartesian coordinates $x^\alpha = (t, x, y, z)$.

In order to compute the quantity $^{(3)}g_{ij}$ at a Cartesian boundary grid point labeled by (t_{inj}, x^*, y^*, z^*), the injection module decomposes the problem of 4-D interpolation into a number of simpler problems:

First a radial interpolation is performed in terms of $\hat{r} = \sqrt{x^2 + y^2 + z^2}$. The 1-D interpolation is done along characteristics labeled by (u, q, p), computing the quantities g^{ij} and (x^α) at the intersection points between these characteristics and the world-tubes $\Lambda^{[I]}$. The results of this first interpolation are the functions g^{ij} and (x^α) at the 2-D surfaces $\Lambda^{[I]}_{u_{n-1/2}}$.

Next the injection module uses the outcome of the same interpolation from previous time-steps, given on $\Lambda^{[I]}_{u_{n-3/2}}, \Lambda^{[I]}_{u_{n-5/2}}$, etc. to perform a 1-D time-interpolation (keeping (q, p) and $\hat{r}$ constant) and obtain the functions g^{ij} and (x^i) at the spheres $\Lambda^{[I]}_{t_{inj}}$.

Given the lapse function α and the shift vector β^i, the contravariant 3-D Cauchy metric $^{(3)}g^{ij}$ is constructed using Eq. (6.12). Then the covariant 3-D Cauchy metric $^{(3)}g_{ij}$ is obtained.

It remains to transfer data from the spheres $\Lambda^{[I]}_{t_{inj}}$ to the actual Cartesian injection points (t_{inj}, x^*, y^*, z^*). Recall that the gridpoints of $\Lambda^{[I]}_{t_{inj}}$ are labeled by Cartesian coordinate values (x, y, z). These values come from a radial and a time interpolation that is performed starting from a Bondi grid. Thus the spherical grid of $\Lambda^{[I]}_{t_{inj}}$ is irregular in the Cartesian frame. The angular dimensions are resolved via spherical decomposition that represents the Cauchy metric $^{(3)}g_{ij}$ with a set of coefficients $c^{[I]ij}_{\ell m}$ for each sphere $\Lambda^{[I]}_{t_{inj}}$. The angular coordinates used in the decomposition are defined on $\Lambda^{[I]}$ by

$$\hat{q}(x^i) = \frac{x}{R^{[I]} \pm z}, \quad \hat{p}(x^i) = \pm\frac{x}{R^{[I]} \pm z} \tag{6.14}$$

on the north $(+)$ and south $(-)$ patches.

Finally, the Cauchy metric $^{(3)}g_{ij}$ is evaluated at the injection points (t_{inj}, x^*, y^*, z^*). When doing so first the angular coordinates (q^*, p^*) of the injection point are computed using the analog of Eq. (6.14). Then the metric functions $^{(3)}g_{ij}$ are reconstructed from the coefficients $c^{[I]ij}_{\ell m}$, at the angular coordinates given by (q^*, p^*), at a number of spheres $\Lambda^{[I]}_{t_{inj}}$ surrounding the Cartesian injection point. Lastly a radial interpolation is performed.

The injection routine has the option to perform all three 1-D interpolations using two, three, or four gridpoints.

6.3 Calibration

All test-beds described for the extraction module have been used to test the CCM algorithm as a whole. When doing so we have proceeded as follows: At $t_{[0]} = u_{[0]} = 0$ give initial data analytically on the Cauchy and characteristic slices. Then give analytic Cauchy data at the next time-level $t_{[1]} = \Delta t$. Use the numeric extraction module, characteristic evolution code, and injection module to compute the Cauchy boundary values, as provided by CCM, in the injection domain surrounding Γ. Then iterate the procedure, i.e. give Cauchy data at $t_{[2]} = 2\Delta t$, use extraction, null evolution and injection, and so on until some final time $t = t_f$. At this final time-step the error in the injection is compared to the analytic Cauchy metric. Repeating the procedure for higher and higher grid-sizes provides information about the convergence rate of CCM as $\Delta \to 0$. An overall second-order convergence was confirmed.

In addition, to obtain a stricter test of the injection module, the following approach was used. Take a solution that is known in Bondi and in Cartesian coordinates, as well as the coordinate transformation as computed in the extraction module. Using these, build analytically the results that the injection module will produce with an error of $O(\Delta^2)$. Recall that injection is designed to be an $O(\lambda^2)$ algorithm. Since $\lambda > \Delta x$, for certain grid sizes an error larger than $O(\Delta^2)$ might be masked by the $O(\lambda^2)$ error. By performing the operations prescribed for the injection in some computer algebra utility, one can construct the functions $x^\alpha = f(y^\beta) + O(\lambda^2)$ in the same fashion as in the injection. Then the Cauchy metric components can be constructed. The computer algebra result must be identical with the numerical result except for the $O(\Delta^2)$ discretization error in the injection module.

The test was performed for the linear quadrupole waves. Obtaining the solution in Bondi coordinates is a nontrivial problem by itself that is addressed in Appendix C. Here only the outcome of the numerical convergence test is quoted.

All interpolation routines and the spherical decomposition-reconstruction routines were checked for convergence and showed the correct convergence rates. It should be noted that although interpolation can be done up to $O(\Delta^4)$, there are a number of operations in injection that are performed to $O(\Delta^2)$. See Eq. (6.13) for an example. A convergence plot of the whole injection module is given in Figure 6.1, using the various interpolation routines. The graph shows second order convergence. Besides testing the outcome of the whole injection module, tests were performed to ensure that the Cartesian coordinates of the characteristic gridpoints (x^α), the Jacobian terms $\partial x^i / \partial y^\beta$, the Bondi metric $\eta^{\alpha\beta}$, and the Cauchy metric components
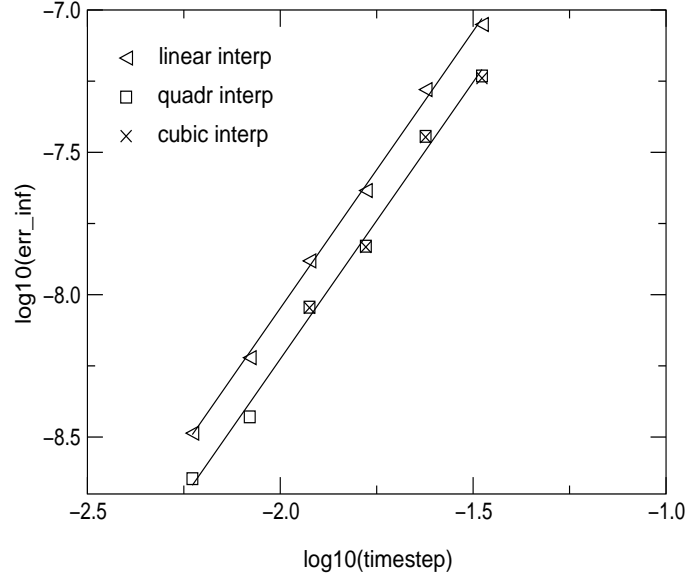
Fig. 6.1: g_{xy} as provided by the injection module at Cauchy boundary points. The test-bed is based on the quadrupole linear waves with parameters $t = 1, R_\Gamma = 1, \varpi = 0.5$, and $\varepsilon = 10^{-8}$. The spherical decomposition was done up to $\ell = 4$, with a discretization error of $O(\Delta^2)$. The error in g_{xy} was measured with the ℓ_∞ norm to be less than $O(\Delta^{1.94})$.

g^{ij}, $^{(3)}g^{ij}$ and $^{(3)}g_{ij}$ are computed to $O(\Delta^2)$ with respect to the analytic λ-expansion.

7. STABILITY OF CCM

In this chapter a variety of numerical experiments are presented to test the CCM modules in a numeric environment. While both the extraction and the injection modules show second-order accuracy with respect to a number of test-beds, this does not guarantee the numerical stability of CCM as an interface between the general relativistic Cauchy and characteristic evolution codes. The Cauchy system used in this chapter is the ADM formulation (see section 2.3.2, also [2, 3]), developed by the Binary Black Hole Grand Challenge Alliance [116].

7.1 Blending

After the implementation and calibration of the CCM modules, it was found that unstable (exponentially growing) numerical modes arise at the interface between the two evolution codes. Since the wavelength of those modes was typically $O(\Delta)$, various smoothing techniques were tested. Least-square fitting (see Section 5.1.2) did not bring the expected improvement. A technique that improved the fore-stated exponential growths in certain circumstances is the following "blending" technique [117].

The 3-D metric $^{(3)}g_{ij}^{(Cauchy)}$ is determined by the Cauchy evolution at all Cartesian evolution gridpoints. In order to provide boundary data $^{(3)}g_{ij}^{(Bdry)}$, one can apply the condition

$$^{(3)}g_{ij} = f(x^i) \cdot {}^{(3)}g_{ij}^{(Cauchy)} + (1 - f(x^i)) \cdot {}^{(3)}g_{ij}^{(Bdry)} \qquad (7.1)$$

where $f(x^i)$ is a smooth function that vanishes at the boundary grid-points and has the value 1 for all evolution gridpoints that are at least a distance w away from the boundary point. The zone over which $1 < f < 0$ is the blending zone, with a blending width w. A blending zone of width zero amounts to Dirichlet boundary conditions.

Applying analytic boundary conditions with no blending results in an unstable ADM evolution for the linearized quadrupole waves. Analytic boundary conditions blended over an $O(\Delta)$ region give an improved behavior for the same analytic solution. Also, the full non-linear ADM system

with smooth initial data of linear order and blended flat boundary conditions (i.e., in Eq. (7.1) set $^{(3)}g_{ij}^{(Bdry)} = \delta_{ij}$) run for hundreds of crossing times without any signs of instability [117]. Blending has also brought improvement in matching Cauchy evolution to perturbative spherical evolution [118].

Even though the use of blending postpones the appearance of exponential modes in most settings, it does not remove the numerical instability in all cases. For instance, constraint violating random initial data with blended flat boundary conditions resulted in a numerically unstable run.

7.2 "No feedback" experiments

As shown in Figure 7.1, matching consists of a closed loop. If the numerical amplification matrix of the finite-difference algorithm has any eigenvalue with absolute value greater than one, an exponential mode is generated that poisons the evolution of physical data. A finite-difference stability analysis of the coupled code is too complicated to be carried out. Thus the numerical stability of the system is investigated via numerical experiments.

To investigate the potential problems arising from feedback, a series of numerical experiments was designed where the loop is broken at various points with analytic data.

The experiments were based on the quadrupole linearized solution. The Cauchy metric is defined in Section 5.3.2. The characteristic metric is provided as an expansion in terms of the affine parameter λ and is given in Appendix C.

The radius of the extraction world-tube is set to $R_\Gamma = 1$. The amplitude and the width of the time-symmetric wave packet are set to $\varepsilon = 10^{-8}$, $\varpi = 0.5$. The CFL ratio is given by $\Delta t/\Delta x = 0.25$.

In all of these experiments the injected Cauchy metric is worked out up to $O(\lambda^3)$. Blending is used over a region of three Cauchy gridpoints. Since runs with a closed loop show rapidly growing instabilities, most runs were performed up to $t = 20R_\Gamma$. Each set of experiments was run with a number of different grid sizes.

7.2.1 Analytic injection data

In the first set of experiments the Cauchy boundary data is an analytic expansion up to $O(\lambda^3)$ of the exact solution

$$g_{ij}^{injected} = g_{ij}^{exact} + O(\lambda^3). \tag{7.2}$$

A schematic diagram of the setup of the run can be seen on the left side of Figure 7.2.
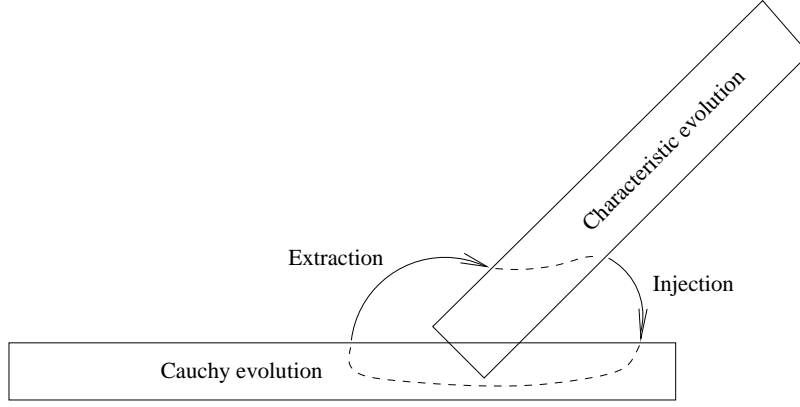
Fig. 7.1: The loop created by CCM. Extraction data is taken from the Cauchy code and used as boundary data for the characteristic code. This is evolved along the characteristics and feeds into the injection module which constructs the Cauchy boundary data. Lastly, the Cauchy evolution propagates data from its boundaries back to the domain of dependence of the extraction module.

The experiment tests whether the $O(\lambda^3)$ error induces any short-range instabilities. Runs were performed with grid sizes $32^3, 48^3, 64^3, 80^3$, up to $t = 20$. As it can be seen in Figure 7.3, short-term instabilities did not develop.

7.2.2 Analytic extraction and characteristic data

In the next set of runs the injection is numeric, but it is fed by analytic extraction and characteristic data. The Bondi metric variables (J, β, U, W) are given as an $O(\lambda^7)$ expansion around the extraction world-tube Γ. Similar to the case of analytic injection data, no short-time instabilities were seen. Runs were performed for grid sizes 48^3 and 64^3. See the right-hand plot of Figure 7.2 for a schematic diagram of the numerical setup. Surface plots of $^{(3)}g_{xy}$ after the first time-step and at $t = 20$ are provided in Figure 7.4. At the time-scale of the run no boundary instabilities were seen.

7.2.3 Analytic extraction data

In the third stage characteristic evolution and injection are numeric. Thus the discretization noise of the characteristic evolution and the injection are fed into the Cauchy evolution. Extraction data in these runs is analytic. In other words the extraction module is replaced by a set of functions that
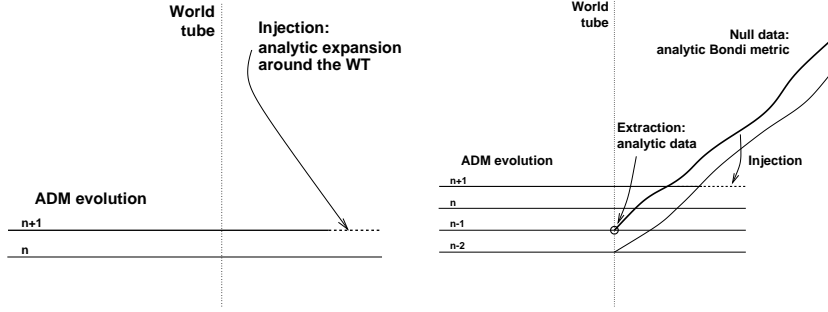
Fig. 7.2: Left: the scheme of the runs performed with analytic $O(\lambda^3)$ injection data. Right: the scheme of the runs performed with analytic extraction and characteristic data, and numeric injection data.

provide the extraction results analytically. These analytic results are used as boundary data for the characteristic evolution and in the injection. A scheme of the setup can be seen in Figure 7.5, on the left. Runs were made up to $t = 20$, for grid sizes of $32^3, 48^3$, and 64^3. Figure 7.6 contains surface plots of $^{(3)}g_{xy}$ at the beginning and the end of the runs. The runs did not reveal short time-scale instabilities.

7.2.4 Extraction from analytic Cauchy data

In the next stage the extraction, characteristic evolution and injection are numeric. However, in order to avoid a closed loop, input data for the extraction module is provided by a Cartesian grid containing analytic Cauchy data. Thus, in addition to the previous run, the numerical noise coming from the extraction module is fed into the characteristic evolution and the injection. The right hand side of Figure 7.5 shows the setup of the runs. Grid sizes were 32^3 and 40^3. Surface plots of $^{(3)}g_{xy}$ at $z = 0$ are provided in Figure 7.7. These runs revealed no exponentially growing modes.

7.2.5 Extraction from decoupled numeric Cauchy data

In the last set of runs there are two Cauchy codes involved. The first is provided analytic boundary data, and it serves as numeric input for the extraction module, characteristic evolution, and injection that provide boundary data for the second Cauchy code. A schematic diagram illustrating the numerical setup can be seen on Figure 7.8. Grid sizes were 32^3 and 48^3. Due to the extensive hard-disk usage of the experiment, the runs lasted only up to $t = 10$. Surface plots of the metric component $^{(3)}g_{xy}$ at $z = 0$ can be
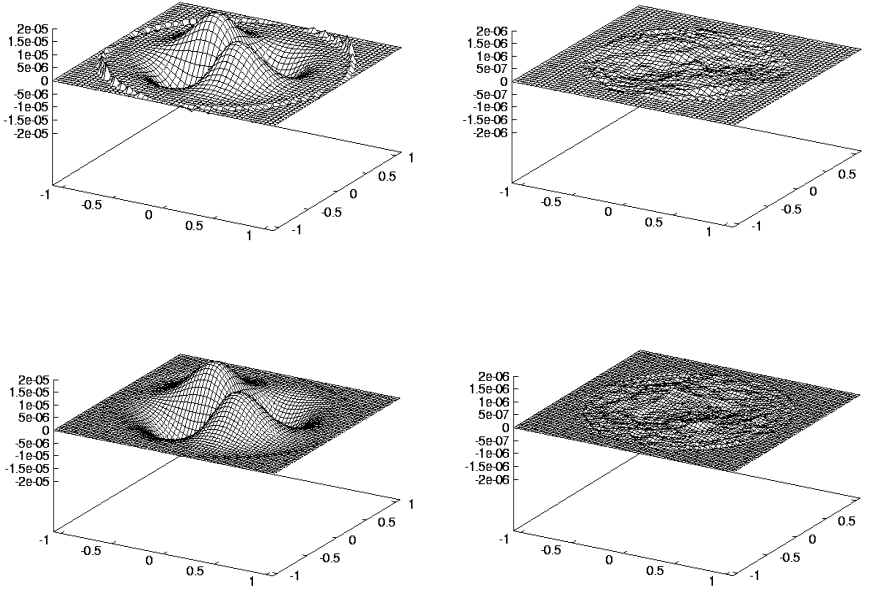
Fig. 7.3: Cauchy run with analytic boundary data as an expansion around the extraction world-tube. All plots represent $z = 0$ slices of the metric component $^{(3)}g_{xy}$. Top left: the Cauchy data is shown after one time-step for a grid size of 48^3. The same run, at time $t = 20$ can be seen on the top right plot. The bottom left and right plots are the first and the last time-step of a 64^3 grid run up to $t = 20$. Comparing the initial time-step for the two different grids, one can see that as the injection zone converges to the extraction world-tube, the effects of the λ-expansion converge to zero.
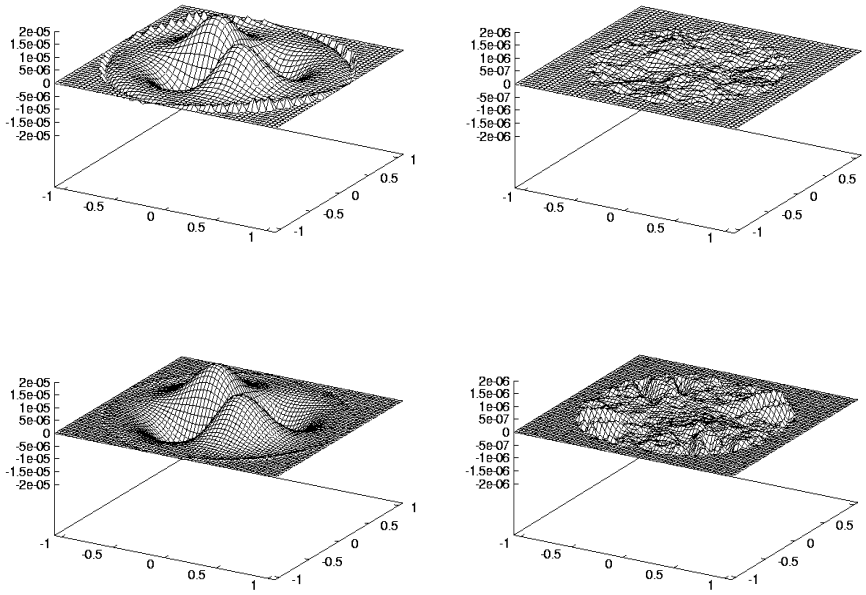
Fig. 7.4: Cauchy run with analytic extraction and characteristic data, with numeric injection. All plots represent $z = 0$ slices of the metric component $^{(3)}g_{xy}$. Top left: the Cauchy data is given after one time-step, for a grid size of 48^3. The same run, at time $t = 20$ can be seen on the top right plot. The bottom left and right plots are the first and the last time-step of a 64^3 grid run up to $t = 20$.
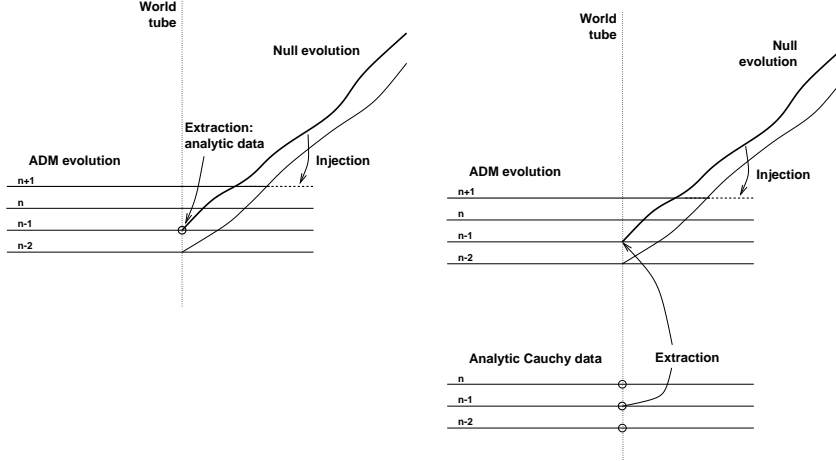
Fig. 7.5: Left: the scheme of the runs performed with analytic extraction data, numeric characteristic evolution and injection. Right: the scheme of the runs performed with numeric extraction fed by analytic Cauchy data.

seen on Figure 7.9. Although the numerical noise left in the grid is larger in this case then for the previous runs, no numerical instabilities were seen at the time-scale of the run.

7.3   The fully coupled problem

The main conclusion of the runs from the previous section is that numerical noise by itself will not destabilize the Cauchy-CCM system on a short term. The question then is: What is destabilizing the full Cauchy-CCM system? In order to shed light on the issue a run was performed using the fully coupled system, a Cartesian grid of 32^3 points, with a blending width of $3\Delta x$. Then the run was repeated using the same grid-spacing Δx and same world-tube radius but with blending over a region of $6\Delta x$. The result from the two runs is plotted in Figure 7.10. As it can be seen, the smaller the cavity between the extraction world-tube Γ and the outermost injection world-tube Σ ($= \Sigma^{[M]}$), the steeper the exponential time dependence of the ℓ_∞ norm of $^{(3)}g_{ij}$. But even if one uses a large $\Gamma - \Sigma$ cavity, the exponential mode is there. Furthermore the convergence radius of the λ-expansion used in the injection module is limited, and thus one must not separate the two world-tubes excessively.

An alternative to the Dirichlet data used at the Cauchy boundary is
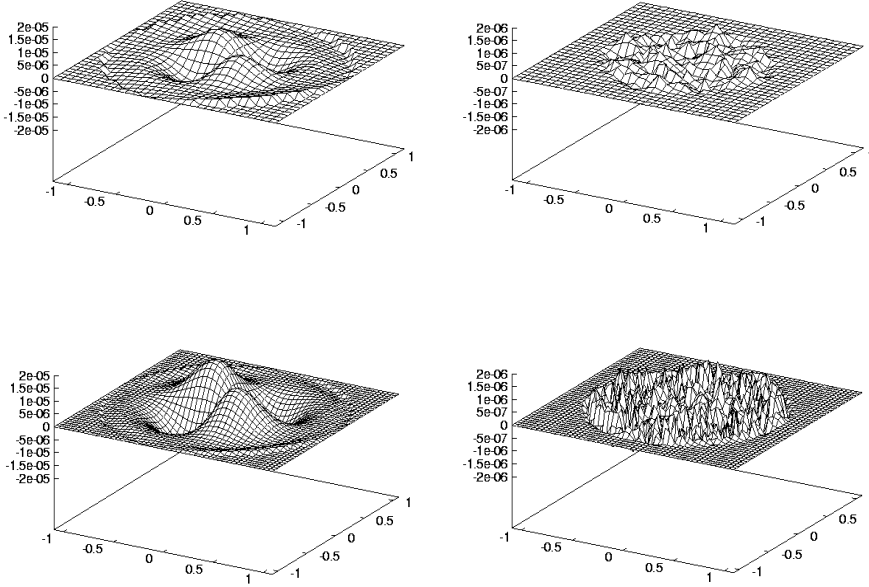
Fig. 7.6: Cauchy run with analytic extraction data, numeric characteristic evolution and injection. All plots represent $z = 0$ slices of the metric component $^{(3)}g_{xy}$. Top left: the Cauchy data is shown after one time-step for a grid size of 32^3. The same run, at time $t = 20$ can be seen on the top right plot. The bottom left and right plots are the first and the last time-step of a 48^3 grid run up to $t = 20$.
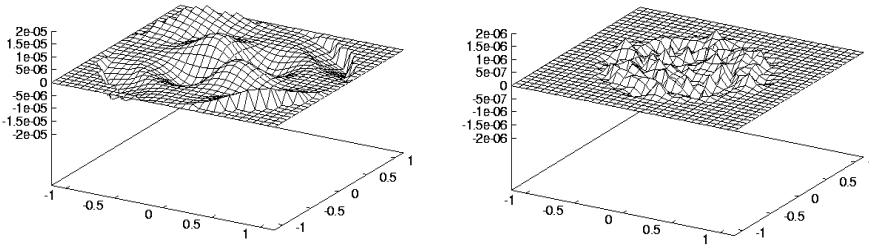
Fig. 7.7: Cauchy run with numeric extraction data, with the extraction module fed by analytic Cauchy data. Characteristic evolution and injection are numeric as well. All plots represent $z = 0$ slices of the metric component $^{(3)}g_{xy}$. Left: the Cauchy data is shown after one time-step for a grid size of 32^3. The same run at time $t = 20$ can be seen on the right plot.
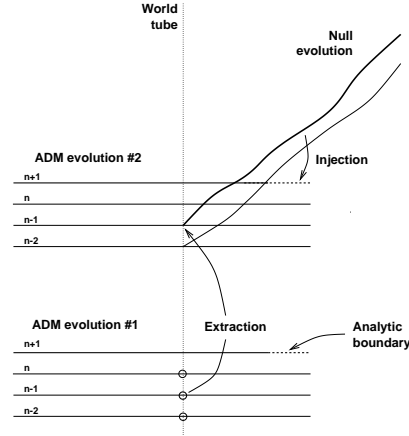
Fig. 7.8: Double Cauchy evolution. The first code serves as a numeric input for the CCM routines attached to the second Cauchy code.
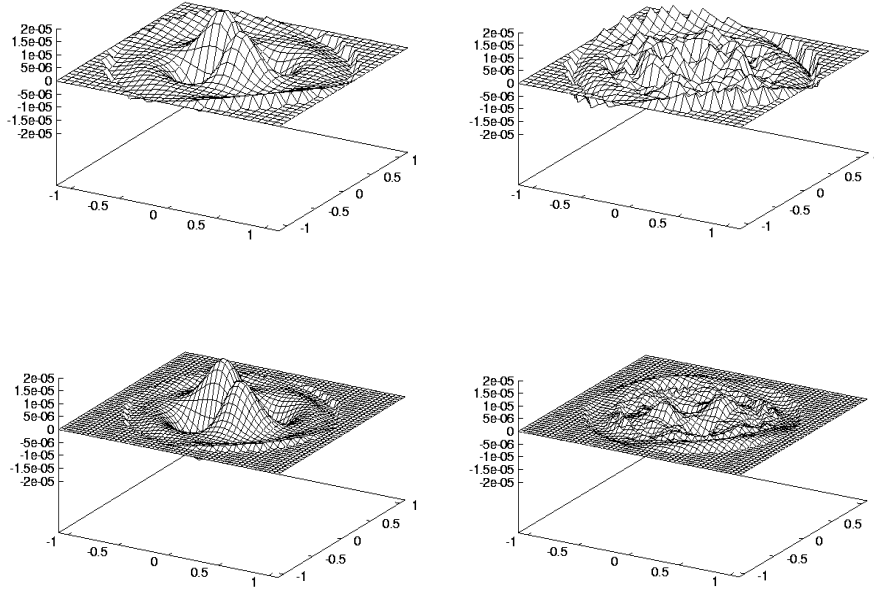
Fig. 7.9: Results for the double set of Cauchy runs. All plots represent $z = 0$ slices of the metric component $^{(3)}g_{xy}$. Top left: the Cauchy data is shown after one time-step for a grid size of 32^3. The same run at time $t = 10$ can be seen on the top right plot. The bottom left and right plots are the first and the last time-step of a 48^3 grid run up to $t = 10$.
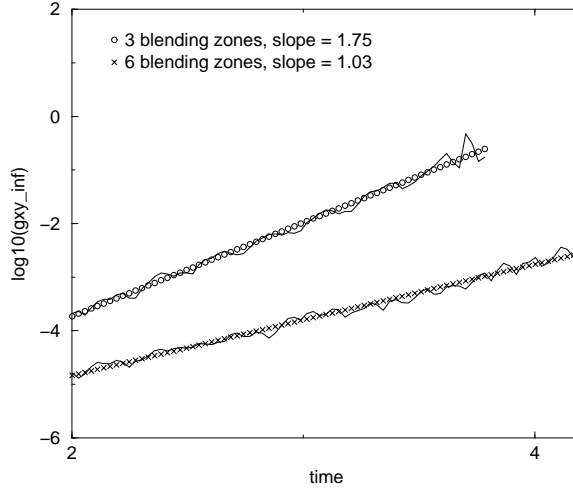
Fig. 7.10: The runs with the fully coupled Cauchy+Characteristic codes demonstrate exponential growth versus the number of blending zones. Grid size for both runs is 32^3.

a Sommerfeld outgoing radiation condition. It performed better then the Dirichlet condition, so a "modified Sommerfeld" version of the injection module has been implemented.[1] The details of implementation will not be given, for not even the outgoing radiation condition has solved the problem. During the period of time when these experiments were done, it was found that the iterative Crank-Nicholson evolution scheme[2] is not unconditionally stable with respect to the number of iterations performed. One must do two or three, or six or seven, etc. iterations but not four or five iterations, etc. [119]. Still, with the lessons applied, the boundary module did not achieve stability.

In order to shed light on the problem, we undertook a systematic study of the linearized ADM equations and properties of a variety of evolution codes and boundary conditions. Chapters 8 and 9 describe this study. As it is shown, the coupled set of partial-differential equations that form the principal part of the ADM equations needs appropriate boundary conditions. In particular, one should not specify boundary-values to six metric compo-

---

[1] The modified Sommerfeld version in a CCM context is written in the form

$$(\partial_t + \partial_r)\,^{(3)}g_{ij}^{Cauchy} = (\partial_t + \partial_r)\,^{(3)}g_{ij}^{characteristic}. \tag{7.3}$$

See [4] for implementation of the modified Sommerfeld condition for the case of SWE.

[2] See Section 8.2.5 for a description of the iterative Crank-Nicholson evolution scheme.

nents, but provide the two radiation degrees of freedom and use a set of boundary constraints that determine the remaining four components of the metric tensor at the boundary. Thus the fact that CCM (as well as all other boundary conditions used so far with the ADM code) sets boundary values to all six metric components gives rise to an ill-posed problem. This accounts for at least one source of the instabilities that are seen. There might be other numerical problems, but those cannot be studied before implementation of a consistent spherical boundary is worked out for a Cartesian Cauchy code.

8. LINEARIZED CARTESIAN CAUCHY EVOLUTION

This chapter discusses the stability properties of numerical implementations of the linearized ADM equations in Cartesian coordinates, as defined in Section 8.1. Throughout this chapter the slicing is geodesic, that is the lapse and shift are fixed by

$$\alpha = 1, \quad \beta^i = 0. \tag{8.1}$$

Four different finite-difference algorithms are compared. The issue of consistent boundary conditions is also addressed. A robust stability test is defined and used to check the stability properties of the various evolution algorithms with various boundary conditions. Some of the results presented in this chapter can be also found in [62].

Throughout this Chapter we use Greek letters for space-time indices and Latin letters for spatial indices. Four dimensional geometric quantities are explicitly indicated, such as $^{(4)}R_{\alpha\beta}$ and $^{(4)}G_{\alpha\beta}$ for the Ricci and Einstein tensors of the space-time, whereas R_{ij} and R refer to the Ricci tensor and Ricci scalar of the Cauchy hypersurfaces. These quantities are computed to linear order throughout this and the following Chapter.

The main question we ask for a number of numerical codes is whether they are "stable" or "unstable". In the case of a scalar field we call an evolution unstable if the ℓ_∞ norm of the field grows exponentially with time. Otherwise the evolution is called "stable". In the case of the Linearized Gravitational (LG) equations we use the Hamiltonian constraint to monitor if exponential modes are present in the evolution. An exponentially growing Hamiltonian constraint is the signature of an unstable run.

8.1   Linearized field equations in Cartesian coordinates

The space-time is treated as a perturbation around flat space. In Cartesian coordinates (t, x, y, z) the linearized metric can be written as

$$^{(4)}g_{\alpha\beta} = {}^{(4)}\eta_{\alpha\beta} + {}^{(4)}h_{\alpha\beta}, \tag{8.2}$$

where $^{(4)}\eta_{\alpha\beta}$ is the Minkowski metric $^{(4)}\eta_{\alpha\beta} = \mathrm{diag}(-1, 1, 1, 1)$. The gauge condition Eq. (8.1) implies $^{(4)}h_{t\alpha} = 0$.

We also use the notation

$$
\begin{aligned}
\dot{f} &\equiv \partial_t f\,, & (8.3) \\
h &\equiv \eta^{ij} h_{ij} = h_i^i\,, & (8.4) \\
h^{ij} &\equiv \eta^{in} \eta^{jm} h_{nm}\,. & (8.5)
\end{aligned}
$$

The Hamiltonian and momentum constraints are

$$
\mathcal{C} := {}^{(4)}G_{tt}\,, \quad \mathcal{C}_i := -{}^{(4)}G_{ti}\,. \tag{8.6}
$$

The evolution equations $\mathcal{E}_{ij}$ are built from the spatial components of the linearized Ricci tensor, the background metric and the Hamiltonian constraint:

$$
\mathcal{E}_{ij} := {}^{(4)}R_{ij} + \frac{1}{2}\lambda\eta_{ij}\mathcal{C}, \tag{8.7}
$$

where the case $\lambda = -1$ corresponds to the spatial components of the Einstein tensor while $\lambda = 0$ corresponds to the "Standard ADM" system as described in Section 2.3.2. The parameter λ must satisfy $1 + \lambda > 0$ for a well-posed hyperbolic initial value problem for the system of equations governing constraint evolution [120, 121]. Indeed, the linearized Bianchi identities $\partial_\beta {}^{(4)}G_\alpha^\beta \equiv 0$ imply that

$$
\begin{aligned}
\dot{\mathcal{C}}^i + (1+\lambda)\partial^i C + \partial_j \mathcal{E}^{ij} &\equiv 0, & (8.8) \\
\dot{\mathcal{C}} + \partial_i \mathcal{C}^i &\equiv 0. & (8.9)
\end{aligned}
$$

When the evolution equations are satisfied the Hamiltonian constraint satisfies the wave equation

$$
\ddot{\mathcal{C}} - (1+\lambda)\partial^k\partial_k\mathcal{C} = 0, \tag{8.10}
$$

propagating with speed $v_{\mathcal{C}} = \sqrt{1+\lambda}$. Early codes [3] have used the case $\lambda = 0$ (in which the Hamiltonian constraint propagates along the light cone). Here the behavior of the Hamiltonian constraint $\mathcal{C}$ in codes running with different values of λ is studied.

The Ricci tensor components ${}^{(4)}R_{ij}$ can be written as

$$
{}^{(4)}R_{ij} = R_{ij} + \frac{1}{2}\ddot{h}_{ij}\,, \tag{8.11}
$$

where the 3-D curvature tensor R_{ij} is given by

$$
R_{ij} = \frac{1}{2}\left\{ \partial^k\partial_i h_{jk} + \partial^k\partial_j h_{ik} - \partial^k\partial_k h_{ij} - \partial_i\partial_j h \right\}. \tag{8.12}
$$

The Hamiltonian and momentum constraints are

$$\mathcal{C} = \frac{1}{2} \left(\partial_i \partial_j h^{ij} - \partial_i \partial_j \eta^{ij} h \right), \tag{8.13}$$

$$\mathcal{C}^i = -\frac{1}{2} \left(\partial_j \dot{h}^{ij} - \eta^{ij} \partial_j \dot{h} \right). \tag{8.14}$$

In some of the algorithms the evolution equations $\mathcal{E}_{ij}$ are written in a form that is first-differential-order in time and second-differential-order in space:

$$\dot{h}_{ij} = -2K_{ij}, \tag{8.15}$$

$$\dot{K}_{ij} = R_{ij} + \frac{1}{2}\lambda\eta_{ij}\mathcal{C}, \tag{8.16}$$

where Eq. (8.11) was substituted into Eq. (8.7). Except for numerical roundoff error, using the variables g_{ij} instead of h_{ij} makes no difference, since the two tensors differ only by a constant tensor $\eta_{ij} = \delta_{ij}$ (in Cartesian coordinates). In Section 8.2 the variable g_{ij} is used while the codes described in Section 8.3 use h_{ij}.

Since evolving the linearized GR equations implies propagating scalar waves (along with gauge modes), the scalar wave equation will provide a useful test bed in ruling out bad choices of finite-difference approximations. Algorithms that fail for the scalar wave equation (SWE) will necessarily fail for the (linearized) evolution equations describing gravity.

In addition, finite difference algorithms and boundary conditions were first tested in the 1-D case. This provides a numerically inexpensive environment for ruling out unstable evolution schemes.

8.2   Study of the 1-D case

This section describes a large number of 1-D numerical experiments. Many of the results quoted in this section are superseded by the 3-D results in Section 8.3. The work done in 1-D is described in detail to indicate how lower dimensions provide a first criteria in ruling out bad choices of finite-difference algorithms.

8.2.1   Scalar wave equation

In one dimension the SWE takes the form

$$\partial_{tt}\phi - \partial_{xx}\phi = 0. \tag{8.17}$$

Equation (8.17) can be split into two equations that are first-order in time, and second-order in space:

$$\partial_t \phi = \xi, \tag{8.18}$$

$$\partial_t \xi = \partial_{xx} \phi. \tag{8.19}$$

Note that $\phi(x,t) = t$ is a solution of the SWE. To rule it out one needs to use proper initial and/or boundary data. However, such secular growth should not be interpreted as an instability.

8.2.2 1-D linearized gravity

Plane-wave solutions for a 1-dimensional version of gravitational equations were also studied. The Cartesian metric tensor $^{(4)}g_{\mu\nu}$ takes the form

$$^{(4)}g_{\mu\nu}(t,x) = {}^{(4)}\eta_{\mu\nu} + {}^{(4)}h_{\mu\nu}(t,x). \tag{8.20}$$

In this 1-D study the parameter λ in Eq. (8.7) is set to zero, so that the evolution equations (8.7) reduce to

$$^{(4)}R_{ij} = R_{ij} + \frac{1}{2}\ddot{g}_{ij} = 0. \tag{8.21}$$

The first-differential-order in time form of Eq. (8.21) is

$$\dot{g}_{ij} = -2K_{ij}, \tag{8.22}$$

$$\dot{K}_{ij} = R_{ij}. \tag{8.23}$$

Recall from Section 2.3.2 that K_{ij} stands for the extrinsic curvature of the $t = $ constant Cauchy slice.

The constraint equations (8.13) - (8.14) are

$$g_{yy,xx} + g_{zz,xx} = 0, \tag{8.24}$$

$$g_{xy,xt} = g_{xz,xt} = 0, \tag{8.25}$$

$$g_{yy,xt} + g_{zz,xt} = 0. \tag{8.26}$$

These are not imposed in the evolution code; therefore this is a case of unconstrained evolution. The tensor R_{ij} is computed via Eq. (8.12):

$$R_{xx} = -\frac{1}{2}\left[g_{yy,xx} + g_{zz,xx}\right],$$

$$R_{xy} = 0,$$

$$
\begin{aligned}
R_{xz} &= 0, \\
R_{yy} &= -\frac{1}{2}g_{yy,xx}, \\
R_{yz} &= -\frac{1}{2}g_{yz,xx}, \\
R_{zz} &= -\frac{1}{2}g_{zz,xx}.
\end{aligned}
\tag{8.27}
$$

The mode $g_{ij} = \eta_{ij} + a_{ij}t$ is a solution of Eq. (8.21) with a_{ij} symmetric and constant. Since the corresponding Ricci tensor is zero this is a pure gauge mode that, if present, is introduced by initial data. Another way of seeing that a pure gauge transformation can lead to linearly growing modes is to apply the infinitesimal gauge (coordinate) transformation

$$
\delta g^{\alpha\beta} = g^{\alpha\mu}\zeta^{\beta}_{,\mu} + g^{\beta\mu}\zeta^{\alpha}_{,\mu}
\tag{8.28}
$$

with the choice

$$
\zeta^{\alpha} = (\varepsilon xy, \varepsilon yt, \varepsilon xt, 0).
\tag{8.29}
$$

This immediately gives

$$
\delta g^{00} = \delta g^{0i} = 0,
\tag{8.30}
$$

so that the gauge transformation (8.29) is consistent with the geodesic gauge condition Eq. (8.1). For the spatial components the result is

$$
\delta g^{ij} = \begin{pmatrix} 0 & 2\varepsilon t & 0 \\ 2\varepsilon t & 0 & 0 \\ 0 & 0 & 0 \end{pmatrix}.
\tag{8.31}
$$

For the purpose of defining various (discretized) evolution schemes for the SWE and the linearized gravitational equations in 1-D, physical fields are represented on a set of equally spaced points. Grid conventions are as follows:

$$
x_I = I\Delta x, \quad t_N = N\Delta t, \quad \phi(x_I, t_N) = \phi^{[N]}_{[I]},
$$

where $I = 1 \ldots I_{max}$ and $N \geq 0$.

8.2.3 Non-staggered leap-frog (LF1) for the 1-D SWE

This section describes the non-staggered leap-frog evolution algorithm for Eqs. (8.18) - (8.19).

Given $\phi^{[0]}$ and $\xi^{[0]}$ (i.e. initial data at $t = 0$) the quantities $\phi^{[1]}$ and $\xi^{[1]}$ are updated as follows:

$$\phi_{[I]}^{[1]} = \phi_{[I]}^{[0]} + \Delta t \cdot \xi_{[I]}^{[0]}, \tag{8.32}$$

$$\xi_{[I]}^{[1]} = \xi_{[I]}^{[0]} + \frac{\Delta t}{(\Delta x)^2} \cdot \left[\phi_{[I+1]}^{[0]} - 2\phi_{[I]}^{[0]} + \phi_{[I-1]}^{[0]} \right], \tag{8.33}$$

which amounts to a time-step first-order in time from level $N = 0$ to level $N = 1$. The explicit form of the evolution scheme is:

$$\phi_{[I]}^{[N]} = \phi_{[I]}^{[N-2]} + 2\Delta t \cdot \xi_{[I]}^{[N-1]}, \tag{8.34}$$

$$\xi_{[I]}^{[N]} = \xi_{[I]}^{[N-2]} + \frac{2\Delta t}{(\Delta x)^2} \cdot \left[\phi_{[I+1]}^{[N-1]} - 2\phi_{[I]}^{[N-1]} + \phi_{[I-1]}^{[N-1]} \right]. \tag{8.35}$$

8.2.4   Second-order evolution scheme (2ND)

Scalar wave equation

The second-order in time form of the wave-equation (8.17) is discretized in the following way:

$$\phi_{[I]}^{[N]} = 2\phi_{[I]}^{[N-1]} - \phi_{[I]}^{[N-2]} + \left(\frac{\Delta t}{\Delta x} \right)^2 \cdot \left[\phi_{[I+1]}^{[N-1]} - 2\phi_{[I]}^{[N-1]} + \phi_{[I-1]}^{[N-1]} \right] \tag{8.36}$$

Initial data is $\phi^{[0]} = \phi(x, t = 0)$ and $\phi^{[1]} = \phi(x, t = \Delta t)$.

Linearized gravity

The LG equations (8.21) are discretized in the following way:

$$g_{xx[I]}^{[N]} = 2g_{xx[I]}^{[N-1]} - g_{xx[I]}^{[N-2]} +$$
$$+ \left(\frac{\Delta t}{\Delta x} \right)^2 \cdot \left[g_{yy[I+1]}^{[N-1]} - 2g_{yy[I]}^{[N-1]} + g_{yy[I-1]}^{[N-1]} \right.$$
$$\left. + g_{zz[I+1]}^{[N-1]} - 2g_{zz[I]}^{[N-1]} + g_{zz[I-1]}^{[N-1]} \right],$$
$$g_{xy[I]}^{[N]} = 2g_{xy[I]}^{[N-1]} - g_{xy[I]}^{[N-2]},$$
$$g_{xz[I]}^{[N]} = 2g_{xz[I]}^{[N-1]} - g_{xz[I]}^{[N-2]},$$
$$g_{yy[I]}^{[N]} = 2g_{yy[I]}^{[N-1]} - g_{yy[I]}^{[N-2]} + \left(\frac{\Delta t}{\Delta x} \right)^2 \cdot \left[g_{yy[I+1]}^{[N-1]} - 2g_{yy[I]}^{[N-1]} + g_{yy[I-1]}^{[N-1]} \right],$$

$$g_{yz[I]}^{[N]} = 2g_{yz[I]}^{[N-1]} - g_{yz[I]}^{[N-2]} + \left(\frac{\Delta t}{\Delta x}\right)^2 \cdot \left[g_{yz[I+1]}^{[N-1]} - 2g_{yz[I]}^{[N-1]} + g_{yz[I-1]}^{[N-1]}\right],$$

$$g_{zz[I]}^{[N]} = 2g_{zz[I]}^{[N-1]} - g_{zz[I]}^{[N-2]} + \left(\frac{\Delta t}{\Delta x}\right)^2 \cdot \left[g_{zz[I+1]}^{[N-1]} - 2g_{zz[I]}^{[N-1]} + g_{zz[I-1]}^{[N-1]}\right].$$

$$(8.37)$$

Required initial data is $g_{ij}^{[0]}$ and $g_{ij}^{[1]}$.

8.2.5   Iterative Crank-Nicholson evolution scheme (ICN)

Scalar wave equation

The wave-equation is solved in its first-order form given by Eqs. (8.18) - (8.19).

For each time-step one performs a given number of Crank-Nicholson iterations. The first one is first-order in time (counted for as iteration 0), and the rest of them are second-order in time. The sequence of operations executed for each time-step is the following:

1. Compute $\overset{(0)}{\phi}{}^{[N+1]}$ and $\overset{(0)}{\xi}{}^{[N+1]}$ first-order in time:

$$\overset{(0)}{\phi}{}_{[I]}^{[N+1]} = \phi_{[I]}^{[N]} + \Delta t \cdot \xi_{[I]}^{[N]}, \tag{8.38}$$

$$\overset{(0)}{\xi}{}_{[I]}^{[N+1]} = \xi_{[I]}^{[N]} + \frac{\Delta t}{(\Delta x)^2} \cdot \left\{\phi_{[I+1]}^{[N]} - 2\phi_{[I]}^{[N]} + \phi_{[I-1]}^{[N]}\right\}. \tag{8.39}$$

2. Compute $\overset{(i)}{\phi}{}^{[N+1/2]}$ and $\overset{(i)}{\xi}{}^{[N+1/2]}$ by averaging:

$$\overset{(i)}{\phi}{}^{[N+1/2]} = \frac{1}{2}\left\{\phi^{[N]} + \overset{(i)}{\phi}{}^{[N+1]}\right\}, \tag{8.40}$$

$$\overset{(i)}{\xi}{}^{[N+1/2]} = \frac{1}{2}\left\{\xi^{[N]} + \overset{(i)}{\xi}{}^{[N+1]}\right\}. \tag{8.41}$$

3. Compute $\overset{(i+1)}{\phi}{}^{[N+1]}, \overset{(i+1)}{\xi}{}^{[N+1]}$ using levels N and $N+1/2$:

$$\overset{(i+1)}{\phi}{}_{[I]}^{[N+1]} = \phi_{[I]}^{[N]} + \Delta t \cdot \overset{(i)}{\xi}{}_{[I]}^{[N+1/2]}, \tag{8.42}$$

$$
\overset{(i+1)}{\xi}{}^{[N+1]}_{[I]} \;=\; \xi^{[N]}_{[I]} + \frac{\Delta t}{(\Delta x)^2} \cdot \left\{ \overset{(i)}{\phi}{}^{[N+1/2]}_{[I+1]} \right.
$$

$$
\left. -2\,\overset{(i)}{\phi}{}^{[N+1/2]}_{[I]} + \overset{(i)}{\phi}{}^{[N+1/2]}_{[I-1]} \right\}. \tag{8.43}
$$

4. Increment i by one, then go back to step 2, until the desired number of iterations is reached.

Initial data is $\phi^{[0]}$ and $\xi^{[0]}$.

A discretized stability analysis of the evolution scheme shows [119] that the algorithm is stable for two and three iterations, unstable for four and five iterations, stable for six and seven iterations, etc.

Linearized gravity

Starting from Eqs. (8.22) - (8.23), the ICN algorithm is:

1. Compute $\overset{(0)}{g}_{ij}{}^{[N+1]}$ and $\overset{(0)}{K}_{ij}{}^{[N+1]}$ first-order in time:

$$
\overset{(0)}{g}{}^{[N+1]}_{ij\,[I]} \;=\; g^{[N]}_{ij\,[I]} - 2\,\Delta t \cdot K^{[N]}_{ij\,[I]},
$$

$$
\overset{(0)}{K}{}^{[N+1]}_{xx\,[I]} \;=\; K^{[N]}_{xx\,[I]} - \frac{1}{2}\frac{\Delta t}{(\Delta x)^2} \times
$$

$$
\times\; \left\{ g^{[N]}_{yy\,[I+1]} - 2g^{[N]}_{yy\,[I]} + g^{[N]}_{yy\,[I-1]} \right.
$$

$$
\left. + g^{[N]}_{zz\,[I+1]} - 2g^{[N]}_{zz\,[I]} + g^{[N]}_{zz\,[I-1]} \right\},
$$

$$
\overset{(0)}{K}{}^{[N+1]}_{xy\,[I]} \;=\; K^{[N]}_{xy\,[I]},
$$

$$
\overset{(0)}{K}{}^{[N+1]}_{xz\,[I]} \;=\; K^{[N]}_{xz\,[I]},
$$

$$
\overset{(0)}{K}{}^{[N+1]}_{yy\,[I]} \;=\; K^{[N]}_{yy\,[I]} - \frac{1}{2}\frac{\Delta t}{(\Delta x)^2} \cdot \left\{ g^{[N]}_{yy\,[I+1]} - 2g^{[N]}_{yy\,[I]} + g^{[N]}_{yy\,[I-1]} \right\},
$$

$$
\overset{(0)}{K}{}^{[N+1]}_{yz\,[I]} \;=\; K^{[N]}_{yz\,[I]} - \frac{1}{2}\frac{\Delta t}{(\Delta x)^2} \cdot \left\{ g^{[N]}_{yz\,[I+1]} - 2g^{[N]}_{yz\,[I]} + g^{[N]}_{yz\,[I-1]} \right\},
$$

$$
\overset{(0)}{K}{}^{[N+1]}_{zz\,[I]} \;=\; K^{[N]}_{zz\,[I]} - \frac{1}{2}\frac{\Delta t}{(\Delta x)^2} \cdot \left\{ g^{[N]}_{zz\,[I+1]} - 2g^{[N]}_{zz\,[I]} + g^{[N]}_{zz\,[I-1]} \right\}. \tag{8.44}
$$

2. Compute $\overset{(i)}{\phi}{}^{[N+1/2]}$ and $\overset{(i)}{\xi}{}^{[N+1/2]}$ by averaging:

$$\overset{(i)}{g}_{ij}{}^{[N+1/2]} = \frac{1}{2}\left\{g_{ij}^{[N]} + \overset{(i)}{g}_{ij}{}^{[N+1]}\right\}, \qquad (8.45)$$

$$\overset{(i)}{K}_{ij}{}^{[N+1/2]} = \frac{1}{2}\left\{K_{ij}^{[N]} + \overset{(i)}{K}_{ij}{}^{[N+1]}\right\}. \qquad (8.46)$$

3. Compute $\overset{(i+1)}{g}_{ij}{}^{[N+1]}$, $\overset{(i+1)}{K}_{ij}{}^{[N+1]}$ using levels N and $N+1/2$:

$$\overset{(i+1)}{g}_{ij}{}^{[N+1]}_{[I]} = g_{ij\,[I]}^{[N]} - 2\,\Delta t \cdot \overset{(i)}{K}_{ij}{}^{[N+1/2]}_{[I]},$$

$$\overset{(i+1)}{K}_{xx}{}^{[N+1]}_{[I]} = K_{xx\,[I]}^{[N]} - \frac{1}{2}\frac{\Delta t}{(\Delta x)^2}$$

$$\times \left\{\overset{(i)}{g}_{yy}{}^{[N+1/2]}_{[I+1]} - 2\,\overset{(i)}{g}_{yy}{}^{[N+1/2]}_{[I]} + \overset{(i)}{g}_{yy}{}^{[N+1/2]}_{[I-1]}\right.$$

$$\left. + \overset{(i)}{g}_{zz}{}^{[N+1/2]}_{[I+1]} - 2\,\overset{(i)}{g}_{zz}{}^{[N+1/2]}_{[I]} + \overset{(i)}{g}_{zz}{}^{[N+1/2]}_{[I-1]}\right\},$$

$$\overset{(i+1)}{K}_{xy}{}^{[N+1]}_{[I]} = K_{xy\,[I]}^{[N]},$$

$$\overset{(i+1)}{K}_{xz}{}^{[N+1]}_{[I]} = K_{xz\,[I]}^{[N]},$$

$$\overset{(i+1)}{K}_{yy}{}^{[N+1]}_{[I]} = K_{yy\,[I]}^{[N]} - \frac{1}{2}\frac{\Delta t}{(\Delta x)^2} \times$$

$$\times \left\{\overset{(i)}{g}_{yy}{}^{[N+1/2]}_{[I+1]} - 2\,\overset{(i)}{g}_{yy}{}^{[N+1/2]}_{[I]} + \overset{(i)}{g}_{yy}{}^{[N+1/2]}_{[I-1]}\right\},$$

$$\overset{(i+1)}{K}_{yz}{}^{[N+1]}_{[I]} = K_{yz\,[I]}^{[N]} - \frac{1}{2}\frac{\Delta t}{(\Delta x)^2} \times$$

$$\times \left\{\overset{(i)}{g}_{yz}{}^{[N+1/2]}_{[I+1]} - 2\,\overset{(i)}{g}_{yz}{}^{[N+1/2]}_{[I]} + \overset{(i)}{g}_{yz}{}^{[N+1/2]}_{[I-1]}\right\},$$

$$\overset{(i+1)}{K}_{zz}{}^{[N+1]}_{[I]} = K_{zz\,[I]}^{[N]} - \frac{1}{2}\frac{\Delta t}{(\Delta x)^2} \times$$

$$\times \left\{\overset{(i)}{g}_{zz}{}^{[N+1/2]}_{[I+1]} - 2\,\overset{(i)}{g}_{zz}{}^{[N+1/2]}_{[I]} + \overset{(i)}{g}_{zz}{}^{[N+1/2]}_{[I-1]}\right\}. $$

$$(8.47)$$

4. Increment i by one, then go back to step 2, until the desired number of iterations is reached.

Initial data is $g_{ij}^{[0]}$ and $K_{ij}^{[0]}$.

8.2.6 Boundary conditions

Analytic formulation

Let L be the size of the evolution domain:

$$x \in [0, L]. \tag{8.48}$$

Codes were run with the following types of boundary conditions:

- Periodic boundaries:

$$\phi(x + L, t) = \phi(x, t) \tag{8.49}$$

- Reflecting boundaries:

$$\phi(0, t) = \phi(L, t) = 0 \tag{8.50}$$

- Sommerfeld boundaries (outgoing radiation condition): based on the assumption that there is no incoming radiation at the boundaries, one obtains

$$[(\partial_t - \partial_x)\phi]_{|x=0} = 0, \tag{8.51}$$
$$[(\partial_t + \partial_x)\phi]_{|x=L} = 0. \tag{8.52}$$

Discretized formulation

Periodic boundary conditions consist of the identification

$$\phi_{[0]} \equiv \phi_{[I_{max}]}, \tag{8.53}$$
$$\phi_{[I_{max}+1]} \equiv \phi_{[1]}. \tag{8.54}$$

Reflecting boundary conditions are imposed by setting

$$\phi_{[1]} = \phi_{[I_{max}]} = 0. \tag{8.55}$$

Sommerfeld boundary conditions are tested in first- and in second-order form. The first-order form of the 1-D outgoing boundary condition is:

$$\phi_{[1]}^{[N]} = \frac{1}{\Delta t + \Delta x} \left[\Delta t \cdot \phi_{[2]}^{[N]} + \Delta x \cdot \phi_{[1]}^{[N-1]} \right], \qquad (8.56)$$

$$\phi_{[I_{max}]}^{[N]} = \frac{1}{\Delta t + \Delta x} \left[\Delta t \cdot \phi_{[I_{max}-1]}^{[N]} + \Delta x \cdot \phi_{[I_{max}]}^{[N-1]} \right], \qquad (8.57)$$

while the second-order form is:

$$\phi_{[1]}^{[N]} = \frac{1}{3(\Delta t + \Delta x)} \times \left[4\Delta t \cdot \phi_{[2]}^{[N]} - \Delta t \cdot \phi_{[3]}^{[N]} \right.$$
$$\left. + 4\Delta x \cdot \phi_{[1]}^{[N-1]} - \Delta x \cdot \phi_{[1]}^{[N-2]} \right], \qquad (8.58)$$

$$\phi_{[I_{max}]}^{[N]} = \frac{1}{3(\Delta t + \Delta x)} \times \left[4\Delta t \cdot \phi_{[I_{max}-1]}^{[N]} - \Delta t \cdot \phi_{[I_{max}-2]}^{[N]} \right.$$
$$\left. + 4\Delta x \cdot \phi_{[I_{max}]}^{[N-1]} - \Delta x \cdot \phi_{[I_{max}]}^{[N-2]} \right]. \qquad (8.59)$$

Non-periodic boundary conditions were imposed either on ϕ or on ξ. Since ξ is computed as a spatial derivative of ϕ, if a boundary condition is imposed on $\phi_{[1]}$ and $\phi_{[I_{max}]}$, the field ξ is evolved only in the points $x_{[2]} \dots x_{[I_{max}-1]}$. Since ϕ is computed as a time derivative of ξ, imposing boundary conditions on $\xi_{[1]}$ and $\xi_{[I_{max}]}$ allows evolution of the field ϕ in the whole numerical grid.

8.2.7 Code tests for the 1-D scalar wave equation

This section investigates the stability properties of different evolution schemes with periodic, reflecting, and outgoing (Sommerfeld) boundary data. The different codes were tested qualitatively with a pulse of compact support:

$$\phi(x,t) = \begin{cases} \phi(x,t) = A \cdot \left[\frac{(t-\epsilon \cdot x)^2}{w^2} - 1 \right]^4, & |\epsilon \cdot x - t| < w \\ 0, & |\epsilon \cdot x - t| \geq w. \end{cases} \qquad (8.60)$$

These runs were done for 10 crossing times on a grid that goes from -1 to 1 with the choices

$$A = 1, \ w = 0.75, \ \epsilon = \pm 1.$$

The codes did not show any unexpected qualitative properties. The amount of dispersion was insignificant.

The stability properties of the codes were tested for $\sim 10^3$ crossing times. Initial data was generated by multiplying the right-hand-side of
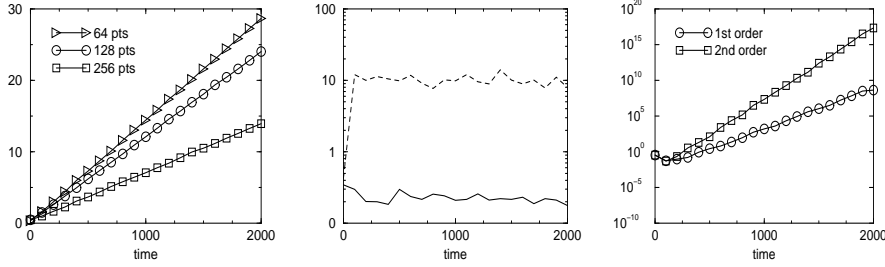
Fig. 8.1: Stability runs with the LF1 evolution scheme. Left: $||\phi||_\infty$ as a function of time for different grid sizes, using periodic boundary conditions. Middle: $||\phi||_\infty$ (dashed line) and $||\xi||_\infty$ (continuous line) for a grid size of 64, using reflecting boundary conditions applied to ξ. Right: $||\phi||_\infty$ as a function of time for 64 points, using first- and second-order radiation boundary condition applied to ϕ.

Eq. (8.60) with a set of random numbers distributed between -0.5 and 0.5. When running the SWE with random initial data, one introduces the mode $\phi = t$. However, when applying freezing or Sommerfeld boundary conditions this mode is ruled out.

LF1 evolution scheme

Runs were made at a CFL factor of $\Delta t/\Delta x = 0.25$ (which is at half of the CFL limit), using grid sizes of $64, 128, 256$. Results are as follows:

- Periodic boundaries display linearly growing $||\phi||_\infty$ as a function of time, while $||\xi||_\infty$ stays bounded, i.e. $||\xi||_\infty \leq C$ with C constant.

- Reflecting boundary conditions applied to either ϕ or ξ result in stable runs. Moreover, both $||\phi||_\infty$ and $||\xi||_\infty$ stay bounded.

- The outgoing radiation condition in first-order or second-order form applied to ϕ or to ξ gives *unstable* runs, showing an exponentially growing time dependence of both $||\phi||_\infty$ and $||\xi||_\infty$.

Plots of these three sets of runs are shown in Figure 8.1.

2ND evolution scheme

Runs were made for 1000 crossing times (i.e. up to $t = 2000$), for grid sizes of 64, 128, 256. The CFL factor was $\Delta t/\Delta x = 0.50$ (which is at half of the CFL limit). Boundary conditions were periodic, reflecting, first- and
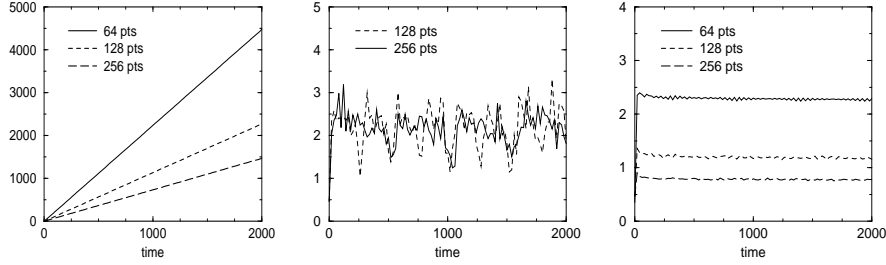
Fig. 8.2: Stability runs for the 2ND evolution scheme. $||\phi||_\infty$ is shown as a function of time for different grid sizes, using the following boundary conditions: periodic (on the left), reflecting (in the middle), and first-order outgoing radiation (on the right).

second-order outgoing radiation condition, with the non-periodic boundary conditions being applied either to ϕ or to ξ. The code proved to be stable in all cases (see Figure 8.2). Periodic boundary conditions allowed for a linear growth of $||\phi||_\infty$. In terms of stability there was no significant difference between applying first- or second-order Sommerfeld boundary conditions.

ICN evolution scheme

The setup of the stability runs was similar to those for the 2ND scheme except for the CFL factor, which in this case was $\Delta t/\Delta x = 0.25$. Boundary conditions applied were periodic, reflecting, and first- and second-order outgoing radiation condition. The code was found to be stable for all of these cases, as shown in Figure 8.3. None of the runs produced exponentially growing time-dependences.

The roundoff problem

Next the SWE ICN code was run with periodic boundary conditions, grid sizes of 64, 128, 256, using the following initial data:

$$\phi(x,0) \;=\; 1 + A \cdot \varrho_c, \tag{8.61}$$

$$\xi(x,0) \;=\; A \cdot \varrho_c, \tag{8.62}$$

where ϱ_c stands for random data of compact support.

When choosing $A = 10^{-1}$ the behavior of $\xi(x,t)$ is linear with respect to time. For $A = 10^{-11}$ the function $||\xi(x,t)||_\infty$ becomes a higher order polynomial as a function of time:

$$64 \text{ pts: } ||\xi||_\infty \;=\; 1 + O(10^{-12}) + O(10^{-13}) \cdot t$$
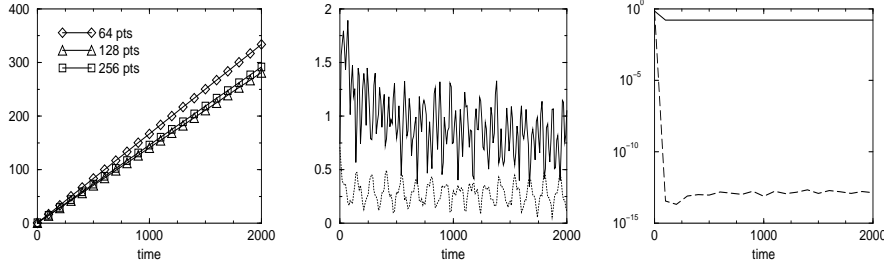
Fig. 8.3: Stability runs with an ICN evolution scheme. Left: $||\phi||_\infty$ as a function of time for different grid sizes, periodic boundary conditions. Middle: $||\phi||_\infty$ (dotted line) and $||\xi||_\infty$ (continuous line) for a grid size of 64, using reflecting boundary conditions applied to ϕ. Right: $||\phi||_\infty$ (continuous line) and $||\xi||_\infty$ (dotted line) for a grid size of 64, using second-order outgoing radiation boundary conditions applied to ξ.

$$
\begin{aligned}
&\qquad\qquad +O(10^{-13}) \cdot t^2 + O(10^{-19}) \cdot t^3 \ldots \\
128 \text{ pts: } ||\xi||_\infty &= 1 + O(10^{-10}) + O(10^{-12}) \cdot t \\
&\qquad\qquad +O(10^{-12}) \cdot t^2 + O(10^{-19}) \cdot t^3 \ldots \\
256 \text{ pts: } ||\xi||_\infty &= 1 + O(10^{-10}) + O(10^{-12}) \cdot t \\
&\qquad\qquad +O(10^{-11}) \cdot t^2 + O(10^{-18}) \cdot t^3 \ldots
\end{aligned}
$$

This quadratic time dependence was displayed as expected by the functions g_{yy} and g_{zz} when solving the LG equations for g_{ij} with an ICN evolution scheme. Plots of g_{yy} are shown in Figure 8.5 (left).

This higher order polynomial behavior is not present when using the 2ND evolution scheme, nor is it present when evolving the SWE for the function $\phi(x, 0)$ where the constant 1 does not enter.

All these runs were made on a CRAY C90 architecture in single precision which corresponds to a roundoff error of $O(10^{-14})$ when representing an $O(1)$ quantity.

8.2.8   Code tests for the 1-D LG equations

The different codes were tested for proper qualitative behavior using a pulse of compact support:

$$
g_{ij} = \begin{pmatrix} 1 & 0 & 0 \\ 0 & 1 + \phi(x,t) & 0 \\ 0 & 0 & 1 - \phi(x,t) \end{pmatrix} \tag{8.63}
$$

with the function $\phi(x,t)$ defined in Eq. (8.60). These runs were done for ~ 10 crossing times, on a grid that goes from -1 to 1 with the choices

$$A = 10^{-6}, \; w = 0.75, \; \epsilon = \pm 1.$$

No significant dispersion was observed.

Stability of the codes was tested for $\sim 10^3$ crossing times. Initial data for each component of $g_{ij} - \eta_{ij}$ was generated by multiplying the function $\phi(x,t)$ defined in Eq. (8.60) with a set of random numbers distributed between -0.5 and 0.5. The same procedure was followed for initializing K_{ij} when using the ICN evolution scheme.

2ND evolution scheme

Runs were made for 1000 crossing times, with grid sizes of 64, 128, and 256, and a CFL factor of $\Delta t/\Delta x = 0.50$. The results are as follows:

- Periodic boundaries: $||h_{ij}||_\infty = ||g_{ij} - \eta_{ij}||_\infty$ grew linearly in time.

- Reflecting (freezing) boundaries:

  - h_{xx}, h_{xy}, h_{xz}: the ℓ_∞ norm grew like $t \cdot O(10^{-4})$,
  - h_{yy}, h_{yz}, h_{zz}: these functions stay $O(10^{-6})$.

- Sommerfeld (first- and second-order):

  - h_{xx}, h_{xy}, h_{xz}: the ℓ_∞ norm grew linearly in time with a slope $O(10^{-4})$,
  - h_{yy}, h_{yz}, h_{zz}: these functions slowly decreased with time, being $O(10^{-6})$.

  There was no qualitative difference between the runs with first and second order Sommerfeld boundary condition.

ICN evolution scheme

Runs were made for 1000 crossing times, with grid sizes of 64, 128, and 256. The CFL factor was $\Delta t/\Delta x = 0.25$. At each time-step the code performed two Crank-Nicholson iterations. The results are as follows:

- Periodic boundaries:

  - $h_{xx}, h_{xy}, h_{xz}, h_{yz}$: the ℓ_∞ norms grew linearly in time. The slope is $O(10^{-6})$ for h_{xi}, and it is $O(10^{-9})$ for h_{yz}.
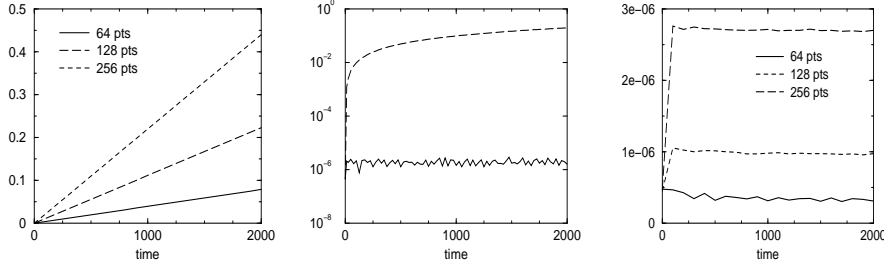
Fig. 8.4: Stability runs with a second-order evolution scheme. Left: $||h_{xy}||_\infty$ as a function of time for different grid sizes, using periodic boundary conditions. Middle: $||h_{xy}||_\infty$ (dashed line) and $||h_{yz}||_\infty$ (continuous line) for a grid size of 128, using reflecting boundary conditions. Right: $||h_{yz}||_\infty$ as a function of time for different grid sizes, using first-order Sommerfeld boundary conditions.

- h_{yy}, h_{zz}: the ℓ_∞ norm of these components showed a polynomial behavior as a function of time. This is the same roundoff behavior as the one described in Section 8.2.7.

- Reflecting (freezing) boundaries:

  - the ℓ_∞ norms of h_{xx}, h_{xy}, h_{xz} grew linearly in time with a slope of $O(10^{-6})$,

  - h_{yy}, h_{yz}, h_{zz} were slowly decreasing in time,

  - $K_{xx}, K_{yy}, K_{yz}, K_{zz}$ were slowly decreasing in time,

  - the ℓ_∞ norms of K_{xy}, K_{xz} were time-independent.

  Applying reflecting boundary conditions to g_{ij} instead of K_{ij} did not influence the stability properties of the code.

- Sommerfeld boundaries (first- and second-order):

  Runs were made up to $t = 4000$. Applying first or second order Sommerfeld boundary condition to the components of either g_{ij} or K_{ij} gave stable runs. As expected from the form of the evolution equations (8.21), the ℓ_∞ norms of h_{xx}, h_{xy}, and h_{xz} showed a linear growth with time.

These results indicate that there are several choices of evolution algorithms that seem to perform equally well with periodic and Dirichlet boundary conditions. The non-staggered leap-frog algorithm failed for the outgoing radiation boundaries (Sommerfeld conditions).
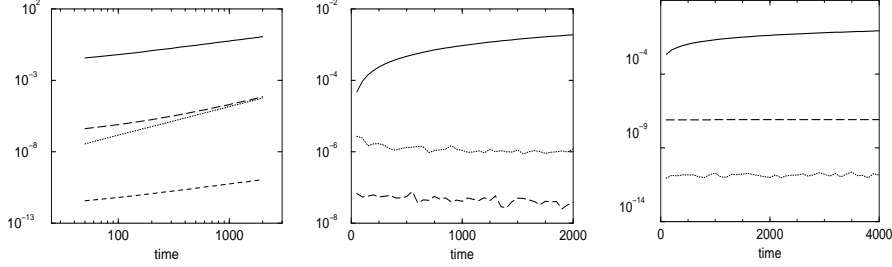
Fig. 8.5: Stability runs with an ICN evolution scheme. Left: $||g_{yy}-1||_\infty$ using periodic boundary condition, 256 points. The top three curves correspond to solving the equations for g_{ij}, using as initial data $g_{yy} = 1 + O(10^{-1})$ (solid line), $g_{yy} = 1 + O(10^{-6})$ (long dashed line), $g_{yy} = 1 + O(10^{-11})$ (dotted line); the bottom curve (dashed line) corresponds to solving the equations for h_{ij}, using $h_{yy} = O(10^{-11})$ as initial data. Middle: reflecting boundary conditions applied to g_{ij}, showing $||g_{xy}||_\infty$ in the top (solid line), $||g_{yz}||_\infty$ in the bottom (dashed line), $||K_{xx}||_\infty$ in the middle (dotted line). Right: first-order Sommerfeld boundary conditions applied to K_{ij} using 128 gridpoints. The top (continuous) curve shows $||g_{xx} - 1||_\infty$, the middle (dashed) line corresponds to $||g_{zz} - 1||_\infty$ while the bottom (dotted) curve represents $||k_{zz}||_\infty$.

8.3   SWE and LG equations in 3-D

This section studies the numerical stability of 3-D evolution codes for linearized gravity with various boundary conditions. Evolution algorithms are described (and tested) first for the scalar wave equation. Next the LG equations are studied for periodic boundaries. Furthermore runs are described with a variety of boundary conditions on the $z =$ constant faces of the numerical grid, keeping the x- and y-directions periodic. These tests are first performed with the second-order evolution scheme. Then the best boundary algorithms are tested for the ICN and for the leap-frog algorithms. At the end a robustly stable algorithm is presented for evolving a region of space-time contained within a cube, using random initial and random boundary data.

8.3.1   Evolution schemes

Four different evolution schemes were used for the scalar wave equation

$$\partial^\mu \partial_\mu \phi = 0. \tag{8.64}$$

With the exception of the algorithm 2ND, the numerical algorithms evolve the SWE in first-order in time form

$$\partial_t \phi = \xi \tag{8.65}$$

$$\partial_t \xi = \nabla^2 \phi. \tag{8.66}$$

The generalization of the finite-difference algorithms to the LG equations is straightforward.

Non-staggered leap-frog (LF1)

The first algorithm, LF1, is a standard leap-frog implementation of the Eqs. (8.65) - (8.66):

$$\phi^{[N+1]}_{[I,J,K]} = \phi^{[N-1]}_{[I,J,K]} - 4\xi^n_{[I,J,K]}\Delta t$$

$$\xi^{[N+1]}_{[I,J,K]} = \xi^{[N-1]}_{[I,J,K]} - \nabla^2\phi^n_{[I,J,K]}\Delta t, \tag{8.67}$$

where ∇^2 is the second-order accurate centered difference approximation to the Laplacian. It is known that this algorithm has a time-splitting instability in the presence of dissipative and non-linear effects [122].

Staggered leap-frog (LF2)

The second algorithm, LF2, is a staggered in time leap-frog scheme which is not subject to the time-splitting instability:

$$\phi^{[N+1]}_{[I,J,K]} = \phi^{[N]}_{[I,J,K]} - 2\xi^{[N+1/2]}_{[I,J,K]}\Delta t \tag{8.68}$$

$$\xi^{[N+1/2]}_{[I,J,K]} = \xi^{[N-1/2]}_{[I,J,K]} - \frac{1}{2}\nabla^2\phi^n_{[I,J,K]}\Delta t. \tag{8.69}$$

Here ξ is evaluated on the half grid. By subtracting the equation

$$\phi^{[N]}_{[I,J,K]} = \phi^{[N-1]}_{[I,J,K]} - 2\xi^{[N-1/2]}_{[I,J,K]}\Delta t \tag{8.70}$$

from Eq. (8.68) and using Eq. (8.69) to eliminate ξ, it can be seen that LF2 is equivalent to the standard leap-frog scheme for the second-differential-order in time form of the wave equation (8.64), in which ϕ lies on integral time levels and ξ is not introduced.

Second-order scheme (2ND)

The scalar wave equation (8.64) is approximated by a the three-level, second-differential-order in time algorithm:

$$\phi^{[N+1]}_{[I,J,K]} = 2\phi^n_{[I,J,K]} - \phi^{[N-1]}_{[I,J,K]} + \Delta t^2\nabla^2\phi^{[N]}_{[I,J,K]}. \tag{8.71}$$

Iterative Crank-Nicholson (ICN)

The fourth algorithm is an iterative Crank-Nicholson algorithm with two iterations. The following sequence of operations is executed for each time-step:

1. Compute the first-order accurate quantities

$$
\begin{aligned}
\overset{(0)}{\phi}{}^{[N+1]}_{[I,J,K]} &= \phi^{[N]}_{[I,J,K]} - 2\xi^{[N]}_{[I,J,K]}\Delta t, \\
\overset{(0)}{\xi}{}^{[N+1]}_{[I,J,K]} &= \xi^{[N]}_{[I,J,K]} - \frac{1}{2}\nabla^2\phi^{[N]}_{[I,J,K]}\Delta t.
\end{aligned} \tag{8.72}
$$

2. Compute the mid-level values

$$
\begin{aligned}
\overset{(i)}{\phi}{}^{[N+1/2]}_{[I,J,K]} &= \frac{1}{2}\left(\phi^{[N]}_{[I,J,K]} + \overset{(i)}{\phi}{}^{[N+1]}_{[I,J,K]}\right), \\
\overset{(i)}{\xi}{}^{[N+1/2]}_{[I,J,K]} &= \frac{1}{2}\left(\xi^{[N]}_{[I,J,K]} + \overset{(i)}{\xi}{}^{[N+1]}_{[I,J,K]}\right).
\end{aligned} \tag{8.73}
$$

3. Update using levels n and $n + 1/2$:

$$
\begin{aligned}
\overset{(i+1)}{\phi}{}^{[N+1]}_{[I,J,K]} &= \phi^{[N]}_{[I,J,K]} - 2\,\overset{(i)}{\xi}{}^{[N+1/2]}_{[I,J,K]}\Delta t, \\
\overset{(i+1)}{\xi}{}^{[N+1]}_{[I,J,K]} &= \xi^{[N]}_{[I,J,K]} - \frac{1}{2}\nabla^2\,\overset{(i)}{\phi}{}^{[N+1/2]}_{[I,J,K]}\Delta t.
\end{aligned} \tag{8.74}
$$

4. Increment i by one and return to step 2 until $i = 2$ is reached.

8.3.2 *Periodic boundary conditions*

The LG equations (8.7) were studied with respect to the parameter λ, using periodic boundary conditions and the 2ND evolution algorithm with a CFL factor of 0.25. Initial data for these runs was unconstrained (i.e. a set of random numbers, scattered between $-0.5 \cdot 10^{-6} \ldots 0.5 \cdot 10^{-6}$). The grid size was 16^3. Non-exponentially growing runs were made up to 1000 crossing times (i.e. up to $t = 2000$, with a grid going from -1 to 1.), unless stated otherwise. Numerical experiments showed the following:

- Runs for $\lambda \in \{-4.0, -2.0, -1.2, -1.0, -0.8, -0.4\}$ were unstable. The choice $\lambda = -1$ gives a growth rate that is significantly smaller than the other values, yet it gives an unstable run. Runs for $\lambda \in \{4.4, 6.0, 8.0\}$ were unstable as well.

- Runs for $\lambda \in \{0.0,\ 0.8,\ 1.6,\ 2.4,\ 3.2,\ 4.0\}$ were stable, as follows:

  – The case $\lambda = 0$ gave a linear growth of the Hamiltonian constraint, with a slope of $O(10^{-3})$.
  – The case $\lambda = 4$ gave a linear growth of the Hamiltonian constraint, with a slope of $O(10^{-5})$.
  – The cases $0 < \lambda < 4$ gave runs where the Hamiltonian constraint remained bounded, with a magnitude of $O(10^{-4})$.

Similar results were reproduced when using the schemes ICN, LF1, LF2. In the case of ICN there was an additional (isolated) value $\lambda = -1$ that resulted in a stable evolution. Plots of the stable runs performed with ICN can be found in Figure 8.6 (right).

To check that $\lambda = 0$ is indeed the edge of the stability domain, runs were made with values of $\lambda/4 = 10^{-1}, 10^{-2}, 10^{-3}, 10^{-4}, 10^{-5}, 10^{-6}, -10^{-6}$ for a grid size of 48^3, up to 100 crossing times. The run with negative λ resulted in a slow exponential growth of the Hamiltonian constraint. Runs with positive values of λ are shown in Figure 8.6 (left), each of them being stable.

For the values $\lambda = 0.0, 2.0$, and 4.0, test runs were made with a grid size of 48^3 and 2000 crossing times. The code revealed no unstable modes.

As suggested by Eq. (8.10), the larger the value of λ the faster certain quantities propagate across the numerical grid. For any given value of the $\Delta t / \Delta x$ ratio, there are values of λ large enough such that the CFL condition is violated, e.g. the velocity $v_{\mathcal{C}}$ of the Hamiltonian constraint gets larger than the numerical velocity intrinsic to the evolution scheme. To support this argument a run was made with $\Delta t = \Delta x / 8$ (half the time-step of the standard runs) and $\lambda = 20$, 2000 crossing times. It showed no exponential growth.

8.3.3 Dirichlet boundary conditions

Next various boundary conditions were tested for the SWE and LG equations. First a test bed was defined so as to efficiently reveal unstable (boundary) algorithms. Then this test bed was applied to the SWE and a number of boundary routines for the LG equations, using the 2ND evolution scheme. The boundary algorithms that performed best were tested for the other three evolution schemes LF1, LF2, and ICN. A stable algorithm is finally formulated for the LG equations with a cubic boundary.

Definition of test bed for Dirichlet boundary condition

The stability test bed is defined as follows:
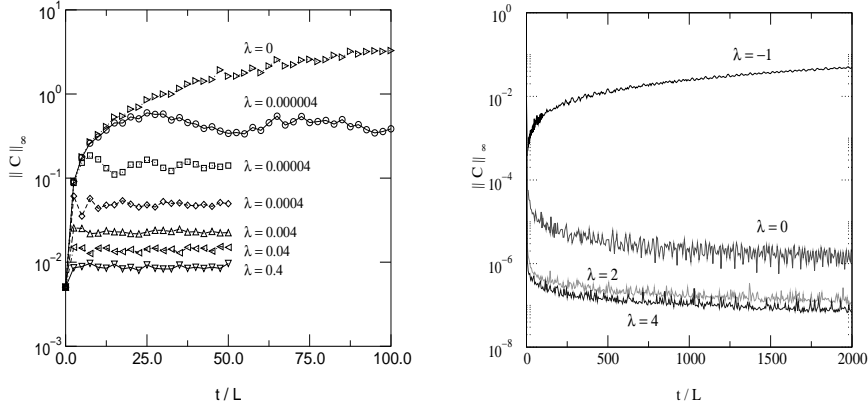
Fig. 8.6: The ℓ_∞ norm of the Hamiltonian constraint versus time (in crossing times) for the algorithms 2ND (left) and ICN (right), periodic boundary conditions. Runs were made with 48 gridpoints, random initial data of $O(10^{-6})$, various choices of λ. The ratio $\Delta t/\Delta x$ was chosen to be 0.25.

- random initial data for all dynamic quantities

- random data for all free functions on the boundary

- grid size of at least 48^3, evolving the code for at least 2000 crossing times.

In this context random data means a set of numbers equally distributed in the interval $[-a, +a]$. The value of the parameter a was chosen to be $O(10^{-6})$.

If an unstable mode reveals itself for grid sizes smaller than 48^3, the larger grid size test becomes irrelevant.

Scalar wave code with Dirichlet boundary condition

The test bed was tried with a scalar wave code, 2ND evolution algorithm, using periodic boundary conditions in the x- and y-directions, and random Dirichlet boundary condition on the $z = $ constant faces. For a grid size of 48^3 and a CFL factor of 0.25, the code ran stably for 2000 crossing times, showing a growth that is not stronger than linear for the quantity $||\phi||_\infty$ as a function of time.

The ADM equations with "plain" Dirichlet boundary condition

The term "plain" Dirichlet boundary condition denotes setting all six metric functions to random numbers on the $z = $ constant faces of the evolution domain with the x- and y-directions kept periodic. This boundary condition was unstable for the choices $\lambda = 0.0, 1.0, 2.0$ or 3.0. The grid size was 16^3 and the runs lasted less than 1000 crossing times.

The choice of $\lambda = 4.0$ was more robust, but for a grid size of 48^3 the instability emerged after only 150 crossing times.

The following analytic argument indicates what goes wrong [121]. Let us define

$$\Psi := \partial_A \partial^A h_B^B - \partial^A \partial^B h_{AB}. \tag{8.75}$$

The evolution equations $^{(4)}R_{ij} = 0$ imply that the quantity Ψ propagates as a scalar wave, i.e. $\Box \Psi = 0$. The question arises: what boundary condition is applied to Ψ when h_{ij} is set to zero at the boundary? Clearly $h_{ij}|_{bdry} = 0$ implies $\Psi|_{bdry} = 0$. On the other hand

$$2\partial_A{}^{(4)}G_z^A = \partial_A \ddot{h}_z^A - \partial_A \partial_B(\partial^B h_z^A - \partial^A h_z^B) - \partial_z \Psi = 0. \tag{8.76}$$

One can see that setting h_{ij} to zero at the boundary implies an *additional* condition on the boundary value of Ψ, namely $\partial_z \Psi|_{bdry} = 0$. Using Dirichlet and Neumann conditions as simultaneous boundary conditions on a scalar wave is over-determined. *Therefore setting $h_{ij}|_{bdry} = 0$ gives rise to an inconsistent boundary condition.*

The characteristic code with "plain" Dirichlet boundaries

For comparison a similar test was performed with the characteristic code, as described in Chapter 3. Since non-linear terms are included in the code, the amplitude of the initial and boundary data was set to $a = 10^{-6} \cdot (\Delta t)^2$, and the non-linear term $\beta_{,r}$ was set to zero on the initial slice as well as on the inner boundary. The code revealed no unstable modes. Not even a linearly growing mode was present. The radial grid size was set to 49, the 2-D angular grid using 55^2 points per stereographic patch. The inner boundary was placed at $r = 1$ at which $\Delta t / \Delta r \simeq 0.5$. The run was made up to $t = 4000$.

A systematic search for a stable, Dirichlet boundary condition

Although the question of initial boundary value problem for symmetric hyperbolic systems is discussed in [123, 124], the ADM evolution equations are neither first-order nor hyperbolic. Thus we are left with the option of studying the boundary problem via systematic experiments.

Analytic discussion

We first studied reflecting boundary conditions on the $z = $ constant faces of a cube that has periodic boundary conditions in the x- and y-directions.

The strategy was to apply Dirichlet boundary conditions to only some of the components of the metric tensor h_{ij}, the others were constrained by demanding that various combinations of the following quantities vanish on the boundary:

$$
\begin{aligned}
-2\,\mathcal{C}^z &\equiv \partial_j \dot{h}^{zj} - \partial^z \dot{h}; & (8.77)\\
-2\,\mathcal{C}^A &\equiv \partial_j \dot{h}^{Aj} - \partial^A \dot{h}; & (8.78)\\
2\,^{(4)}R_t^t &\equiv \ddot{h}; & (8.79)\\
2\,^{(4)}G_{zz} &\equiv -\ddot{h}_A^A + \partial^B \partial_B h_A^A - \partial_A \partial_B h^{AB}; & (8.80)\\
2\,^{(4)}G_z^A &\equiv \ddot{h}_z^A - \partial_B(\partial^B h_z^A - \partial^A h_z^B) \\
& \quad -\partial_z \partial^A h_B^B + \partial_z \partial^B h_B^A; & (8.81)
\end{aligned}
$$

$$
\begin{aligned}
2\left(-\dot{\mathcal{C}}^A + \partial^A\,^{(4)}R_t^t\right) &:= \partial_j \dddot{h}^{Aj}; & (8.82)\\
2\left(-\dot{\mathcal{C}}^z + \partial^z\,^{(4)}R_t^t\right) &:= \partial_j \dddot{h}^{zj}. & (8.83)
\end{aligned}
$$

Here uppercase Latin letters indicate the directions in the plane of the boundary (i.e. the x- and y-directions). In formulating sets of boundary constraints one should recall that use of the Hamiltonian constraint and of the three momentum constraints does not give four independent conditions [38], these quantities being related via the Bianchi identities.

The following boundary conditions were tested:

1.

$$
\begin{aligned}
h^{xx} - h^{yy} = h^{xy} &= 0, & (8.84)\\
\dot{h}^{ij}_{,j} - \eta^{ij}\dot{h}_{,j} &= 0, & (8.85)\\
\ddot{h} &= 0. & (8.86)
\end{aligned}
$$

2.

$$
\begin{aligned}
h^{xx} = h^{yy} = h^{xy} &= 0, & (8.87)\\
\ddot{h}^{ij}_{,j} &= 0. & (8.88)
\end{aligned}
$$

3.

$$
\begin{aligned}
h^{xx} - h^{yy} = h^{xy} &= 0, & (8.89)\\
\ddot{h}^{ij}_{,j} &= 0, & (8.90)\\
\ddot{h} &= 0. & (8.91)
\end{aligned}
$$

4.

$$h^{xx} = h^{yy} = h^{xy} \quad = \quad 0, \tag{8.92}$$
$$\dot{h}_{,i}^{Ai} - \eta^{Ai}\dot{h}_{,i} \quad = \quad 0, \tag{8.93}$$
$$\ddot{h}_{,i}^{zi} \quad = \quad 0. \tag{8.94}$$
$$\tag{8.95}$$

5.

$$h^{xx} - h^{yy} = h^{xy} \quad = \quad 0, \tag{8.96}$$
$$\dot{h}_{,i}^{Ai} - \eta^{Ai}\dot{h}_{,i} \quad = \quad 0, \tag{8.97}$$
$$\ddot{h}_{,i}^{zi} \quad = \quad 0, \tag{8.98}$$
$$\ddot{h} \quad = \quad 0. \tag{8.99}$$

6.

$$h^{xx} = h^{yy} = h^{xy} \quad = \quad 0, \tag{8.100}$$
$$\ddot{h}_{,j}^{ij} - \frac{1}{2}\eta^{ij}\,\ddot{h}_{,j} \quad = \quad 0. \tag{8.101}$$

Finite differencing

Applying the various proposed algorithms requires solving finite-difference equations that involve time and space derivatives. A function F is represented by a discrete set of values $F_{[I,J,K]}^{[N]}$ where N labels the time level, and I, J, K correspond to grid indices along the coordinates x, y, z.

The x- and y-derivatives are either centered at the gridpoints

$$\partial_x F_{[I,J,K]} = \frac{1}{2h}\left[F_{[I+1,J,K]} - F_{[I-1,J,K]}\right] + O(\Delta^2), \tag{8.102}$$

$$\partial_y F_{[I,J,K]} = \frac{1}{2h}\left[F_{[I,J+1,K]} - F_{[I,J-1,K]}\right] + O(\Delta^2), \tag{8.103}$$

or in the middle of the 2-D cells:

$$\partial_x F_{[I+1/2,J,K]} = \frac{1}{h}\left[F_{[I+1,J,K]} - F_{[I,J,K]}\right] + O(\Delta^2), \tag{8.104}$$

$$\partial_y F_{[I,J+1/2,K]} = \frac{1}{h}\left[F_{[I,J+1,K]} - F_{[I,J,K]}\right] + O(\Delta^2). \tag{8.105}$$

The z-derivatives are computed either at the boundary:

$$\partial_z F_{[I,J,1]} = \frac{1}{2h}\left[-3F_{[I,J,1]} + 4F_{[I,J,2]} - F_{[I,J,3]}\right] + O(\Delta^2), \quad (8.106)$$

$$\partial_z F_{[I,J,K_{max}]} = \frac{1}{2h}\left[F_{[I,J,K_{max}-2]} - 4F_{[I,J,K_{max}-1]} + 3F_{[I,J,K_{max}]}\right]$$
$$+ O(\Delta^2), \quad (8.107)$$

or at the point next to the boundary:

$$\partial_z F_{[I,J,2]} = \frac{1}{2h}\left[F_{[I,J,3]} - F_{[I,J,1]}\right] + O(\Delta^2), \quad (8.108)$$

$$\partial_z F_{[I,J,K_{max}-1]} = \frac{1}{2h}\left[F_{[I,J,K_{max}]} - F_{[I,J,K_{max}-2]}\right] + O(\Delta^2), \quad (8.109)$$

or between the boundary point and its' nearest neighbor:

$$\partial_z F_{[I,J,1+1/2]} = \frac{1}{h}\left[F_{[I,J,2]} - F_{[I,J,1]}\right] + O(\Delta^2), \quad (8.110)$$

$$\partial_z F_{[I,J,K_{max}-1/2]} = \frac{1}{h}\left[F_{[I,J,K_{max}]} - F_{[I,J,K_{max}-1]}\right] + O(\Delta^2). \quad (8.111)$$

Runs were made with various choices of λ, using the 2ND evolution algorithm. Initial data was a set of random numbers of $O(10^{-6})$ in a domain of compact support, unless stated otherwise.

All of the boundary constraints listed above have the form $\dot{\mathcal{F}}(h^{ij}, h^{ij}_{,k}) = 0$ or $\ddot{\mathcal{F}}(h^{ij}, h^{ij}_{,k}) = 0$. Since initial data in the neighborhood of the boundary is zero, the functions $\mathcal{F}$ vanish for the first few time levels. Analytically the function $\mathcal{F}$ and its first time derivative are initially zero (in the neighborhood of the boundary). Thus imposing $\dot{\mathcal{F}} = 0$ or $\ddot{\mathcal{F}} = 0$ amounts to asking that $\mathcal{F} = 0$ at all times. In other words, the use of initial data of compact support implies that the time derivatives in the various boundary conditions play no effective role. For this reason all runs were made with the same stencils for first-order time derivatives, centered between the last two time levels.

Boundary algorithm

In order to understand the implementation of the above boundary constraints consider the case defined by Eqs. (8.87) - (8.88). Written out in an explicit form, the boundary constraints (8.88) become

$$\ddot{h}^{xx}_{,x} + \ddot{h}^{xy}_{,y} + \ddot{h}^{xz}_{,z} = 0, \quad (8.112)$$

$$\ddot{h}^{yx}_{,x} + \ddot{h}^{yy}_{,y} + \ddot{h}^{yz}_{,z} = 0, \tag{8.113}$$

$$\ddot{h}^{zx}_{,x} + \ddot{h}^{zy}_{,y} + \ddot{h}^{zz}_{,z} = 0. \tag{8.114}$$

With the boundary values of h^{xx}, h^{xy} and h^{yy} set to zero, the boundary constraints (8.112) - (8.113) serve as Neumann-type conditions on h^{xz} and h^{yz}. Having determined these two functions at the boundary point, one can use Eq. (8.114) to compute the boundary value for h^{zz}.

The other boundary systems do not provide such a clean method of updating boundary points: the boundary equations are a set of coupled PDEs, involve quantities whose boundary values are not yet known. For example, the system (8.89) - (8.91) provides only two functions at the boundary, $h^{xx} - h^{yy}$ and h^{xy} with the additional constraint $\ddot{h}^{xx} + \ddot{h}^{yy} + \ddot{h}^{zz} = 0$. This means that the boundary values of h^{xx} and h^{yy} are functions of h^{zz}, which is determined by Eq. (8.90) which also involves the boundary values of h^{xx} and h^{yy}. An iterative approach was adopted to solve such coupled systems.

In fact, a non-iterative approach could be used only for the system (8.87) - (8.88), solved with x- and y-derivatives centered on the gridpoints.

Numeric results

The first set of runs was made for a grid size of 16^3, with a CFL factor of 0.25, for 500 crossing times (i.e. on a grid of $-1...1$ up to $t = 1000$), with the choice of $\lambda = 4$ as defined in Eq. (8.7).

The results were:

- The condition

$$h^{xx} = h^{yy} = h^{xx} = 0, \tag{8.115}$$
$$\ddot{h}^{ij}_{,j} = 0 \tag{8.116}$$

  showed no signs of instability for the following two stencils:

  1. z-derivative computed at the boundary, x- and y-derivatives centered on the point;

  2. z-derivative centered between the last two points, x- and y-derivatives centered in the 2-D cells.

- The condition

$$h^{xx} - h^{yy} = h^{xx} = 0, \tag{8.117}$$
$$\ddot{h}^{ij}_{,j} = 0, \tag{8.118}$$
$$\ddot{h} = 0 \tag{8.119}$$

showed no signs of instability for the stencil in which z-derivative is centered between the last two points, and the x- and y-derivatives are centered in the 2-D cells.

- All other (non-periodic) boundary conditions gave unstable runs.

Next the three well-behaved cases were tested with homogeneous boundary data and random initial data (without compact support).

The runs with Eqs. (8.115) - (8.116) showed no qualitative difference. The Hamiltonian constraint was still a linear function of time.

The runs with Eqs. (8.117) - (8.119) resulted in

$$\begin{aligned}||\mathcal{C}||_\infty &= O(10^{-2}) + t \cdot O(10^{-4}) + t^2 \cdot O(10^{-4}) \\ &\quad + t^3 \cdot O(10^{-3}) + t^4 \cdot O(10^{-12}) + \cdots\end{aligned}$$

Running with 32^3 gridpoints gave similar results. When running with 48^3 points for 1000 crossing times, with derivatives centered on the cell, both the condition Eqs. (8.115) - (8.116) and Eqs. (8.117) - (8.119) revealed an unstable mode. The only boundary condition surviving the stability tests is Eqs. (8.115) - (8.116), using z-derivatives computed at the boundary and x- and y-derivatives centered on the point.

Next, boundary values for h^{xx}, h^{yy} and h^{xy} were set to random numbers. The Hamiltonian constraint remained a linear function of time.

Even though the results were significantly better than for the "plain" Dirichlet boundary condition, the picture is still unclear. Ideally one should have to specify two functions at the boundary (the two polarization modes). Then, starting from these, one should be able to reconstruct boundary values for all six metric functions by use of four boundary constraints.

The following boundary condition is proposed:

- provide h^{xy} and $h^{xx} - h^{yy}$ freely (i.e. set the polarization modes to random numbers), and

- compute $h^{xx} + h^{yy}, h^{zx}, h^{zy}, h^{zz}$ using Eqs. (8.80), (8.82) and (8.83).

Initial data is a set of random numbers (without compact support), for each metric function. The code was run for 2000 crossing times.

This boundary condition caused exponential growth of the Hamiltonian constraint after 1000 crossing times for a grid size of 48^3 with the value of $\lambda = 4.0$. The value $\lambda = 3.0$ was unstable after 800 crossing times.

Convergence test

In order to study its convergence properties, the above boundary algorithm is extended to the edges and corners of the cube-shaped boundary. This is done done using the following rules:

1. On edges and corners use the equation

$$\ddot{h} = 0 \qquad (8.120)$$

together with the two "+"-modes given on the neighboring sides to compute the diagonal components of the metric.

2. On edges use the equation

$$\ddot{h}^{ij}_j = 0 \qquad (8.121)$$

with sideways finite difference derivatives to compute the missing non-diagonal component.

Although the boundary algorithm is unstable, the exponential growth is slow enough to allow a short time convergence test. This was done using $\ell = 4$ time-symmetric linear waves [125] of amplitude 10^{-6}, width 1, at t=8, bounding box $-4\ldots4$, grid sizes $50, 60, 70, 80$. The measured convergence rates of the six metric functions were better than $O(h^{2.04})$.

8.3.4 *Boundary constraints and the first-order schemes*

The previous sections have identified a few algorithms that work significantly better than the inconsistent choice $h_{ij}|_{bdry} = 0$. As a next step, a number of boundary algorithms were tested with the other evolution schemes: LF1, LF2, and ICN.

First the the boundary constraints Eqs. (8.78) - (8.83) are rewritten in terms of the variables h_{ij} and $K_{ij} = -\frac{1}{2}\dot{h}_{ij}$:

$$2\,^{(4)}G_{zz} = 2\dot{K}^A_A + \partial^B\partial_B h^A_A - \partial_A\partial_B h^{AB}, \qquad (8.122)$$

$$\dot{\mathcal{C}}^A - \partial^A\,^{(4)}R^t_t = \partial_z\dot{K}^{Az} + \partial_B\dot{K}^{AB}, \qquad (8.123)$$

$$\mathcal{C}^A = \partial_z K^{Az} + \partial_B K^{AB} - \partial^A K, \qquad (8.124)$$

$$2\,^{(4)}G^A_z = -2\dot{K}^A_z - \partial_B(\partial^B h^A_z - \partial^A h^B_z)$$
$$-\partial_z\partial^A h^B_B + \partial_z\partial^B h^A_B, \qquad (8.125)$$

$$^{(4)}R^t_t = -\dot{K}, \qquad (8.126)$$

$$\dot{\mathcal{C}}^z - \partial^z\,^{(4)}R^t_t = \partial_z\dot{K}^{zz} + \partial_B\dot{K}^{zB}. \qquad (8.127)$$

Given the h_{TT} components[1] h^{xy} and $h^{xx} - h^{yy}$, equation (8.122) determines the missing component of the 2-tensor h_{AB}. The h^{zA} components can then be determined via any of the equations (8.123) - (8.125). Either of

---

[1] These functions correspond to the gravitational wave that propagates (in this case) in the z-direction, two polarization modes. (See Section 3.3.)

the remaining expressions, (8.126) or (8.127), can be used to compute the component h_{zz}. These equations provide five[2] alternative sets of boundary constraints:

No.	Equations involved:
1)	(8.122), (8.124) and (8.126),
2)	(8.122), (8.123) and (8.126),
3)	(8.122), (8.123) and (8.127),
4)	(8.122), (8.125) and (8.126),
5)	(8.122), (8.125) and (8.127).

The linearized ADM equations (8.15)-(8.16) have the form

$$\dot{h}_{ij} = -2K_{ij}, \tag{8.128}$$

$$K_{ij} = \sum_{k,l,m,n} c[k,l,m,n;i,j]\partial_k\partial_l h_{mn}, \tag{8.129}$$

with $c[k,l,m,n;i,j]$ being a set of numeric coefficients. The metric h_{ij} can be updated at each gridpoint where K_{ij} is known. In other words there is no need for boundary data for h_{ij}. On the other hand updating K_{ij} involves finite-difference expressions involving h_{ij}. This implies that the tensor K_{ij} cannot be updated at the boundary via the evolution algorithm. A separate boundary algorithm is necessary. This algorithm uses a set of boundary constraints and the free functions K_{TT}.

When approximating the boundary constraints by finite-difference equations, those derivatives that are parallel to the boundary are centered on the gridpoint. Derivatives perpendicular to the boundary (the z-derivatives) are computed using 3-point, second-order formulae (see Eqs. (8.106) - (8.107)). Time derivatives are centered in the mid-level $N + 1/2$. Since the momentum constraint $\mathcal{C}^A$ does not contain explicit time derivatives, it is imposed on the time level t_N. These rules furnish finite-difference approximations for any of the boundary constraints. For example, Eq. (8.122) is approximated by

$$\frac{1}{\Delta t}\left[\left(K_A^A\right)_{[I,J,1]}^{[N+1]} - \left(K_A^A\right)_{[I,J,1]}^{[N]}\right] = \frac{1}{4(\Delta x)^2} \times$$

$$\left(-2h_{xx[I,J-1,1]}^{[N+1/2]} + 4h_{xx[I,J,1]}^{[N+1/2]} - 2h_{xx[I,J+1,1]}^{[N+1/2]} \right.$$

$$-2h_{yy[I-1,J,1]}^{[N+1/2]} + 4h_{yy[I,J,1]}^{[N+1/2]} - 2h_{yy[I+1,J,1]}^{[N+1/2]}$$

---

[2] There is one more combination of constraints, (8.122), (8.124), and (8.127), whose numerical implementation was not clear and so we have not insisted in working it out.

$$-h_{xy[I+1,J-1,1]}^{[N+1/2]} - h_{xy[I-1,J+1,1]}^{[N+1/2]}$$
$$+h_{xy[I+1,J+1,1]}^{[N+1/2]} + h_{xy[I-1,J-1,1]}^{[N+1/2]} \Big) \qquad (8.130)$$

and used to update $\left(K_A^A\right)_{[I,J,1]}^{[N+1]}$; similarly, Eq. (8.127) is approximated by

$$\frac{1}{2\Delta t \Delta x}\Big\{ \Big[3K_{[I,J,1]}^{zz[N+1]} - 4K_{[I,J,2]}^{zz[N+1]} + K_{[I,J,3]}^{zz[N+1]}\Big] -$$
$$\Big[3K_{[I,J,1]}^{zz[N]} - 4K_{[I,J,2]}^{zz[N]} + K_{[I,J,3]}^{zz[N]}\Big] \Big\} \quad +$$
$$\frac{1}{2\Delta t \Delta x}\Big\{ \Big[K_{[I+1,J,1]}^{xz[N+1]} - K_{[I-1,J,1]}^{xz[N+1]}\Big] - \Big[K_{[I+1,J,1]}^{xz[N]} - K_{[I-1,J,1]}^{xz[N]}\Big] \Big\} \quad +$$
$$\frac{1}{2\Delta t \Delta x}\Big\{ \Big[K_{[I,J+1,1]}^{yz[N+1]} - K_{[I,J-1,1]}^{yz[N+1]}\Big] - \Big[K_{[I,J+1,1]}^{yz[N]} - K_{[I,J-1,1]}^{yz[N]}\Big] \Big\} \quad = \quad 0$$
$$(8.131)$$

and used to update $K_{[I,J,1]}^{zz[N+1]}$.

Stability tests were made for 2000 crossing times, grid size of 48^3, $\Delta t = \Delta x/4$, random initial data and random boundary values for the K_{TT} functions. All five systems were tested for $\lambda = 2$, with all evolution algorithms. Only the runs with ICN were stable. In addition system (1) was tested using $\lambda = 0$ and $\lambda = 4$, with all evolution algorithms. Again, all runs became unstable except for ICN. System (5) was tested for $\lambda = 0$ and $\lambda = 4$ as well; it remained stable for ICN and became unstable in a short time for the leap-frog algorithms.

Five stable boundary-algorithms have been found for the LG equations evolved via an ICN scheme. None of these boundary algorithms were stable when evolved with the leap-frog schemes. Figure 8.7 plots of the ℓ_∞ norm of the Hamiltonian constraint as a function of time for ICN and LF2.

8.3.5 Outgoing radiation boundary conditions

A few runs were performed with the "modified" Sommerfeld boundary conditions. "Modified" in the present context means

$$[(\partial_t - \partial_x)F]_{|x_{min}} = S_{|x_{min}}, \quad [(\partial_t + \partial_x)F]_{|x_{max}} = S_{|x_{max}} \qquad (8.132)$$

where S is a source, describing incoming radiation. In the numerical experiments we set S to random numbers.

Our efforts in this direction were limited. We have not been able to find a stable boundary algorithm for the LG equations, when using Sommerfeld radiation conditions. In particular, we applied Sommerfeld condition on the radiation degrees of freedom combined with different sets of boundary constraints. These experiments produced unstable runs.
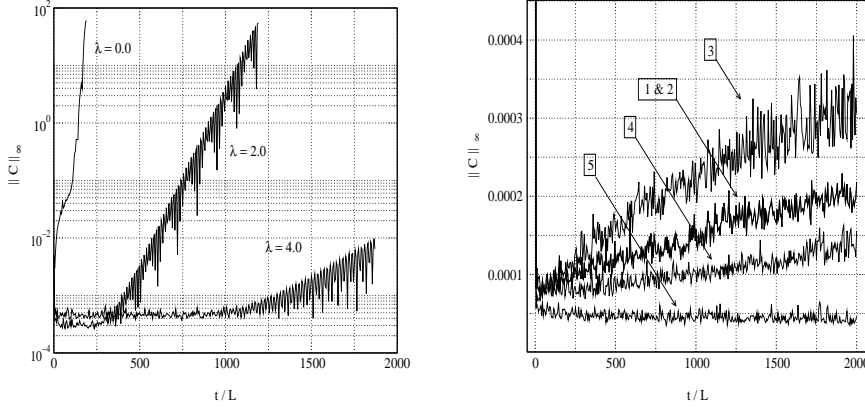
Fig. 8.7: The ℓ_∞ norm of the Hamiltonian constraint versus time (in crossing times) for stability runs with random initial and h_{TT} boundary data of $O(10^{-6})$, with $\Delta t = \Delta x/4$. The x- and y-directions have periodic boundary condition. Left: algorithm LF2. The boundary constraints are given by system (1), with runs being made for $\lambda = 0, 2$, and 4. Right: algorithm ICN. $\lambda = 2$, for all five boundary-constraint systems.

8.3.6 Evolution of a bounded space-time region

Next we want to extend the boundary algorithm to all faces of a cube. The edges and corners must be handled separately.

Algorithm (5) was used on all faces. The two components $K_{TT} = -\frac{1}{2}\dot{h}_{TT}$ are treated as free data (they are specified randomly) on all faces, edges, and corners. While this means two free quantities and four constraints on the faces, there are four free quantities on the edges, so only two constraints are needed. Similarly, on the corners, there are five free quantities, for the identity $[K_{xx} - K_{yy}] + [K_{yy} - K_{zz}] + [K_{zz} - K_{xx}] = 0$ reduces the total number of six TT components to five that are independent. Thus only one constraint is needed at the corners.

All non-diagonal components are provided at the corners. Given $[K_{xx} - K_{yy}]$ and $[K_{zz} - K_{xx}]$ the missing diagonal component is K_{xx}, which can be computed from

$$3K_{xx} = K + [K_{xx} - K_{yy}] + [K_{xx} - K_{zz}].$$

The trace K is updated using the condition

$$^{(4)}R_t^t = -\dot{K} = 0.$$

On the edges parallel to the x-axis one already has K_{xy} and K_{xz} as boundary data. The missing boundary data K_{yz} is computed using $^{(4)}G_{yz}$,
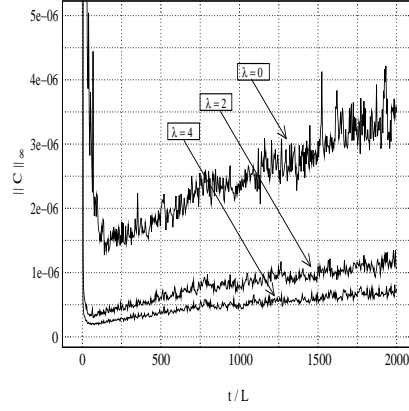
Fig. 8.8: Results of the stability tests for a code evolving the interior region of a cube with constrained boundaries at the faces, edges, and corners of the cube. The Hamiltonian constraint is measured via the ℓ_∞ norm. Initial data and the h_{TT} boundary data are random of $O(10^{-6})$. The CFL ratio is $\Delta t / \Delta x = 0.25$. Runs were performed for 2000 crossing times, using, $\lambda = 0, 2$, and 4.

an equation that is also used on both neighboring faces. Derivatives in the y- and z-directions are computed by sideways, 3-point, finite difference formulae. The diagonal components of the 3-metric are computed the same way as on the corners.

Note that the routine that solves the constraint

$$(-\dot{\mathcal{C}}^n + \partial^{n\,(4)} R_t^t) = 0$$

on a face of the cube (with normal in the n-direction) must be called *after* the missing non-diagonal components have been updated on the edges surrounding that face. Otherwise, in the case of the $z = $ constant face, when computing the quantity $K_{yz,y}$ on the top time level, with centered finite differencing, one would be using values of K_{yz} on the edge parallel to the x-axis that had not yet been updated.

Runs performed with $\lambda = 0, 2, 4$. showed that the above algorithm is robustly stable. All three runs were given random initial and boundary data. A graph showing the Hamiltonian constraint as a function of time is shown in Figure 8.8.

9. SPHERICAL BOUNDARIES

The previous chapter described how to stably evolve the linearized ADM system in Cartesian coordinates, with boundaries on the faces of a cube. However the Cauchy boundary required by CCM is a sphere; it is not aligned to the Cartesian-grid-structure. We need to adapt the boundary algorithm found for the faces of the cube to the case of a spherical boundary.

The approach we present here uses a spherical grid that forms a boundary for the Cartesian evolution domain. This spherical boundary is connected to the evolution points via an interpolation algorithm. First we describe how such an approach works for the SWE case. Next the linearized ADM system is analyzed. Throughout the chapter the evolution scheme is ICN.

9.1 The scalar wave problem

On a Cartesian set of grid-points $\{x_I, y_J, z_K\}$ that lie inside a sphere of radius R, the scalar wave equation takes the first-order in time discretized form

$$
\begin{aligned}
(\partial_t \phi)_{[I,J,K]} &= \xi_{[I,J,K]}, \\
(\partial_t \xi)_{[I,J,K]} &= \tfrac{1}{(\Delta x)^2} \big(\quad \phi_{[I+1,J,K]} - 2\phi_{[I,J,K]} + \phi_{[I-1,J,K]} \\
&\qquad\qquad \phi_{[I,J+1,K]} - 2\phi_{[I,J,K]} + \phi_{[I,J-1,K]} \\
&\qquad\qquad \phi_{[I,J,K+1]} - 2\phi_{[I,J,K]} + \phi_{[I,J,K-1]} \quad \big) + O(\Delta^2).
\end{aligned}
$$

$$(9.1)$$

In order to properly update the point $[I, J, K]$, one needs values of ϕ at the neighboring points $[I \pm 1, J, K], [I, J \pm 1, K], [I, J, K \pm 1]$. These points are at most a distance Δx outside of the sphere R. The boundary algorithm adopted from [4] is the following:

- Let S_1 denote the spherical boundary of the evolution domain, with radius R_1. Let S_2 and S_3 be two additional spheres, concentric with S_1, radii $R_2 = R_1 + \Delta x, \quad R_3 = R_1 + 2\Delta x$. The spheres are described by a stereographic grid-structure corresponding to the coordinate patches ζ_N, ζ_S.

- Let D be a point outside S_1 with at least one of its nearest neighbors in the Cartesian evolution domain.

- We define the most normal direction through D as the direction given by a vector $\vec{n}$ parallel to either the x-, or the y-, or the z-axis, chosen such that it is closest to the radial direction through D.

- Let C, E, and F be the intersection points of the most normal direction through D and the spheres S_1, S_2 and S_3. Let A and B be the nearest two Cartesian evolution grid-points of D in the most normal direction.

- Given any smooth function ϕ on the Cartesian grid-points inside S_1 and on the spherical gridpoints of S_2 and S_3, one can obtain ϕ_C and ϕ_D by interpolation:

  - The points E and F do not necessarily coincide with stereographic gridpoints, and so the values ϕ_E and ϕ_F are constructed using 2-D quadratic interpolators in the plane $q = \Re(\zeta), p = \Im(\zeta)$.
  - Next, using a 1-D quadratic interpolator in the most normal direction, the values of ϕ_C and ϕ_D are obtained from the values of ϕ at $A, B, E,$ and F.

  An illustration of the interpolation algorithm can be seen in Figure 9.1.

The algorithm presented above requires knowledge of ϕ on the Cartesian evolution gridpoints as well as on the outer two spheres. The sphere S_3 is the boundary of the system, the field ϕ on can be specified arbitrarily on S_3. The value of ϕ on the sphere S_2 is updated using the scalar wave equation, expressed in spherical coordinates. The field ϕ on the sphere S_1 is updated by the interpolation algorithm and is used in the evolution of ϕ on S_2.

The algorithm was found to be numerically stable with the usual settings of 48^3 Cartesian grid-points, 2000 crossing times, a CFL ratio of $\Delta t/\Delta x = 0.25$, random initial data and random boundary data on S_3.

9.2   The linearized ADM system in spherical coordinates

9.2.1   Conventions

We introduce spherical coordinates $[t, r, q, p]$, where stereographic patching is used for the angular coordinates (q, p). The space-time metric takes the
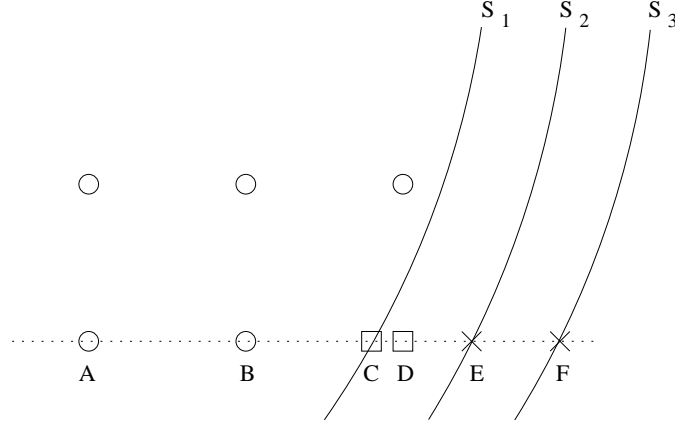
Fig. 9.1: Interpolation scheme providing spherical boundary to a Cartesian code.

form

$$^{(4)}g_{\mu\nu} = {}^{(4)}\eta_{\mu\nu} + {}^{(4)}h_{\mu\nu} = \tag{9.2}$$

$$= \begin{bmatrix} -1 & 0 & 0 & 0 \\ 0 & 1 - Wr & -\frac{2r^2 \Re(U)}{P} & -\frac{2r^2 \Im(U)}{P} \\ 0 & -\frac{2r^2 \Re(U)}{P} & 4\frac{r^2}{P^2}\left[1 + K + \Re(J)\right] & 4\frac{r^2}{P^2}\Im(J) \\ 0 & -\frac{2r^2 \Im(U)}{P} & 4\frac{r^2}{P^2}\Im(J) & 4\frac{r^2}{P^2}\left[1 + K - \Re(J)\right] \end{bmatrix},$$

where $P = 1 + q^2 + p^2$ and $\eta_{\mu\nu} = \mathrm{diag}(-1, 1, \frac{4r^2}{P^2}, \frac{4r^2}{P^2})$.
    We define the vectors:

$$q^\mu = \left[0, 0, \frac{P}{2}, I\frac{P}{2}\right], \tag{9.3}$$

$$r^\mu = [0, 1, 0, 0]. \tag{9.4}$$

9.2.2   Evolution equations

The ADM equations $^{(4)}R_{ij} = 0$ decompose into spin-weighted equations that provide the evolution equations for J, K, U, W:

$$\mathcal{E}_W \quad := \quad r^\mu r^\nu \, {}^{(4)}R_{\mu\nu} = \frac{1}{2r^2}\Big\{r^3\ddot{W} + 2r(rW)_{,r}$$

$$-r\eth\bar{\eth}\bar{\eth}W + \left[r^2\left(\bar{\eth}U + \eth\bar{U}\right)\right]_{,r} + 2[r^2K_{,r}]_{,r}\Big\} = 0, \tag{9.5}$$

$$\mathcal{E}_K := q^\mu\bar{q}^\nu\,{}^{(4)}R_{\mu\nu} =$$

$$\frac{1}{2r^2}\Big\{-2r^4\ddot{K} + 2r^2(r^2K)_{,rr} + 2r^2\eth\bar{\eth}K - r^2(\eth\eth\bar{J} + \bar{\eth}\bar{\eth}J)$$

$$+\left[r^4(\eth\bar{U} + \bar{\eth}U)\right]_{,r} + 2r(r^3W)_{,r} - r^3\eth\bar{\eth}W\Big\} = 0, \tag{9.6}$$

$$\mathcal{E}_U := q^\mu r^\nu\,{}^{(4)}R_{\mu\nu} = \frac{1}{4}\Big\{2r^2\ddot{U} - 4U$$

$$+\eth\eth\bar{U} - \eth\bar{\eth}U - 2\bar{\eth}J_{,r} + 2\eth K_{,r} + 2\eth W\Big\} = 0, \tag{9.7}$$

$$\mathcal{E}_J := q^\mu q^\nu\,{}^{(4)}R_{\mu\nu} = -r^2\ddot{J} + (r^2J_{,r})_{,r} - \frac{1}{2}\,r\,\eth\eth W + (r^2\,\eth U)_{,r} = 0. \tag{9.8}$$

9.2.3   Multipole expansions

Next the metric functions K, W, J, U are written as an expansion in terms of the spherical harmonics:

$$K = \sum_{\ell=0}^{\infty}\sum_{m=-\ell}^{\ell} k^{(\ell,m)}(t,r)\,Y_m^\ell(\theta,\phi), \tag{9.9}$$

$$W = \sum_{\ell=0}^{\infty}\sum_{m=-\ell}^{\ell} w^{(\ell,m)}(t,r)\,Y_m^\ell(\theta,\phi), \tag{9.10}$$

$$J = \sum_{\ell=0}^{\infty}\sum_{m=-\ell}^{\ell} j^{(\ell,m)}(t,r)\,\eth\eth\,Y_m^\ell(\theta,\phi), \tag{9.11}$$

$$U = \sum_{\ell=0}^{\infty}\sum_{m=-\ell}^{\ell} u^{(\ell,m)}(t,r)\,\eth\,Y_m^\ell(\theta,\phi), \tag{9.12}$$

with $(\theta,\phi) = f(q,p)$ defined by

$$\zeta_{North} = q_N + Ip_N = \sqrt{\frac{1-\cos\theta}{1+\cos\theta}}\,e^{I\phi}, \tag{9.13}$$

$$\zeta_{South} = q_S + Ip_S = \sqrt{\frac{1+\cos\theta}{1-\cos\theta}}\,e^{-I\phi}. \tag{9.14}$$

The identities

$$\eth Y_0^0 = 0, \tag{9.15}$$

$$\eth\eth Y_0^1 = \eth\eth Y_{\pm 1}^1 = 0 \tag{9.16}$$

imply that no $\ell = 0$ mode is present in U and that the lowest non-zero term in the expansion of J is a quadrupole.

The equations (9.5) - (9.8), written for the expanded metric variables (9.9) - (9.12), become a series of equations for the coefficients

$$\left\{ k^{(\ell,m)}, w^{(\ell,m)}, j^{(\ell,m)}, u^{(\ell,m)} \right\},$$

with no coupling between different spherical harmonics.

9.2.4 Stability

A numerically stable algorithm must satisfy the von Neumann stability criterion. The von Neumann analysis assumes that the constant coefficient version of the evolution equations has no exponentially growing spatially periodic modes. In order to analyze such modes, we write the evolution equations corresponding to the multipole modes in a constant-coefficient form and study their solutions. The analysis proceeds in the neighborhood of some shell $r = r_0$, in order to avoid the coordinate singularity at $r = 0$ (which is irrelevant for the purpose of CCM).

The methodology we adopt is the following: Consider first the monopole mode $\ell = 0$. This provides a set of two PDEs in the variables (t, r). Assume that the fundamental metric variables of the system are of the form $\tilde{W} = r^m W, \tilde{K} = r^n K$. Next write down the evolution equations for the coefficients $\tilde{k}^{(0,0)}$ and $\tilde{w}^{(0,0)}$ around $r = r_0$. Assuming periodic boundary conditions in the radial direction, choose the values of (n, m) such that exponentially growing modes are ruled out.

Given the values (n, m) from the $\ell = 0$ analysis repeat the procedure for $\ell = 1, m = 0$. This results in a system of three PDEs for the coefficients $k^{(1,0)}, w^{(1,0)}$ and $u^{(1,0)}$. Assume that the fundamental variables of the system are the $\tilde{K}$ and $\tilde{W}$ defined by the $\ell = 0$ analysis, and $\tilde{U} = r^s U$. As it is shown, assuming periodic r-dependence around $r = r_0$ will necessarily imply the presence of exponentially growing modes.

Monopole terms

The monopole amplitudes $\left\{ k^{(0,0)}, w^{(0,0)} \right\}$ evolve according to the equations

$$
\begin{aligned}
\mathcal{E}_K^{(0,0)} &= \frac{1}{r} \left[-r^3 \ddot{k}^{(0,0)} + r \left(r^2 k^{(0,0)} \right)_{,rr} + \left(r^3 w^{(0,0)} \right)_{,r} \right] = 0, \\
&\qquad\qquad\qquad\qquad\qquad\qquad\qquad\qquad\qquad (9.17) \\
\mathcal{E}_W^{(0,0)} &= \frac{1}{2r^2} \left[r^3 \ddot{w}^{(0,0)} + 2r \left(r w^{(0,0)} \right)_{,r} + 2 \left(r^2 k_{,r}^{(0,0)} \right)_{,r} \right] = 0.
\end{aligned}
$$

$$(9.18)$$

up to some overall numerical factors that from now on are neglected.

In order to select an appropriate choice of fundamental variables, the evolution equations (9.17) - (9.18) are rewritten in terms of $\tilde{W} = r^m \cdot W$, $\tilde{K} = r^n \cdot K$:

$$
\begin{aligned}
\mathcal{E}_{\tilde{K}}\big|_{r=r_0} = \ & -r_0{}^{2-n}\tilde{k}^{(0,0)}_{,tt} + r_0{}^{2-n}\tilde{k}^{(0,0)}_{,rr} - 2\,r_0{}^{1-n}\,(n-2)\,\tilde{k}^{(0,0)}_{,r} \\
& +r_0{}^{-n}\,(n-1)\,(n-2)\,\tilde{k}^{(0,0)} \\
& +r_0{}^{-m+2}\tilde{w}^{(0,0)}_{,r} - r_0{}^{1-m}\,(m-3)\,\tilde{w}^{(0,0)} = 0,
\end{aligned}
$$
$$(9.19)$$

$$
\begin{aligned}
\mathcal{E}_{\tilde{W}}\big|_{r=r_0} = \ & \frac{1}{2r}\Big[\tilde{w}^{(0,0)}_{,tt}\,r_0{}^{-m+2} + 2\,r_0{}^{1-m}\tilde{w}^{(0,0)}_{,r} - 2\,r_0{}^{-m}\,(m-1)\,\tilde{w}^{(0,0)} \\
& +2\,r_0{}^{1-n}\tilde{k}^{(0,0)}_{,rr} - 4\,r_0{}^{-n}\,(n-1)\,\tilde{k}^{(0,0)}_{,r} \\
& +2\,r_0{}^{-n-1}n\,(n-1)\,\tilde{k}^{(0,0)}\Big] = 0.
\end{aligned}
$$
$$(9.20)$$

Assume the following behavior for $\tilde{k}^{(0,0)}$ and $\tilde{w}^{(0,0)}$:

$$
\begin{aligned}
\tilde{k}^{(0,0)}(t,r) &= e^{I(\alpha t + \beta r)}k_0, \\
\tilde{w}^{(0,0)}(t,r) &= e^{I(\alpha t + \beta r)}w_0.
\end{aligned}
$$
$$(9.21)$$
$$(9.22)$$

The evolution equations (9.19) - (9.20) then impose conditions on α, β, k_0 and w_0:

$$
\begin{aligned}
\big[I r_0{}^{-m+2}\beta - r_0{}^{1-m}\,(m-3)\big]\ & w_0 \\
+ \big[r_0{}^{2-n}\alpha^2 - r_0{}^{2-n}\beta^2 - 2\,I r_0{}^{1-n}\,(-2+n)\,\beta & \\
+ r_0{}^{-n}\,(n-1)\,(-2+n)\big]\ & k_0 = 0,
\end{aligned}
$$
$$(9.23)$$

$$
\begin{aligned}
\big[-\alpha^2 r_0{}^{-m+2} + 2\,I r_0{}^{1-m}\beta - 2\,r_0{}^{-m}\,(m-1)\big]\ & w_0 \\
+ \big[-2\,r_0{}^{1-n}\beta^2 - 4\,I r_0{}^{-n}\,(n-1)\,\beta + 2\,r_0{}^{-n-1}n\,(n-1)\big]\ & k_0 = 0.
\end{aligned}
$$
$$(9.24)$$

The system of equations (9.23) - (9.24) admits nontrivial solutions (k_0, w_0) if and only if the determinant of the Jacobian of the system vanishes, that is

$$
\begin{aligned}
\frac{1}{r_0^{m+n}}\Big\{\alpha^4 r_0{}^4 + \big[-r_0{}^4\beta^2 - 2\,I r_0{}^3\,(n-1)\,\beta + r_0{}^2\,(-3n+n^2+2m)\big]\alpha^2 \\
+4\,I r_0\,(m-n)\,\beta - 4\,(n-1)\,(m-n-1)\Big\} = 0.
\end{aligned}
$$
$$(9.25)$$

Assuming periodic r-dependence implies a real value for β. Then, unless the imaginary part of $\alpha = f(\beta, r_0)$ is non-negative, the evolution equations (9.19) - (9.20) allow exponentially growing modes. The determinant condition (9.25) is a second-order polynomial in terms of α^2, with solutions of the form

$$\alpha = \pm\sqrt{A \pm \sqrt{B}}. \qquad (9.26)$$

The condition $\Im(\alpha) \geq 0$ implies that all coefficients of Eq. (9.25) must be real. This implies $n = m = 1$. Thus the determinant condition (9.25) leads to

$$\alpha_{1,2} = 0, \quad \alpha_{3,4} = \pm\beta.$$

The fundamental variables identified so far are $\tilde{W} = r \cdot W$ and $\tilde{K} = r \cdot K$.

Dipole terms

The equations evolving the dipole coefficients $\left\{u^{(1,0)}, k^{(1,0)}, w^{(1,0)}\right\}$ are

$$
\begin{aligned}
\mathcal{E}_U^{(1,0)} &= \frac{\zeta}{1 + \zeta\bar{\zeta}} \times \\
&\times \left\{ -r^2 u_{,tt}^{(1,0)} - k_{,r}^{(1,0)} - w^{(1,0)} + u^{(1,0)} + \bar{u}^{(1,0)} \right\} = 0, \qquad (9.27) \\
\mathcal{E}_K^{(1,0)} &= \frac{1}{r^2} \frac{1 - \zeta\bar{\zeta}}{1 + \zeta\bar{\zeta}} \times \\
&\times \left\{ -r^4 k_{,tt}^{(1,0)} + \left[r^4 \left(k_{,r}^{(1,0)} + w^{(1,0)} - u^{(1,0)} - \bar{u}^{(1,0)} \right) \right]_{,r} \right\} = 0,
\end{aligned}
$$
$$(9.28)$$
$$
\begin{aligned}
\mathcal{E}_W^{(1,0)} &= \frac{1}{r^2} \frac{1 - \zeta\bar{\zeta}}{1 + \zeta\bar{\zeta}} \times \\
&\times \left\{ \frac{1}{2} r^3 w_{,tt}^{(1,0)} + \left[r^2 \left(k_{,r}^{(1,0)} + w^{(1,0)} - u^{(1,0)} - \bar{u}^{(1,0)} \right) \right]_{,r} \right\} = 0.
\end{aligned}
$$
$$(9.29)$$

As already mentioned, the dipole term in J vanishes.

Repeating the procedure from the $\ell = 0$ case; the evolution equations (9.27) - (9.29) can be rewritten using the variables $\tilde{U} = r^s \cdot U, \tilde{W} = r \cdot W, \tilde{K} = r \cdot K$. A behavior of the form

$$
\begin{aligned}
\tilde{u}^{(1,0)}(t, r) &= e^{I(\alpha t + \beta r)} u_0, & (9.30) \\
\tilde{k}^{(1,0)}(t, r) &= e^{I(\alpha t + \beta r)} k_0, & (9.31) \\
\tilde{w}^{(1,0)}(t, r) &= e^{I(\alpha t + \beta r)} w_0 & (9.32)
\end{aligned}
$$

is assumed.

The equations $\left\{ \mathcal{E}_{\tilde{U}}^{(1,0)}, \bar{\mathcal{E}}_{\tilde{U}}^{(1,0)}, \mathcal{E}_{\tilde{K}}^{(1,0)}, \mathcal{E}_{\tilde{W}}^{(1,0)} \right\}_{r=r_0}$ are a linear system for the variables $\{\Re(u_0), \Im(u_0), k_0, w_0\}$. The existence of nontrivial solutions leads to the determinant condition satisfied:

$$r_0^8 \alpha^8 - (2 + r_0^2 \beta^2) r_0^6 \alpha^6 + \left(12 - 6s + 2I(s-4)r_0 \beta - 2r_0^2 \beta^2\right) r_0^4 \alpha^4 = 0. \quad (9.33)$$

Similar to the case of Eq. (9.25), we assume periodic r-dependence. Thus β must be real. A well-behaved solution requires that all coefficients of the polynomial Eq. (9.33) be real, which implies $s = 4$. However, this still allows exponential growth. For instance, taking $r_0 = 1, \beta = 0$, a solution of Eq. (9.33) is $-\sqrt{1 - \sqrt{13}}$, which has a negative imaginary part.

The failure of the previous approach to a spherical ADM code indicates that one must adopt a more sophisticated strategy to treat the powers of r that arise in the transformation from Cartesian to spherical coordinates. The fact that the same set of coupled PDEs can be implemented stably using Cartesian coordinates indicates that there should be a stable way to implement ADM in spherical coordinates. That is the subject of future work.

10. SUMMARY

This thesis presents a concentrated effort to develop and calibrate the implementation of the Cauchy-Characteristic Matching problem for 3-dimensional strongly gravitating systems. The related problems of Characteristic and ADM evolution and their boundaries, have been discussed.

First we give a brief description of the Cauchy and Characteristic formulations of the equations of General Relativity, as well as of the concept of Cauchy Characteristic Matching (CCM). Next the Pitt Null Code is described. The underlying physics is presented, i.e. the characteristic slicing, the spin-weighted metric functions and the equations describing the evolution of space-time. We also show how one can use characteristic evolution to numerically evolve black-hole space-times.

In the following we define the concept of Cauchy Characteristic Matching first for a spherically symmetric scalar wave, next for a 3-D scalar field. Then the same concept is outlined for the case of general relativity. To make the understanding of the details easier, first a geometrical description is given, and then a detailed description follows. As described, the extraction first interpolates Cauchy data from the Cartesian grid onto the extraction world-tube, then computes the Jacobian of the coordinate transformation from Cartesian to Bondi coordinates and lastly it computes the Bondi metric functions and provides these as boundary data to the Characteristic evolution. The injection, in turn, uses the Jacobian obtained in the extraction to compute the reverse coordinate transformation from Bondi to Cartesian coordinates and then performs a 4-D interpolation to transfer data from the characteristic grid onto the Cauchy boundary gridpoints. Along with the presentation of the matching modules, calibration tests are provided to show proper second-order accuracy for a number of test-beds.

Next we study the stability properties of CCM. As it is shown, the numerical noise of the individual modules do not excite any short-time instabilities. However, in order to analyze the long-term stability properties of matching, one needs to assure that both the Cauchy and the characteristic evolution codes are able to deal with the discretization error that is inherent to numerical boundary algorithms. This issue is also addressed. As it is shown, the characteristic code is able to deal with constraint violating

boundary modes of high frequency without signs of numerical instabilities. However, the Cauchy code using the ADM equations is numerically unstable unless the boundary conditions are treated properly. A major contribution of this thesis is that, in the context of linearized gravitational theory, we have elucidated the appropriate boundary conditions for the coupled set of partial-differential equations that form the principal part of the ADM equations. In particular, one should not specify boundary values for six metric components but provide boundary data for the two radiation degrees of freedom and use a set of boundary constraints to determine the remaining four components of the spatial metric tensor.

The stability of the injection module requires a spherical boundary condition for the Cartesian Cauchy code. For the ADM system this implies use of boundary constraints in spherical coordinates. The question of spherical boundary constraints applied to a Cartesian grid is a complicated problem that includes implementation of a spherical ADM evolution code, which provides the subject of future work.

APPENDIX

A. ALGEBRAIC EXPRESSIONS FOR THE LINEARIZED QUADRUPOLE WAVES

Using the notations

$$e_1 = \exp\left[-\frac{(u - R_\Gamma)^2}{\varpi^4}\right], \qquad \text{(A.1)}$$

$$e_2 = \exp\left[-\frac{(u + R_\Gamma)^2}{\varpi^4}\right], \qquad \text{(A.2)}$$

$$e_3 = \exp\left[\frac{4uR_\Gamma}{\varpi^2}\right], \qquad \text{(A.3)}$$

the functions $\gamma_{1\ldots11}$ referred to in Section 5.3.2 have the following explicit form:

$$
\begin{aligned}
\gamma_1 = {} & -12 \Big(12\, R_\Gamma{}^2\, \varpi^4\, u + 18\, e_3\, \varpi^4\, R_\Gamma\, u^2 - 32\, e_3\, R_\Gamma{}^6\, u \\
& -12\, e_3\, \varpi^4\, R_\Gamma{}^2\, u + 8\, e_3\, R_\Gamma{}^3\, u^4 + 32\, R_\Gamma{}^6\, u \\
& +16\, R_\Gamma{}^2\, \varpi^2\, u^3 - 8\, \varpi^2\, R_\Gamma{}^5 + 48\, e_3\, R_\Gamma{}^5\, u^2 \\
& -16\, e_3\, \varpi^2\, R_\Gamma{}^2\, u^3 + 24\, e_3\, R_\Gamma{}^3\, \varpi^2\, u^2 + 8\, R_\Gamma{}^3\, u^4 \\
& +8\, e_3\, R_\Gamma{}^7 - 9\, e_3\, \varpi^6\, u - 8\, e_3\, R_\Gamma{}^5\, \varpi^2 \\
& +48\, R_\Gamma{}^5\, u^2 + 18\, R_\Gamma\, \varpi^4\, u^2 - 32\, e_3\, R_\Gamma{}^4\, u^3 \\
& +32\, R_\Gamma{}^4\, u^3 + 9\, \varpi^6\, u + 24\, R_\Gamma{}^3\, \varpi^2\, u^2 \\
& +8\, R_\Gamma{}^7 \Big) \cdot e_2/\varpi^8/R_\Gamma{}^5, \qquad \text{(A.4)}
\end{aligned}
$$

$$
\begin{aligned}
\gamma_2 = {} & 24 \Big(-12\, e_3\, R_\Gamma{}^4\, \varpi^2\, u + 12\, R_\Gamma{}^4\, \varpi^2\, u + 16\, R_\Gamma{}^3\, u^4 \\
& +96\, R_\Gamma{}^5\, u^2 + 64\, R_\Gamma{}^4\, u^3 + 64\, R_\Gamma{}^6\, u \\
& +16\, e_3\, R_\Gamma{}^7 + 21\, \varpi^6\, u - 12\, \varpi^2\, R_\Gamma{}^5 \\
& +16\, R_\Gamma{}^7 + 60\, R_\Gamma{}^3\, \varpi^2\, u^2 + 36\, R_\Gamma{}^2\, \varpi^2\, u^3 \\
& +42\, R_\Gamma\, \varpi^4\, u^2 + 30\, R_\Gamma{}^2\, \varpi^4\, u + 16\, e_3\, R_\Gamma{}^3\, u^4 \\
& -21\, e_3\, \varpi^6\, u - 12\, e_3\, R_\Gamma{}^5\, \varpi^2 + 96\, e_3\, R_\Gamma{}^5\, u^2 \\
& -36\, e_3\, \varpi^2\, R_\Gamma{}^2\, u^3 + 42\, e_3\, \varpi^4\, R_\Gamma\, u^2 - 30\, e_3\, \varpi^4\, R_\Gamma{}^2\, u
\end{aligned}
$$

$$+60\, e_3\, R_\Gamma{}^3\, \varpi^2\, u^2 - 64\, e_3\, R_\Gamma{}^6\, u - 64\, e_3\, R_\Gamma{}^4\, u^3\Big)$$

$$\cdot e_2/\varpi^8/R_\Gamma{}^5, \tag{A.5}$$

$$\gamma_3 \;=\; \pm 6\,\Big(-4\, e_3\, R_\Gamma{}^2\, u^3 + 4\, R_\Gamma{}^2\, u^3 + 6\, \varpi^2\, R_\Gamma{}^2\, u$$

$$+12\, R_\Gamma{}^3\, u^2 + 12\, e_3\, R_\Gamma{}^3\, u^2 + 6\, \varpi^2\, R_\Gamma\, u^2$$

$$+6\, \varpi^2\, e_3\, R_\Gamma\, u^2 - 12\, e_3\, R_\Gamma{}^4\, u - 3\, \varpi^4\, e_3\, u$$

$$+4\, R_\Gamma{}^5 + 3\, \varpi^4\, u - 6\, \varpi^2\, e_3\, R_\Gamma{}^2\, u$$

$$+4\, e_3\, R_\Gamma{}^5 + 12\, R_\Gamma{}^4\, u\Big)\cdot e_2/\varpi^6\,/R_\Gamma{}^5, \tag{A.6}$$

$$\gamma_4 \;=\; \mp 48\,\Big(-2\, \varpi^2\, R_\Gamma{}^5 - 2\, e_3\, R_\Gamma{}^5\, \varpi^2 - 6\, e_3\, R_\Gamma{}^4\, \varpi^2\, u$$

$$-9\, e_3\, \varpi^4\, R_\Gamma{}^2\, u + 18\, e_3\, R_\Gamma{}^3\, \varpi^2\, u^2 - 10\, e_3\, \varpi^2\, R_\Gamma{}^2\, u^3$$

$$+12\, e_3\, \varpi^4\, R_\Gamma\, u^2 + 18\, R_\Gamma{}^3\, \varpi^2\, u^2 + 10\, R_\Gamma{}^2\, \varpi^2\, u^3$$

$$+12\, R_\Gamma\, \varpi^4\, u^2 - 6\, e_3\, \varpi^6\, u + 6\, R_\Gamma{}^4\, \varpi^2\, u$$

$$+6\, \varpi^6\, u + 4\, e_3\, R_\Gamma{}^7 + 24\, R_\Gamma{}^5\, u^2$$

$$+4\, R_\Gamma{}^3\, u^4 + 16\, R_\Gamma{}^6\, u + 16\, R_\Gamma{}^4\, u^3$$

$$+24\, e_3\, R_\Gamma{}^5\, u^2 - 16\, e_3\, R_\Gamma{}^6\, u + 4\, e_3\, R_\Gamma{}^3\, u^4$$

$$+4\, R_\Gamma{}^7 - 16\, e_3\, R_\Gamma{}^4\, u^3 + 9\, R_\Gamma{}^2\, \varpi^4\, u\Big)$$

$$\cdot e_2/\varpi^8/R_\Gamma{}^5, \tag{A.7}$$

$$\gamma_5 \;=\; -24\,\Big(15\, u\, \varpi^8\, e_3 - 9\, \varpi^6\, R_\Gamma{}^3\, e_3 + 40\, \varpi^2\, R_\Gamma{}^7$$

$$-54\, R_\Gamma{}^2\, \varpi^4\, u^3 - 42\, u^2\, R_\Gamma\, \varpi^6 - 40\, R_\Gamma{}^3\, \varpi^2\, u^4$$

$$+6\, \varpi^8\, R_\Gamma - 80\, R_\Gamma{}^8\, u - 160\, R_\Gamma{}^6\, u^3$$

$$+80\, R_\Gamma{}^6\, \varpi^2\, u + 6\, R_\Gamma{}^2\, \varpi^4\, e_3\, u^3 - 6\, \varpi^4\, R_\Gamma{}^5\, e_3$$

$$-18\, R_\Gamma{}^3\, \varpi^4\, e_3\, u^2 + 27\, u\, R_\Gamma{}^2\, \varpi^6\, e_3 - 160\, R_\Gamma{}^7\, u^2$$

$$+18\, R_\Gamma{}^4\, \varpi^4\, u - 15\, u\, \varpi^8 - 3\, u\, R_\Gamma{}^2\, \varpi^6$$

$$-16\, R_\Gamma{}^9 - 16\, R_\Gamma{}^4\, u^5 - 80\, R_\Gamma{}^5\, u^4$$

$$+9\, \varpi^6\, R_\Gamma{}^3 + 6\, \varpi^4\, R_\Gamma{}^5 - 6\, \varpi^8\, R_\Gamma\, e_3$$

$$-80\, R_\Gamma{}^4\, \varpi^2\, u^3 - 42\, R_\Gamma{}^3\, \varpi^4\, u^2 + 18\, R_\Gamma{}^4\, \varpi^4\, u\, e_3$$

$$-18\, u^2\, R_\Gamma\, \varpi^6\, e_3\Big)\cdot e_2/\varpi^{10}\,/R_\Gamma{}^6, \tag{A.8}$$

$$\gamma_6 \;=\; 24\,\Big(-48\, \varpi^6\, R_\Gamma{}^3\, e_3 + 224\, R_\Gamma{}^6\, \varpi^2\, u + 8\, \varpi^2\, R_\Gamma{}^7\, e_3$$

$$-264\, R_\Gamma{}^2\, \varpi^4\, u^3 - 240\, R_\Gamma{}^3\, \varpi^4\, u^2 - 416\, R_\Gamma{}^4\, \varpi^2\, u^3$$

$$-24\, u\, R_\Gamma{}^2\, \varpi^6 - 210\, u^2\, R_\Gamma\, \varpi^6 + 75\, u\, \varpi^8\, e_3$$

$$-320\, R_\Gamma{}^5\, u^4 - 48\, \varpi^4\, R_\Gamma{}^5\, e_3 + 72\, R_\Gamma{}^4\, \varpi^4\, u$$

$$-184\,R_\Gamma{}^3\,\varpi^2\,u^4 - 144\,R_\Gamma{}^5\,\varpi^2\,u^2 - 96\,R_\Gamma{}^3\,\varpi^4\,e_3\,u^2$$
$$-32\,R_\Gamma{}^6\,\varpi^2\,u\,e_3 + 8\,R_\Gamma{}^3\,\varpi^2\,e_3\,u^4 - 90\,u^2\,R_\Gamma\,\varpi^6\,e_3$$
$$+120\,R_\Gamma{}^4\,\varpi^4\,u\,e_3 + 144\,u\,R_\Gamma{}^2\,\varpi^6\,e_3 + 48\,R_\Gamma{}^5\,\varpi^2\,u^2\,e_3$$
$$-32\,R_\Gamma{}^4\,\varpi^2\,e_3\,u^3 + 24\,R_\Gamma{}^2\,\varpi^4\,e_3\,u^3 + 48\,\varpi^6\,R_\Gamma{}^3$$
$$+30\,\varpi^8\,R_\Gamma - 64\,R_\Gamma{}^4\,u^5 - 640\,R_\Gamma{}^6\,u^3$$
$$-640\,R_\Gamma{}^7\,u^2 - 30\,\varpi^8\,R_\Gamma\,e_3 + 136\,\varpi^2\,R_\Gamma{}^7$$
$$+48\,\varpi^4\,R_\Gamma{}^5 - 64\,R_\Gamma{}^9 - 320\,R_\Gamma{}^8\,u$$
$$-75\,u\,\varpi^8\Big)\cdot e_2/\varpi^{10}\,/R_\Gamma{}^6, \tag{A.9}$$

$$\gamma_7 \;=\; \pm 6/\varpi^8\Big(-48\,R_\Gamma{}^2\,\varpi^2\,u^3 - 6\,\varpi^6\,R_\Gamma\,e_3 - 12\,\varpi^4\,R_\Gamma{}^3\,e_3$$
$$-72\,R_\Gamma{}^3\,\varpi^2\,u^2 - 42\,R_\Gamma\,\varpi^4\,u^2 - 32\,e_3\,R_\Gamma{}^4\,u^3$$
$$-32\,e_3\,R_\Gamma{}^6\,u + 15\,e_3\,\varpi^6\,u + 8\,e_3\,R_\Gamma{}^3\,u^4$$
$$+48\,e_3\,R_\Gamma{}^5\,u^2 - 96\,R_\Gamma{}^4\,u^3 - 15\,\varpi^6\,u$$
$$+6\,\varpi^6\,R_\Gamma + 48\,e_3\,R_\Gamma{}^4\,\varpi^2\,u - 24\,R_\Gamma{}^7$$
$$+12\,\varpi^4\,R_\Gamma{}^3 - 24\,e_3\,R_\Gamma{}^3\,\varpi^2\,u^2 - 96\,R_\Gamma{}^6\,u$$
$$-144\,R_\Gamma{}^5\,u^2 + 8\,e_3\,R_\Gamma{}^7 - 24\,R_\Gamma{}^3\,u^4$$
$$+36\,e_3\,\varpi^4\,R_\Gamma{}^2\,u - 18\,e_3\,\varpi^4\,R_\Gamma\,u^2 + 24\,\varpi^2\,R_\Gamma{}^5$$
$$-24\,e_3\,R_\Gamma{}^5\,\varpi^2 - 12\,R_\Gamma{}^2\,\varpi^4\,u\Big)\cdot e_2/R_\Gamma{}^6, \tag{A.10}$$

$$\gamma_8 \;=\; \mp 24\Big(56\,\varpi^2\,R_\Gamma{}^7 + 12\,R_\Gamma{}^2\,\varpi^4\,e_3\,u^3 + 90\,u\,R_\Gamma{}^2\,\varpi^6\,e_3$$
$$+84\,R_\Gamma{}^4\,\varpi^4\,u\,e_3 - 54\,u^2\,R_\Gamma\,\varpi^6\,e_3 + 8\,R_\Gamma{}^3\,\varpi^2\,e_3\,u^4$$
$$-32\,R_\Gamma{}^4\,\varpi^2\,e_3\,u^3 + 48\,R_\Gamma{}^5\,\varpi^2\,u^2\,e_3 - 60\,R_\Gamma{}^3\,\varpi^4\,e_3\,u^2$$
$$-32\,R_\Gamma{}^6\,\varpi^2\,u\,e_3 + 36\,\varpi^4\,R_\Gamma{}^5 - 32\,R_\Gamma{}^9$$
$$-36\,\varpi^4\,R_\Gamma{}^5\,e_3 - 30\,\varpi^6\,R_\Gamma{}^3\,e_3 + 36\,R_\Gamma{}^4\,\varpi^4\,u$$
$$+64\,R_\Gamma{}^6\,\varpi^2\,u - 156\,R_\Gamma{}^3\,\varpi^4\,u^2 - 256\,R_\Gamma{}^4\,\varpi^2\,u^3$$
$$-18\,u\,R_\Gamma{}^2\,\varpi^6 - 126\,u^2\,R_\Gamma\,\varpi^6 + 45\,u\,\varpi^8\,e_3$$
$$+8\,\varpi^2\,R_\Gamma{}^7\,e_3 - 104\,R_\Gamma{}^3\,\varpi^2\,u^4 - 156\,R_\Gamma{}^2\,\varpi^4\,u^3$$
$$-320\,R_\Gamma{}^7\,u^2 - 18\,\varpi^8\,R_\Gamma\,e_3 - 32\,R_\Gamma{}^4\,u^5$$
$$+30\,\varpi^6\,R_\Gamma{}^3 - 144\,R_\Gamma{}^5\,\varpi^2\,u^2 - 160\,R_\Gamma{}^5\,u^4$$
$$-45\,u\,\varpi^8 - 320\,R_\Gamma{}^6\,u^3 - 160\,R_\Gamma{}^8\,u$$
$$+18\,\varpi^8\,R_\Gamma\Big)\cdot e_2/\varpi^{10}\,/R_\Gamma{}^6, \tag{A.11}$$

$$\gamma_9 \;=\; 6\Big(-6\,e_3\,\varpi^4\,u^2 + 12\,\varpi^2\,u^3\,R_\Gamma + 3\,\varpi^6\,e_3$$
$$-48\,R_\Gamma{}^4\,e_3\,u^2 + 6\,\varpi^4\,u^2 + 12\,\varpi^2\,R_\Gamma{}^4\,e_3$$

$$-8\,{R_\Gamma}^2\,e_3\,u^4 + 48\,{R_\Gamma}^4\,u^2 + 32\,{R_\Gamma}^3\,e_3\,u^3$$
$$+32\,u\,{R_\Gamma}^5\,e_3 + 32\,u\,{R_\Gamma}^5 + 6\,\varpi^4\,{R_\Gamma}^2\,e_3$$
$$-12\,\varpi^2\,u\,{R_\Gamma}^3 - 6\,u\,\varpi^4\,R_\Gamma - 12\,\varpi^2\,{R_\Gamma}^4$$
$$-3\,\varpi^6 + 8\,{R_\Gamma}^6 - 12\,\varpi^2\,u\,{R_\Gamma}^3\,e_3$$
$$-6\,{R_\Gamma}^2\,\varpi^4 + 8\,{R_\Gamma}^2\,u^4 - 6\,\varpi^4\,u\,e_3\,R_\Gamma$$
$$+12\,\varpi^2\,u^3\,R_\Gamma\,e_3 - 12\,\varpi^2\,u^2\,{R_\Gamma}^2\,e_3 - 8\,{R_\Gamma}^6\,e_3$$
$$+32\,{R_\Gamma}^3\,u^3 + 12\,\varpi^2\,u^2\,{R_\Gamma}^2) \cdot e_2/\varpi^8/{R_\Gamma}^5\,, \tag{A.12}$$

$$\gamma_{10} \;=\; 3\Big(-6\,u^2\,\varpi^2\,R_\Gamma - 6\,\varpi^2\,u\,{R_\Gamma}^2 - 4\,e_3\,{R_\Gamma}^5$$
$$-12\,u\,{R_\Gamma}^4 - 12\,u^2\,{R_\Gamma}^3 - 3\,u\,\varpi^4$$
$$-4\,u^3\,{R_\Gamma}^2 - 6\,e_3\,u^2\,\varpi^2\,R_\Gamma - 12\,e_3\,u^2\,{R_\Gamma}^3$$
$$+3\,e_3\,u\,\varpi^4 + 4\,e_3\,u^3\,{R_\Gamma}^2 - 4\,{R_\Gamma}^5$$
$$+12\,e_3\,u\,{R_\Gamma}^4 + 6\,e_3\,\varpi^2\,u\,{R_\Gamma}^2\Big) \cdot e_2/{R_\Gamma}^4/\varpi^6\,, \tag{A.13}$$

$$\gamma_{11} \;=\; 3\Big(6\,\varpi^4\,{R_\Gamma}^3 - 24\,e_3\,\varpi^2\,u^3\,{R_\Gamma}^2 + 18\,e_3\,u^2\,\varpi^4\,R_\Gamma$$
$$+16\,e_3\,{R_\Gamma}^7 - 64\,e_3\,u^3\,{R_\Gamma}^4 + 24\,e_3\,u\,{R_\Gamma}^4\,\varpi^2$$
$$+24\,e_3\,u^2\,\varpi^2\,{R_\Gamma}^3 - 6\,e_3\,u\,\varpi^6 - 64\,e_3\,u\,{R_\Gamma}^6$$
$$-3\,e_3\,R_\Gamma\,\varpi^6 + 16\,e_3\,u^4\,{R_\Gamma}^3 - 6\,e_3\,\varpi^4\,{R_\Gamma}^3$$
$$+96\,e_3\,u^2\,{R_\Gamma}^5 - 24\,e_3\,\varpi^2\,{R_\Gamma}^5 + 6\,u\,\varpi^6$$
$$+3\,R_\Gamma\,\varpi^6 + 6\,u^2\,\varpi^4\,R_\Gamma + 12\,\varpi^4\,u\,{R_\Gamma}^2\Big)$$
$$\cdot e_2/\varpi^8/{R_\Gamma}^5\,. \tag{A.14}$$

In addition, the functions $\gamma_{12\ldots17}$ used in expressing J, U and W are given by:

$$\gamma_{12} \;=\; 2\Big(270\,{R_\Gamma}^8\,\varpi^{18}\,e_1\,u - 720\,{R_\Gamma}^{10}\,\varpi^{12}\,e_1\,u^5$$
$$-135\,{R_\Gamma}^6\,\varpi^{20}\,e_1\,u + 3600\,{R_\Gamma}^{11}\,\varpi^{12}\,e_1\,u^4$$
$$+7920\,{R_\Gamma}^{12}\,\varpi^{14}\,e_1\,u + 720\,{R_\Gamma}^{15}\,\varpi^{12}\,e_2$$
$$+1080\,{R_\Gamma}^{11}\,\varpi^{16}\,e_2 + 720\,{R_\Gamma}^{10}\,\varpi^{12}\,e_2\,u^5$$
$$+3600\,{R_\Gamma}^{14}\,\varpi^{12}\,e_2\,u + 3600\,{R_\Gamma}^{11}\,\varpi^{12}\,e_2\,u^4$$
$$+7200\,{R_\Gamma}^{12}\,\varpi^{12}\,e_2\,u^3 + 7200\,{R_\Gamma}^{13}\,\varpi^{12}\,e_2\,u^2$$
$$-7920\,{R_\Gamma}^{12}\,\varpi^{14}\,e_2\,u + 1080\,{R_\Gamma}^{11}\,\varpi^{16}\,e_1$$
$$+540\,{R_\Gamma}^8\,\varpi^{16}\,e_2\,u^3 - 540\,{R_\Gamma}^9\,\varpi^{16}\,e_2\,u^2$$
$$-6480\,{R_\Gamma}^{11}\,\varpi^{14}\,e_2\,u^2 - 720\,{R_\Gamma}^{10}\,\varpi^{14}\,e_2\,u^3$$
$$+270\,{R_\Gamma}^7\,\varpi^{18}\,e_2\,u^2 + 720\,{R_\Gamma}^9\,\varpi^{14}\,e_2\,u^4$$

$$+135\,R_\Gamma{}^6\,\varpi^{20}\,e_2\,u + 270\,R_\Gamma{}^7\,\varpi^{18}\,e_1\,u^2$$
$$-270\,R_\Gamma{}^8\,\varpi^{18}\,e_2\,u - 6480\,R_\Gamma{}^{11}\,\varpi^{14}\,e_1\,u^2$$
$$+720\,R_\Gamma{}^{10}\,\varpi^{14}\,e_1\,u^3 + 720\,R_\Gamma{}^9\,\varpi^{14}\,e_1\,u^4$$
$$-540\,R_\Gamma{}^8\,\varpi^{16}\,e_1\,u^3 - 540\,R_\Gamma{}^9\,\varpi^{16}\,e_1\,u^2$$
$$-3600\,R_\Gamma{}^{14}\,\varpi^{12}\,e_1\,u + 7200\,R_\Gamma{}^{13}\,\varpi^{12}\,e_1\,u^2$$
$$-7200\,R_\Gamma{}^{12}\,\varpi^{12}\,e_1\,u^3 + 720\,R_\Gamma{}^{15}\,\varpi^{12}\,e_1$$
$$-2880\,R_\Gamma{}^{13}\,\varpi^{14}\,e_1 - 2880\,R_\Gamma{}^{13}\,\varpi^{14}\,e_2\Big)$$
$$/R_\Gamma{}^{11}/\varpi^{22}/15, \qquad\qquad\qquad \text{(A.15)}$$

$$\gamma_{13} \;=\; 2\Big(18000\,\varpi^{12}\,R_\Gamma{}^{14}\,e_2 - 16560\,\varpi^{14}\,R_\Gamma{}^{12}\,e_2$$

$$+135\,\varpi^{20}\,R_\Gamma{}^6\,e_2 - 2160\,\varpi^{16}\,R_\Gamma{}^{10}\,e_2$$
$$-2160\,\varpi^{16}\,R_\Gamma{}^{10}\,e_1 - 2880\,\varpi^{10}\,R_\Gamma{}^{16}\,e_2$$
$$-3600\,\varpi^{12}\,R_\Gamma{}^{10}\,e_1\,u^4 + 3600\,\varpi^{12}\,R_\Gamma{}^{13}\,e_1\,u$$
$$-10800\,\varpi^{14}\,R_\Gamma{}^{11}\,e_1\,u + 7200\,\varpi^{12}\,R_\Gamma{}^{11}\,e_1\,u^3$$
$$+720\,\varpi^{12}\,R_\Gamma{}^9\,e_1\,u^5 - 1350\,\varpi^{18}\,R_\Gamma{}^7\,e_1\,u$$
$$+1080\,\varpi^{18}\,R_\Gamma{}^6\,e_1\,u^2 - 405\,\varpi^{20}\,R_\Gamma{}^5\,e_1\,u$$
$$-7200\,\varpi^{12}\,R_\Gamma{}^{12}\,e_1\,u^2 + 3600\,\varpi^{14}\,R_\Gamma{}^{12}\,e_1$$
$$-57600\,\varpi^{10}\,R_\Gamma{}^{13}\,e_2\,u^3 - 19440\,\varpi^{14}\,R_\Gamma{}^{11}\,e_2\,u$$
$$-43200\,\varpi^{10}\,R_\Gamma{}^{14}\,e_2\,u^2 + 3600\,\varpi^{12}\,R_\Gamma{}^{10}\,e_2\,u^4$$
$$+540\,\varpi^{18}\,R_\Gamma{}^6\,e_2\,u^2 - 2160\,\varpi^{14}\,R_\Gamma{}^8\,e_2\,u^4$$
$$+4860\,\varpi^{16}\,R_\Gamma{}^8\,e_2\,u^2 - 2880\,\varpi^{10}\,R_\Gamma{}^{10}\,e_2\,u^6$$
$$-540\,\varpi^{16}\,R_\Gamma{}^7\,e_2\,u^3 - 17280\,\varpi^{10}\,R_\Gamma{}^{15}\,e_2\,u$$
$$+9360\,\varpi^{14}\,R_\Gamma{}^9\,e_2\,u^3 + 68400\,\varpi^{12}\,R_\Gamma{}^{13}\,e_2\,u$$
$$-2160\,\varpi^{16}\,R_\Gamma{}^9\,e_2\,u - 720\,\varpi^{12}\,R_\Gamma{}^{14}\,e_1$$
$$-43200\,\varpi^{10}\,R_\Gamma{}^{12}\,e_2\,u^4 + 93600\,\varpi^{12}\,R_\Gamma{}^{12}\,e_2\,u^2$$
$$+8640\,\varpi^{14}\,R_\Gamma{}^{10}\,e_2\,u^2 + 1890\,\varpi^{18}\,R_\Gamma{}^7\,e_2\,u$$
$$+405\,\varpi^{20}\,R_\Gamma{}^5\,e_2\,u - 17280\,\varpi^{10}\,R_\Gamma{}^{11}\,e_2\,u^5$$
$$+1080\,\varpi^{16}\,R_\Gamma{}^9\,e_1\,u - 540\,\varpi^{16}\,R_\Gamma{}^7\,e_1\,u^3$$
$$+1620\,\varpi^{16}\,R_\Gamma{}^8\,e_1\,u^2 - 3600\,\varpi^{14}\,R_\Gamma{}^9\,e_1\,u^3$$
$$+10800\,\varpi^{14}\,R_\Gamma{}^{10}\,e_1\,u^2 - 3600\,\varpi^{12}\,R_\Gamma{}^9\,e_2\,u^5$$
$$+50400\,\varpi^{12}\,R_\Gamma{}^{11}\,e_2\,u^3 - 135\,\varpi^{20}\,R_\Gamma{}^6\,e_1$$
$$+270\,\varpi^{18}\,R_\Gamma{}^8\,e_1 - 270\,\varpi^{18}\,R_\Gamma{}^8\,e_2\Big)$$
$$/15/R_\Gamma{}^{11}/\varpi^{22}, \qquad\qquad\qquad \text{(A.16)}$$

$$\gamma_{14} = -2\Big(-540\,R_\Gamma{}^{11}\,\varpi^{14}\,e_2 - 1620\,R_\Gamma{}^9\,\varpi^{14}\,e_1\,u^2$$

$$+540\,R_\Gamma{}^8\,\varpi^{14}\,e_1\,u^3 + 1620\,R_\Gamma{}^{10}\,\varpi^{14}\,e_1\,u$$

$$-540\,R_\Gamma{}^8\,\varpi^{14}\,e_2\,u^3 - 1620\,R_\Gamma{}^9\,\varpi^{14}\,e_2\,u^2$$

$$-1620\,R_\Gamma{}^{10}\,\varpi^{14}\,e_2\,u - 810\,R_\Gamma{}^7\,\varpi^{16}\,e_2\,u^2$$

$$-810\,R_\Gamma{}^7\,\varpi^{16}\,e_1\,u^2 - 810\,R_\Gamma{}^8\,\varpi^{16}\,e_2\,u$$

$$-405\,R_\Gamma{}^6\,\varpi^{18}\,e_2\,u + 810\,R_\Gamma{}^8\,\varpi^{16}\,e_1\,u$$

$$-540\,R_\Gamma{}^{11}\,\varpi^{14}\,e_1 + 405\,R_\Gamma{}^6\,\varpi^{18}\,e_1\,u\Big)$$

$$/R_\Gamma{}^{12}/\varpi^{20}/15, \tag{A.17}$$

$$\gamma_{15} = -2\Big(-14400\,R_\Gamma{}^{12}\,\varpi^{10}\,e_2\,u^2 - 270\,R_\Gamma{}^6\,\varpi^{16}\,e_2\,u^2$$

$$-7200\,R_\Gamma{}^{10}\,\varpi^{10}\,e_2\,u^4 + 5040\,R_\Gamma{}^{12}\,\varpi^{12}\,e_2$$

$$-1440\,R_\Gamma{}^9\,\varpi^{10}\,e_2\,u^5 - 14400\,R_\Gamma{}^{11}\,\varpi^{10}\,e_2\,u^3$$

$$-1440\,R_\Gamma{}^9\,\varpi^{12}\,e_2\,u^3 + 8640\,R_\Gamma{}^{10}\,\varpi^{12}\,e_2\,u^2$$

$$-2160\,R_\Gamma{}^8\,\varpi^{12}\,e_2\,u^4 + 12960\,R_\Gamma{}^{11}\,\varpi^{12}\,e_2\,u$$

$$-1440\,R_\Gamma{}^{14}\,\varpi^{10}\,e_2 + 7200\,R_\Gamma{}^{10}\,\varpi^{10}\,e_1\,u^4$$

$$+1440\,R_\Gamma{}^{14}\,\varpi^{10}\,e_1 + 21600\,R_\Gamma{}^{11}\,\varpi^{12}\,e_1\,u$$

$$+7200\,R_\Gamma{}^9\,\varpi^{12}\,e_1\,u^3 - 1440\,R_\Gamma{}^9\,\varpi^{10}\,e_1\,u^5$$

$$+1080\,R_\Gamma{}^7\,\varpi^{16}\,e_2\,u - 14400\,R_\Gamma{}^{11}\,\varpi^{10}\,e_1\,u^3$$

$$-21600\,R_\Gamma{}^{10}\,\varpi^{12}\,e_1\,u^2 - 5400\,R_\Gamma{}^9\,\varpi^{14}\,e_1\,u$$

$$-7200\,R_\Gamma{}^{13}\,\varpi^{10}\,e_1\,u + 14400\,R_\Gamma{}^{12}\,\varpi^{10}\,e_1\,u^2$$

$$+5400\,R_\Gamma{}^{10}\,\varpi^{14}\,e_1 - 7200\,R_\Gamma{}^{12}\,\varpi^{12}\,e_1$$

$$+270\,R_\Gamma{}^6\,\varpi^{16}\,e_1\,u^2 - 540\,R_\Gamma{}^7\,\varpi^{16}\,e_1\,u$$

$$-7200\,R_\Gamma{}^{13}\,\varpi^{10}\,e_2\,u - 135\,R_\Gamma{}^6\,\varpi^{18}\,e_1$$

$$-270\,R_\Gamma{}^8\,\varpi^{16}\,e_2 + 4320\,R_\Gamma{}^9\,\varpi^{14}\,e_2\,u$$

$$-1080\,R_\Gamma{}^7\,\varpi^{14}\,e_2\,u^3 + 3240\,R_\Gamma{}^8\,\varpi^{14}\,e_2\,u^2$$

$$+270\,R_\Gamma{}^8\,\varpi^{16}\,e_1 + 135\,R_\Gamma{}^6\,\varpi^{18}\,e_2\Big)$$

$$/15/R_\Gamma{}^{12}/\varpi^{20}, \tag{A.18}$$

$$\gamma_{16} = -\Big(1080\,R_\Gamma{}^8\,\varpi^{12}\,e_2\,u^3 + 810\,R_\Gamma{}^7\,\varpi^{14}\,e_2\,u^2$$

$$+4320\,R_\Gamma{}^{11}\,\varpi^{10}\,e_2\,u^2 - 1080\,R_\Gamma{}^{10}\,\varpi^{12}\,e_2\,u$$

$$+270\,R_\Gamma{}^7\,\varpi^{14}\,e_1\,u^2 + 720\,R_\Gamma{}^9\,\varpi^{10}\,e_2\,u^4$$

$$+2880\,R_\Gamma{}^{12}\,\varpi^{10}\,e_2\,u + 135\,R_\Gamma{}^7\,\varpi^{16}\,e_1$$

$$+270\,R_\Gamma{}^6\,\varpi^{16}\,e_2\,u - 270\,R_\Gamma{}^6\,\varpi^{16}\,e_1\,u$$

$$+1080\,R_{\Gamma}{}^{9}\,\varpi^{12}\,e_2\,u^2 - 540\,R_{\Gamma}{}^{8}\,\varpi^{14}\,e_1\,u$$
$$+2880\,R_{\Gamma}{}^{10}\,\varpi^{10}\,e_2\,u^3 + 720\,R_{\Gamma}{}^{13}\,\varpi^{10}\,e_2$$
$$-1080\,R_{\Gamma}{}^{11}\,\varpi^{12}\,e_2 - 135\,R_{\Gamma}{}^{7}\,\varpi^{16}\,e_2$$
$$-270\,R_{\Gamma}{}^{9}\,\varpi^{14}\,e_2 + 270\,R_{\Gamma}{}^{9}\,\varpi^{14}\,e_1\Big)$$

$$/\varpi^{18}/R_{\Gamma}{}^{12}/15 \tag{A.19}$$

$$\gamma_{17} = \Big(-27\,R_{\Gamma}{}^{6}\,\varpi^{16}\,e_1 + 48\,R_{\Gamma}{}^{8}\,\varpi^{10}\,e_2\,u^4$$
$$-288\,R_{\Gamma}{}^{9}\,\varpi^{12}\,e_2\,u + 288\,R_{\Gamma}{}^{10}\,\varpi^{10}\,e_2\,u^2$$
$$-144\,R_{\Gamma}{}^{8}\,\varpi^{12}\,e_2\,u^2 - 18\,R_{\Gamma}{}^{6}\,\varpi^{14}\,e_2\,u^2$$
$$-36\,R_{\Gamma}{}^{7}\,\varpi^{14}\,e_2\,u + 192\,R_{\Gamma}{}^{11}\,\varpi^{10}\,e_2\,u$$
$$+192\,R_{\Gamma}{}^{9}\,\varpi^{10}\,e_2\,u^3 + 90\,R_{\Gamma}{}^{6}\,\varpi^{14}\,e_1\,u^2$$
$$+144\,R_{\Gamma}{}^{7}\,\varpi^{14}\,e_1\,u - 18\,R_{\Gamma}{}^{5}\,\varpi^{16}\,e_1\,u$$
$$-216\,R_{\Gamma}{}^{7}\,\varpi^{12}\,e_1\,u^3 - 216\,R_{\Gamma}{}^{8}\,\varpi^{12}\,e_1\,u^2$$
$$+1920\,R_{\Gamma}{}^{12}\,\varpi^{8}\,e_1\,u^2 - 192\,R_{\Gamma}{}^{9}\,\varpi^{8}\,e_1\,u^5$$
$$+1728\,R_{\Gamma}{}^{11}\,\varpi^{10}\,e_1\,u + 18\,R_{\Gamma}{}^{5}\,\varpi^{16}\,e_2\,u$$
$$+288\,R_{\Gamma}{}^{8}\,\varpi^{10}\,e_1\,u^4 + 960\,R_{\Gamma}{}^{10}\,\varpi^{8}\,e_1\,u^4$$
$$-960\,R_{\Gamma}{}^{13}\,\varpi^{8}\,e_1\,u + 360\,R_{\Gamma}{}^{9}\,\varpi^{12}\,e_1\,u$$
$$-1920\,R_{\Gamma}{}^{11}\,\varpi^{8}\,e_1\,u^3 - 192\,R_{\Gamma}{}^{9}\,\varpi^{10}\,e_1\,u^3$$
$$-1152\,R_{\Gamma}{}^{10}\,\varpi^{10}\,e_1\,u^2 + 192\,R_{\Gamma}{}^{14}\,\varpi^{8}\,e_1$$
$$+72\,R_{\Gamma}{}^{10}\,\varpi^{12}\,e_1 + 48\,R_{\Gamma}{}^{12}\,\varpi^{10}\,e_2$$
$$-18\,R_{\Gamma}{}^{8}\,\varpi^{14}\,e_1 + 27\,R_{\Gamma}{}^{6}\,\varpi^{16}\,e_2$$
$$-672\,R_{\Gamma}{}^{12}\,\varpi^{10}\,e_1 + 18\,R_{\Gamma}{}^{8}\,\varpi^{14}\,e_2$$
$$-144\,R_{\Gamma}{}^{10}\,\varpi^{12}\,e_2\Big)/\varpi^{18}/R_{\Gamma}{}^{12}. \tag{A.20}$$

B. BONDI FUNCTIONS FOR THE SOLUTION SIMPLE

Here the formulae obtained for the static solution SIMPLE, in the gauge described in Section 5.3.3 are listed. Since the solution is time-independent, the functions r, J, β, U, W and their λ-derivatives on the world-tube depend only on the angular variables (q, p). The function $r^{(0)}(q, p)$ is given by

$$
\begin{aligned}
r^{(0)} = {} & R_\Gamma - \frac{1}{80}\, R_\Gamma^5\, \beth_1^2 a^4 + \frac{1}{112}\, R_\Gamma^6\, \beth_1^3 a^6 \\
& - \frac{11}{1920}\, R_\Gamma^8\, \beth_1^4 a^8 + \frac{179}{49280}\, R_\Gamma^{10}\, \beth_1^5 a^{10} + \cdots,
\end{aligned}
\tag{B.1}
$$

where

$$
\beth_1 = \frac{\left(-4\,p^2 + P^2\right)}{P^2}, \quad P = 1 + q^2 + p^2.
\tag{B.2}
$$

Using the same notations and further introducing

$$
\beth_2 = \frac{\zeta^2 + 1}{1 + \zeta\bar\zeta} = \frac{(q + Ip)^2 + 1}{P},
\tag{B.3}
$$

$$
\beth_3 = \frac{\zeta - \bar\zeta}{1 + \zeta\bar\zeta} = \frac{2Ip}{P},
\tag{B.4}
$$

the Bondi functions and their λ-derivatives are given by

$$
\begin{aligned}
J^{(0)} = {} & -\frac{1}{2}\,\beth_2^2 R_\Gamma^2 a^2 + \frac{3}{16}\,\bar\beth_2\,\beth_2^3 R_\Gamma^4 a^4 - \frac{9}{80}\,\bar\beth_2^2\beth_2^4 R_\Gamma^6 a^6 \\
& + \frac{1317}{17920}\,\bar\beth_2^3\beth_2^5 R_\Gamma^8 a^8 - \frac{26647}{537600}\,\bar\beth_2^4\beth_2^6 R_\Gamma^{10} a^{10} + \cdots,
\end{aligned}
\tag{B.5}
$$

$$
\begin{aligned}
J^{(0)}_{,\lambda} = {} & -\beth_2^2 R_\Gamma a^2 + \frac{3}{4}\,\bar\beth_2\,\beth_2^3 R_\Gamma^3 a^4 - \frac{27}{40}\,\bar\beth_2^2\beth_2^4 R_\Gamma^5 a^6 \\
& + \frac{1317}{2240}\,\bar\beth_2^3\beth_2^5 R_\Gamma^7 a^8 - \frac{26647}{5376z0}\,\bar\beth_2^4\beth_2^6 R_\Gamma^9 a^{10} + \cdots,
\end{aligned}
\tag{B.6}
$$

$$
\begin{aligned}
\beta^{(0)} = {} & \frac{1}{32}R_\Gamma^4\beth_1^2 a^4 - \frac{1}{32}R_\Gamma^6\beth_1^3 a^6 + \frac{137}{5120}R_\Gamma^8\beth_1^4 a^8 \\
& - \frac{393}{17920}R_\Gamma^{10}\beth_1^5 a^{10}\cdots,
\end{aligned}
\tag{B.7}
$$

$$\beta^{(0)}_{,\lambda} = \frac{1}{8}R_\Gamma^3 ⅃_1^2 a^4 - \frac{3}{16}R_\Gamma^5 ⅃_1^3 a^6 + \frac{137}{640}R_\Gamma^7 ⅃_1^4 a^8$$
$$- \frac{393}{1792}R_\Gamma^9 ⅃_1^5 a^{10} + \cdots, \tag{B.8}$$

$$U^{(0)} = ⅃_3 ⅃_2\, R_\Gamma\, a^2 - \frac{1}{2}⅃_3\, \bar{⅃}_2\, ⅃_2^2 R_\Gamma^3 a^4 + \frac{29}{80}⅃_3\, \bar{⅃}_2^2 ⅃_2^3 R_\Gamma^5 a^6$$
$$- \frac{319}{1120}⅃_3\, \bar{⅃}_2^3 ⅃_2^4 R_\Gamma^7 a^8 + \frac{3103}{13440}⅃_3\, \bar{⅃}_2^4 ⅃_2^5 R_\Gamma^9 a^{10} + \cdots, \tag{B.9}$$

$$U^{(0)}_{,\lambda} = ⅃_3 ⅃_2\, a^2 - \frac{3}{2}⅃_3\, \bar{⅃}_2\, ⅃_2^2 R_\Gamma^2 a^4 + \frac{29}{16}⅃_3\, \bar{⅃}_2^2 ⅃_2^3 R_\Gamma^4 a^6$$
$$- \frac{319}{160}⅃_3\, \bar{⅃}_2^3 ⅃_2^4 R_\Gamma^6 a^8 + \frac{9309}{4480}⅃_3\, \bar{⅃}_2^4 ⅃_2^5 R_\Gamma^8 a^{10} + \cdots, \tag{B.10}$$

$$W^{(0)} = \frac{1}{2}\left(-2+3⅃_1\right) R_\Gamma\, a^2 - \frac{1}{8}\left(-4+5⅃_1\right) ⅃_1\, R_\Gamma^3\, a^4$$
$$+ \frac{1}{160}\left(-58+67⅃_1\right) ⅃_1^2\, R_\Gamma^5\, a^6$$
$$- \frac{1}{2240}\left(-638+705⅃_1\right) ⅃_1^3\, R_\Gamma^7\, a^8$$
$$+ \frac{1}{26880}\left(-6206+6669⅃_1\right) ⅃_1^4\, R_\Gamma^9\, a^{10} + \cdots, \tag{B.11}$$

$$W^{(0)}_{,\lambda} = \frac{1}{2}\left(-2+3⅃_1\right) a^2 - \frac{3}{8}\left(-4+5⅃_1\right) ⅃_1\, R_\Gamma^2\, a^4$$
$$+ \frac{1}{32}\left(-58+67⅃_1\right) ⅃_1^2\, R_\Gamma^4\, a^6$$
$$- \frac{1}{320}\left(-638+705⅃_1\right) ⅃_1^3\, R_\Gamma^6\, a^8$$
$$+ \frac{3}{8960}\left(-6206+6669⅃_1\right) ⅃_1^4\, R_\Gamma^8\, a^{10} + \cdots. \tag{B.12}$$

C. LINEARIZED QUADRUPOLE WAVE SOLUTION IN BONDI COORDINATES

This appendix is a description of the algebraic steps performed to obtain the linearized quadrupole wave solution in Bondi coordinates. At the end explicit expressions are provided for the Bondi metric functions. The work described below (and most of the work from the entire thesis) could not have been accomplished without a significant input from [121].

The starting point is the linearized quadrupole solution in coordinates $x^\alpha = (t, r, x^A)$, as given in Section 5.3.2. The contravariant metric is written in the form $g^{\alpha\beta} = \eta^{\alpha\beta} - h^{\alpha\beta}$, where computations are done up to order $O(h^2)$.

C.1   Approximate null coordinates

The approximate null coordinates $y'^{\mu'} = (u, \lambda, y^A)$ are defined by $u = t - r, \lambda = r - R_\Gamma$. This leads to a metric of the form

$$g'^{\mu'\nu'} = \frac{\partial y'^{\mu'}}{\partial x^\alpha} \frac{\partial y'^{\nu'}}{\partial x^\beta} g^{\alpha\beta} = \eta'^{\mu'\nu'} - h'^{\mu'\nu'}, \tag{C.1}$$

where $h'^{\mu'\nu'}$ is

$$h'^{\mu'\nu'} = \frac{\partial y'^{\mu'}}{\partial x^\alpha} \frac{\partial y'^{\nu'}}{\partial x^\beta} h^{\alpha\beta} \tag{C.2}$$

and $\eta'^{\mu'\nu'}$ is the background null metric:

$$\eta'^{\mu'\nu'} = \begin{pmatrix} 0 & -1 & 0 \\ -1 & 1 & \\ 0 & & \frac{q^{AB}}{(\lambda+R_\Gamma)^2} \end{pmatrix}. \tag{C.3}$$

C.2   Affine null coordinates

As a further step the affine null coordinates are introduced in the following way:

$$\tilde{y}^{\mu} = y'^{\mu} + \xi^{\mu}, \quad \text{where} \quad \xi^{\mu}|_{\mathrm{R}_{\Gamma}} = 0. \tag{C.4}$$

This leads to a metric that can be written as

$$\tilde{g}^{\tilde{\mu}\tilde{\nu}}(\tilde{y}) = \frac{\partial \tilde{y}^{\tilde{\mu}}}{\partial y'^{\alpha'}} \frac{\partial \tilde{y}^{\tilde{\nu}}}{\partial y'^{\beta'}} g'^{\alpha'\beta'}(y') = \tilde{\eta}^{\tilde{\mu}\tilde{\nu}}(\tilde{y}) - \tilde{h}^{\tilde{\mu}\tilde{\nu}}. \tag{C.5}$$

Here again $\tilde{\eta}^{\mu\nu}$ is the background metric in null coordinates, while

$$\tilde{h}^{\tilde{\mu}\tilde{\nu}} = h'^{\mu'\nu'} - \xi^{\mu}_{,\alpha'}\eta^{\nu'\alpha'} - \xi^{\nu}_{,\alpha'}\eta^{\mu'\alpha'} + \eta^{\mu'\nu'}_{,\alpha'}\xi^{\alpha}. \tag{C.6}$$

The vector ξ^{μ} is fixed by the requirement that $\tilde{g}^{\tilde{\mu}\tilde{\nu}}$ be a null metric, that is

$$\tilde{h}^{\tilde{u}\tilde{u}} = 0 \quad \Rightarrow \quad 0 = h'^{u'u'} + 2\,\xi^{u}_{,\lambda}$$

$$\Rightarrow \quad \xi^{u} = \int_{0}^{\lambda}\left[-\frac{1}{2}h'^{u'u'}\right]d\lambda, \tag{C.7}$$

$$\tilde{h}^{\tilde{u}\tilde{A}} = 0 \quad \Rightarrow \quad 0 = h'^{u'A'} - \xi^{u}_{,B}\,\eta^{A'B'} + \xi^{A}_{,\lambda}$$

$$\Rightarrow \quad \xi^{A} = \int_{0}^{\lambda}\left[-h'^{u'A'} + \xi^{u}_{,B'}\,\eta^{A'B'}\right]d\lambda, \tag{C.8}$$

$$\tilde{h}^{\tilde{u}\tilde{\lambda}} = 0 \quad \Rightarrow \quad 0 = h'^{u'\lambda'} + \xi^{u}_{,u} - \xi^{u}_{,\lambda} + \xi^{\lambda}_{,\lambda}$$

$$\Rightarrow \quad \xi^{\lambda} = \int_{0}^{\lambda}\left[-h'^{u'\lambda'} - \xi^{u}_{,u} - \frac{1}{2}h^{u'u'}\right]d\lambda. \tag{C.9}$$

C.3   Bondi coordinates

In order to get the null metric in Bondi coordinates $y^{\mu} = (u, r_b, y^{A})$ the following coordinate transformation is defined

$$y^{\mu} = \tilde{y}^{\tilde{\mu}} + \eta^{\mu}, \quad \text{where} \quad \eta^{u} = \eta^{A} = 0. \tag{C.10}$$

The above coordinate transformation translates into

$$r_b = \tilde{\lambda} + R_{\Gamma} + \eta^{r}. \tag{C.11}$$

Carrying it out provides the following metric:

$$g_b^{\mu\nu}(y) = \frac{\partial y^{\mu}}{\partial \tilde{y}^{\tilde{\alpha}}} \frac{\partial y^{\nu}}{\partial \tilde{y}^{\tilde{\beta}}} \tilde{g}^{\tilde{\alpha}\tilde{\beta}} = \eta_b^{\mu\nu}(y) - h_b^{\mu\nu}(y), \tag{C.12}$$

where $\eta_b^{\mu\nu}$ is the background metric in Bondi coordinates which is identical with the same metric in null coordinates. The expression for $h_b^{\mu\nu}$ is

$$h_b^{\mu\nu} = h^{\tilde\mu\tilde\nu} - \eta^\mu_{,\tilde\alpha}\tilde\eta^{\tilde\alpha\tilde\nu} - \eta^\nu_{,\tilde\alpha}\tilde\eta^{\tilde\alpha\tilde\mu} + \eta^{\tilde\mu\tilde\nu}_{,\tilde\alpha}\eta^\alpha. \tag{C.13}$$

As a condition upon η^r the following gauge condition is imposed:

$$\eta_{AB}h_b^{AB} = \eta_{AB}\tilde h^{AB} + \eta_{AB}\eta^{AB}_{,\lambda}\eta^r = 0. \tag{C.14}$$

Using

$$\eta_{AB}\eta^{AB}_{,\lambda} = -\frac{4}{\lambda},$$

this translates into

$$\eta^r = \frac{\lambda}{4}\eta_{AB}\tilde h^{AB}. \tag{C.15}$$

If the determinant condition is imposed to the Bondi metric g_b^{AB}, one obtains

$$\frac{1}{r_b^4 q} = \left|g_b^{AB}(y)\right| = \left|\tilde g^{\tilde A\tilde B}(\tilde y)\right| = \left|\eta^{\tilde A\tilde B}(\tilde y) - \tilde h^{\tilde A\tilde B}(\tilde y)\right| \tag{C.16}$$

$$= \left|\eta^{\tilde A\tilde B}(\tilde y)\right|\left(1 - \eta_{\tilde A\tilde B}(\tilde y)\,\tilde h^{\tilde A\tilde B}(\tilde y)\right), \tag{C.17}$$

which is equivalent to satisfying the gauge condition specified in Eq. (C.14).

C.4   Inverting the relation $r_b = r_b(\tilde\lambda)$

Once the metric is obtained in Bondi coordinates, computing the dependence $\tilde\lambda(r_b)$ is straightforward. The expression for $\partial r_b/\partial\tilde\lambda$ can be obtained directly from

$$\partial r_b/\partial\tilde\lambda = e^{-2\beta} = -g_b^{ru}. \tag{C.18}$$

The value of $\partial^2 r_b/\partial\tilde\lambda^2$ is determined by the value of $\beta_{,\tilde\lambda}$, which vanishes in linearized theory (see Eq. (5.76)). Thus $\partial^2 r_b/\partial\tilde\lambda^2 = 0$, or in other words, the dependence $r_b = r_b(\tilde\lambda)$ is linear.

C.5   Explicit results for the Bondi functions

Most of the coordinate transformations described in Sections C.1-C.4 are relatively easy to carry out with the exception of the integrals (C.7) - (C.9). These cannot be evaluated in a closed form, and they were approximated by a high-order expansion in the affine parameter λ. The resulting expressions for the Bondi variables J, U, W as functions of (u, λ, q, p) are listed below. As described in Section C.4, replacing the variable λ with the Bondi r is straightforward.

The function $J(u, \lambda, q, p)$ takes the form

$$
J = \varepsilon \left(\frac{q^2 - p^2 + 2Iqp}{P^2} \right) \times \left[J^{(0)}(u) + \frac{\lambda^1}{1!} J^{(1)}(u) + \right.
$$
$$
\left. + \cdots + \frac{\lambda^6}{6!} J^{(6)}(u) + O(\lambda^7) \right] + O(\varepsilon^2), \tag{C.19}
$$

where the coefficients $J^{(0)}, \ldots J^{(6)}$ are given by

$$
\begin{aligned}
J^{(0)} = & \Big(270\, R_\Gamma^8 \, \varpi^{18} \, e_1 \, u - 720\, R_\Gamma^{10} \, \varpi^{12} \, e_1 \, u^5 \\
& - 135\, R_\Gamma^6 \, \varpi^{20} \, e_1 \, u + 3600\, R_\Gamma^{11} \, \varpi^{12} \, e_1 \, u^4 \\
& + 7920\, R_\Gamma^{12} \, \varpi^{14} \, e_1 \, u + 720\, R_\Gamma^{15} \, \varpi^{12} \, e_2 \\
& + 1080\, R_\Gamma^{11} \, \varpi^{16} \, e_2 + 720\, R_\Gamma^{10} \, \varpi^{12} \, e_2 \, u^5 \\
& + 3600\, R_\Gamma^{14} \, \varpi^{12} \, e_2 \, u + 3600\, R_\Gamma^{11} \, \varpi^{12} \, e_2 \, u^4 \\
& + 7200\, R_\Gamma^{12} \, \varpi^{12} \, e_2 \, u^3 + 7200\, R_\Gamma^{13} \, \varpi^{12} \, e_2 \, u^2 \\
& - 7920\, R_\Gamma^{12} \, \varpi^{14} \, e_2 \, u + 1080\, R_\Gamma^{11} \, \varpi^{16} \, e_1 \\
& + 540\, R_\Gamma^8 \, \varpi^{16} \, e_2 \, u^3 - 540\, R_\Gamma^9 \, \varpi^{16} \, e_2 \, u^2 \\
& - 6480\, R_\Gamma^{11} \, \varpi^{14} \, e_2 \, u^2 - 720\, R_\Gamma^{10} \, \varpi^{14} \, e_2 \, u^3 \\
& + 270\, R_\Gamma^7 \, \varpi^{18} \, e_2 \, u^2 + 720\, R_\Gamma^9 \, \varpi^{14} \, e_2 \, u^4 \\
& + 135\, R_\Gamma^6 \, \varpi^{20} \, e_2 \, u + 270\, R_\Gamma^7 \, \varpi^{18} \, e_1 \, u^2 \\
& - 270\, R_\Gamma^8 \, \varpi^{18} \, e_2 \, u - 6480\, R_\Gamma^{11} \, \varpi^{14} \, e_1 \, u^2 \\
& + 720\, R_\Gamma^{10} \, \varpi^{14} \, e_1 \, u^3 + 720\, R_\Gamma^9 \, \varpi^{14} \, e_1 \, u^4 \\
& - 540\, R_\Gamma^8 \, \varpi^{16} \, e_1 \, u^3 - 540\, R_\Gamma^9 \, \varpi^{16} \, e_1 \, u^2 \\
& - 3600\, R_\Gamma^{14} \, \varpi^{12} \, e_1 \, u + 7200\, R_\Gamma^{13} \, \varpi^{12} \, e_1 \, u^2 \\
& - 7200\, R_\Gamma^{12} \, \varpi^{12} \, e_1 \, u^3 + 720\, R_\Gamma^{15} \, \varpi^{12} \, e_1 \\
& - 2880\, R_\Gamma^{13} \, \varpi^{14} \, e_1 - 2880\, R_\Gamma^{13} \, \varpi^{14} \, e_2 \Big) \times \\
& 2/15 / R_\Gamma^{11} / \varpi^{22}, \tag{C.20}
\end{aligned}
$$

$$
\begin{aligned}
J^{(1)} = & \Big(18000\, \varpi^{12} \, R_\Gamma^{14} \, e_2 - 16560\, \varpi^{14} \, R_\Gamma^{12} \, e_2 \\
& + 135\, \varpi^{20} \, R_\Gamma^6 \, e_2 - 2160\, \varpi^{16} \, R_\Gamma^{10} \, e_2 \\
& - 2160\, \varpi^{16} \, R_\Gamma^{10} \, e_1 - 2880\, \varpi^{10} \, R_\Gamma^{16} \, e_2 \\
& - 3600\, \varpi^{12} \, R_\Gamma^{10} \, e_1 \, u^4 + 3600\, \varpi^{12} \, R_\Gamma^{13} \, e_1 \, u \\
& - 10800\, \varpi^{14} \, R_\Gamma^{11} \, e_1 \, u + 7200\, \varpi^{12} \, R_\Gamma^{11} \, e_1 \, u^3 \\
& + 720\, \varpi^{12} \, R_\Gamma^9 \, e_1 \, u^5 - 1350\, \varpi^{18} \, R_\Gamma^7 \, e_1 \, u \\
& + 1080\, \varpi^{18} \, R_\Gamma^6 \, e_1 \, u^2 - 405\, \varpi^{20} \, R_\Gamma^5 \, e_1 \, u \\
& - 7200\, \varpi^{12} \, R_\Gamma^{12} \, e_1 \, u^2 + 3600\, \varpi^{14} \, R_\Gamma^{12} \, e_1
\end{aligned}
$$

$$-57600\,\varpi^{10}\,R_\Gamma^{13}\,e_2\,u^3 - 19440\,\varpi^{14}\,R_\Gamma^{11}\,e_2\,u$$
$$-43200\,\varpi^{10}\,R_\Gamma^{14}\,e_2\,u^2 + 3600\,\varpi^{12}\,R_\Gamma^{10}\,e_2\,u^4$$
$$+540\,\varpi^{18}\,R_\Gamma^{6}\,e_2\,u^2 - 2160\,\varpi^{14}\,R_\Gamma^{8}\,e_2\,u^4$$
$$+4860\,\varpi^{16}\,R_\Gamma^{8}\,e_2\,u^2 - 2880\,\varpi^{10}\,R_\Gamma^{10}\,e_2\,u^6$$
$$-540\,\varpi^{16}\,R_\Gamma^{7}\,e_2\,u^3 - 17280\,\varpi^{10}\,R_\Gamma^{15}\,e_2\,u$$
$$+9360\,\varpi^{14}\,R_\Gamma^{9}\,e_2\,u^3 + 68400\,\varpi^{12}\,R_\Gamma^{13}\,e_2\,u$$
$$-2160\,\varpi^{16}\,R_\Gamma^{9}\,e_2\,u - 720\,\varpi^{12}\,R_\Gamma^{14}\,e_1$$
$$-43200\,\varpi^{10}\,R_\Gamma^{12}\,e_2\,u^4 + 93600\,\varpi^{12}\,R_\Gamma^{12}\,e_2\,u^2$$
$$+8640\,\varpi^{14}\,R_\Gamma^{10}\,e_2\,u^2 + 1890\,\varpi^{18}\,R_\Gamma^{7}\,e_2\,u$$
$$+405\,\varpi^{20}\,R_\Gamma^{5}\,e_2\,u - 17280\,\varpi^{10}\,R_\Gamma^{11}\,e_2\,u^5$$
$$+1080\,\varpi^{16}\,R_\Gamma^{9}\,e_1\,u - 540\,\varpi^{16}\,R_\Gamma^{7}\,e_1\,u^3$$
$$+1620\,\varpi^{16}\,R_\Gamma^{8}\,e_1\,u^2 - 3600\,\varpi^{14}\,R_\Gamma^{9}\,e_1\,u^3$$
$$+10800\,\varpi^{14}\,R_\Gamma^{10}\,e_1\,u^2 - 3600\,\varpi^{12}\,R_\Gamma^{9}\,e_2\,u^5$$
$$+50400\,\varpi^{12}\,R_\Gamma^{11}\,e_2\,u^3 - 135\,\varpi^{20}\,R_\Gamma^{6}\,e_1$$
$$+270\,\varpi^{18}\,R_\Gamma^{8}\,e_1 - 270\,\varpi^{18}\,R_\Gamma^{8}\,e_2 \Big) \times$$
$$2/15/R_\Gamma^{11}/\varpi^{22}, \tag{C.21}$$

$$J^{(2)} = \Big(2160\,\varpi^{18}\,R_\Gamma^{7}\,e_2 - 27360\,\varpi^{14}\,R_\Gamma^{11}\,e_2$$
$$-14400\,\varpi^{12}\,R_\Gamma^{10}\,e_1\,u^3 - 50400\,\varpi^{12}\,R_\Gamma^{9}\,e_2\,u^4$$
$$+11520\,\varpi^{8}\,R_\Gamma^{17}\,e_2 - 2160\,\varpi^{18}\,R_\Gamma^{7}\,e_1$$
$$-7200\,\varpi^{14}\,R_\Gamma^{11}\,e_1 - 270\,\varpi^{20}\,R_\Gamma^{5}\,e_2$$
$$+270\,\varpi^{20}\,R_\Gamma^{5}\,e_1 + 4320\,\varpi^{18}\,R_\Gamma^{6}\,e_1\,u$$
$$+7200\,\varpi^{14}\,R_\Gamma^{8}\,e_1\,u^3 - 5400\,\varpi^{16}\,R_\Gamma^{8}\,e_1\,u$$
$$-1080\,\varpi^{18}\,R_\Gamma^{5}\,e_2\,u^2 + 7200\,\varpi^{12}\,R_\Gamma^{9}\,e_1\,u^4$$
$$+11520\,\varpi^{8}\,R_\Gamma^{10}\,e_2\,u^7 + 34560\,\varpi^{14}\,R_\Gamma^{10}\,e_2\,u$$
$$+8640\,\varpi^{14}\,R_\Gamma^{9}\,e_2\,u^2 - 17280\,\varpi^{10}\,R_\Gamma^{10}\,e_2\,u^5$$
$$-57600\,\varpi^{12}\,R_\Gamma^{10}\,e_2\,u^3 + 241920\,\varpi^{8}\,R_\Gamma^{12}\,e_2\,u^5$$
$$+15840\,\varpi^{12}\,R_\Gamma^{8}\,e_2\,u^5 - 864000\,\varpi^{10}\,R_\Gamma^{12}\,e_2\,u^3$$
$$-345600\,\varpi^{10}\,R_\Gamma^{11}\,e_2\,u^4 + 80640\,\varpi^{8}\,R_\Gamma^{11}\,e_2\,u^6$$
$$+8640\,\varpi^{14}\,R_\Gamma^{7}\,e_2\,u^4 + 1440\,\varpi^{12}\,R_\Gamma^{13}\,e_1$$
$$-950400\,\varpi^{10}\,R_\Gamma^{13}\,e_2\,u^2 + 403200\,\varpi^{8}\,R_\Gamma^{14}\,e_2\,u^3$$
$$-5400\,\varpi^{18}\,R_\Gamma^{6}\,e_2\,u - 44640\,\varpi^{14}\,R_\Gamma^{8}\,e_2\,u^3$$
$$+241920\,\varpi^{8}\,R_\Gamma^{15}\,e_2\,u^2 - 501120\,\varpi^{10}\,R_\Gamma^{14}\,e_2\,u$$

$$
\begin{aligned}
&+403200\,\varpi^{8}\,R_{\Gamma}^{13}\,e_{2}\,u^{4}+17280\,\varpi^{10}\,R_{\Gamma}^{9}\,e_{2}\,u^{6}\\
&-19440\,\varpi^{16}\,R_{\Gamma}^{7}\,e_{2}\,u^{2}+288000\,\varpi^{12}\,R_{\Gamma}^{11}\,e_{2}\,u^{2}\\
&+468000\,\varpi^{12}\,R_{\Gamma}^{12}\,e_{2}\,u+2160\,\varpi^{16}\,R_{\Gamma}^{6}\,e_{2}\,u^{3}\\
&+14040\,\varpi^{16}\,R_{\Gamma}^{8}\,e_{2}\,u+80640\,\varpi^{8}\,R_{\Gamma}^{16}\,e_{2}\,u\\
&-810\,\varpi^{20}\,R_{\Gamma}^{4}\,e_{2}\,u-7200\,\varpi^{12}\,R_{\Gamma}^{12}\,e_{1}\,u\\
&+14400\,\varpi^{12}\,R_{\Gamma}^{11}\,e_{1}\,u^{2}-1440\,\varpi^{12}\,R_{\Gamma}^{8}\,e_{1}\,u^{5}\\
&+21600\,\varpi^{14}\,R_{\Gamma}^{10}\,e_{1}\,u-21600\,\varpi^{14}\,R_{\Gamma}^{9}\,e_{1}\,u^{2}\\
&-2160\,\varpi^{18}\,R_{\Gamma}^{5}\,e_{1}\,u^{2}+810\,\varpi^{20}\,R_{\Gamma}^{4}\,e_{1}\,u\\
&+188640\,\varpi^{12}\,R_{\Gamma}^{13}\,e_{2}-103680\,\varpi^{10}\,R_{\Gamma}^{15}\,e_{2}\\
&+5400\,\varpi^{16}\,R_{\Gamma}^{9}\,e_{1}+3240\,\varpi^{16}\,R_{\Gamma}^{9}\,e_{2}\Big)\times\\
&2/15/R_{\Gamma}^{11}/\varpi^{22}, \hspace{5cm}\text{(C.22)}\\
J^{(3)} =\; &\Big(-2430\,\varpi^{20}\,R_{\Gamma}^{3}\,e_{1}\,u+29160\,\varpi^{16}\,R_{\Gamma}^{7}\,e_{1}\,u\\
&+4320\,\varpi^{16}\,R_{\Gamma}^{5}\,e_{1}\,u^{3}+21600\,\varpi^{12}\,R_{\Gamma}^{11}\,e_{1}\,u\\
&-2580480\,\varpi^{6}\,R_{\Gamma}^{15}\,e_{2}\,u^{3}-43200\,\varpi^{12}\,R_{\Gamma}^{10}\,e_{1}\,u^{2}\\
&-12960\,\varpi^{16}\,R_{\Gamma}^{6}\,e_{1}\,u^{2}-64800\,\varpi^{14}\,R_{\Gamma}^{9}\,e_{1}\,u\\
&-21600\,\varpi^{14}\,R_{\Gamma}^{7}\,e_{1}\,u^{3}+64800\,\varpi^{14}\,R_{\Gamma}^{8}\,e_{1}\,u^{2}\\
&+43200\,\varpi^{12}\,R_{\Gamma}^{9}\,e_{1}\,u^{3}-21600\,\varpi^{12}\,R_{\Gamma}^{8}\,e_{1}\,u^{4}\\
&+4320\,\varpi^{12}\,R_{\Gamma}^{7}\,e_{1}\,u^{5}-1290240\,\varpi^{6}\,R_{\Gamma}^{16}\,e_{2}\,u^{2}\\
&+3306240\,\varpi^{8}\,R_{\Gamma}^{15}\,e_{2}\,u+3240\,\varpi^{18}\,R_{\Gamma}^{4}\,e_{2}\,u^{2}\\
&+2430\,\varpi^{20}\,R_{\Gamma}^{3}\,e_{2}\,u-81000\,\varpi^{16}\,R_{\Gamma}^{7}\,e_{2}\,u\\
&+22680\,\varpi^{18}\,R_{\Gamma}^{5}\,e_{2}\,u-10800\,\varpi^{16}\,R_{\Gamma}^{5}\,e_{2}\,u^{3}\\
&+97200\,\varpi^{16}\,R_{\Gamma}^{6}\,e_{2}\,u^{2}-368640\,\varpi^{6}\,R_{\Gamma}^{17}\,e_{2}\,u\\
&+564480\,\varpi^{8}\,R_{\Gamma}^{16}\,e_{2}-1670400\,\varpi^{10}\,R_{\Gamma}^{14}\,e_{2}\\
&-810\,\varpi^{20}\,R_{\Gamma}^{4}\,e_{1}+21600\,\varpi^{14}\,R_{\Gamma}^{10}\,e_{1}\\
&+12960\,\varpi^{18}\,R_{\Gamma}^{6}\,e_{1}+345600\,\varpi^{10}\,R_{\Gamma}^{10}\,e_{2}\,u^{4}\\
&-43200\,\varpi^{14}\,R_{\Gamma}^{6}\,e_{2}\,u^{4}+2177280\,\varpi^{8}\,R_{\Gamma}^{11}\,e_{2}\,u^{5}\\
&-3168000\,\varpi^{10}\,R_{\Gamma}^{11}\,e_{2}\,u^{3}+7983360\,\varpi^{8}\,R_{\Gamma}^{14}\,e_{2}\,u^{2}\\
&-3225600\,\varpi^{6}\,R_{\Gamma}^{14}\,e_{2}\,u^{4}-97920\,\varpi^{10}\,R_{\Gamma}^{8}\,e_{2}\,u^{6}\\
&+259200\,\varpi^{10}\,R_{\Gamma}^{9}\,e_{2}\,u^{5}+80640\,\varpi^{8}\,R_{\Gamma}^{10}\,e_{2}\,u^{6}\\
&-46080\,\varpi^{6}\,R_{\Gamma}^{10}\,e_{2}\,u^{8}-7516800\,\varpi^{10}\,R_{\Gamma}^{12}\,e_{2}\,u^{2}\\
&-80640\,\varpi^{8}\,R_{\Gamma}^{9}\,e_{2}\,u^{7}-368640\,\varpi^{6}\,R_{\Gamma}^{11}\,e_{2}\,u^{7}\\
&-6030720\,\varpi^{10}\,R_{\Gamma}^{13}\,e_{2}\,u-82080\,\varpi^{12}\,R_{\Gamma}^{7}\,e_{2}\,u^{5}
\end{aligned}
$$

$$-2580480\,\varpi^6\,R_\Gamma^{13}\,e_2\,u^5 - 345600\,\varpi^{12}\,R_\Gamma^{10}\,e_2\,u^2$$
$$-86400\,\varpi^{14}\,R_\Gamma^9\,e_2\,u + 237600\,\varpi^{14}\,R_\Gamma^7\,e_2\,u^3$$
$$-19440\,\varpi^{18}\,R_\Gamma^5\,e_1\,u + 6480\,\varpi^{18}\,R_\Gamma^4\,e_1\,u^2$$
$$-129600\,\varpi^{14}\,R_\Gamma^8\,e_2\,u^2 + 1015200\,\varpi^{12}\,R_\Gamma^{11}\,e_2\,u$$
$$+0.1008{\cdot}10^8\,\varpi^8\,R_\Gamma^{13}\,e_2\,u^3 + 324000\,\varpi^{12}\,R_\Gamma^8\,e_2\,u^4$$
$$+6854400\,\varpi^8\,R_\Gamma^{12}\,e_2\,u^4 - 1290240\,\varpi^6\,R_\Gamma^{12}\,e_2\,u^6$$
$$-12960\,\varpi^{18}\,R_\Gamma^6\,e_2 + 954720\,\varpi^{12}\,R_\Gamma^{12}\,e_2$$
$$-4320\,\varpi^{12}\,R_\Gamma^{12}\,e_1 + 21600\,\varpi^{14}\,R_\Gamma^{10}\,e_2$$
$$-20520\,\varpi^{16}\,R_\Gamma^8\,e_1 - 5400\,\varpi^{16}\,R_\Gamma^8\,e_2$$
$$-46080\,\varpi^6\,R_\Gamma^{18}\,e_2 + 810\,\varpi^{20}\,R_\Gamma^4\,e_2\Big) \times$$
$$2/15/R_\Gamma^{11}/\varpi^{22}, \tag{C.23}$$

$$J^{(4)} = \Big(0.5999616{\cdot}10^8\,\varpi^8\,R_\Gamma^{14}\,e_2\,u - 0.202752{\cdot}10^8\,\varpi^6\,R_\Gamma^{16}\,e_2\,u$$
$$+0.1548288{\cdot}10^8\,\varpi^4\,R_\Gamma^{16}\,e_2\,u^3 - 9720\,\varpi^{20}\,R_\Gamma^2\,e_2\,u$$
$$+1658880\,\varpi^4\,R_\Gamma^{18}\,e_2\,u + 518400\,\varpi^{16}\,R_\Gamma^6\,e_2\,u$$
$$-0.9547776{\cdot}10^8\,\varpi^6\,R_\Gamma^{14}\,e_2\,u^3 - 38880\,\varpi^{16}\,R_\Gamma^4\,e_1\,u^3$$
$$+116640\,\varpi^{16}\,R_\Gamma^5\,e_1\,u^2 + 259200\,\varpi^{14}\,R_\Gamma^8\,e_1\,u$$
$$-181440\,\varpi^{16}\,R_\Gamma^6\,e_1\,u + 84240\,\varpi^{18}\,R_\Gamma^5\,e_2$$
$$-172800\,\varpi^{12}\,R_\Gamma^8\,e_1\,u^3 - 17280\,\varpi^{12}\,R_\Gamma^6\,e_1\,u^5$$
$$+86400\,\varpi^{14}\,R_\Gamma^6\,e_1\,u^3 - 25920\,\varpi^{18}\,R_\Gamma^3\,e_1\,u^2$$
$$-86400\,\varpi^{12}\,R_\Gamma^{10}\,e_1\,u + 86400\,\varpi^{12}\,R_\Gamma^7\,e_1\,u^4$$
$$-259200\,\varpi^{14}\,R_\Gamma^7\,e_1\,u^2 + 110160\,\varpi^{18}\,R_\Gamma^4\,e_1\,u$$
$$-86400\,\varpi^{14}\,R_\Gamma^9\,e_2 + 184320\,\varpi^4\,R_\Gamma^{19}\,e_2$$
$$-368640\,\varpi^6\,R_\Gamma^{10}\,e_2\,u^7 + 622080\,\varpi^{10}\,R_\Gamma^7\,e_2\,u^6$$
$$+9720\,\varpi^{20}\,R_\Gamma^2\,e_1\,u - 2073600\,\varpi^{10}\,R_\Gamma^8\,e_2\,u^5$$
$$-1290240\,\varpi^8\,R_\Gamma^9\,e_2\,u^6 + 552960\,\varpi^8\,R_\Gamma^8\,e_2\,u^7$$
$$+103680\,\varpi^{16}\,R_\Gamma^7\,e_1 - 84240\,\varpi^{18}\,R_\Gamma^5\,e_1$$
$$+368640\,\varpi^6\,R_\Gamma^9\,e_2\,u^8 + 1209600\,\varpi^{12}\,R_\Gamma^9\,e_2\,u^2$$
$$-432000\,\varpi^{12}\,R_\Gamma^{10}\,e_2\,u + 184320\,\varpi^4\,R_\Gamma^{10}\,e_2\,u^9$$
$$+2764800\,\varpi^{10}\,R_\Gamma^{10}\,e_2\,u^3 - 345600\,\varpi^{10}\,R_\Gamma^9\,e_2\,u^4$$
$$+0.1548288{\cdot}10^8\,\varpi^4\,R_\Gamma^{13}\,e_2\,u^6 + 1658880\,\varpi^4\,R_\Gamma^{11}\,e_2\,u^8$$
$$+0.290304{\cdot}10^8\,\varpi^8\,R_\Gamma^{11}\,e_2\,u^4 - 0.129024{\cdot}10^8\,\varpi^6\,R_\Gamma^{11}\,e_2\,u^6$$
$$-0.903168{\cdot}10^8\,\varpi^6\,R_\Gamma^{13}\,e_2\,u^4 - 1935360\,\varpi^8\,R_\Gamma^{10}\,e_2\,u^5$$

$$-0.196992 \cdot 10^8 \, \varpi^{10} \, R_\Gamma^{11} \, e_2 \, u^2 - 2160000 \, \varpi^{12} \, R_\Gamma^7 \, e_2 \, u^4$$

$$-0.3497472 \cdot 10^8 \, \varpi^{10} \, R_\Gamma^{12} \, e_2 \, u + 864000 \, \varpi^{12} \, R_\Gamma^8 \, e_2 \, u^3$$

$$+501120 \, \varpi^{12} \, R_\Gamma^6 \, e_2 \, u^5 + 0.2322432 \cdot 10^8 \, \varpi^4 \, R_\Gamma^{14} \, e_2 \, u^5$$

$$+259200 \, \varpi^{14} \, R_\Gamma^8 \, e_2 \, u - 0.4902912 \cdot 10^8 \, \varpi^6 \, R_\Gamma^{12} \, e_2 \, u^5$$

$$-123120 \, \varpi^{18} \, R_\Gamma^4 \, e_2 \, u + 17280 \, \varpi^{12} \, R_\Gamma^{11} \, e_1$$

$$-12960 \, \varpi^{18} \, R_\Gamma^3 \, e_2 \, u^2 + 0.903168 \cdot 10^8 \, \varpi^8 \, R_\Gamma^{12} \, e_2 \, u^3$$

$$+6635520 \, \varpi^4 \, R_\Gamma^{12} \, e_2 \, u^7 - 1468800 \, \varpi^{14} \, R_\Gamma^6 \, e_2 \, u^3$$

$$+1036800 \, \varpi^{14} \, R_\Gamma^7 \, e_2 \, u^2 - 583200 \, \varpi^{16} \, R_\Gamma^5 \, e_2 \, u^2$$

$$+172800 \, \varpi^{12} \, R_\Gamma^9 \, e_1 \, u^2 + 0.2322432 \cdot 10^8 \, \varpi^4 \, R_\Gamma^{15} \, e_2 \, u^4$$

$$-0.5935104 \cdot 10^8 \, \varpi^6 \, R_\Gamma^{15} \, e_2 \, u^2 + 259200 \, \varpi^{14} \, R_\Gamma^5 \, e_2 \, u^4$$

$$+6635520 \, \varpi^4 \, R_\Gamma^{17} \, e_2 \, u^2 - 3240 \, \varpi^{20} \, R_\Gamma^3 \, e_2$$

$$+0.1083802 \cdot 10^9 \, \varpi^8 \, R_\Gamma^{13} \, e_2 \, u^2 + 64800 \, \varpi^{16} \, R_\Gamma^4 \, e_2 \, u^3$$

$$-0.148608 \cdot 10^8 \, \varpi^{10} \, R_\Gamma^{13} \, e_2 + 3240 \, \varpi^{20} \, R_\Gamma^3 \, e_1$$

$$-86400 \, \varpi^{14} \, R_\Gamma^9 \, e_1 - 2949120 \, \varpi^6 \, R_\Gamma^{17} \, e_2$$

$$+0.1281024 \cdot 10^8 \, \varpi^8 \, R_\Gamma^{15} \, e_2 + 1883520 \, \varpi^{12} \, R_\Gamma^{11} \, e_2 \Big) \times$$

$$2/15/R_\Gamma^{11}/\varpi^{22}, \tag{C.24}$$

$$J^{(5)} \;=\; \Big(810000 \, \varpi^{18} \, R_\Gamma^3 \, e_2 \, u + 0.1177805 \cdot 10^9 \, \varpi^4 \, R_\Gamma^{17} \, e_2 \, u$$

$$+48600 \, \varpi^{20} \, R_\Gamma \, e_2 \, u + 6266880 \, \varpi^6 \, R_\Gamma^9 \, e_2 \, u^7$$

$$-7372800 \, \varpi^2 \, R_\Gamma^{19} \, e_2 \, u + 64800 \, \varpi^{18} \, R_\Gamma^2 \, e_2 \, u^2$$

$$-2949120 \, \varpi^6 \, R_\Gamma^8 \, e_2 \, u^8 - 0.331776 \cdot 10^8 \, \varpi^2 \, R_\Gamma^{12} \, e_2 \, u^8$$

$$+0.7064064 \cdot 10^9 \, \varpi^8 \, R_\Gamma^{12} \, e_2 \, u^2 - 7372800 \, \varpi^2 \, R_\Gamma^{11} \, e_2 \, u^9$$

$$-737280 \, \varpi^2 \, R_\Gamma^{10} \, e_2 \, u^{10} + 0.165888 \cdot 10^8 \, \varpi^{10} \, R_\Gamma^7 \, e_2 \, u^5$$

$$+1658880 \, \varpi^4 \, R_\Gamma^{10} \, e_2 \, u^8 - 1658880 \, \varpi^4 \, R_\Gamma^9 \, e_2 \, u^9$$

$$-0.903168 \cdot 10^9 \, \varpi^6 \, R_\Gamma^{12} \, e_2 \, u^4 - 0.124416 \cdot 10^8 \, \varpi^{10} \, R_\Gamma^9 \, e_2 \, u^3$$

$$-4492800 \, \varpi^{10} \, R_\Gamma^8 \, e_2 \, u^4 + 5184000 \, \varpi^{10} \, R_\Gamma^{10} \, e_2 \, u^2$$

$$+0.274176 \cdot 10^9 \, \varpi^8 \, R_\Gamma^{11} \, e_2 \, u^3 + 0.7299072 \cdot 10^8 \, \varpi^4 \, R_\Gamma^{11} \, e_2 \, u^7$$

$$-615600 \, \varpi^{18} \, R_\Gamma^4 \, e_2 - 48600 \, \varpi^{20} \, R_\Gamma \, e_1 \, u$$

$$-864000 \, \varpi^{12} \, R_\Gamma^8 \, e_1 \, u^2 + 432000 \, \varpi^{12} \, R_\Gamma^9 \, e_1 \, u$$

$$+864000 \, \varpi^{12} \, R_\Gamma^7 \, e_1 \, u^3 + 86400 \, \varpi^{12} \, R_\Gamma^5 \, e_1 \, u^5$$

$$-432000 \, \varpi^{14} \, R_\Gamma^5 \, e_1 \, u^3 + 1296000 \, \varpi^{16} \, R_\Gamma^5 \, e_1 \, u$$

$$-1296000 \, \varpi^{14} \, R_\Gamma^7 \, e_1 \, u + 129600 \, \varpi^{18} \, R_\Gamma^2 \, e_1 \, u^2$$

$$+324000 \, \varpi^{16} \, R_\Gamma^3 \, e_1 \, u^3 - 745200 \, \varpi^{18} \, R_\Gamma^3 \, e_1 \, u$$

$$-0.1857946{\cdot}10^9\,\varpi^2\,R_\Gamma^{15}\,e_2\,u^5 - 0.5113037{\cdot}10^9\,\varpi^6\,R_\Gamma^{15}\,e_2\,u$$
$$-0.1548288{\cdot}10^9\,\varpi^2\,R_\Gamma^{14}\,e_2\,u^6 + 0.1492992{\cdot}10^8\,\varpi^4\,R_\Gamma^{18}\,e_2$$
$$-16200\,\varpi^{20}\,R_\Gamma^2\,e_1 - 0.8921088{\cdot}10^8\,\varpi^6\,R_\Gamma^{16}\,e_2$$
$$+0.3251405{\cdot}10^9\,\varpi^4\,R_\Gamma^{12}\,e_2\,u^6 - 0.801792{\cdot}10^8\,\varpi^{10}\,R_\Gamma^{11}\,e_2\,u$$
$$-0.2348237{\cdot}10^9\,\varpi^6\,R_\Gamma^{11}\,e_2\,u^5 - 5011200\,\varpi^{12}\,R_\Gamma^8\,e_2\,u^2$$
$$+0.1225728{\cdot}10^8\,\varpi^8\,R_\Gamma^8\,e_2\,u^6 + 2160000\,\varpi^{12}\,R_\Gamma^9\,e_2\,u$$
$$+0.15984{\cdot}10^8\,\varpi^{12}\,R_\Gamma^6\,e_2\,u^4 - 3542400\,\varpi^{12}\,R_\Gamma^5\,e_2\,u^5$$
$$-86400\,\varpi^{12}\,R_\Gamma^{10}\,e_1 - 4492800\,\varpi^{10}\,R_\Gamma^6\,e_2\,u^6$$
$$-9504000\,\varpi^{12}\,R_\Gamma^7\,e_2\,u^3 + 0.9521971{\cdot}10^9\,\varpi^4\,R_\Gamma^{14}\,e_2\,u^4$$
$$+0.7199539{\cdot}10^9\,\varpi^4\,R_\Gamma^{13}\,e_2\,u^5 - 4147200\,\varpi^8\,R_\Gamma^7\,e_2\,u^7$$
$$-777600\,\varpi^{14}\,R_\Gamma^7\,e_2\,u - 0.1442488{\cdot}10^{10}\,\varpi^6\,R_\Gamma^{13}\,e_2\,u^3$$
$$-1814400\,\varpi^{14}\,R_\Gamma^4\,e_2\,u^4 - 453600\,\varpi^{16}\,R_\Gamma^3\,e_2\,u^3$$
$$-0.722304{\cdot}10^8\,\varpi^{10}\,R_\Gamma^{12}\,e_2 - 648000\,\varpi^{16}\,R_\Gamma^6\,e_1$$
$$-86400\,\varpi^{12}\,R_\Gamma^{10}\,e_2 + 615600\,\varpi^{18}\,R_\Gamma^4\,e_1$$
$$+432000\,\varpi^{14}\,R_\Gamma^8\,e_2 + 129600\,\varpi^{16}\,R_\Gamma^6\,e_2$$
$$-0.884736{\cdot}10^8\,\varpi^2\,R_\Gamma^{13}\,e_2\,u^7 - 0.193536{\cdot}10^8\,\varpi^8\,R_\Gamma^{10}\,e_2\,u^4$$
$$+0.104544{\cdot}10^8\,\varpi^{14}\,R_\Gamma^5\,e_2\,u^3 + 0.1032192{\cdot}10^8\,\varpi^6\,R_\Gamma^{10}\,e_2\,u^6$$
$$-8294400\,\varpi^{14}\,R_\Gamma^6\,e_2\,u^2 + 0.5960909{\cdot}10^9\,\varpi^8\,R_\Gamma^{13}\,e_2\,u$$
$$+0.4047667{\cdot}10^9\,\varpi^4\,R_\Gamma^{16}\,e_2\,u^2 - 3758400\,\varpi^{16}\,R_\Gamma^5\,e_2\,u$$
$$-0.1548288{\cdot}10^9\,\varpi^2\,R_\Gamma^{16}\,e_2\,u^4 - 0.1197343{\cdot}10^{10}\,\varpi^6\,R_\Gamma^{14}\,e_2\,u^2$$
$$+0.7896269{\cdot}10^9\,\varpi^4\,R_\Gamma^{15}\,e_2\,u^3 + 1296000\,\varpi^{14}\,R_\Gamma^6\,e_1\,u^2$$
$$-972000\,\varpi^{16}\,R_\Gamma^4\,e_1\,u^2 - 432000\,\varpi^{12}\,R_\Gamma^6\,e_1\,u^4$$
$$-0.331776{\cdot}10^8\,\varpi^2\,R_\Gamma^{18}\,e_2\,u^2 + 4082400\,\varpi^{16}\,R_\Gamma^4\,e_2\,u^2$$
$$-0.884736{\cdot}10^8\,\varpi^2\,R_\Gamma^{17}\,e_2\,u^3 + 3870720\,\varpi^8\,R_\Gamma^9\,e_2\,u^5$$
$$-737280\,\varpi^2\,R_\Gamma^{20}\,e_2 + 16200\,\varpi^{20}\,R_\Gamma^2\,e_2$$
$$+432000\,\varpi^{14}\,R_\Gamma^8\,e_1 + 0.1706803{\cdot}10^9\,\varpi^8\,R_\Gamma^{14}\,e_2\Big)\times$$
$$2/15/R_\Gamma^{11}/\varpi^{22}, \tag{C.25}$$

$$J^{(6)} = \Big(-2851200\,\varpi^{16}\,R_\Gamma^2\,e_1\,u^3 + 0.1397053{\cdot}10^{10}\,\varpi^8\,e_2\,R_\Gamma^{13}$$
$$-2592000\,\varpi^{12}\,R_\Gamma^8\,e_1\,u + 0.307152{\cdot}10^8\,\varpi^{16}\,R_\Gamma^4\,e_2\,u$$
$$+2592000\,\varpi^{12}\,R_\Gamma^5\,e_1\,u^4 + 3628800\,\varpi^{16}\,R_\Gamma^2\,e_2\,u^3$$
$$-0.48384{\cdot}10^8\,\varpi^8\,e_2\,R_\Gamma^{10}\,u^3 - 6220800\,\varpi^{18}\,R_\Gamma^2\,e_2\,u$$
$$-388800\,\varpi^{18}\,e_2\,R_\Gamma\,u^2 + 2949120\,e_2\,R_\Gamma^{21}$$

$$-0.326592 \cdot 10^8\, \varpi^{16}\, R_\Gamma^3\, e_2\, u^2 - 0.6561792 \cdot 10^9\, e_2\, R_\Gamma^{18}\, u\, \varpi^2$$

$$+2073600\, \varpi^{10}\, e_2\, R_\Gamma^{10}\, u + 7372800\, e_2\, R_\Gamma^9\, u^{10}\, \varpi^2$$

$$+0.649728 \cdot 10^8\, \varpi^{10}\, e_2\, R_\Gamma^8\, u^3 - 0.3096576 \cdot 10^8\, e_2\, R_\Gamma^9\, u^6\, \varpi^6$$

$$+0.2543616 \cdot 10^8\, e_2\, R_\Gamma^7\, u^8\, \varpi^6 + 0.1064448 \cdot 10^9\, \varpi^8\, e_2\, R_\Gamma^9\, u^4$$

$$-0.2985984 \cdot 10^8\, e_2\, R_\Gamma^9\, u^8\, \varpi^4 - 0.6856704 \cdot 10^8\, \varpi^6\, e_2\, R_\Gamma^8\, u^7$$

$$-0.2587853 \cdot 10^{10}\, e_2\, R_\Gamma^{17}\, u^2\, \varpi^2 + 0.1511424 \cdot 10^8\, e_2\, R_\Gamma^8\, u^9\, \varpi^4$$

$$+0.1741824 \cdot 10^8\, \varpi^8\, e_2\, R_\Gamma^8\, u^5 + 0.3456 \cdot 10^8\, \varpi^8\, e_2\, R_\Gamma^6\, u^7$$

$$-0.5927731 \cdot 10^{10}\, e_2\, R_\Gamma^{16}\, u^3\, \varpi^2 + 518400\, \varpi^{12}\, R_\Gamma^9\, e_1$$

$$-0.73728 \cdot 10^8\, e_2\, R_\Gamma^{19}\, \varpi^2 + 291600\, \varpi^{20}\, e_1\, u$$

$$-0.1640079 \cdot 10^{10}\, e_2\, R_\Gamma^{15}\, \varpi^6 - 2592000\, \varpi^{14}\, R_\Gamma^7\, e_2$$

$$+0.228096 \cdot 10^8\, \varpi^{12}\, R_\Gamma^7\, e_2\, u^2 + 0.1734083 \cdot 10^{10}\, e_2\, R_\Gamma^{11}\, u^6\, \varpi^4$$

$$-0.3096576 \cdot 10^{10}\, e_2\, R_\Gamma^{11}\, u^4\, \varpi^6 + 0.1583899 \cdot 10^{11}\, e_2\, R_\Gamma^{13}\, u^4\, \varpi^4$$

$$-0.132192 \cdot 10^9\, \varpi^{12}\, R_\Gamma^5\, e_2\, u^4 - 0.8360755 \cdot 10^{10}\, e_2\, R_\Gamma^{14}\, u^5\, \varpi^2$$

$$+0.123863 \cdot 10^9\, e_2\, R_\Gamma^{10}\, u^5\, \varpi^6 - 0.8670413 \cdot 10^{10}\, e_2\, R_\Gamma^{15}\, u^4\, \varpi^2$$

$$+0.112273 \cdot 10^{11}\, e_2\, R_\Gamma^{15}\, u^2\, \varpi^4 - 7372800\, e_2\, R_\Gamma^{10}\, u^9\, \varpi^2$$

$$-777600\, \varpi^{18}\, e_1\, R_\Gamma\, u^2 - 0.7506985 \cdot 10^{10}\, e_2\, R_\Gamma^{14}\, u\, \varpi^6$$

$$+5832000\, \varpi^{18}\, R_\Gamma^2\, e_1\, u + 8553600\, \varpi^{16}\, R_\Gamma^3\, e_1\, u^2$$

$$-0.104976 \cdot 10^8\, \varpi^{16}\, R_\Gamma^4\, e_1\, u + 2592000\, \varpi^{14}\, R_\Gamma^4\, e_1\, u^3$$

$$-0.1430784 \cdot 10^9\, \varpi^{10}\, e_2\, R_\Gamma^6\, u^5 - 0.3981312 \cdot 10^9\, \varpi^2\, e_2\, R_\Gamma^{11}\, u^8$$

$$+0.1828915 \cdot 10^{10}\, \varpi^8\, e_2\, R_\Gamma^{11}\, u^2 + 5184000\, \varpi^{12}\, R_\Gamma^7\, e_1\, u^2$$

$$-518400\, \varpi^{12}\, R_\Gamma^4\, e_1\, u^5 + 7776000\, \varpi^{14}\, R_\Gamma^6\, e_1\, u$$

$$-7776000\, \varpi^{14}\, R_\Gamma^5\, e_1\, u^2 - 5184000\, \varpi^{12}\, R_\Gamma^6\, e_1\, u^3$$

$$+97200\, \varpi^{20}\, R_\Gamma\, e_1 + 0.1622016 \cdot 10^9\, e_2\, R_\Gamma^{19}\, u^2$$

$$-1684800\, \varpi^{16}\, R_\Gamma^5\, e_2 + 0.4866048 \cdot 10^9\, e_2\, R_\Gamma^{18}\, u^3$$

$$+0.28512 \cdot 10^8\, \varpi^{12}\, R_\Gamma^4\, e_2\, u^5 + 0.7942717 \cdot 10^{10}\, e_2\, R_\Gamma^{12}\, u^5\, \varpi^4$$

$$-0.1141862 \cdot 10^9\, \varpi^8\, e_2\, R_\Gamma^7\, u^6 + 0.3918275 \cdot 10^{10}\, e_2\, R_\Gamma^{16}\, u\, \varpi^4$$

$$-0.31104 \cdot 10^8\, \varpi^{10}\, e_2\, R_\Gamma^9\, u^2 + 0.705024 \cdot 10^8\, \varpi^{10}\, e_2\, R_\Gamma^7\, u^4$$

$$+0.366336 \cdot 10^8\, \varpi^{10}\, e_2\, R_\Gamma^5\, u^6 + 0.1752662 \cdot 10^{11}\, e_2\, R_\Gamma^{14}\, u^3\, \varpi^4$$

$$+1036800\, \varpi^{14}\, R_\Gamma^6\, e_2\, u + 0.715392 \cdot 10^8\, \varpi^{14}\, R_\Gamma^5\, e_2\, u^2$$

$$-0.844992 \cdot 10^8\, \varpi^{14}\, R_\Gamma^4\, e_2\, u^3 + 0.145152 \cdot 10^8\, \varpi^{14}\, R_\Gamma^3\, e_2\, u^4$$

$$-0.5264179 \cdot 10^{10}\, e_2\, R_\Gamma^{13}\, u^6\, \varpi^2 - 0.1312948 \cdot 10^{11}\, e_2\, R_\Gamma^{13}\, u^2\, \varpi^6$$

$$-0.2034893 \cdot 10^{10}\, e_2\, R_\Gamma^{12}\, u^7\, \varpi^2 - 0.1041998 \cdot 10^{11}\, e_2\, R_\Gamma^{12}\, u^3\, \varpi^6$$

$$+0.3214633 \cdot 10^{10}\, \varpi^8\, e_2\, R_\Gamma^{12}\, u - 0.5308416 \cdot 10^8\, e_2\, R_\Gamma^{10}\, u^7\, \varpi^4$$

$$-0.1296{\cdot}10^8\,\varpi^{12}\,e_2\,R_\Gamma^8\,u + 0.93312{\cdot}10^8\,\varpi^{12}\,R_\Gamma^6\,e_2\,u^3$$
$$-97200\,\varpi^{20}\,R_\Gamma\,e_2 - 5054400\,\varpi^{18}\,R_\Gamma^3\,e_1$$
$$-291600\,\varpi^{20}\,e_2\,u + 0.3244032{\cdot}10^8\,e_2\,R_\Gamma^{11}\,u^{10}$$
$$+0.4866048{\cdot}10^9\,e_2\,R_\Gamma^{13}\,u^8 + 0.1362493{\cdot}10^{10}\,e_2\,R_\Gamma^{15}\,u^6$$
$$+518400\,\varpi^{12}\,R_\Gamma^9\,e_2 + 0.9732096{\cdot}10^9\,e_2\,R_\Gamma^{17}\,u^4$$
$$+4795200\,\varpi^{16}\,R_\Gamma^5\,e_1 - 2592000\,\varpi^{14}\,R_\Gamma^7\,e_1$$
$$+0.1362493{\cdot}10^{10}\,e_2\,R_\Gamma^{16}\,u^5 + 5054400\,\varpi^{18}\,R_\Gamma^3\,e_2$$
$$+0.1622016{\cdot}10^9\,e_2\,R_\Gamma^{12}\,u^9 + 0.3244032{\cdot}10^8\,e_2\,R_\Gamma^{20}\,u$$
$$+0.9732096{\cdot}10^9\,e_2\,R_\Gamma^{14}\,u^7 + 0.5791334{\cdot}10^9\,e_2\,R_\Gamma^{17}\,\varpi^4$$
$$-0.152064{\cdot}10^9\,\varpi^{10}\,e_2\,R_\Gamma^{11} + 2949120\,e_2\,R_\Gamma^{10}\,u^{11}\Big) \times$$
$$2/15/R_\Gamma^{11}/\varpi^{22}. \tag{C.26}$$

The function $U(u, \lambda, q, p)$ expanded in terms of λ takes the form

$$U \;=\; \varepsilon\left(\frac{(P-2)(q+I\,p)}{P^2}\right) \times \Big[U^{(0)}(u) + \frac{\lambda^1}{1!}U^{(1)}(u) +$$
$$+\cdots+ \frac{\lambda^6}{6!}U^{(6)}(u) + O(\lambda^7)\Big] + O(\varepsilon^2), \tag{C.27}$$

where

$$U^{(0)} \;=\; -2/15\Big(-540\,R_\Gamma^{11}\,\varpi^{14}\,e_2 - 1620\,R_\Gamma^9\,\varpi^{14}\,e_1\,u^2$$
$$+540\,R_\Gamma^8\,\varpi^{14}\,e_1\,u^3 + 1620\,R_\Gamma^{10}\,\varpi^{14}\,e_1\,u$$
$$-540\,R_\Gamma^8\,\varpi^{14}\,e_2\,u^3 - 1620\,R_\Gamma^9\,\varpi^{14}\,e_2\,u^2$$
$$-1620\,R_\Gamma^{10}\,\varpi^{14}\,e_2\,u - 810\,R_\Gamma^7\,\varpi^{16}\,e_2\,u^2$$
$$-810\,R_\Gamma^7\,\varpi^{16}\,e_1\,u^2 - 810\,R_\Gamma^8\,\varpi^{16}\,e_2\,u$$
$$-405\,R_\Gamma^6\,\varpi^{18}\,e_2\,u + 810\,R_\Gamma^8\,\varpi^{16}\,e_1\,u$$
$$-540\,R_\Gamma^{11}\,\varpi^{14}\,e_1 + 405\,R_\Gamma^6\,\varpi^{18}\,e_1\,u\Big)/R_\Gamma^{12}/\varpi^{20}, \tag{C.28}$$

$$U^{(1)} \;=\; -\Big(-14400\,R_\Gamma^{12}\,\varpi^{10}\,e_2\,u^2 - 270\,R_\Gamma^6\,\varpi^{16}\,e_2\,u^2$$
$$-7200\,R_\Gamma^{10}\,\varpi^{10}\,e_2\,u^4 + 5040\,R_\Gamma^{12}\,\varpi^{12}\,e_2$$
$$-1440\,R_\Gamma^9\,\varpi^{10}\,e_2\,u^5 - 14400\,R_\Gamma^{11}\,\varpi^{10}\,e_2\,u^3$$
$$-1440\,R_\Gamma^9\,\varpi^{12}\,e_2\,u^3 + 8640\,R_\Gamma^{10}\,\varpi^{12}\,e_2\,u^2$$
$$-2160\,R_\Gamma^8\,\varpi^{12}\,e_2\,u^4 + 12960\,R_\Gamma^{11}\,\varpi^{12}\,e_2\,u$$
$$-1440\,R_\Gamma^{14}\,\varpi^{10}\,e_2 + 7200\,R_\Gamma^{10}\,\varpi^{10}\,e_1\,u^4$$
$$+1440\,R_\Gamma^{14}\,\varpi^{10}\,e_1 + 21600\,R_\Gamma^{11}\,\varpi^{12}\,e_1\,u$$

$$+7200\,R_\Gamma^9\,\varpi^{12}\,e_1\,u^3 - 1440\,R_\Gamma^9\,\varpi^{10}\,e_1\,u^5$$

$$+1080\,R_\Gamma^7\,\varpi^{16}\,e_2\,u - 14400\,R_\Gamma^{11}\,\varpi^{10}\,e_1\,u^3$$

$$-21600\,R_\Gamma^{10}\,\varpi^{12}\,e_1\,u^2 - 5400\,R_\Gamma^9\,\varpi^{14}\,e_1\,u$$

$$-7200\,R_\Gamma^{13}\,\varpi^{10}\,e_1\,u + 14400\,R_\Gamma^{12}\,\varpi^{10}\,e_1\,u^2$$

$$+5400\,R_\Gamma^{10}\,\varpi^{14}\,e_1 - 7200\,R_\Gamma^{12}\,\varpi^{12}\,e_1$$

$$+270\,R_\Gamma^6\,\varpi^{16}\,e_1\,u^2 - 540\,R_\Gamma^7\,\varpi^{16}\,e_1\,u$$

$$-7200\,R_\Gamma^{13}\,\varpi^{10}\,e_2\,u - 135\,R_\Gamma^6\,\varpi^{18}\,e_1$$

$$-270\,R_\Gamma^8\,\varpi^{16}\,e_2 + 4320\,R_\Gamma^9\,\varpi^{14}\,e_2\,u$$

$$-1080\,R_\Gamma^7\,\varpi^{14}\,e_2\,u^3 + 3240\,R_\Gamma^8\,\varpi^{14}\,e_2\,u^2$$

$$+270\,R_\Gamma^8\,\varpi^{16}\,e_1 + 135\,R_\Gamma^6\,\varpi^{18}\,e_2\Big)\,\times$$

$$2/15/R_\Gamma^{12}/\varpi^{20}, \tag{C.29}$$

$$U^{(2)} = -\Big(-3240\,R_\Gamma^7\,\varpi^{16}\,e_1 + 12960\,R_\Gamma^7\,\varpi^{12}\,e_2\,u^4$$

$$+86400\,R_\Gamma^{11}\,\varpi^8\,e_2\,u^4 - 108000\,R_\Gamma^{12}\,\varpi^{10}\,e_2\,u$$

$$+115200\,R_\Gamma^{12}\,\varpi^8\,e_2\,u^3 - 43200\,R_\Gamma^{10}\,\varpi^{10}\,e_2\,u^3$$

$$-129600\,R_\Gamma^{11}\,\varpi^{10}\,e_2\,u^2 + 34560\,R_\Gamma^{10}\,\varpi^8\,e_2\,u^5$$

$$+12960\,R_\Gamma^8\,\varpi^{10}\,e_2\,u^5 + 21600\,R_\Gamma^9\,\varpi^{10}\,e_2\,u^4$$

$$+5760\,R_\Gamma^9\,\varpi^8\,e_2\,u^6 + 21600\,R_\Gamma^{12}\,\varpi^{10}\,e_1\,u$$

$$-5400\,R_\Gamma^6\,\varpi^{14}\,e_1\,u^3 + 4320\,R_\Gamma^9\,\varpi^{14}\,e_2$$

$$+4320\,R_\Gamma^7\,\varpi^{12}\,e_1\,u^4 - 38880\,R_\Gamma^8\,\varpi^{12}\,e_1\,u^3$$

$$+1620\,R_\Gamma^5\,\varpi^{16}\,e_1\,u^2 - 810\,R_\Gamma^4\,\varpi^{18}\,e_1\,u$$

$$+90720\,R_\Gamma^9\,\varpi^{12}\,e_1\,u^2 - 82080\,R_\Gamma^{10}\,\varpi^{12}\,e_1\,u$$

$$+4860\,R_\Gamma^6\,\varpi^{16}\,e_1\,u + 4320\,R_\Gamma^8\,\varpi^{10}\,e_1\,u^5$$

$$+5760\,R_\Gamma^{15}\,\varpi^8\,e_2 - 22680\,R_\Gamma^7\,\varpi^{14}\,e_2\,u^2$$

$$-12960\,R_\Gamma^8\,\varpi^{14}\,e_2\,u - 23760\,R_\Gamma^9\,\varpi^{14}\,e_1$$

$$+3240\,R_\Gamma^7\,\varpi^{16}\,e_2 + 34560\,R_\Gamma^{14}\,\varpi^8\,e_2\,u$$

$$+5400\,R_\Gamma^6\,\varpi^{14}\,e_2\,u^3 + 86400\,R_\Gamma^{13}\,\varpi^8\,e_2\,u^2$$

$$-51840\,R_\Gamma^9\,\varpi^{12}\,e_2\,u^2 - 12960\,R_\Gamma^8\,\varpi^{12}\,e_2\,u^3$$

$$+810\,R_\Gamma^4\,\varpi^{18}\,e_2\,u + 1620\,R_\Gamma^5\,\varpi^{16}\,e_2\,u^2$$

$$-4860\,R_\Gamma^6\,\varpi^{16}\,e_2\,u - 12960\,R_\Gamma^{10}\,\varpi^{12}\,e_2\,u$$

$$+43200\,R_\Gamma^{10}\,\varpi^{10}\,e_1\,u^3 - 43200\,R_\Gamma^{11}\,\varpi^{10}\,e_1\,u^2$$

$$+3240\,R_\Gamma^7\,\varpi^{14}\,e_1\,u^2 + 25920\,R_\Gamma^8\,\varpi^{14}\,e_1\,u$$

$$-21600\,R_\Gamma^9\,\varpi^{10}\,e_1\,u^4 + 12960\,R_\Gamma^{11}\,\varpi^{12}\,e_2$$

$$
\begin{aligned}
&+25920\,R_\Gamma^{11}\,\varpi^{12}\,e_1 - 30240\,R_\Gamma^{13}\,\varpi^{10}\,e_2 \\
&\left.-4320\,R_\Gamma^{13}\,\varpi^{10}\,e_1\right) \times 2/15/R_\Gamma^{12}/\varpi^{20}, \tag{C.30}
\end{aligned}
$$

$$
\begin{aligned}
U^{(3)} = -\Big(&172800\,R_\Gamma^{7}\,\varpi^{12}\,e_2\,u^3 - 86400\,R_\Gamma^{6}\,\varpi^{12}\,e_2\,u^4 \\
&-43200\,R_\Gamma^{9}\,\varpi^{12}\,e_2\,u + 259200\,R_\Gamma^{8}\,\varpi^{12}\,e_2\,u^2 \\
&-32400\,R_\Gamma^{5}\,\varpi^{14}\,e_2\,u^3 + 162000\,R_\Gamma^{6}\,\varpi^{14}\,e_2\,u^2 \\
&+32400\,R_\Gamma^{7}\,\varpi^{14}\,e_2\,u + 32400\,R_\Gamma^{5}\,\varpi^{16}\,e_2\,u \\
&-161280\,R_\Gamma^{15}\,\varpi^{6}\,e_2\,u - 8100\,R_\Gamma^{4}\,\varpi^{16}\,e_2\,u^2 \\
&+4860\,R_\Gamma^{3}\,\varpi^{18}\,e_1\,u + 380160\,R_\Gamma^{9}\,\varpi^{12}\,e_1\,u \\
&+207360\,R_\Gamma^{7}\,\varpi^{12}\,e_1\,u^3 - 172800\,R_\Gamma^{9}\,\varpi^{10}\,e_1\,u^3 \\
&+172800\,R_\Gamma^{10}\,\varpi^{10}\,e_1\,u^2 - 17280\,R_\Gamma^{7}\,\varpi^{10}\,e_1\,u^5 \\
&+86400\,R_\Gamma^{8}\,\varpi^{10}\,e_1\,u^4 + 794880\,R_\Gamma^{13}\,\varpi^{8}\,e_2\,u \\
&-483840\,R_\Gamma^{14}\,\varpi^{6}\,e_2\,u^2 + 432000\,R_\Gamma^{9}\,\varpi^{10}\,e_2\,u^3 \\
&-4860\,R_\Gamma^{3}\,\varpi^{18}\,e_2\,u - 483840\,R_\Gamma^{11}\,\varpi^{6}\,e_2\,u^5 \\
&+1036800\,R_\Gamma^{11}\,\varpi^{8}\,e_2\,u^3 - 259200\,R_\Gamma^{11}\,\varpi^{10}\,e_2\,u \\
&-810\,R_\Gamma^{4}\,\varpi^{18}\,e_2 + 17280\,R_\Gamma^{12}\,\varpi^{10}\,e_1 \\
&-116640\,R_\Gamma^{10}\,\varpi^{12}\,e_1 - 32400\,R_\Gamma^{8}\,\varpi^{14}\,e_2 \\
&+24300\,R_\Gamma^{6}\,\varpi^{16}\,e_1 - 23040\,R_\Gamma^{16}\,\varpi^{6}\,e_2 \\
&+810\,R_\Gamma^{4}\,\varpi^{18}\,e_1 + 172800\,R_\Gamma^{14}\,\varpi^{8}\,e_2 \\
&-190080\,R_\Gamma^{12}\,\varpi^{10}\,e_2 - 24300\,R_\Gamma^{6}\,\varpi^{16}\,e_2 \\
&+116640\,R_\Gamma^{8}\,\varpi^{14}\,e_1 - 30240\,R_\Gamma^{6}\,\varpi^{12}\,e_1\,u^4 \\
&-440640\,R_\Gamma^{8}\,\varpi^{12}\,e_1\,u^2 - 35640\,R_\Gamma^{5}\,\varpi^{16}\,e_1\,u \\
&-11340\,R_\Gamma^{4}\,\varpi^{16}\,e_1\,u^2 - 129600\,R_\Gamma^{7}\,\varpi^{14}\,e_1\,u \\
&+38880\,R_\Gamma^{5}\,\varpi^{14}\,e_1\,u^3 - 25920\,R_\Gamma^{6}\,\varpi^{14}\,e_1\,u^2 \\
&-86400\,R_\Gamma^{11}\,\varpi^{10}\,e_1\,u + 172800\,R_\Gamma^{10}\,\varpi^{8}\,e_2\,u^4 \\
&-103680\,R_\Gamma^{7}\,\varpi^{10}\,e_2\,u^5 - 161280\,R_\Gamma^{10}\,\varpi^{6}\,e_2\,u^6 \\
&-69120\,R_\Gamma^{8}\,\varpi^{8}\,e_2\,u^6 - 23040\,R_\Gamma^{9}\,\varpi^{6}\,e_2\,u^7 \\
&-806400\,R_\Gamma^{13}\,\varpi^{6}\,e_2\,u^3 - 172800\,R_\Gamma^{9}\,\varpi^{8}\,e_2\,u^5 \\
&+259200\,R_\Gamma^{10}\,\varpi^{10}\,e_2\,u^2 - 806400\,R_\Gamma^{12}\,\varpi^{6}\,e_2\,u^4 \\
&\left.+1382400\,R_\Gamma^{12}\,\varpi^{8}\,e_2\,u^2 - 43200\,R_\Gamma^{10}\,\varpi^{12}\,e_2\right) \times \\
&2/15/R_\Gamma^{12}/\varpi^{20}, \tag{C.31}
\end{aligned}
$$

$$
U^{(4)} = -\Big(2580480\,R_\Gamma^{11}\,\varpi^{4}\,e_2\,u^6 + 5356800\,R_\Gamma^{12}\,\varpi^{8}\,e_2\,u
$$

$$+648000\,R_\Gamma^8\,\varpi^{12}\,e_2\,u - 0.137088{\cdot}10^8\,R_\Gamma^{12}\,\varpi^6\,e_2\,u^3$$
$$-86400\,R_\Gamma^{11}\,\varpi^{10}\,e_1 - 86400\,R_\Gamma^{11}\,\varpi^{10}\,e_2$$
$$+226800\,R_\Gamma^7\,\varpi^{14}\,e_2 - 5322240\,R_\Gamma^{14}\,\varpi^6\,e_2\,u$$
$$+172800\,R_\Gamma^9\,\varpi^{12}\,e_2 - 29160\,R_\Gamma^2\,\varpi^{18}\,e_1\,u$$
$$-0.12096{\cdot}10^8\,R_\Gamma^{13}\,\varpi^6\,e_2\,u^2 + 1900800\,R_\Gamma^{13}\,\varpi^8\,e_2$$
$$-667440\,R_\Gamma^7\,\varpi^{14}\,e_1 + 6480\,R_\Gamma^3\,\varpi^{18}\,e_2$$
$$+639360\,R_\Gamma^9\,\varpi^{12}\,e_1 + 92160\,R_\Gamma^{17}\,\varpi^4\,e_2$$
$$-944640\,R_\Gamma^{15}\,\varpi^6\,e_2 - 864000\,R_\Gamma^9\,\varpi^{10}\,e_1\,u^2$$
$$+207360\,R_\Gamma^5\,\varpi^{12}\,e_1\,u^4 + 71280\,R_\Gamma^3\,\varpi^{16}\,e_1\,u^2$$
$$-278640\,R_\Gamma^4\,\varpi^{14}\,e_1\,u^3 + 732240\,R_\Gamma^6\,\varpi^{14}\,e_1\,u$$
$$+213840\,R_\Gamma^5\,\varpi^{14}\,e_1\,u^2 - 2125440\,R_\Gamma^8\,\varpi^{12}\,e_1\,u$$
$$-1261440\,R_\Gamma^6\,\varpi^{12}\,e_1\,u^3 + 2540160\,R_\Gamma^7\,\varpi^{12}\,e_1\,u^2$$
$$+275400\,R_\Gamma^4\,\varpi^{16}\,e_1\,u + 86400\,R_\Gamma^6\,\varpi^{10}\,e_1\,u^5$$
$$+737280\,R_\Gamma^{10}\,\varpi^4\,e_2\,u^7 + 32400\,R_\Gamma^6\,\varpi^{14}\,e_2\,u$$
$$-1263600\,R_\Gamma^5\,\varpi^{14}\,e_2\,u^2 - 1728000\,R_\Gamma^6\,\varpi^{12}\,e_2\,u^3$$
$$+5160960\,R_\Gamma^{12}\,\varpi^4\,e_2\,u^5 + 2580480\,R_\Gamma^{15}\,\varpi^4\,e_2\,u^2$$
$$-1296000\,R_\Gamma^7\,\varpi^{12}\,e_2\,u^2 - 7257600\,R_\Gamma^{11}\,\varpi^6\,e_2\,u^4$$
$$+226800\,R_\Gamma^4\,\varpi^{14}\,e_2\,u^3 + 5160960\,R_\Gamma^{14}\,\varpi^4\,e_2\,u^3$$
$$+29160\,R_\Gamma^2\,\varpi^{18}\,e_2\,u + 45360\,R_\Gamma^3\,\varpi^{16}\,e_2\,u^2$$
$$+737280\,R_\Gamma^{16}\,\varpi^4\,e_2\,u - 249480\,R_\Gamma^4\,\varpi^{16}\,e_2\,u$$
$$+864000\,R_\Gamma^8\,\varpi^{10}\,e_1\,u^3 - 432000\,R_\Gamma^7\,\varpi^{10}\,e_1\,u^4$$
$$+432000\,R_\Gamma^{10}\,\varpi^{10}\,e_1\,u + 864000\,R_\Gamma^6\,\varpi^{10}\,e_2\,u^5$$
$$+3110400\,R_\Gamma^{11}\,\varpi^8\,e_2\,u^2 + 345600\,R_\Gamma^8\,\varpi^6\,e_2\,u^7$$
$$+518400\,R_\Gamma^8\,\varpi^8\,e_2\,u^5 + 691200\,R_\Gamma^7\,\varpi^8\,e_2\,u^6$$
$$-86400\,R_\Gamma^9\,\varpi^{10}\,e_2\,u^2 - 483840\,R_\Gamma^{10}\,\varpi^6\,e_2\,u^5$$
$$-3024000\,R_\Gamma^8\,\varpi^{10}\,e_2\,u^3 + 1123200\,R_\Gamma^{10}\,\varpi^{10}\,e_2\,u$$
$$+648000\,R_\Gamma^5\,\varpi^{12}\,e_2\,u^4 - 864000\,R_\Gamma^7\,\varpi^{10}\,e_2\,u^4$$
$$+6451200\,R_\Gamma^{13}\,\varpi^4\,e_2\,u^4 - 2937600\,R_\Gamma^9\,\varpi^8\,e_2\,u^4$$
$$+92160\,R_\Gamma^9\,\varpi^4\,e_2\,u^8 - 3110400\,R_\Gamma^{10}\,\varpi^8\,e_2\,u^3$$
$$+1128960\,R_\Gamma^9\,\varpi^6\,e_2\,u^6 + 191160\,R_\Gamma^5\,\varpi^{16}\,e_2$$
$$-191160\,R_\Gamma^5\,\varpi^{16}\,e_1 - 6480\,R_\Gamma^3\,\varpi^{18}\,e_1\Big)\times$$
$$2/15/R_\Gamma^{12}/\varpi^{20}, \tag{C.32}$$

$$
\begin{aligned}
U^{(5)} \quad = \quad & -\Big(2203200\, R_\Gamma^3\, \varpi^{14}\, e_1\, u^3 - 4665600\, R_\Gamma^5\, \varpi^{14}\, e_1\, u \\
& -2332800\, R_\Gamma^3\, \varpi^{16}\, e_1\, u + 194400\, R_\Gamma\, \varpi^{18}\, e_1\, u \\
& -486000\, R_\Gamma^2\, \varpi^{16}\, e_1\, u^2 + 0.139968{\cdot}10^8\, R_\Gamma^7\, \varpi^{12}\, e_1\, u \\
& -1555200\, R_\Gamma^4\, \varpi^{12}\, e_1\, u^4 + 8812800\, R_\Gamma^5\, \varpi^{12}\, e_1\, u^3 \\
& -0.171072{\cdot}10^8\, R_\Gamma^6\, \varpi^{12}\, e_1\, u^2 - 518400\, R_\Gamma^5\, \varpi^{10}\, e_1\, u^5 \\
& +2592000\, R_\Gamma^6\, \varpi^{10}\, e_1\, u^4 - 5184000\, R_\Gamma^7\, \varpi^{10}\, e_1\, u^3 \\
& +5184000\, R_\Gamma^8\, \varpi^{10}\, e_1\, u^2 - 2592000\, R_\Gamma^9\, \varpi^{10}\, e_1\, u \\
& -6220800\, R_\Gamma^8\, \varpi^{10}\, e_2\, u^2 - 5702400\, R_\Gamma^9\, \varpi^{10}\, e_2\, u \\
& +6220800\, R_\Gamma^6\, \varpi^{12}\, e_2\, u^2 + 0.171072{\cdot}10^8\, R_\Gamma^5\, \varpi^{12}\, e_2\, u^3 \\
& -5443200\, R_\Gamma^4\, \varpi^{12}\, e_2\, u^4 - 1658880\, R_\Gamma^8\, \varpi^4\, e_2\, u^8 \\
& +2073600\, R_\Gamma^{11}\, \varpi^8\, e_2\, u - 0.1327104{\cdot}10^8\, R_\Gamma^{11}\, \varpi^2\, e_2\, u^7 \\
& +0.4644864{\cdot}10^8\, R_\Gamma^{11}\, \varpi^4\, e_2\, u^5 + 0.20736{\cdot}10^8\, R_\Gamma^7\, \varpi^{10}\, e_2\, u^3 \\
& -7776000\, R_\Gamma^5\, \varpi^{10}\, e_2\, u^5 + 0.1296{\cdot}10^8\, R_\Gamma^6\, \varpi^{10}\, e_2\, u^4 \\
& -0.290304{\cdot}10^8\, R_\Gamma^{11}\, \varpi^6\, e_2\, u^3 - 0.870912{\cdot}10^8\, R_\Gamma^{12}\, \varpi^6\, e_2\, u^2 \\
& +0.1161216{\cdot}10^9\, R_\Gamma^{12}\, \varpi^4\, e_2\, u^4 - 0.3096576{\cdot}10^8\, R_\Gamma^{12}\, \varpi^2\, e_2\, u^6 \\
& -0.165888{\cdot}10^8\, R_\Gamma^{10}\, \varpi^8\, e_2\, u^2 - 3317760\, R_\Gamma^{10}\, \varpi^2\, e_2\, u^8 \\
& -4147200\, R_\Gamma^8\, \varpi^{12}\, e_1 - 777600\, R_\Gamma^8\, \varpi^{12}\, e_2 \\
& +518400\, R_\Gamma^{10}\, \varpi^{10}\, e_2 + 7603200\, R_\Gamma^{12}\, \varpi^8\, e_2 \\
& +4976640\, R_\Gamma^{16}\, \varpi^4\, e_2 + 1652400\, R_\Gamma^4\, \varpi^{16}\, e_1 \\
& +48600\, R_\Gamma^2\, \varpi^{18}\, e_1 + 4406400\, R_\Gamma^6\, \varpi^{14}\, e_1 \\
& +518400\, R_\Gamma^{10}\, \varpi^{10}\, e_1 + 6912000\, R_\Gamma^9\, \varpi^8\, e_2\, u^3 \\
& -368640\, R_\Gamma^9\, \varpi^2\, e_2\, u^9 + 0.108864{\cdot}10^8\, R_\Gamma^4\, \varpi^{14}\, e_2\, u^2 \\
& +0.331776{\cdot}10^8\, R_\Gamma^{15}\, \varpi^4\, e_2\, u - 0.3096576{\cdot}10^8\, R_\Gamma^{15}\, \varpi^2\, e_2\, u^3 \\
& -1652400\, R_\Gamma^4\, \varpi^{16}\, e_2 - 0.6386688{\cdot}10^8\, R_\Gamma^{13}\, \varpi^6\, e_2\, u \\
& -0.4644864{\cdot}10^8\, R_\Gamma^{13}\, \varpi^2\, e_2\, u^5 + 2138400\, R_\Gamma^3\, \varpi^{16}\, e_2\, u \\
& -194400\, R_\Gamma\, \varpi^{18}\, e_2\, u - 291600\, R_\Gamma^2\, \varpi^{16}\, e_2\, u^2 \\
& -3317760\, R_\Gamma^{17}\, \varpi^2\, e_2\, u + 0.1393459{\cdot}10^9\, R_\Gamma^{13}\, \varpi^4\, e_2\, u^3 \\
& -48600\, R_\Gamma^2\, \varpi^{18}\, e_2 - 1944000\, R_\Gamma^5\, \varpi^{14}\, e_2\, u \\
& -0.1327104{\cdot}10^8\, R_\Gamma^{16}\, \varpi^2\, e_2\, u^2 - 0.4644864{\cdot}10^8\, R_\Gamma^{14}\, \varpi^2\, e_2\, u^4 \\
& -4147200\, R_\Gamma^7\, \varpi^6\, e_2\, u^7 - 6912000\, R_\Gamma^6\, \varpi^8\, e_2\, u^6 \\
& -6635520\, R_\Gamma^9\, \varpi^4\, e_2\, u^7 + 0.9289728{\cdot}10^8\, R_\Gamma^{14}\, \varpi^4\, e_2\, u^2 \\
& -5806080\, R_\Gamma^8\, \varpi^6\, e_2\, u^6 - 368640\, R_\Gamma^{18}\, \varpi^2\, e_2 \\
& -0.1575936{\cdot}10^8\, R_\Gamma^{14}\, \varpi^6\, e_2 + 0.269568{\cdot}10^8\, R_\Gamma^8\, \varpi^8\, e_2\, u^4
\end{aligned}
$$

$$+2073600\,R_\Gamma^7\,\varpi^8\,e_2\,u^5 - 1814400\,R_\Gamma^3\,\varpi^{14}\,e_2\,u^3$$
$$+0.1741824{\cdot}10^8\,R_\Gamma^9\,\varpi^6\,e_2\,u^5 + 0.290304{\cdot}10^8\,R_\Gamma^{10}\,\varpi^6\,e_2\,u^4$$
$$-6220800\,R_\Gamma^7\,\varpi^{12}\,e_2\,u - 1944000\,R_\Gamma^4\,\varpi^{14}\,e_1\,u^2$$
$$-1684800\,R_\Gamma^6\,\varpi^{14}\,e_2\Big) \times 2/15/R_\Gamma^{12}/\varpi^{20}, \qquad\qquad \text{(C.33)}$$

$$U^{(6)} \;=\; -\Big(-0.1957478{\cdot}10^9\,e_2\,R_\Gamma^{16}\,\varpi^2\,u + 0.36288{\cdot}10^8\,\varpi^{10}\,R_\Gamma^6\,e_1\,u^3$$
$$+3628800\,\varpi^{10}\,R_\Gamma^4\,e_1\,u^5 + 0.1296{\cdot}10^8\,\varpi^{12}\,R_\Gamma^3\,e_1\,u^4$$
$$+0.132192{\cdot}10^9\,\varpi^{12}\,R_\Gamma^5\,e_1\,u^2 - 0.106272{\cdot}10^9\,\varpi^{12}\,R_\Gamma^6\,e_1\,u$$
$$-0.69984{\cdot}10^8\,\varpi^{12}\,R_\Gamma^4\,e_1\,u^3 - 0.36288{\cdot}10^8\,\varpi^{10}\,R_\Gamma^7\,e_1\,u^2$$
$$-0.18144{\cdot}10^8\,\varpi^{10}\,R_\Gamma^5\,e_1\,u^4 + 0.18144{\cdot}10^8\,\varpi^{10}\,R_\Gamma^8\,e_1\,u$$
$$-0.217728{\cdot}10^8\,\varpi^{12}\,e_2\,R_\Gamma^5\,u^2 + 0.1207665{\cdot}10^{10}\,e_2\,R_\Gamma^{13}\,\varpi^4\,u^2$$
$$+0.508032{\cdot}10^8\,\varpi^{12}\,e_2\,R_\Gamma^3\,u^4 - 0.290304{\cdot}10^8\,e_2\,R_\Gamma^{11}\,u^2\,\varpi^6$$
$$+0.870912{\cdot}10^8\,\varpi^{10}\,e_2\,R_\Gamma^7\,u^2 - 0.163296{\cdot}10^9\,\varpi^{10}\,e_2\,R_\Gamma^5\,u^4$$
$$+0.3096576{\cdot}10^9\,e_2\,R_\Gamma^{13}\,u^6 + 0.326592{\cdot}10^8\,\varpi^{10}\,e_2\,R_\Gamma^8\,u$$
$$+0.580608{\cdot}10^8\,\varpi^{12}\,e_2\,R_\Gamma^6\,u + 0.2322432{\cdot}10^9\,e_2\,R_\Gamma^{11}\,u^4\,\varpi^4$$
$$-0.1778112{\cdot}10^9\,\varpi^{12}\,e_2\,R_\Gamma^4\,u^3 - 0.1347011{\cdot}10^{10}\,e_2\,R_\Gamma^{13}\,\varpi^2\,u^4$$
$$-0.650281{\cdot}10^9\,e_2\,R_\Gamma^{15}\,\varpi^2\,u^2 + 0.6038323{\cdot}10^9\,e_2\,R_\Gamma^{14}\,\varpi^4\,u$$
$$-0.1207665{\cdot}10^{10}\,e_2\,R_\Gamma^{14}\,\varpi^2\,u^3 + 0.163296{\cdot}10^8\,\varpi^{14}\,e_2\,R_\Gamma^2\,u^3$$
$$+0.299376{\cdot}10^8\,\varpi^{14}\,e_2\,R_\Gamma^4\,u - 0.202176{\cdot}10^8\,\varpi^{16}\,e_2\,R_\Gamma^2\,u$$
$$+0.1354752{\cdot}10^8\,e_2\,R_\Gamma^7\,u^6\,\varpi^6 - 0.145152{\cdot}10^9\,e_2\,R_\Gamma^6\,\varpi^{10}\,u^3$$
$$-0.2786918{\cdot}10^9\,e_2\,R_\Gamma^{11}\,u^6\,\varpi^2 + 0.1327104{\cdot}10^8\,e_2\,R_\Gamma^{10}\,u^7\,\varpi^2$$
$$+0.1068319{\cdot}10^{10}\,e_2\,R_\Gamma^{12}\,\varpi^4\,u^3 + 0.3649536{\cdot}10^8\,e_2\,R_\Gamma^9\,u^8\,\varpi^2$$
$$+0.1016064{\cdot}10^9\,\varpi^8\,e_2\,R_\Gamma^9\,u^2 - 0.9289728{\cdot}10^8\,e_2\,R_\Gamma^9\,u^6\,\varpi^4$$
$$-0.1064448{\cdot}10^9\,e_2\,R_\Gamma^9\,u^4\,\varpi^6 - 0.145152{\cdot}10^8\,\varpi^8\,e_2\,R_\Gamma^{10}\,u$$
$$+7741440\,e_2\,R_\Gamma^8\,u^9\,\varpi^2 - 0.2322432{\cdot}10^9\,e_2\,R_\Gamma^{10}\,u^5\,\varpi^4$$
$$+0.1838592{\cdot}10^9\,e_2\,R_\Gamma^{10}\,u^3\,\varpi^6 - 0.1257984{\cdot}10^9\,e_2\,R_\Gamma^{13}\,\varpi^6$$
$$+0.157464{\cdot}10^8\,\varpi^{16}\,e_2\,R_\Gamma^3 + 3628800\,\varpi^{12}\,e_2\,R_\Gamma^7$$
$$+0.13608{\cdot}10^8\,\varpi^{14}\,e_2\,R_\Gamma^5 + 0.31104{\cdot}10^8\,\varpi^{12}\,R_\Gamma^7\,e_1$$
$$+0.1161216{\cdot}10^9\,e_2\,R_\Gamma^{15}\,\varpi^4 - 3628800\,\varpi^{10}\,e_2\,R_\Gamma^9$$
$$+0.147456{\cdot}10^8\,e_2\,R_\Gamma^{18}\,u - 388800\,\varpi^{18}\,R_\Gamma\,e_1$$
$$-1458000\,\varpi^{18}\,e_1\,u - 0.8825242{\cdot}10^9\,e_2\,R_\Gamma^{12}\,\varpi^2\,u^5$$
$$+1474560\,e_2\,R_\Gamma^9\,u^{10} + 1458000\,\varpi^{18}\,e_2\,u$$
$$-0.157464{\cdot}10^8\,\varpi^{16}\,e_1\,R_\Gamma^3 + 0.663552{\cdot}10^8\,e_2\,R_\Gamma^{17}\,u^2$$

$$+0.1769472 \cdot 10^9 \, e_2 \, R_\Gamma^{16} \, u^3 + 388800 \, \varpi^{18} \, R_\Gamma \, e_2$$
$$-0.2543616 \cdot 10^8 \, e_2 \, R_\Gamma^{17} \, \varpi^2 - 3628800 \, \varpi^{10} \, R_\Gamma^9 \, e_1$$
$$+0.3096576 \cdot 10^9 \, e_2 \, R_\Gamma^{15} \, u^4 + 0.147456 \cdot 10^8 \, e_2 \, R_\Gamma^{10} \, u^9$$
$$+0.3715891 \cdot 10^9 \, e_2 \, R_\Gamma^{14} \, u^5 + 3693600 \, \varpi^{16} \, e_1 \, R_\Gamma \, u^2$$
$$+0.217728 \cdot 10^8 \, \varpi^{16} \, e_1 \, R_\Gamma^2 \, u + 0.1944 \cdot 10^8 \, \varpi^{14} \, e_1 \, R_\Gamma^3 \, u^2$$
$$-0.1944 \cdot 10^8 \, \varpi^{14} \, e_1 \, R_\Gamma^2 \, u^3 + 0.33048 \cdot 10^8 \, \varpi^{14} \, e_1 \, R_\Gamma^4 \, u$$
$$+0.762048 \cdot 10^8 \, \varpi^{10} \, R_\Gamma^4 \, e_2 \, u^5 + 0.4644864 \cdot 10^8 \, e_2 \, R_\Gamma^8 \, u^7 \, \varpi^4$$
$$+0.48384 \cdot 10^8 \, e_2 \, R_\Gamma^6 \, \varpi^6 \, u^7 - 0.2032128 \cdot 10^9 \, e_2 \, R_\Gamma^8 \, u^5 \, \varpi^6$$
$$-0.72576 \cdot 10^8 \, \varpi^8 \, e_2 \, R_\Gamma^6 \, u^5 + 0.290304 \cdot 10^8 \, \varpi^8 \, e_2 \, R_\Gamma^8 \, u^3$$
$$-0.2322432 \cdot 10^9 \, \varpi^8 \, e_2 \, R_\Gamma^7 \, u^4 + 0.72576 \cdot 10^8 \, \varpi^8 \, e_2 \, R_\Gamma^5 \, u^6$$
$$+0.2322432 \cdot 10^8 \, e_2 \, R_\Gamma^7 \, u^8 \, \varpi^4 - 0.2767565 \cdot 10^9 \, e_2 \, R_\Gamma^{12} \, u \, \varpi^6$$
$$+1474560 \, e_2 \, R_\Gamma^{19} - 0.33048 \cdot 10^8 \, \varpi^{14} \, R_\Gamma^5 \, e_1$$
$$+2138400 \, \varpi^{16} \, e_2 \, R_\Gamma \, u^2 + 0.1769472 \cdot 10^9 \, e_2 \, R_\Gamma^{12} \, u^7$$
$$-0.1034208 \cdot 10^9 \, \varpi^{14} \, e_2 \, R_\Gamma^3 \, u^2 + 0.663552 \cdot 10^8 \, e_2 \, R_\Gamma^{11} \, u^8 \Big) \times$$
$$2/15/R_\Gamma^{12}/\varpi^{20}. \tag{C.34}$$

Finally, the expansion of $W(u, \lambda, q, p)$ is given by

$$
W \;=\; \varepsilon \left(\frac{6 - 6P + P^2}{P^2} \right) \times \left[W^{(0)}(u) + \frac{\lambda^1}{1!} W^{(1)}(u) + \right.
$$
$$
\left. + \cdots + \frac{\lambda^6}{6!} W^{(6)}(u) + O(\lambda^7) \right] + O(\varepsilon^2), \tag{C.35}
$$

with

$$
\begin{aligned}
W^{(0)} \;=\; -\Big(& 1080 \, R_\Gamma^8 \, \varpi^{12} \, e_2 \, u^3 + 810 \, R_\Gamma^7 \, \varpi^{14} \, e_2 \, u^2 \\
& +4320 \, R_\Gamma^{11} \, \varpi^{10} \, e_2 \, u^2 - 1080 \, R_\Gamma^{10} \, \varpi^{12} \, e_2 \, u \\
& +270 \, R_\Gamma^7 \, \varpi^{14} \, e_1 \, u^2 + 720 \, R_\Gamma^9 \, \varpi^{10} \, e_2 \, u^4 \\
& +2880 \, R_\Gamma^{12} \, \varpi^{10} \, e_2 \, u + 135 \, R_\Gamma^7 \, \varpi^{16} \, e_1 \\
& +270 \, R_\Gamma^6 \, \varpi^{16} \, e_2 \, u - 270 \, R_\Gamma^6 \, \varpi^{16} \, e_1 \, u \\
& +1080 \, R_\Gamma^9 \, \varpi^{12} \, e_2 \, u^2 - 540 \, R_\Gamma^8 \, \varpi^{14} \, e_1 \, u \\
& +2880 \, R_\Gamma^{10} \, \varpi^{10} \, e_2 \, u^3 + 720 \, R_\Gamma^{13} \, \varpi^{10} \, e_2 \\
& -1080 \, R_\Gamma^{11} \, \varpi^{12} \, e_2 - 135 \, R_\Gamma^7 \, \varpi^{16} \, e_2 \\
& -270 \, R_\Gamma^9 \, \varpi^{14} \, e_2 + 270 \, R_\Gamma^9 \, \varpi^{14} \, e_1 \Big) \\
& /\varpi^{18}/R_\Gamma^{12}/15, \tag{C.36}
\end{aligned}
$$

$$
\begin{aligned}
W^{(1)} \;=\; \Big(&-27\,R_\Gamma^6\,\varpi^{16}\,e_1 + 48\,R_\Gamma^8\,\varpi^{10}\,e_2\,u^4 \\
&-288\,R_\Gamma^9\,\varpi^{12}\,e_2\,u + 288\,R_\Gamma^{10}\,\varpi^{10}\,e_2\,u^2 \\
&-144\,R_\Gamma^8\,\varpi^{12}\,e_2\,u^2 - 18\,R_\Gamma^6\,\varpi^{14}\,e_2\,u^2 \\
&-36\,R_\Gamma^7\,\varpi^{14}\,e_2\,u + 192\,R_\Gamma^{11}\,\varpi^{10}\,e_2\,u \\
&+192\,R_\Gamma^9\,\varpi^{10}\,e_2\,u^3 + 90\,R_\Gamma^6\,\varpi^{14}\,e_1\,u^2 \\
&+144\,R_\Gamma^7\,\varpi^{14}\,e_1\,u - 18\,R_\Gamma^5\,\varpi^{16}\,e_1\,u \\
&-216\,R_\Gamma^7\,\varpi^{12}\,e_1\,u^3 - 216\,R_\Gamma^8\,\varpi^{12}\,e_1\,u^2 \\
&+1920\,R_\Gamma^{12}\,\varpi^8\,e_1\,u^2 - 192\,R_\Gamma^9\,\varpi^8\,e_1\,u^5 \\
&+1728\,R_\Gamma^{11}\,\varpi^{10}\,e_1\,u + 18\,R_\Gamma^5\,\varpi^{16}\,e_2\,u \\
&+288\,R_\Gamma^8\,\varpi^{10}\,e_1\,u^4 + 960\,R_\Gamma^{10}\,\varpi^8\,e_1\,u^4 \\
&-960\,R_\Gamma^{13}\,\varpi^8\,e_1\,u + 360\,R_\Gamma^9\,\varpi^{12}\,e_1\,u \\
&-1920\,R_\Gamma^{11}\,\varpi^8\,e_1\,u^3 - 192\,R_\Gamma^9\,\varpi^{10}\,e_1\,u^3 \\
&-1152\,R_\Gamma^{10}\,\varpi^{10}\,e_1\,u^2 + 192\,R_\Gamma^{14}\,\varpi^8\,e_1 \\
&+72\,R_\Gamma^{10}\,\varpi^{12}\,e_1 + 48\,R_\Gamma^{12}\,\varpi^{10}\,e_2 \\
&-18\,R_\Gamma^8\,\varpi^{14}\,e_1 + 27\,R_\Gamma^6\,\varpi^{16}\,e_2 \\
&-672\,R_\Gamma^{12}\,\varpi^{10}\,e_1 + 18\,R_\Gamma^8\,\varpi^{14}\,e_2 \\
&-144\,R_\Gamma^{10}\,\varpi^{12}\,e_2\Big)/\varpi^{18}/R_\Gamma^{12}, \qquad\qquad \text{(C.37)}
\end{aligned}
$$

$$
\begin{aligned}
W^{(2)} \;=\; \Big(&-144\,R_\Gamma^9\,\varpi^{12}\,e_1 + 36\,R_\Gamma^7\,\varpi^{14}\,e_1 \\
&-1920\,R_\Gamma^{11}\,\varpi^8\,e_2\,u^2 + 1344\,R_\Gamma^{10}\,\varpi^{10}\,e_2\,u \\
&+576\,R_\Gamma^9\,\varpi^{10}\,e_2\,u^2 + 720\,R_\Gamma^7\,\varpi^{12}\,e_2\,u^2 \\
&-144\,R_\Gamma^6\,\varpi^{12}\,e_2\,u^3 - 36\,R_\Gamma^4\,\varpi^{16}\,e_2\,u \\
&-192\,R_\Gamma^8\,\varpi^8\,e_2\,u^5 + 288\,R_\Gamma^6\,\varpi^{14}\,e_2\,u \\
&-960\,R_\Gamma^{12}\,\varpi^8\,e_2\,u + 36\,R_\Gamma^5\,\varpi^{14}\,e_2\,u^2 \\
&+1152\,R_\Gamma^8\,\varpi^{12}\,e_2\,u - 1920\,R_\Gamma^{10}\,\varpi^8\,e_2\,u^3 \\
&+54\,R_\Gamma^5\,\varpi^{16}\,e_1 + 3456\,R_\Gamma^9\,\varpi^{10}\,e_1\,u^2 \\
&+5760\,R_\Gamma^{10}\,\varpi^8\,e_1\,u^3 + 576\,R_\Gamma^8\,\varpi^{10}\,e_1\,u^3 \\
&+36\,R_\Gamma^4\,\varpi^{16}\,e_1\,u - 2880\,R_\Gamma^9\,\varpi^8\,e_1\,u^4 \\
&-864\,R_\Gamma^7\,\varpi^{10}\,e_1\,u^4 - 504\,R_\Gamma^6\,\varpi^{14}\,e_1\,u \\
&-5184\,R_\Gamma^{10}\,\varpi^{10}\,e_1\,u + 576\,R_\Gamma^6\,\varpi^{12}\,e_1\,u^3 \\
&+2880\,R_\Gamma^{12}\,\varpi^8\,e_1\,u - 5760\,R_\Gamma^{11}\,\varpi^8\,e_1\,u^2 \\
&-180\,R_\Gamma^5\,\varpi^{14}\,e_1\,u^2 + 864\,R_\Gamma^7\,\varpi^{12}\,e_1\,u^2 \\
&-1296\,R_\Gamma^8\,\varpi^{12}\,e_1\,u - 384\,R_\Gamma^7\,\varpi^{10}\,e_2\,u^4
\end{aligned}
$$

$$+576\,R_\Gamma^8\,\varpi^8\,e_1\,u^5 - 960\,R_\Gamma^9\,\varpi^8\,e_2\,u^4$$
$$-576\,R_\Gamma^8\,\varpi^{10}\,e_2\,u^3 - 192\,R_\Gamma^{13}\,\varpi^8\,e_2$$
$$+288\,R_\Gamma^9\,\varpi^{12}\,e_2 + 576\,R_\Gamma^{11}\,\varpi^{10}\,e_2$$
$$+2016\,R_\Gamma^{11}\,\varpi^{10}\,e_1 - 576\,R_\Gamma^{13}\,\varpi^8\,e_1$$
$$-36\,R_\Gamma^7\,\varpi^{14}\,e_2 - 54\,R_\Gamma^5\,\varpi^{16}\,e_2\Big)/\varpi^{18}/R_\Gamma^{12}, \tag{C.38}$$

$$
\begin{aligned}
W^{(3)} &= \Big(-7776\,R_\Gamma^{10}\,\varpi^{10}\,e_1 - 288\,R_\Gamma^8\,\varpi^{12}\,e_2\\
&\quad -324\,R_\Gamma^6\,\varpi^{14}\,e_1 + 11520\,R_\Gamma^8\,\varpi^8\,e_1\,u^4\\
&\quad -2448\,R_\Gamma^5\,\varpi^{12}\,e_1\,u^3 + 6480\,R_\Gamma^7\,\varpi^{12}\,e_1\,u\\
&\quad -2304\,R_\Gamma^7\,\varpi^8\,e_1\,u^5 - 23040\,R_\Gamma^9\,\varpi^8\,e_1\,u^3\\
&\quad -108\,R_\Gamma^3\,\varpi^{16}\,e_1\,u + 2592\,R_\Gamma^5\,\varpi^{14}\,e_1\,u\\
&\quad +540\,R_\Gamma^4\,\varpi^{14}\,e_1\,u^2 - 11520\,R_\Gamma^{11}\,\varpi^8\,e_1\,u\\
&\quad +3744\,R_\Gamma^6\,\varpi^{10}\,e_1\,u^4 + 19584\,R_\Gamma^9\,\varpi^{10}\,e_1\,u\\
&\quad -3456\,R_\Gamma^7\,\varpi^{10}\,e_1\,u^3 - 3888\,R_\Gamma^6\,\varpi^{12}\,e_1\,u^2\\
&\quad +1152\,R_\Gamma^5\,\varpi^{12}\,e_2\,u^3 + 2880\,R_\Gamma^6\,\varpi^{10}\,e_2\,u^4\\
&\quad -5184\,R_\Gamma^6\,\varpi^{12}\,e_2\,u^2 - 8640\,R_\Gamma^8\,\varpi^{10}\,e_2\,u^2\\
&\quad +11520\,R_\Gamma^{12}\,\varpi^6\,e_2\,u^2 + 2304\,R_\Gamma^7\,\varpi^8\,e_2\,u^5\\
&\quad -12096\,R_\Gamma^8\,\varpi^{10}\,e_1\,u^2 + 324\,R_\Gamma^6\,\varpi^{14}\,e_2\\
&\quad -144\,R_\Gamma^8\,\varpi^{12}\,e_1 + 162\,R_\Gamma^4\,\varpi^{16}\,e_2\\
&\quad +5760\,R_\Gamma^8\,\varpi^8\,e_2\,u^4 + 11520\,R_\Gamma^{10}\,\varpi^6\,e_2\,u^4\\
&\quad -11520\,R_\Gamma^{11}\,\varpi^8\,e_2\,u - 11520\,R_\Gamma^{10}\,\varpi^8\,e_2\,u^2\\
&\quad +768\,R_\Gamma^8\,\varpi^6\,e_2\,u^6 - 5760\,R_\Gamma^9\,\varpi^{10}\,e_2\,u\\
&\quad -1944\,R_\Gamma^5\,\varpi^{14}\,e_2\,u - 108\,R_\Gamma^4\,\varpi^{14}\,e_2\,u^2\\
&\quad +4608\,R_\Gamma^9\,\varpi^6\,e_2\,u^5 + 15360\,R_\Gamma^{11}\,\varpi^6\,e_2\,u^3\\
&\quad +23040\,R_\Gamma^{10}\,\varpi^8\,e_1\,u^2 - 5184\,R_\Gamma^7\,\varpi^{12}\,e_2\,u\\
&\quad +4608\,R_\Gamma^{13}\,\varpi^6\,e_2\,u + 108\,R_\Gamma^3\,\varpi^{16}\,e_2\,u\\
&\quad +768\,R_\Gamma^{14}\,\varpi^6\,e_2 + 2304\,R_\Gamma^{12}\,\varpi^8\,e_1\\
&\quad -3456\,R_\Gamma^{12}\,\varpi^8\,e_2 - 162\,R_\Gamma^4\,\varpi^{16}\,e_1\Big)/\varpi^{18}/R_\Gamma^{12}, \tag{C.39}
\end{aligned}
$$

$$
\begin{aligned}
W^{(4)} &= \Big(-3168\,R_\Gamma^7\,\varpi^{12}\,e_2 - 3072\,R_\Gamma^{15}\,\varpi^4\,e_2\\
&\quad -648\,R_\Gamma^3\,\varpi^{16}\,e_2 - 432\,R_\Gamma^2\,\varpi^{16}\,e_2\,u\\
&\quad -16848\,R_\Gamma^4\,\varpi^{14}\,e_1\,u - 23040\,R_\Gamma^7\,\varpi^8\,e_2\,u^4\\
&\quad +14256\,R_\Gamma^4\,\varpi^{14}\,e_2\,u - 8928\,R_\Gamma^4\,\varpi^{12}\,e_2\,u^3
\end{aligned}
$$

$$-64512\, R_\Gamma^{13}\, \varpi^4\, e_2\, u^2 - 23040\, R_\Gamma^6\, \varpi^8\, e_2\, u^5$$

$$-107520\, R_\Gamma^{12}\, \varpi^4\, e_2\, u^3 + 87552\, R_\Gamma^{12}\, \varpi^6\, e_2\, u$$

$$+42336\, R_\Gamma^5\, \varpi^{12}\, e_2\, u^2 + 69120\, R_\Gamma^7\, \varpi^{10}\, e_2\, u^2$$

$$-107520\, R_\Gamma^{11}\, \varpi^4\, e_2\, u^4 - 5760\, R_\Gamma^9\, \varpi^{10}\, e_2$$

$$+138240\, R_\Gamma^{11}\, \varpi^6\, e_2\, u^2 + 4896\, R_\Gamma^7\, \varpi^{12}\, e_1$$

$$+25056\, R_\Gamma^6\, \varpi^{12}\, e_2\, u - 21504\, R_\Gamma^{14}\, \varpi^4\, e_2\, u$$

$$+432\, R_\Gamma^3\, \varpi^{14}\, e_2\, u^2 + 17280\, R_\Gamma^8\, \varpi^{10}\, e_2\, u$$

$$+648\, R_\Gamma^3\, \varpi^{16}\, e_1 - 11520\, R_\Gamma^{11}\, \varpi^8\, e_2$$

$$+19968\, R_\Gamma^{13}\, \varpi^6\, e_2 - 3456\, R_\Gamma^5\, \varpi^{14}\, e_2$$

$$-23040\, R_\Gamma^5\, \varpi^{10}\, e_2\, u^4 - 12288\, R_\Gamma^7\, \varpi^6\, e_2\, u^6$$

$$-21504\, R_\Gamma^9\, \varpi^4\, e_2\, u^6 + 11520\, R_\Gamma^{10}\, \varpi^8\, e_2\, u$$

$$-64512\, R_\Gamma^{10}\, \varpi^4\, e_2\, u^5 + 76800\, R_\Gamma^{10}\, \varpi^6\, e_2\, u^3$$

$$+23040\, R_\Gamma^6\, \varpi^{10}\, e_2\, u^3 + 57600\, R_\Gamma^8\, \varpi^8\, e_2\, u^3$$

$$-23040\, R_\Gamma^9\, \varpi^6\, e_2\, u^4 + 80640\, R_\Gamma^9\, \varpi^8\, e_2\, u^2$$

$$+57600\, R_\Gamma^{10}\, \varpi^8\, e_1\, u - 57600\, R_\Gamma^7\, \varpi^8\, e_1\, u^4$$

$$+25344\, R_\Gamma^6\, \varpi^{10}\, e_1\, u^3 - 41472\, R_\Gamma^8\, \varpi^6\, e_2\, u^5$$

$$-3072\, R_\Gamma^8\, \varpi^4\, e_2\, u^7 + 36864\, R_\Gamma^9\, \varpi^{10}\, e_1$$

$$-11520\, R_\Gamma^{11}\, \varpi^8\, e_1 + 3456\, R_\Gamma^5\, \varpi^{14}\, e_1$$

$$-20736\, R_\Gamma^5\, \varpi^{10}\, e_1\, u^4 - 89856\, R_\Gamma^8\, \varpi^{10}\, e_1\, u$$

$$+432\, R_\Gamma^2\, \varpi^{16}\, e_1\, u - 2160\, R_\Gamma^3\, \varpi^{14}\, e_1\, u^2$$

$$+48384\, R_\Gamma^7\, \varpi^{10}\, e_1\, u^2 - 38880\, R_\Gamma^6\, \varpi^{12}\, e_1\, u$$

$$+14112\, R_\Gamma^4\, \varpi^{12}\, e_1\, u^3 + 19872\, R_\Gamma^5\, \varpi^{12}\, e_1\, u^2$$

$$+11520\, R_\Gamma^6\, \varpi^8\, e_1\, u^5 - 115200\, R_\Gamma^9\, \varpi^8\, e_1\, u^2$$

$$+115200\, R_\Gamma^8\, \varpi^8\, e_1\, u^3\Big)/\varpi^{18}/R_\Gamma^{12}, \tag{C.40}$$

$$W^{(5)} = \Big(345600\, R_\Gamma^6\, \varpi^8\, e_1\, u^4 + 10800\, R_\Gamma^2\, \varpi^{14}\, e_1\, u^2$$

$$-2160\, R_\Gamma\, \varpi^{16}\, e_1\, u + 276480\, R_\Gamma^{11}\, \varpi^6\, e_2\, u$$

$$+688128\, R_\Gamma^{11}\, \varpi^2\, e_2\, u^5 - 1290240\, R_\Gamma^{11}\, \varpi^4\, e_2\, u^3$$

$$-1290240\, R_\Gamma^{12}\, \varpi^4\, e_2\, u^2 - 100800\, R_\Gamma^3\, \varpi^{12}\, e_1\, u^3$$

$$+860160\, R_\Gamma^{12}\, \varpi^2\, e_2\, u^4 - 345600\, R_\Gamma^5\, \varpi^{10}\, e_2\, u^3$$

$$+267840\, R_\Gamma^5\, \varpi^{12}\, e_1\, u - 69120\, R_\Gamma^5\, \varpi^8\, e_1\, u^5$$

$$-380160\, R_\Gamma^4\, \varpi^{12}\, e_2\, u^2 + 688128\, R_\Gamma^{13}\, \varpi^2\, e_2\, u^3$$

$$-430080\, R_\Gamma^{10}\, \varpi^4\, e_2\, u^4 + 344064\, R_\Gamma^{10}\, \varpi^2\, e_2\, u^6$$

$$-276480\,R_\Gamma^{10}\,\varpi^6\,e_2\,u^2 - 798720\,R_\Gamma^9\,\varpi^6\,e_2\,u^3$$

$$+92160\,R_\Gamma^9\,\varpi^8\,e_2\,u + 258048\,R_\Gamma^8\,\varpi^4\,e_2\,u^6$$

$$-276480\,R_\Gamma^8\,\varpi^6\,e_2\,u^4 - 691200\,R_\Gamma^7\,\varpi^8\,e_2\,u^3$$

$$+230400\,R_\Gamma^5\,\varpi^8\,e_2\,u^5 + 201600\,R_\Gamma^4\,\varpi^{10}\,e_2\,u^4$$

$$+12288\,R_\Gamma^8\,\varpi^2\,e_2\,u^8 - 518400\,R_\Gamma^6\,\varpi^{10}\,e_2\,u^2$$

$$-414720\,R_\Gamma^8\,\varpi^8\,e_2\,u^2 + 61440\,R_\Gamma^7\,\varpi^4\,e_2\,u^7$$

$$+98304\,R_\Gamma^9\,\varpi^2\,e_2\,u^7 + 258048\,R_\Gamma^9\,\varpi^4\,e_2\,u^5$$

$$-120960\,R_\Gamma^5\,\varpi^{12}\,e_2\,u + 2160\,R_\Gamma\,\varpi^{16}\,e_2\,u$$

$$+74880\,R_\Gamma^3\,\varpi^{12}\,e_2\,u^3 - 116640\,R_\Gamma^3\,\varpi^{14}\,e_2\,u$$

$$+344064\,R_\Gamma^{14}\,\varpi^2\,e_2\,u^2 + 98304\,R_\Gamma^{15}\,\varpi^2\,e_2\,u$$

$$-2160\,R_\Gamma^2\,\varpi^{14}\,e_2\,u^2 - 602112\,R_\Gamma^{13}\,\varpi^4\,e_2\,u$$

$$-110592\,R_\Gamma^{14}\,\varpi^4\,e_2 - 54720\,R_\Gamma^6\,\varpi^{12}\,e_1$$

$$+3240\,R_\Gamma^2\,\varpi^{16}\,e_2 + 51840\,R_\Gamma^8\,\varpi^{10}\,e_2$$

$$+12288\,R_\Gamma^{16}\,\varpi^2\,e_2 + 69120\,R_\Gamma^{10}\,\varpi^8\,e_1$$

$$+46080\,R_\Gamma^6\,\varpi^{12}\,e_2 - 36720\,R_\Gamma^4\,\varpi^{14}\,e_1$$

$$-207360\,R_\Gamma^8\,\varpi^{10}\,e_1 + 36720\,R_\Gamma^4\,\varpi^{14}\,e_2$$

$$-3240\,R_\Gamma^2\,\varpi^{16}\,e_1 + 153600\,R_\Gamma^{12}\,\varpi^6\,e_2$$

$$+46080\,R_\Gamma^{10}\,\varpi^8\,e_2 - 345600\,R_\Gamma^9\,\varpi^8\,e_1\,u$$

$$-207360\,R_\Gamma^6\,\varpi^{10}\,e_1\,u^2 - 691200\,R_\Gamma^7\,\varpi^8\,e_1\,u^3$$

$$+483840\,R_\Gamma^7\,\varpi^{10}\,e_1\,u + 691200\,R_\Gamma^8\,\varpi^8\,e_1\,u^2$$

$$-112320\,R_\Gamma^4\,\varpi^{12}\,e_1\,u^2 + 129600\,R_\Gamma^3\,\varpi^{14}\,e_1\,u$$

$$+276480\,R_\Gamma^7\,\varpi^6\,e_2\,u^5 + 153600\,R_\Gamma^6\,\varpi^6\,e_2\,u^6$$

$$+138240\,R_\Gamma^4\,\varpi^{10}\,e_1\,u^4 - 207360\,R_\Gamma^5\,\varpi^{10}\,e_1\,u^3\Big)$$

$$/\varpi^{18}/R_\Gamma^{12}, \tag{C.41}$$

$$W^{(6)} = \Big(-12960\,\varpi^{16}\,e_2\,u + 5253120\,e_2\,R_\Gamma^7\,u^4\,\varpi^6$$

$$+1728000\,\varpi^8\,R_\Gamma^5\,e_2\,u^4 + 1658880\,\varpi^8\,R_\Gamma^7\,e_2\,u^2$$

$$-2322432\,e_2\,R_\Gamma^7\,u^6\,\varpi^4 - 1843200\,\varpi^6\,e_2\,R_\Gamma^5\,u^6$$

$$-829440\,\varpi^{10}\,R_\Gamma^6\,e_2\,u + 3939840\,\varpi^{10}\,R_\Gamma^5\,e_2\,u^2$$

$$+774144\,e_2\,R_\Gamma^8\,u^5\,\varpi^4 - 921600\,e_2\,R_\Gamma^6\,u^7\,\varpi^4$$

$$+5713920\,e_2\,R_\Gamma^8\,u^3\,\varpi^6 - 49152\,e_2\,R_\Gamma^{17}$$

$$-2419200\,\varpi^8\,R_\Gamma^4\,e_2\,u^5 - 1474560\,e_2\,R_\Gamma^8\,\varpi^2\,u^7$$

$$+6451200\,e_2\,R_\Gamma^9\,u^4\,\varpi^4 - 552960\,e_2\,R_\Gamma^9\,u^2\,\varpi^6$$

$$-1382400\, e_2\, R_\Gamma^{10}\, u\, \varpi^6 - 1935360\, \varpi^{10}\, R_\Gamma^3\, e_2\, u^4$$

$$-2064384\, e_2\, R_\Gamma^9\, \varpi^2\, u^6 + 4354560\, \varpi^{10}\, R_\Gamma^4\, e_2\, u^3$$

$$+2064384\, e_2\, R_\Gamma^{10}\, \varpi^2\, u^5 + 3870720\, e_2\, R_\Gamma^{10}\, u^3\, \varpi^4$$

$$+19440\, \varpi^{16}\, R_\Gamma\, e_1 - 414720\, \varpi^{10}\, R_\Gamma^7\, e_2$$

$$+401760\, \varpi^{14}\, R_\Gamma^3\, e_1 + 12960\, \varpi^{16}\, e_1\, u$$

$$-442368\, e_2\, R_\Gamma^{16}\, u + 3732480\, \varpi^{12}\, R_\Gamma^3\, e_2\, u^2$$

$$+466560\, \varpi^{12}\, R_\Gamma^4\, e_2\, u - 691200\, \varpi^{12}\, R_\Gamma^2\, e_2\, u^3$$

$$+3833856\, e_2\, R_\Gamma^{14}\, \varpi^2\, u + 0.1032192{\cdot}10^8\, e_2\, R_\Gamma^{11}\, \varpi^2\, u^4$$

$$-3870720\, e_2\, R_\Gamma^{11}\, \varpi^4\, u^2 + 0.1445069{\cdot}10^8\, e_2\, R_\Gamma^{12}\, \varpi^2\, u^3$$

$$+12960\, \varpi^{14}\, e_2\, R_\Gamma\, u^2 + 1062720\, \varpi^{14}\, R_\Gamma^2\, e_2\, u$$

$$-2419200\, \varpi^8\, R_\Gamma^5\, e_1\, u^4 - 64800\, \varpi^{14}\, e_1\, R_\Gamma\, u^2$$

$$-1140480\, \varpi^{14}\, R_\Gamma^2\, e_1\, u + 2419200\, \varpi^8\, R_\Gamma^8\, e_1\, u$$

$$+673920\, \varpi^{12}\, R_\Gamma^3\, e_1\, u^2 + 829440\, \varpi^{10}\, R_\Gamma^5\, e_1\, u^2$$

$$+1866240\, \varpi^{10}\, R_\Gamma^4\, e_1\, u^3 - 2073600\, \varpi^{12}\, R_\Gamma^4\, e_1\, u$$

$$-2972160\, \varpi^{10}\, R_\Gamma^6\, e_1\, u - 1071360\, \varpi^{10}\, R_\Gamma^3\, e_1\, u^4$$

$$+4838400\, \varpi^8\, R_\Gamma^6\, e_1\, u^3 + 483840\, \varpi^8\, R_\Gamma^4\, e_1\, u^5$$

$$-4838400\, \varpi^8\, R_\Gamma^7\, e_1\, u^2 + 846720\, \varpi^{12}\, R_\Gamma^2\, e_1\, u^3$$

$$-4902912\, e_2\, R_\Gamma^{12}\, \varpi^4\, u + 0.1032192{\cdot}10^8\, e_2\, R_\Gamma^{13}\, \varpi^2\, u^2$$

$$+6912000\, \varpi^8\, R_\Gamma^6\, e_2\, u^3 - 1313280\, \varpi^8\, R_\Gamma^8\, e_2\, u$$

$$-294912\, e_2\, R_\Gamma^7\, u^8\, \varpi^2 - 1382400\, e_2\, R_\Gamma^6\, u^5\, \varpi^6$$

$$-401760\, \varpi^{14}\, R_\Gamma^3\, e_2 - 483840\, \varpi^8\, R_\Gamma^9\, e_1$$

$$-1769472\, e_2\, R_\Gamma^{15}\, u^2 - 49152\, e_2\, R_\Gamma^8\, u^9$$

$$-4128768\, e_2\, R_\Gamma^{11}\, u^6 - 6193152\, e_2\, R_\Gamma^{12}\, u^5$$

$$-4128768\, e_2\, R_\Gamma^{14}\, u^3 + 92160\, e_2\, R_\Gamma^{11}\, \varpi^6$$

$$-1437696\, e_2\, R_\Gamma^{13}\, \varpi^4 - 6193152\, e_2\, R_\Gamma^{13}\, u^4$$

$$-501120\, \varpi^{12}\, R_\Gamma^5\, e_2 + 1347840\, \varpi^{10}\, R_\Gamma^7\, e_1$$

$$-442368\, e_2\, R_\Gamma^9\, u^8 + 589824\, e_2\, R_\Gamma^{15}\, \varpi^2$$

$$-1769472\, e_2\, R_\Gamma^{10}\, u^7 + 552960\, \varpi^{12}\, R_\Gamma^5\, e_1$$

$$-19440\, \varpi^{16}\, R_\Gamma\, e_2 - 207360\, \varpi^8\, R_\Gamma^9\, e_2 \Big)$$

$$/\varpi^{18}/R_\Gamma^{12}. \tag{C.42}$$

The symbols e_1 and e_2 are defined in Eqs. (A.1) - (A.2). The function β is independent of λ and is already given in Section 5.3.2.

Evaluated at the extraction world-tube, the expressions for the Bondi

metric and its λ-derivative were identical to what was obtained in Section 5.3.2, using the algebraic procedure of the extraction module. This is quite reassuring since the two sets of results were obtained in entirely different ways.

BIBLIOGRAPHY

[1] H. Bondi, F. Sachs., M. G. J. van der Burg, and A. W. K. Metzner, Proc. R. Soc. **A269**, 21 (1962).

[2] R. Arnowitt, S. Deser, and C. W. Misner, in *Gravitation: An Introduction to Current Research*, edited by L. Witten (John Wiley, New York, 1962), pp. 227–265.

[3] J. York, in *Sources of Gravitational Radiation*, edited by L. Smarr (Cambridge University Press, Cambridge, England, 1979).

[4] N. Bishop, R. Gómez, P. Holvorcem, R. Matzner, P. Papadopoulos, and J. Winicour, J. Comp. Phys. **136**, 140 (1997).

[5] R. Gómez, R. Marsa, and J. Winicour, Phys. Rev. D **56**, 6310 (1997), gr-qc/9708002.

[6] C. Misner, Technical report, Wright Air Development Center, (unpublished), quote is borrowed from the talk of L.Smarr, ITP/UCSB Miniprogram on "Colliding Black Holes: Mathematical Issues in Numerical Relativity", Jan 10, 2000.

[7] D. Christodoulou, Commun. Math. Phys. **105**, 337 (1986).

[8] D. Christodoulou, Commun. Math. Phys. **106**, 587 (1986).

[9] D. Christodoulou, Commun. Math. Phys. **109**, 591 (1987).

[10] D. Christodoulou, Commun. Math. Phys. **109**, 613 (1987).

[11] M. Choptuik, in *Approaches to Numerical Relativity*, edited by R. D'Inverno (Cambridge University Press, Cambridge, England, 1992), p. 202.

[12] M. Choptuik, Phys. Rev. Lett. **70**, 9 (1993).

[13] S. L. Shapiro and S. A. Teukolsky, Phys. Rev. D **45**, 2739 (1992).

[14] P. Anninos, D. Hobill, E. Seidel, L. Smarr, and W.-M. Suen, Phys. Rev. Lett. **71**, 2851 (1993).

[15] S. Hughes, C. R. Keeton II, P. Walker, K. Walsh, S. L. Shapiro, and S. A. Teukolsky, Phys. Rev. D **49**, 4004 (1994).

[16] A. M. Abrahams, G. B. Cook, S. L. Shapiro, and S. A. Teukolsky, Phys. Rev. D **49**, 5153 (1994).

[17] P. Anninos, G. Daues, J. Massó, E. Seidel, and W.-M. Suen, in *The Seventh Marcel Grossmann Meeting: On Recent Developments in Theoretical and Experimental General Relativity, Gravitation, and Relativistic Field Theories*, edited by R. T. Jantzen, G. M. Keiser, and R. Ruffini (World Scientific, Singapore, 1996), p. 637.

[18] J. Libson, J. Massó, E. Seidel, W.-M. Suen, and P. Walker, Phys. Rev. D **53**, 4335 (1996).

[19] T. Damour, P. Jaranowski, and G. Schäfer, gr-qc/9912092, Submitted to Phys. Rev. D.

[20] T. Damour, B. R. Iyer, and B. S. Sathyaprakash, gr-qc/0001023.

[21] R. M. Wald, *General Relativity* (The University of Chicago Press, Chicago, 1984).

[22] Y. Choquet-Bruhat, in *Gravitation: An Introduction to Current Research*, edited by L. Witten (John Wiley, New York, 1962).

[23] R. Sachs, J. Math. Phys. **3**, 908 (1962).

[24] J. Winicour, Living Reviews in Relativity **1**, (1998).

[25] L. Lehner, Ph.D. thesis, University of Pittsburgh, 1998.

[26] A. Abrahams, A. Anderson, Y. Choquet-Bruhat, and J. York, Phys. Rev. Lett. **75**, 3377 (1995).

[27] A. Abrahams, A. Anderson, Y. Choquet-Bruhat, and J. York, Class. Quant. Grav. A9 (1997).

[28] C. Bona and J. Massó, Phys. Rev. Lett. **68**, 1097 (1992).

[29] Y. Choquet-Bruhat and T. Ruggeri, Comm. Math. Phys **89**, 269 (1983).

[30] H. Friedrich, Comm. Math. Phys. **100**, 525 (1985).

[31] S. Frittelli and O. Reula, Phys. Rev. Lett. **76**, 4667 (1996).

[32] M. S. Iriondo, E. O. Leguizamón, and O. A. Reula, Adv. Theor. Math. Phys. 2 1075 (1998).

[33] D. Christodoulou and S. Klainerman, *The global nonlinear stability of the Minkowski space* (Princeton University Press, Princeton, Princeton, 1993).

[34] A. D. Rendall, Commun. Math. Phys. **163**, 89 (1995).

[35] Y. Choquet-Bruhat and J. York, C. R. Acad. Sc. Paris **321**, 1089 (1995).

[36] M. Shibata and T. Nakamura, Phys. Rev. D **52**, 5428 (1995).

[37] T. W. Baumgarte and S. L. Shapiro, Physical Review D **59**, 024007 (1999).

[38] M. Alcubierre, B. Brügmann, M. Miller, and W.-M. Suen, Phys. Rev. D **60**, 064017 (1999), gr-qc/9903030.

[39] S. Frittelli and O. Reula, J. Math. Phys. **40**, 5143-5156 (1999), gr-qc/9904048

[40] H. Friedrich and A. Rendall, in *Einstein's Equations and Their Physical Implications* edited by B. Schmidt, (Springer, New York, 2000).

[41] H. Friedrich, Proc. Roy. Soc. London **A 375**, 169 (1981).

[42] H. Friedrich, Proc. Roy. Soc. London **A 378**, 401 (1981).

[43] P. Hübner, Phys. Rev. D **53**, 701 (1996).

[44] P. Hübner, gr-qc/9804065 (1998).

[45] N. Bishop, Class. Quant. Grav. **10**, 333 (1993).

[46] N. Bishop, R. Gómez, L. Lehner, and J. Winicour, Phys. Rev. D **54**, 6153 (1996).

[47] N. Bishop, R. Isaacson, R. Gómez, L. Lehner, B. Szilágyi, and J. Winicour, in *Black Holes, Gravitational Radiation and the Universe*, edited by B. Iyer and B. Bhawal (Kluwer, Dordrecht, The Netherlands, 1999), p. 393, gr-qc/9801070.

[48] R. Gómez, P. Laguna, P. Papadopoulos, and J. Winicour, Phys. Rev. D **54**, 4719 (1996).

[49] R. Gómez, L. Lehner, P. Papadopoulos, and J. Winicour, Class. Quant. Grav. **14**, 977 (1997).

[50] R. Penrose, in *Perspectives in Geometry and Relativity*, edited by B. Hoffmann (Indiana University Press, Bloomington, 1966), p. 259, and references therein.

[51] R. Gómez, P. Papadopoulos, and J. Winicour, J. Math. Phys. **35**, 4184 (1994).

[52] E. Newman and R. Penrose, J. Math. Phys. **7**, 863 (1966).

[53] R. Penrose and W. Rindler, *Spinors and Spacetime* (Cambridge University Press, Cambridge, England, 1984, 1986), Vol. 1, 2.

[54] J. N. Goldberg, A. J. Macfarlane, E. T. Newman, F. Rohrlich, and E. C. G. Sudarshan, J. Math. Phys. **8**, 2155 (1967).

[55] N. T. Bishop, R. Gómez, L. Lehner, M. Maharaj, and J. Winicour, Phys. Rev. D **56**, 6298 (1997).

[56] J. Winicour, J. Math. Phys. **24**, 1193 (1983).

[57] J. Winicour, J. Math. Phys. **25**, 2506 (1984).

[58] L. Lehner, J. Comp. Phys. **149**, 59 (1999).

[59] R. Isaacson, J. Welling, and J. Winicour, J. Math. Phys. **24**, 1824 (1983).

[60] P. Papadopoulos, Ph.D. thesis, University of Pittsburgh, 1994.

[61] R. Gómez, J. Winicour, and R. A. Isaacson, J. Comp. Phys. **98**, 11 (1992).

[62] B. Szilágyi, R. Gómez, N. Bishop and J. Winicour, (1999), gr-qc/9909026. Submitted to Phys. Rev. D.

[63] C. W. Misner, K. S. Thorne, and J. A. Wheeler, *Gravitation* (W. H. Freeman, San Francisco, 1973), p. 954.

[64] L. D. Landau and E. M. Lifshitz, *Mechanics* (Pergamon Press, New York, 1991).

[65] L. Tamburino and J. Winicour, Phys. Rev. **150**, 1039 (1966).

[66] J. Winicour, Gen. Rel. and Grav. **19**, 281 (1987).

[67] B. F. Shutz, Nature **323**, 310 (1986).

[68] A. Abramovici, W. E. Althouse, R. W. P. Drever, Y. Gürsel, S. Kawamura, F. J. Raab, D. Shoemaker, L. Sievers, R. E. Spero, K. S. Thorne, R. E. Vogt, R. Weiss, S. E. Whitcomb, and M. E. Zucker, Science **256**, 325-333 (1992).

[69] C. Cutler and E. E. Flanagan, Phys. Rev. D **49**, 2658-2697 (1994).

[70] E. E. Flanagan and S. A. Hughes, Phys.Rev. D **57**, 4535-4565 (1998), gr-qc/9701039.

[71] L. Blanchet, T. Damour, and B. R. Iyer, Phys. Rev. D **51** (1995) 5360-5386; Erratum–ibid. D**54** (1996) 1860.

[72] L. Blanchet, T. Damour, B. R. Iyer, C. M. Will, and A. G. Wiseman, Phys.Rev.Lett. **74**, 3515-3518 (1995), gr-qc/9501027.

[73] C. M. Will and A. G. Wiseman, Phys.Rev. D **54**, 4813-4848 (1996), gr-qc/9608012.

[74] L. Blanchet, B. R. Iyer, C. M. Will, and A. G. Wiseman, Class.Quant.Grav. **13**, 575-584 (1996), gr-qc/9602024.

[75] L. E. Kidder, C. M. Will, and A. G. Wiseman, Phys. Rev. D **47**, 3281 (1993); Class. Quant. Grav. **9**, L125 (1992).

[76] G. B. Cook, Phys. Rev. D **50**, 5025 (1994).

[77] K. S. Thorne, in *300 Years of Gravitation*, edited by S. W. Hawking and W. Israel (Cambridge University Press, Cambridge, England, 1987), p. 330.

[78] K. S. Thorne, in *Proceedings of the Snowmass 95 Summer Study on Particle and Nuclear Astrophysics*, edited by E. W. Kolb and R. Peccei (World Scientific, Singapore, 1995), gr-qc/9506086.

[79] A. Ori and K. S. Thorne, gr-qc/0003032, submitted to Phys. Rev. D.

[80] D. Lai and A. G. Wiseman, Phys.Rev. D **54**, 3958-3964 (1996), gr-qc/9609014.

[81] S. A. Teukolsky and W. H. Press, Astrophys. J. **193**, 443 (1974).

[82] S. Chandrasekhar and S. L. Detweiler, Proc. R. Soc. London **A344**, 441 (1975).

[83] F. Echeverria, Phys. Rev. D **40**, 3194 (1988).

[84] L. S. Finn, Phys. Rev. D **46**, 5236 (1992).

[85] D. Sigg, LIGO-P98007-00-D, to be published in the *Proceedings of TASI 98 (Theoretical Advanced Study Institue in Elementray Particle Physics), Boulder, Colorado.*

[86] R. Narayan, T. Piran, and A. Shemi, Astrophys. J. **379**, L17 (1991)

[87] E. S. Phinney, Astrophys. J. **380**, L17 (1991).

[88] E. P. J. Van den Heuvel and D. R. Lorimer, Mon. Not. R. Astron. Soc. **283**, L37-L39 (1996).

[89] A. V. Tutukov and L. R. Yungelson, Mon. Not. Roy. Astron. Soc. **260**, 675 (1993).

[90] H. Yamaoka, T. Shigeyama, and K. Nomoto, Astron. Astrophys. **267**, 433 (1993).

[91] B. F. Schutz, in *NASA, Relativistic Gravitational Experiments in Space*, pp. 7-13 (1989).

[92] P. Bender, I. Ciufolini, K. Danzmann, W. Folkner, J. Hough, D. Robertson, A. Rüdiger, M. Sandford, R. Schilling, B. Schutz, R. Stebbins, T. Summer, P. Touboul, S. Vitale, H. Ward, and W. Winkler, *LISA: Laser Interferometer Space Antenna for the detection and observation of gravitational waves*, Pre-Phase A Report, December 1995 (unpublished).

[93] D. Hils and P. L. Bender, Astrophys. J. **445**, L7 (1995).

[94] E. Poisson, Phys. Rev. D **54**, 5939-5953 (1996), gr-qc/9606024.

[95] M. C. Begelman, R. D. Blandford, M. J. Rees, Nature **287**, 307 (1980).

[96] H. D. Wahlquist, in *NASA, Relativistic Gravitational Experiments in Space* (SEE N90-19940 12-90), p 14-17 (1989).

[97] M. G. Haehnelt, Mon. Not. Roy. Astron. Soc. **269**, 199 (1994); astro-ph/9405032.

[98] J. Thornburg, Class. Quant. Grav. **4**, 1119 (1987).

[99] R. Gómez, L. Lehner, R. Marsa, and J. Winicour, Phys. Rev. D **57**, 4778 (1998), gr-qc/9710138.

[100] R. P. Kerr and A. Schild, Proc. Symp. Appl. Math. **17**, 199 (1965).

[101] E. Newman and R. Penrose, J. Math. Phys. **3**, 575 (1992).

[102] R. Gómez, L. Lehner, R. L. Marsa, J. Winicour, A. M. Abrahams, A. Anderson, P. Anninos, T. W. Baumgarte, N. T. Bishop, S. R. Brandt, J. C. Browne, K. Camarda, M. W. Choptuik, G. B. Cook, R. Correll, C. R. Evans, L. S. Finn, G. C. Fox, T. Haupt, M. F. Huq, L. E. Kidder, S. A. Klasky, P. Laguna, W. Landry, J. Lenaghan, J. Masso, R. A. Matzner, S. Mitra, P. Papadopoulos, M. Parashar, L. Rezzolla, M. E. Rupright, F. Saied, P. E. Saylor, M. A. Scheel, E. Seidel, S. L. Shapiro, D. Shoemaker, L. Smarr, B. Szilágyi, S. A. Teukolsky, M. H. P. M. van Putten, P. Walker, and J. W. York Jr, Phys. Rev. Lett. **80**, 3915 (1998), gr-qc/9801069.

[103] L. Lehner, N. Bishop, R. Gómez, B. Szilágyi, and J. Winicour, Phys.Rev. D **60**, 044005 (1999), gr-qc/9809034.

[104] S. Husa and J. Winicour, Phys.Rev. D **60**, 084019 (1999), gr-qc/9905039.

[105] R. Matzner, E. Seidel, S. Shapiro, L. Smarr, W.-M. Suen, S. Teukolsky, and J. Winicour, Science **270**, 941 (1995).

[106] S. Shapiro, S. Teukolsky, and J. Winicour, Phys. Rev. D **52**, 6982 (1995).

[107] J. Winicour, Prog. of Theor. Phys. Suppl., **136**, 57 (1999), gr-qc/9911106.

[108] N. Bishop, C. Clarke, and R. d'Inverno, Class. Quant. Grav. **7**, L23 (1990).

[109] C. Clarke, R. d'Inverno, and J. Vickers, Phys. Rev. D. **52**, 6863 (1995).

[110] M. Dubal, R. d'Inverno, and C. Clarke, Phys. Rev. D **52**, 6868 (1995).

[111] R. d'Inverno and J. Vickers, Phys. Rev. D **54**, 4919 (1996).

[112] R. d'Inverno and J. Vickers, Phys. Rev. D **56**, 772 (1997).

[113] D. Pollney, Ph.D. thesis, University of Southampton, 2000.

[114] W. H. Press, B. P. Flannery, S. A. Teukolsky, and W. T. Vetterling, *Numerical Recipes* (Cambridge University Press, Cambridge, England, 1986).

[115] K. Eppley, in *Sources of Gravitational Radiation*, edited by L. Smarr (Cambridge University Press, Cambridge, England, 1979), p. 275.

[116] G. B. Cook, M. F. Huq, S. A. Klasky, M. A. Scheel, A. M. Abrahams, A. Anderson, P. Anninos, T. W. Baumgarte, N. T. Bishop, S. R. Brandt, J. C. Browne, K. Camarda, M. W. Choptuik, R. R. Correll, C. R. Evans, L. S. Finn, G. C. Fox, R. Gómez, T. Haupt, L. E. Kidder, P. Laguna, W. Landry, L. Lehner, J. Lenaghan, R. L. Marsa, J. Masso, R. A. Matzner, S. Mitra, P. Papadopoulos, M. Parashar, L. Rezzolla, M. E. Rupright, F. Saied, P. E. Saylor, E. Seidel, S. L. Shapiro, D. Shoemaker, L. Smarr, W. M. Suen, B. Szilágyi, S. A. Teukolsky, M. H. P. M. van Putten, P. Walker, J. Winicour, and J. W. York Jr, Phys. Rev. Lett. **80**, 2512 (1998).

[117] R. Gómez, in talks presented at the Los Alamos Workshop of the Binary Black Hole Grand Challenge Alliance (unpublished).

[118] A. M. Abrahams, L. Rezzolla, M. E. Rupright, A. Anderson, P. Anninos, T. W. Baumgarte, N. T. Bishop, S. R. Brandt, J. C. Browne, K. Camarda, M. W. Choptuik, G. B. Cook, R. R. Correll, C. R. Evans, L. S. Finn, G. C. Fox, R. Gómez, T. Haupt, M. F. Huq, L. E. Kidder, S. A. Klasky, P. Laguna, W. Landry, L. Lehner, J. Lenaghan, R. L. Marsa, J. Masso, R. A. Matzner, S. Mitra, P. Papadopoulos, M. Parashar, F. Saied, P. E. Saylor, M. A. Scheel, E. Seidel, S. L. Shapiro, D. Shoemaker, L. Smarr, B. Szilágyi, S. A. Teukolsky, M. H. P. M. van Putten, P. Walker, J. Winicour, and J. W. York Jr, Phys. Rev. Lett. **80**, 1812 (1998), gr-qc/9709082.

[119] S. Teukolsky, Phys. Rev. D **61**, 087501 (2000), gr-qc/9909026.

[120] S. Frittelli, Phys. Rev. D **55**, 5992 (1997).

[121] J. Winicour, private communication (unpublished).

[122] K. C. B. New, K. Watt, C. W. Misner, and J. M. Centrella, Phys. Rev. D **58**, 064022 (1998), gr-qc/9801110.

[123] H. Friedrich and G. Nagy, Commun. Math. Phys. **201**, 619 (1999).

[124] J. M. Stewart, Class. Quant. Grav. **15**, 2865 (1998).

[125] S. Teukolsky, Phys. Rev. D **26**, 745 (1982).